

CONFERENCE SERIES



© *innsbruck* university press, 2012

Universität Innsbruck

1st edition

All rights reserved.

Cover design: Carmen Drolshagen

Cover photo: © Laurent Salino / Office du tourisme Alpe d'Huez

Printed by Prime Rate Kft.

www.uibk.ac.at/iup

ISBN 978-3-902719-52-2

Marius Lewerenz, Odile Dutuit, Roberto Marquardt (Eds.)

XVIIIth Symposium on Atomic, Cluster and Surface Physics 2012 (SASP 2012)

January 22 - 27, 2012

Alpe d' Huez, France

Contributions



**XVIIIth Symposium on
Atomic, Cluster and Surface Physics
(SASP 2012)**

**January 22-27, 2012
Alpe d'Huez, France**

International Scientific Committee:

Davide Bassi (Università degli Studi di Trento, Italy)
Tilmann D. Märk (Universität Innsbruck, Austria)
Nigel Mason (Open University, UK)
Martin Quack (Eidgenössische Technische Hochschule Zürich, Switzerland)
Tom Rizzo (EPFL Lausanne, Switzerland)
Paul Scheier (Universität Innsbruck, Austria)

Organising Committee:

Local organisation: Institut de Planétologie et d'Astrophysique de Grenoble (IPAG), France

Odile Dutuit (IPAG) and Roberto Marquardt (Univ. Strasbourg), co-chairpersons

Marius Lewerenz (Univ. Paris-Est, Marne la Vallée)
Cecilia Ceccarelli (IPAG)
Vianney Taquet (IPAG)
Nigel Mason (Open Univ., UK)
Valérie Chopin (IPAG)
Béatrice Pibaret (IPAG)

SASP 2012 was sponsored by the EU through the COST Action on the "Chemical Cosmos", Université Paris Est (Marne la Vallée), CNRS-INSU, and IPAG (Institut de Planétologie et d'Astrophysique de Grenoble).

Preface

The international symposium on Atomic, Cluster and Surface Physics, SASP, is one in a continuing biennial series of conferences founded in 1978 by members of the Institute for Ion Physics and Applied Physics of the University of Innsbruck, Austria. SASP symposia aim to promote the growth of scientific knowledge and effective exchange of information among scientists in the fields of atomic, molecular, cluster and surface physics stressing both fundamental concepts and applications across these areas of interdisciplinary science. Five scientific themes have been chosen for SASP 2012:

- Astrophysics and astrochemistry
- Clusters, aggregates, aerosols, ices
- Ions, collisions, dynamics, spectroscopy
- Surface science, catalysis
- Energy: production, storage

Since the beginning, the SASP format has been similar to that of a Gordon Conference, with invited lectures, some hot topics, posters and ample time for discussion. The attendance to the symposium has been kept to about 100 participants to favour interdisciplinary and multidisciplinary discussions.

The COST Action on the “Chemical Cosmos” supported SASP 2012 and offered bursaries to early stage researchers to attend the symposium. A special Media training session is proposed to the bursary recipients.

SASP usually takes place in Austria, but every second time, it may be held in another alpine country. So far, the SASP conferences were held in the following locations:

1978 Zirog, Italy	1996 Engelberg, Switzerland
1980 Maria Alm, Austria	1998 Going, Austria
1982 Maria Alm, Austria	2000 Folgaria, Italy
1984 Maria Alm, Austria	2002 Going, Austria
1986 Obertraun, Austria	2004 La Thuile, Italy
1988 La Plagne, France	2006 Obergurgl, Austria
1990 Obertraun, Austria	2008 Les Diablerets, Switzerland
1992 Pampeago, Italy	2010 Obergurgl, Austria
1994 Maria Alm, Austria	2012 Alpe d’Huez, France

SASP Erwin Schrödinger Gold Medal 2012

The “SASP Award for Outstanding Scientific Achievements” was initiated in 1992 by the SASP International Scientific Committee. This award is granted during the biennial SASP meeting to one or two scientists, chosen among those who have strong connections to the activities of SASP.

Recipients of the SASP award 2012 – in the form of the “Erwin Schrödinger Gold Medal” designed by Zdenek Herman – will be



**Dieter Gerlich, University of Chemnitz,
Germany**



**John Maier, University of Basel,
Switzerland**

Dieter Gerlich, from the University of Chemnitz in Germany, will receive this award for his outstanding contributions to ion chemistry with astrophysical applications (collision dynamics and ion spectroscopy), in particular with the development of innovative experimental instruments based on rf-devices.

John P. Maier, from the University of Basel in Switzerland, will receive this award for his outstanding contributions to molecular spectroscopy with astrophysical applications, in particular for highly reactive radical and ionic carbon chains and rings.

At previous SASP meetings the Schrödinger Gold Medal was awarded to:

- 1992 David Smith, Birmingham, UK
- 1994 Zdenek Herman, Praha, Czech Republic
- 1996 Werner Lindinger and Tilman Märk, Innsbruck, Austria
- 1998 Eldon Ferguson, Boulder, USA and Chava Lifshitz, Jerusalem, Israel
- 2000 Jean H. Futrell, Richland, USA
- 2002 Eugen Illenberger, Berlin, Germany
- 2004 Anna Giardini-Guidoni, Roma, Italy
- 2006 Davide Bassi, Trento, Italy and Martin Quack, Zürich, Switzerland
- 2008 Helmut Schwarz, Berlin, Germany
- 2010 Kurt Becker, New York, USA

Program

Sunday	Monday	Tuesday	Wednesday	Thursday
	9:00 (invited) H. Cederquist	9:00 (invited) A.J.H.M. Meijer	9:00 (invited) R. Signorell	9:00 (invited) P. Scheier
	9:30 (invited) W. Geppert	9:30 (invited) N. Watanabe	9:30 (invited) M. Fárník	09:30 (invited) Ph. Marquetand
	10:00 (invited) H. Rothard	10:00 (invited) J.C. Tremblay	10:00 (invited) G. Muñoz-Caro	10:00 (invited) R. Wester
	10:30 <i>Coffee break</i>	10:30 <i>Coffee break</i>	10:30 <i>Coffee break</i>	10:30 <i>Coffee break</i>
	11:00 (invited) F. Dulieu	11:00 (invited) W. Dong	11:00 (invited) A. Milet	11:00 (invited) P. Tosi
	11:20 (invited) Ch. Joblin	11:20 (invited) L. Hornekaer	11:20 (invited) B. Schmitt	11:20 (invited) A. Osterwalder
	11:40 (invited) A. Faure	11:40 (invited) A.M. Wodtke	11:40 (invited) P. Jungwirth	11:40 (invited) A. Lindinger
	12:00 <i>Discussion</i>	12:00 <i>Discussion</i>	12:00 <i>Discussion</i>	12:00 <i>Discussion</i>
	16:00 <i>Pause</i>	16:00 <i>Pause</i>	16:00 <i>Pause</i>	16:00 <i>Pause</i>
16:30 (COST) Media Training	16:30 (invited) J. Stohner	16:30 (hot topic) S.D. Price	16:30 (hot topic) A.B.C. Patzer	16:30 (hot topic) Y. Nakai
	16:50 (invited) J. H. Bredehöft	16:50 (hot topic) R. Zimmermann	16:50 (hot topic) J. Zabka	16:50 (hot topic) A. Lafosse
	17:10 (invited) S. Bauerecker	17:10 (invited) M. Grätzel	17:10 (hot topic) V. Vuitton	17:10 (hot topic) Ph. Haslinger
	17:30 (invited) A. Campargue	17:40 (invited) P. Sanglan	17:30 (invited) S. Albert	17:30 (invited) M.A. Smith
	18:00 (invited) D.M. Benoit	18:15 <i>Discussion</i>	18:00 (invited) S. Schlemmer	18:00 (invited) S. Willitsch
	19:00 <i>Dinner</i>	19:00 <i>Dinner</i>	19:00 <i>Dinner</i>	19:00 <i>Conference Dinner</i>
20:30 (invited) F. Forget	Poster	20:30 (invited) D. Gerlich	Poster	
		21:15 (invited) J. Maier		

Contents

Invited Papers

Extraterrestrial physics on planet Mars <u>François Forget</u>	22
Ions interacting with clusters of polycyclic aromatic hydrocarbon (PAH) molecules or fullerenes <u>Henrik Cederquist</u>	23
Dissociative recombination – an efficient production and destruction mechanism of molecules in space <u>Wolf Geppert</u>	24
Swift heavy ion interaction with insulators (polymers, astrophysical ices and crystals) <u>Hermann Rothard</u>	25
New syntheses and mechanisms on cold surfaces of astrophysical interest <u>François Dulieu</u>	29
Dissociation and electronic properties of PAH-related species of astrophysical interest <u>Christine Joblin</u>	33
State-to-state molecular collisions in astrophysics <u>Alexandre Faure</u>	37
Spectroscopy of chiral molecules <u>Jürgen Stohner</u>	38
Chiral photochemistry and anisotropy in the solid phase <u>Jan Hendrik Bredehöft</u>	40
Phase changes of supercooled water: from aerosol to freely suspended droplets <u>Sigurd Bauerecker</u> and Tillmann Buttersack	44

Near infrared absorption spectroscopy at ultra high sensitivity: the case of H₂ and CH₄. <u>Alain Campargue</u> and Samir Kassi	45
Understanding surface adsorption through theoretical vibrational spectroscopy <u>David M. Benoit</u>	49
Formation of small molecules on substrates of astrochemical interest Kousik Giri, Benjamin J. Irving and <u>Anthony J. H. M. Meijer</u>	51
Hydrogen chemistry on cold grain surfaces <u>Naoki Watanabe</u> , Hiroshi Hidaka, Tetsuya Hama, Yasuhiro Oba, Akira Kouchi, Takeshi Chigai, Yuki Kimura	53
Don't forget friction: theoretical perspectives on the laser control of adsorbate vibrations at metallic surfaces. <u>Jean Christophe Tremblay</u> , Serge Monturet and Peter Saalfrank	56
Reactive force fields for surface chemical reactions <u>W. Dong</u> , Y. Xiao, H. F. Busnengo, X. J. Shen and X. H. Yan	59
Hydrogen interaction with polycyclic aromatic carbon systems – from graphene to PAHs <u>Liv Hornekaer</u>	61
Multiquantum vibrational excitation of NO scattered from Au(111): benchmark data and comparison to theories of nonadiabatic molecule-surface interactions Russell Cooper, Christof Bartels, Alexander Kandratsenka, Igor Rahinov, Neil Shenvi, Kai Golibrzuch, Zhisheng Li, Daniel J. Auerbach, John C. Tully, <u>Alec M. Wodtke</u>	62
Photon harvesting and charge carrier collection in mesoscopic solar energy conversion systems <u>Michael Grätzel</u>	66
Title to be announced <u>Patrick Sanglan</u>	66
Astrochemistry in Ion Traps: From Cold Hydrogen to Hot Carbon <u>Dieter Gerlich</u>	67
Electronic Spectroscopy of Astrophysically Relevant Molecules <u>John P. Maier</u>	71

Characterization of Clusters and Ultrafine Aerosols by Ultraviolet Photoionization Bruce L. Yoder, Jessica H. Litman, and <u>Ruth Signorell</u>	72
Ice nanoparticles in molecular beam experiments: pick-up cross sections for atmospheric molecules and their photochemistry <u>Michal Fárník</u> , Viktoriya Poterya, Andriy Pysanenko, Jozef Lengyel, Pavla Svrčková, Jaroslav Kočišek, Juraj Fedor, Milan Ončák and Petr Slavíček	73
Ice processes relevant to astrophysics: radiation products, thermal and photodesorption <u>Guillermo Muñoz-Caro</u>	76
Theoretical Study of the insertion of small molecules inside clathrate hydrates using metadynamics <u>Anne Milet</u> , Mircea Oltean, and Nevin Uras-Aytemiz	77
Infrared and Raman Spectroscopy of Clathrate Hydrates <u>Bernard Schmitt</u>	81
Ultrafast Dynamics Following Photoionization in Water: From Clusters to the Aqueous Bulk Ondřej Maršálek, Frank Uhlig, and <u>Pavel Jungwirth</u>	85
Highest resolution Fourier transform infrared (FTIR) spectroscopy of polyatomic molecules with and without synchrotron radiation <u>Sieghard Albert</u> , Karen Keppler Albert, Philippe Lerch and Martin Quack	86
IR and THz spectroscopy of cold molecular ions <u>Stephan Schlemmer</u> , Oskar Asvany and Sandra Brünken	90
Electron driven reactions in doped He nanodroplets Christian Leidlmair, Peter Bartl, Harald Schöbel, Lukas an der Lan, Samuel Zöttl, Matthias Daxner, Odin Mack, Benjamin Puschnigg, Violaine Vizcaino, David Gschliesser, Johannes Postler, Michaela Hager, Stephan Denifl, Andrew M. Ellis, Olof Echt and <u>Paul Scheier</u>	92

Mixed quantum classical dynamics including laser interactions and spin-orbit coupling <u>Philipp Marquetand</u> , Martin Richter, Jesús González-Vázquez, Juan José Bajo, Ignacio Sola, Jesus Santamaria and Leticia González	96
Crossed beam imaging of ion-molecule reactions <u>Roland Wester</u>	100
Molecular growth via ion-molecule and radical reactions. From planetary atmospheres to plasma reforming <u>Paolo Tosi</u> and Daniela Ascenzi	101
Deceleration and Velocity Filtering of Neutral Molecules in Electric Fields Andreas Osterwalder	104
Optimal control by using parametrically polarization shaped laser pulses Albrecht Lindinger	105
Ion-Molecule Reaction Processes in a Molecular Beam-Ring Electrode Trap <u>Mark A. Smith</u> , Bing Yuan and Andrei Sanov	108
Ion-Neutral Reactive Collisions at sub-Kelvin Temperatures <u>Stefan Willitsch</u> , Xin Tong and Felix H.J. Hall	111

Hot Topic Papers

- Low temperature reactions on interstellar dust grains: new surface chemistry for the interstellar medium**
Stephen D Price, Rona E Watson and Michael D Ward 114
- New concepts for on-line monitoring of complex gas mixtures using photo ionisation mass spectrometry**
R. Zimmermann, R. Hertz, A. Fendt, Eschner, T. Streibel 118
- Properties of small TiC clusters: Implications for dust nucleation studies under the conditions of C-rich AGB stars**
A. B. C. Patzer, Ch. Chang and D. Sülzle 119
- Anion Chemistry on Titan: A possible route to large N-bearing hydrocarbons**
J. Zabka, M. Polasek, C. Romanzin, and C. Alcaraz 123
- Laboratory data needs for modeling Titan's atmospheric chemistry**
Véronique Vuitton, Nadia Balucani, Odile Dutuit, Axel Bazin and Roger V. Yelle 127
- Equipment for ionic cluster formation based on ion drift-tube with selected-ion injection**
Yoichi Nakai¹, Hiroshi Hidaka, Naoki Watanabe and Takao M. Kojima 131
- Low energy electron induced resonant processes in terphenyl-thiol SAMs**
Lionel Amiaud, Vincent Humblot, Roger Azria, Claire-Marie Pradier and Anne Lafosse 133
- An ionizing time-domain matter-wave interferometer**
Philipp Haslinger, Nadine Dörre, Philipp Geyer, Jonas Rodewald, Stefan Nimmrichter, Klaus Hornberger and Markus Arndt 134

Contributed Papers (Poster)

- Vibrational Bond-Selectivity in Methane Chemisorption**
Li Chen, Hirokazu Ueta, Régis Bisson, and Rainer D. Beck 140
- Reactivity of Carbon Dioxide Radical Anions in Water Clusters**
Robert F. Höckendorf, O. Petru Balaj, Kirsten Fischmann, Amou Akhgarnusch,
Christian van der Linde, K. Philip Jäger, Qiang Hao, Chi-Kit Siu and Martin K. Beyer 141
- Low-energy electron-induced synthesis of formamide**
E. Böhler, J. H. Bredehöft, P. Swiderek 142
- Effect of organic ligands on electron-induced reactions of Si compounds**
E. Böhler, D.Gschliesser, J.Postler, P. Swiderek, P.Scheier 147
- A Combined Crossed-Beam and Theoretical Study of Radical-Radical Reaction Dynamics of $O(^3P) + C_2H_3$**
Min-Jin Park and Jong-Ho Choi 150
- Toward a new global potential energy surface for the $H_2O - HF$ complex**
Yann Cornaton and Roberto Marquardt 151
- The submersion of sodium clusters in helium nanodroplets:
Identification of the surface \rightarrow transition**
Matthias Daxner, Lukas An der Lan, Peter Bartl, Christian Leidlmair, Harald Schöbel,
Roland Jochum, Stephan Denifl, Tilmann D. Märk, Andrew M. Ellis and Paul Scheier 156
- Excited alkali atoms in He_n : influence of the dimer potential energy curves**
David Dell'Angelo, Grégoire Guillon and Alexandra Viel 160
- State selective study of the recombination of D_3^+ ions with electrons**
Petr Dohnal, Michal Hejduk, Jozef Varju, Peter Rubovič, Sergii Opanasiuk, Radek
Plašil and Juraj Glosík 162
- Photochemistry of essential building blocks of biomolecules in clusters**
Michal Fárník, Viktoriya Poterya, Lukáš Šišťák and Petr Slavíček 166
- Toward the quantum dynamics of the frustrated translation $H_2/Cu(100)$**
Thiago Firmino and Roberto Marquardt 170
- The (Ca/N_2O) reactive system on helium clusters**
Marc-André Gaveau, Marc Briant, Gloria Spighi and Jean-Michel Mestdagh 174

Recombination of spin-polarised Hydrogen Atoms on non-porous Water Ice at 3.5K	176
<u>Thomas R. Govers</u>	
Monte-Carlo modeling of hot O, C, and N particles in the upper atmosphere of Mars and Venus	180
<u>H. Gröller</u> , H. I. M. Lichtenegger, H. Lammer, O. Dutuit, M. Pfleger, V. I. Shematovich, Yu. N. Kulikov	
Spin temperature measurement of thermally desorbed water molecules from water ice prepared at 8K	184
<u>Tetsuya Hama</u> , Naoki Watanabe and Akira Kouchi	
Collisions of slow N_2^+ ions with room temperature and heated fusion relevant surfaces	186
<u>Martina Harnisch</u> , Alan Keim, Samuel Zöttl, Paul Scheier, Tilmann D. Märk, Zdenek Herman	
Scattering of T and He at graphite (0001) surfaces: a 3D time-dependent wave packet study	190
<u>Stefan E. Huber</u> , Tobias Hell, Michael Probst and Alexander Ostermann	
Melting behaviour of pure and coated gold nanowires: Molecular dynamics simulations	194
<u>Stefan E. Huber</u> , Chompunuch Warakulwit, Jumras Limtrakul, Tatsuya Tsukuda and Michael Probst	
Quantum-state Resolved Studies of the Physisorption of Water on Ice	198
<u>P. Morten Hundt</u> , Régis Bisson, Hirokazu Ueta, and Rainer D. Beck	
Formation of molecular hydrogen in the interstellar medium	199
<u>Benjamin J. Irving</u> , Anthony J. H. M. Meijer	
Experimental determination of conditions in the trap: reaction temperature and reactant density	200
<u>P. Jusko</u> , I. Zymak, D. Mulin, Š. Roučka, R. Plašil, D. Gerlich, J. Glosík	

Influence of higher-order dispersion coefficients on near-threshold bound and continuum states	
<u>Alexander Kaiser</u> , Tim-Oliver Müller and Harald Friedrich	204
Hydrogen-fullerene interactions at low temperatures	
<u>Alexander Kaiser</u> , Stefan E. Huber, Oksana Ismailova and Michael Probst	208
Cs–He_N Rydberg series	
Florian Lackner, Günter Krois, Moritz Theisen, <u>Markus Koch</u> and Wolfgang E. Ernst	212
Cr clusters in helium nanodroplets	
Matthias Hasewend, Andreas Kautsch, Martin Raschek, <u>Markus Koch</u> and Wolfgang E. Ernst	216
Developing new accurate PES for Metal Nitrosyls	
<u>B. Murali Krishna</u> and Roberto Marquardt	218
Chemistry and photochemistry on mixed water/nitric acid ice nanoparticles studied in molecular beams	
<u>Jozef Lengyel</u> , Viktoriya Poterya, Andriy Pysanenko and Michal Fárník	222
The solvated electron alias H₃O radical: Photochemistry on ice nanoparticles:	
<u>Jozef Lengyel</u> , Viktoriya Poterya, Andriy Pysanenko, Milan Ončák, Petr Slavíček and Michal Fárník	226
Quantum Simulations of Helium Clusters with Open Shell and Ionic Dopants	
J. Jiang, <u>M. Lewerenz</u> , and M. Mladenović	229
Advanced modelling of He droplets	
<u>Andreas Mauracher</u> , Kersti Hermansson and Daniel Spångberg	231
Three-level system depletion spectroscopy by absorption with cavity ringdown	
<u>Fabio J. Mazzotti</u> , Ranjini Raghunandan, Aaseef M. Esmail , Lizandra Barrios	233

- Inversion tunneling in normal and substituted anilines from infrared spectroscopy and quasiadiabatic channel reaction path Hamiltonian calculations.**
Eduard Miloglyadov, Robert Prentner, Georg Seyfang, Martin Quack 234
- Low Energy Ion Surface Irradiation Experiment**
Elena-Andra Muntean, Tom Field and Bob McCullough 238
- Spin and orbital moments of isolated clusters – synchrotron radiation elucidates nanomagnetism**
Sergey Peredkov, Matthias Neeb, Wolfgang Eberhardt, Jennifer Meyer, Matthias Tombers, Heinrich Kampschulte, and Gereon Niedner-Schatteburg 239
- Low-temperature Surface Reactions of Non-energetic OH Radicals of Astrophysical Interest.**
Yasuhiro Oba, Naoki Watanabe, Tetsuya Hama, Akira Kouchi, and Valerio Pirronello 241
- Comparative Study on Hydrogenated and Deuterated Amorphous Carbon Films Deposited by RF PECVD**
Vilma Bursikova, Adrian Stoica, Vratislav Perina, Romana Miksova, Pavel Slavicek, Valentin Mocanu 242
- Excited state relaxation of diarylethenes: a gas phase study on isolated and deposited molecules on Ar_n clusters**
G. Piani, A. Lietard, R. Pollet, L. Poisson, B. Soep, J.-M. Mestdagh 247
- Analysis of the products of reactions induced in methane-nitrogen plasma generated in the glow discharge**
Lucie Polachova, Gabriel Horvath, Jon Watson, Nigel J. Mason, Frantisek Krcma, Miroslav Zahoran and Stefan Matejcik 248
- The structure of liquid ethylene glycol: MD simulations**
Oksana Ismailova and Michael Probst 252

Characterization and manipulation of explosive compounds and homologues <u>S. Ralser</u> , M. Hager, D. Gschliesser, J. Rodríguez Fernández, C. Urban, J. M. Gallego, R. Otero and P. Scheier	255
Collisional Radiative Recombination of H_3^+ Ion in Low Temperature Plasma <u>Štěpán Roučka</u> , Petr Dohnal, Michal Hejduk, Jozef Varju, Peter Rubovič, Sergii Opanasiuk, Radek Plašil and Juraj Glosík	259
IR-Laser Induced Population Transfer from Highly Populated Rotational Levels of NH_3 in a Molecular Beam Peter Dietiker, Martin Quack, Andreas Schneider, <u>Georg Seyfang</u> and Fatih Ünlü	263
Photofragmentation of amino acids containing a disulfide (S-S) bond <u>S. Soorkia</u> , B. Lucas, J. A. Fayeton, M. Barat and C. Jouvét	268
Control of chemical synthesis by electrons: The making and breaking of bonds Th. Hamann, E. Böhler, T. Borrmann, J. H. Bredehöft, <u>P. Swiderek</u>	269
Modification of polydimethylsiloxane coatings by H_2 RF plasma, Xe_2^* excimer VUV radiation, and low-energy electron beams <u>P. Swiderek</u> , E. Jolondz, J.H. Bredehöft, T. Borrmann, C. Dölle, M. Ott, C. Schmäser, A. Hartwig, V. Danilov, H.-E. Wagner, J. Meichsner	273
Quantum dynamics study on muonium chemical reactions Toshiyuki Takayanagi, Tomokazu Tanaka and Takanori Kobayashi	276
Decay of the dialanine anion formed upon free electron attachment <u>Katrin Tanzer</u> , David Gschliesser, Violaine Vizcaino, Michael Probst, Paul Scheier and Stephan Denifl	279
Multilayer and multiparameter grain surface modeling in prestellar cores and hot corino <u>Vianney Taquet</u> , Cecilia Ceccarelli, Claudia Kahane	283

- Vibrationally bond-selective chemisorption of methane on Pt(111) studied by reflection absorption infrared spectroscopy**
Li Chen, [Hirokazu Ueta](#), Régis Bisson and Rainer D. Beck 285
- State-selected ion-molecule reactions relevant to the chemistry of Titan's ionosphere**
B. Cunha de Miranda, S. Chefdeville, [V. Vuitton](#), [J. Zabka](#), M. Polasek, C. Romanzin, and [C. Alcaraz](#) 287
- Orienting polar molecules without multipole lenses:
Optical state selection with adiabatic orientation**
Tim Schäfer, Nils Bartels, Nils Hocke, Xueming Yang, [Alec M. Wodtke](#) 291
- Quantum simulations for double proton transfer processes**
[T. Yoshikawa](#), T. Takayanagi 295

Invited Papers

Extraterrestrial physics on planet Mars

François Forget¹

¹ *LMD, Institut Pierre Simon Laplace/CNRS, Université P. et M. Curie BP99, 2 place Jussieu 75005 Paris, France. forget@lmd.jussieu.fr*

The Planet Mars that we currently explore with rovers on the surface and satellites in orbit is an active environment controlled by exotic physical process such as the condensation of the atmosphere (mostly composed of CO₂) onto the surface and in the atmosphere, the occurrence of planetary-scale dust storms, the formation of spectacular dust devils, etc. Among the numerous enigma raised by the recent observations, we will discuss the discovery of plumes of methane which have been reported by several observers. Their behaviour seems impossible to explain by known physics and chemistry.

Furthermore, the analysis of the geological records present on the surface of the planets have revealed that the planet environment was very different in the past. On the one hand the Martian climate system has probably experienced large variations related to the oscillations of the parameters of the Martian orbit and rotation a few millions or even thousands of years ago. On Earth variations of obliquity between 22° and 24.5° seem to have resulted in major climate changes. Mars is thought to undergo large chaotic variation from 0° to more than 60°. These oscillations affected surface temperatures and the water cycle, inducing the mobilization and accumulation of large ice deposits (glaciers, polar caps) in various locations on the planets.

On the other hand, the observations of the geology and mineralogy of the oldest surface on Mars (dating back to more than 3 billion years ago) provide evidence that the Martian environment was completely different then, with liquid water on the surface. Such clement conditions are surprising because most experts believe that at that time, the young Sun was less dense than today and its luminosity 25% lower than at present time. Mars may have been warmed by a thicker atmosphere containing greenhouse gas and clouds, a young Sun warmer than expected, high geothermal fluxes, or episodically by large impacts.

To open the SASP 2012 symposium, I will be honoured to tell a few stories about the exploration of planet Mars and the investigations on the exotic physic that control its environment.

Ions interacting with clusters of polycyclic aromatic hydrocarbon (PAH) molecules or fullerenes

Henrik Cederquist

Stockholm University, AlbaNova University Center, Department of Physics, S-10691 Stockholm, Sweden

Dissociative recombination – an efficient production and destruction mechanism of molecules in space

Wolf Geppert

Stockholm University, AlbaNova University Center, Department of Physics, S-10691 Stockholm, Sweden

Swift heavy ion interaction with insulators (polymers, astrophysical ices and crystals)

Hermann Rothard¹

¹ *Centre de Recherche sur les Ion, les Matériaux et la Photonique (CEA/CNRS/ENSICAEN/UCBN), CIMAP-CIRIL-Ganil, BP5133, 14070 Caen Cedex 05, France.(email: rothard@ganil.fr)*

Introduction: Heavy Ion Irradiation Effects

The first stage of the interaction of ionizing radiation such as swift heavy ions with condensed matter consists in excitation of target electrons and may lead to subsequent ejection of electrons. Measurements of electron spectra (differential in energy and angle) give direct information about ionization and electron transport. The energy deposited on the electrons is then transferred to surrounding atoms and molecules, for example via electron-phonon coupling in crystal lattices or diffusion and chemical reactions of radicals following radiolysis of molecules. These processes may finally result in desorption or sputtering, appearance of defects and tracks, destruction and formation of molecules, DNA strand breaks and so on. The ejection of atoms, molecules and clusters from irradiated targets can be used to obtain information about the involved microscopic processes at that stage.

In the following, some examples of effects induced in insulating materials irradiated by swift heavy ions will be presented: 1) The slowing down of fast electrons allows to study charging-up of polymers (Mylar = PET, polypropylene) [1,2]. 2) Ionic crystals such as lithium fluoride LiF are subject to “electronic sputtering”. Effects related to the strong perturbation by heavy ion impact are observed. Most particles are ejected as clusters [3,4]. 3) Specific effects related to strong energy deposition were also observed in swift heavy ion induced electronic sputtering of condensed molecules (CO, CO₂). Sputtering yields show a strong non-linear dependence on the deposited energy in the electronic energy loss regime. The contribution of heavy ion induced desorption from grains must therefore be taken into account for understanding the presence of gas phase molecules in dense interstellar clouds [5,6].

Electron ejection: charging-up of polymers

The slowing down of fast electrons emitted from insulators (Mylar, polypropylene) irradiated with swift ion beams (C, O, Kr, Ag, Xe; 20-64 MeV/u) was measured by the time-of-flight (TOF) method at LNS/Catania and at GANIL/Caen [1,2]. The charge build-up, deduced from convoy- and binary encounter electron peak shifts, leads to target material dependent

potentials (6.0 kV for Mylar, 2.8 kV for PP). The number of projectiles needed for charging up (charging-up time constant) is inversely proportional to the electronic energy loss [2]. After a certain time, a sudden de-charging occurs. A surprising finding is that sandwich targets with gold layers on both surfaces of polymer foils behave in the same way as pure insulators, whereas a single gold layer suppresses the charging and de-charging. The puzzling question whether the observed charging-up is a surface- or a bulk (track) phenomenon or if both processes contribute, remains open. This work is performed in collaboration with E. De Filippo (INFN Catania) and S. Hagmann (IKF Frankfurt and GSI Darmstadt).

Electronic sputtering of Lithium Fluoride

Ion-surface collisions involving swift heavy ions (≈ 10 MeV/u), where the electronic loss S_e is dominant, lead to “electronic sputtering”. The microscopic mechanisms are still under debate (Coulomb explosion, thermal spike, excitonic mechanisms etc.). The measurements of yields, and of energy- and angular distributions of sputtered particles contribute to the understanding of the initial microscopic processes of damage and defect creation in materials. A new UHV system (AODO) [3] allows measuring the mass distributions (“Secondary Ion Mass Spectroscopy”, SIMS) with well prepared target surfaces. By means of a combination of “time-of-flight” and imaging techniques (XY-TOF-SIMS), it is possible to measure the complete velocity vector of the secondary ions and to deduce energy spectra and angular distributions.

Here, we focus on the sputtering of Lithium Fluoride (an ionic crystal, a large band gap insulator ≈ 14 eV) by fast heavy ions (≈ 10 MeV/u) and the dependence of the emission of secondary ions on the electronic stopping power S_e . A striking result is that the secondary ion yield Y dependence on S_e presents two different regimes: At low S_e (< 8 keV/nm), the yields scale as $Y \sim S_e^2$. At high S_e (> 8 keV/nm), in the strong perturbation regime, a saturation $Y = \text{constant}$ is observed. The energy distribution for the secondary ions can be described by a Maxwell-Boltzmann distribution; this could be a hint for a thermal mechanism (thermal spike?). It is also found that most particles are emitted as clusters [3,4]. Moreover, experiments performed with thin LiF films deposited in situ on Cu substrate show that the emission of these clusters depends on the target thickness. First results on the evolution of sputtering of nepheline (a silicate believed to be a good analogue of mercurian and lunar surfaces) by cosmic ray equivalents were obtained with TOF-SIMS. This work is performed in collaboration with Ph. Boduch, H. Hijazi, Th. Langlinay, F. Ropars, A. Cassimi (CIMAP-CIRIL-Ganil Caen), L. S. Farenza (UFSC Florianopolis), E. F. da Silveira (PUC Rio de Janeiro), G. Strazzulla (INAF Catania).

Cosmic rays: Sputtering and Radiolysis of Astrophysical Ices

In the solar system and in dense regions of the interstellar medium, icy layers (e.g. grain mantles) formed from a mixture of small molecules are exposed to ionizing irradiation (UV photons, electrons, ions). The interaction of radiation with the ices induces several physico-chemical processes (fragmentation/radiolysis, followed by chemical reactions and formation of new molecules; structural/phase changes; desorption/sputtering of molecules from the surface). Effects induced by weakly ionizing particles (UV photons, electrons, protons) have been studied since more than 20 years. On the other hand, studies with heavy multiply charged ions are scarce, in particular in the (high projectile velocity) electronic energy loss domain. Although protons and helium are several orders of magnitudes more abundant in the cosmic ray spectrum than heavy ions, the high electronic energy loss of heavy ions can compensate for the lower flux and yield to non-negligible contributions of heavy ion induced physico-chemistry. In particular, we observed a strong non-linear increase of sputtering yields with deposited energy S_e in CO and CO₂ ices bombarded with Ni ions of different energies. [5,6]. This clearly shows that the contribution of heavy ion induced desorption from grains must be taken into account for understanding the presence of gas phase molecules in dense interstellar clouds.

The experiments were performed with μm thick ice layers formed from condensed gases on a CsI window at 15K, which allowed to measure infrared absorption spectra (FTIR) before and after irradiation with ions at different fluences. Another interesting result related to the specificities of the strong electronic energy deposition by heavy ions concerns ion bombardment of frozen Methanol CH₃OH. Its destruction cross sections by fast heavy ion irradiation (Zn and Kr beams) were found to be considerably larger than those for lighter ions (O, He or H beams) [7]. As a scaling law, we found that destruction cross sections increase with the electronic stopping power roughly as $\sigma \sim S_e^{3/2}$. Finally, in the case of H₂O-CO-NH₃ mixed ices irradiated with swift heavy ions, we have observed in the infrared absorption spectra of the residues (after thermal desorption of volatile small molecules) strong indications for the formation of glycine, the simplest proteinaceous amino acid, considered as pre-biotic molecule [8]. This work is performed in collaboration with Ph. Boduch, A. Domaracka, X. Lv (CIMAP-CIRIL-Ganil), E. Dartois (IAS Orsay), E. F. da Silveira, E. Seperuelo-Duarte, A. L. F. Barros, V. Bordalo (PUC Rio de Janeiro) and S. Pilling (UNIVAP São José dos Campos).

References

- [1] E. De Filippo, G. Lanzano, F. Amorini, G. Cardella, E. Geraci, L. Grassi, E. La Guidara, I. Lombardo, G. Politi, F. Rizzo, P. Russotto, C. Volant, S. Hagmann, H. Rothard
Charging of insulators by multiply-charged-ion impact probed by slowing down of fast binary-encounter electrons
Phys. Rev. **A82** (2010) 062901
- [2] E. De Filippo, G. Lanzano, F. Amorini, E. Geraci, L. Grassi, E. La Guidara, I. Lombardo, G. Politi, F. Rizzo, P. Russotto, C. Volant, S. Hagmann, H. Rothard
Slowing down of fast electrons as probe for charging and decharging dynamics of ion-irradiated insulators
Phys. Rev. **A83** (2011) 064901
- [3] H. Hijazi, H. Rothard, P. Boduch, I. Alzaher, F. Ropars, A. Cassimi, J.M. Ramillon, T. Been, B. Ban d'Etat, H. Lebius, L.S. Farenzena, E. F da Silveira
Interaction of swift Ion Beams with Surfaces: Sputtering of Secondary Ions from LiF studied by XY-TOF-SIMS
Nucl. Instrum. Meth. **B269** (2011) 1003-1006
- [4] H. Hijazi, L. S. Farenzena, H. Rothard, P. Boduch, P. L. Grande, E. F. da Silveira
Cluster Ion Emission from LiF induced by MeV N^{9+} projectiles and ^{252}Cf Fission Fragments
Eur. Phys. J. **D63** (2011) 391-400
- [5] E. Seperuelo Duarte, P. Boduch, H. Rothard, T. Been, E. Dartois, L. S. Farenzena, E.F. da Silveira,
Heavy Ion Irradiation of Condensed CO₂: Sputtering and Molecule Formation
Astronomy & Astrophysics **502** (2009) 599-603
- [6] E. Seperuelo Duarte, A. Domaracka, P. Boduch, H. Rothard, E. Dartois, E. F. da Silveira
Laboratory simulation of heavy ion cosmic ray interaction with condensed CO
Astronomy & Astrophysics **512** (2010) A71
- [7] A. L. F. de Barros, A. Domaracka, D.P.P. Andrade, P. Boduch, H. Rothard, E. F. da Silveira,
Radiolysis of frozen methanol by heavy cosmic ray and energetic solar particle analogues
Monthly Notices of the Royal Astronomical Society **418** (2011) 1363-1374
- [8] S. Pilling, E. Seperuelo Duarte, E. F. da Silveira, E. Balanzat, H. Rothard, A. Domaracka, and P. Boduch
Radiolysis of ammonia-containing ices by energetic, heavy and highly charged ions inside dense astrophysical environments
Astronomy & Astrophysics **509** (2010) A87

New syntheses and mechanisms on cold surfaces of astrophysical interest

François Dulieu

¹ LERMA, UMR 8118, Observatoire de Paris et Université de Cergy-Pontoise

5, mail Gay-Lussac, 95000 Cergy-Pontoise, France

francois.dulieu@obspm.fr

Context

When interstellar dust grains are cold enough, they become sites of accretion for gaseous species. If compared with reactants in the gas phase – where collisions happen far more rarely than once per day in most astrophysical media – accreted radicals have an almost infinite time to react on a cold surface. This is why cold dust grains are thought to be catalytic centres.

Unfortunately, molecules trapped in the solid state lose most of their spectroscopic specificity, and even with the new powerful observing tools (HERSHEL, ALMA...), the difficulty to observe individual molecular components in solid phase remains very high. Nevertheless, the chemical richness of the solid phase can sometimes be indirectly revealed, for example in star forming regions where non-refractory species go back to gas phase and can be thus detected by radio-astronomers.

In order to circumvent the observational difficulty to detect solid state components, a large number of laboratory works have been devoted to the study of interstellar ices, and specific instruments like ours (FORMOLISM, see figure 2), have been developed to study the interaction of radicals and their reactivity on cold surfaces. FORMOLISM consists of a UHV chamber, in which an amorphous silicate substrate is temperature-controlled in the 6 - 400K range. Ice samples with well characterised morphology can be grown if required. Two collimated atomic or molecular beams are aimed at the sample which can be probed by Infra-red spectroscopy. Nascent molecules can be probed by a quadrupole mass spectrometer or by a laser and time of flight system. If necessary, the temperature can be raised to evaporate adsorbed molecules. Sub-monolayer and mono-layer regime is mostly studied.

Syntheses on cold surfaces

H is the most abundant element, and H₂ the most abundant molecule, this is why H and H₂ have been the subject of numerous studies [1]. Second, hydrogenation of CO has also been a chemical pathway widely studied [2]. These previous surface processes (H+H → H₂, CO+H → HCO +H → H₂CO+2H → CH₃OH) have both a unique chemical scheme, mostly successive hydrogenations.

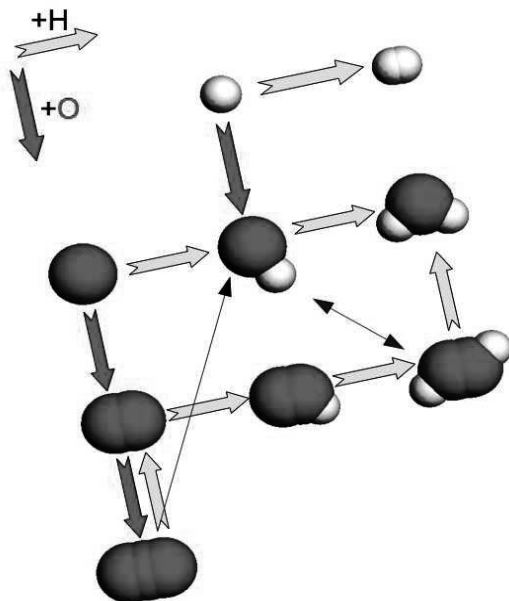


Figure 1: O + H reaction network

We studied the case of the O + H chemistry [3]. But in this case, O + H can give birth to O₂, O₃, H₂, OH, O₂H, H₂O and H₂O₂ (all observed), see figure 1, and this is why the groups have adopted different strategy to solve this problem [4]. We have chosen to separate the initial reactants, and compared O, O₂, and O₃ [5], to solve partly the problem of water formation, which was demonstrated to be the final product of this chemistry.

Using the same strategy, we have studied the CO+OH system isolated on a water or silicate substrate [6]. We observed CO₂ formation with a lower efficiency than that found in previous systems, since this reaction competes with the faster OH+H route. However, this in interstellar conditions it should lead to an efficient CO₂ formation pathway.

Recently we have even synthesised a few N-bearing compounds [7].

Physical mechanisms on surfaces

Especially in the case of direct reaction schemes such as H+H, the chemical result, here H₂, is less important than the physical insight of the reaction. Going more deeply in the physics of the reaction, the temperature, coverage and morphology of the surface will be important parameters. The astrophysical conditions, require low coverage and amorphous surfaces.

We first studied the importance of the coverage and the role of morphology of the surface using molecular interactions. We found that the coverage, even low coverages of H₂ and D₂, can have dramatic effects on the desorption properties and produce segregation effects [8]. We demonstrated that the surface morphology of water is important even at the molecular scale [9], and that the amorphous nature of the substrate does not dominate the adsorption-desorption process as demonstrated by comparing the 3 cases of amorphous silicate substrate, and amorphous and crystalline water [10].

Secondly, we studied the energetic aspects of the reaction. All the reactions mimicked on cold surfaces have to be exo-energetic in our experimental context. The energy released can have found in different forms. The molecule just formed can be chemically desorbed, with some internal energy [11]. The energy can be released to the substrate, and induce secondary effects as the reduction of the porosity of the water template[12], or the energy can be transmitted to surrounding adsorbed molecules [1].

To conclude the talk, I will mention others aspects of the possible mechanisms on the surface, such as nuclear spin conversion[13], isotopes' behaviour differences during the sticking phase [14], and some other physical properties we would like to explore.

References

- [1] Congiu et al, MNRAS Letters, 2009, 397, L96-L100 and references
- [2] See Pr Watanbe's presentation.
- [3] Dulieu et al, Astronomy & Astrophysics, 2010, 512, A30
- [4] Dulieu, Proceedings IAU Symposium No. 280, 2011 J. Cernicharo & R. Bachiller, eds.
- [5] Mokrane et al, Astrophysical Journal Letters, 2009, 705, L195-L198
- [6] Noble et al, The Astrophysical Journal, 2011, 735, 121
- [7] Congiu et al, submitted.
- [8] Kristensen et al, Astronomy & Astrophysics, 2011, 527, A44 and references
- [9] Fillion et al Phys. Chem. Chem. Phys, 2009, 11, 43964402
- [10] Noble et al, accepted in MNRAS with minor revisions.
- [11] Amiaud et al, J. Chem. Phys., 2007, 127, 144709
- [12] Accolla et al, Phys. Chem. Chem. Phys., 2011, 13, 8037-8045
- [13] Chehrouri et al, Phys. Chem. Chem. Phys., 2011, 13, 2172-2178
- [14] Matar et al, J. Chem. Phys., 2010, 133, 104507

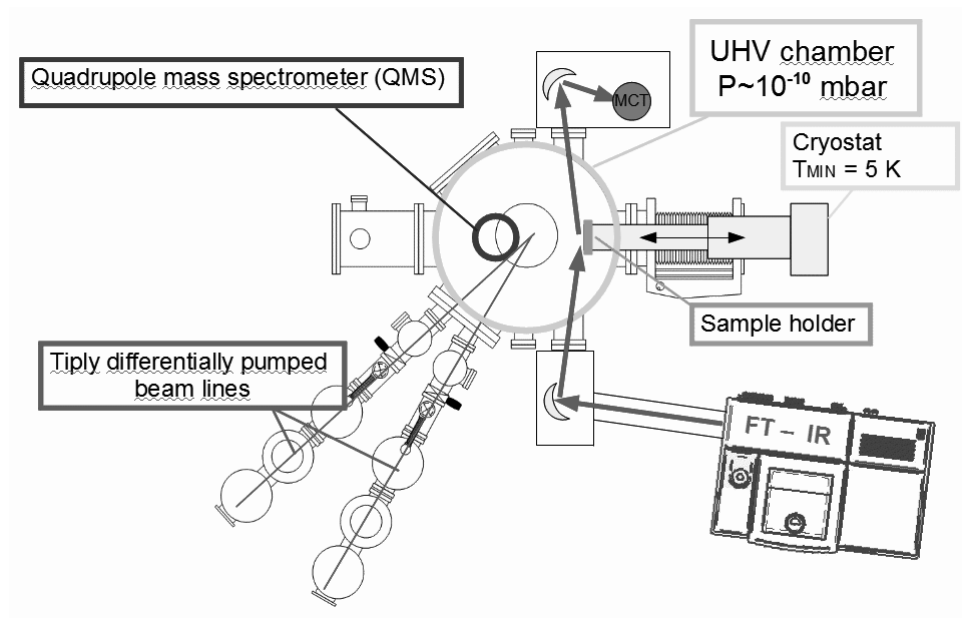


Figure 2 – The FORMOLISM experimental set-up (Cergy-Pontoise)

Dissociation and electronic properties of PAH-related species of astrophysical interest

Christine Joblin^{1,2}

¹ *Université de Toulouse, UPS-OMP, IRAP, Toulouse, France, christine.joblin@irap.omp.eu*

² *CNRS, IRAP, 9 Av. colonel Roche, BP 44346, 31028, Toulouse Cedex 4, France*

The nature of interstellar polycyclic aromatic hydrocarbons (PAHs) is an intriguing problem in astrochemistry [1]. PAHs are thought to be the carriers of the mid-IR emission bands between 3 and 15 μm that are observed in regions exposed to UV photons from stars. In these interstellar or circumstellar environments, PAH species play a major role in the physics and chemistry. Still, no specific molecule could be identified so far on the basis of the comparison of laboratory spectra with astronomical spectra. PAHs represent a large class of species and spectroscopic studies have to be guided by a better understanding of the formation and evolution of these species in astronomical environments.

Contrary to the mid-IR vibrational transitions, the electronic transitions are very specific of individual molecules. The absorption of UV-visible photons can lead to ionisation, radiative relaxation or photodissociation. In this presentation, I will focus on the electronic properties and dissociation of some specific PAHs of astrophysical interest and show how these studies can be addressed in the laboratory using the cold ion trap set-up, PIRENEA, that allows the production and storage of PAH-related species in conditions that approach those found in interstellar space [2]. Whereas spectroscopic signatures can be compared directly with astronomical spectra, dissociation rates are used as inputs in chemical evolution models to study the survival of these species in astronomical environments.

Photodissociation studies and astrophysical modelling

In the PIRENEA set-up, trapped PAH cations can be submitted to the continuous irradiation of a Xe lamp. Boissel et al. [3] have shown that, in these conditions, PAHs absorb sequentially near-UV and visible photons. This leads to an increase of the internal energy and subsequent photodissociation, if the heating rate is faster than the cooling rate. We have derived dissociation rates for the coronene cation $\text{C}_{24}\text{H}_{12}^+$ and its dehydrogenated derivatives $\text{C}_{24}\text{H}_p^+$ [$p=[1,12]$] from the analysis of the experimental data using a kinetic Monte Carlo method in a microcanonical scheme [4,5]. We have also shown that the photodissociation cascade of PAHs leads to the formation of carbon clusters C_n^+ (cf. Fig. 1).

The obtained dissociation rates were used as inputs in a numerical model in which the evolution of interstellar PAHs is described. There is a critical size below which interstellar PAHs evolve into carbon clusters (cf. [6] and Fig. 2). We note that the C_{60} fullerene molecule was recently detected in these environments [7].

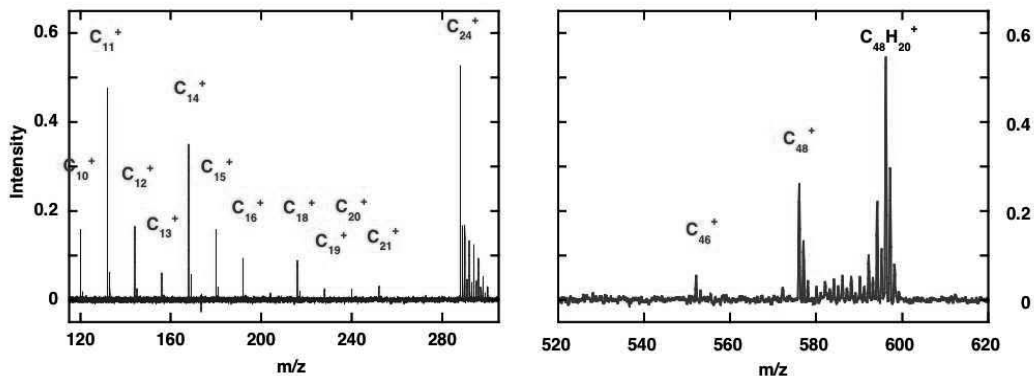


Figure 1: Photodissociation in PIRENEA of the PAH species $C_{24}H_{12}^+$ and $C_{48}H_{20}^+$; dissociation cascades and production of carbon clusters.

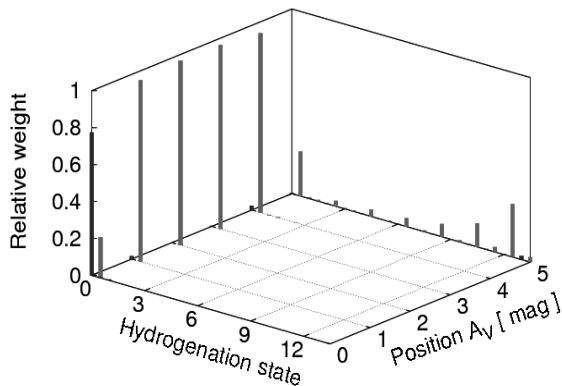


Figure 2: Modelling of the charge and hydrogenation states of interstellar PAHs; Case of coronene $C_{24}H_{12}$ in the reflection nebula NGC 7023 NW. The impinging radiation field is attenuated by a factor 26 and 236 at $A_V=3$ and 5, respectively. Red represents neutrals and blue cations (from [6]).

Electronic spectroscopy and the diffuse interstellar bands

PAHs are considered as attractive candidates for the Diffuse Interstellar Bands, some discrete absorption features observed throughout the visible and near-infrared spectral range whose origin is still investigated (cf. for instance [8–9]). Electronic transitions are very specific. However, so far, not a single PAH species has been identified on the basis of a spectral agreement. This indicates either that the molecular diversity is very large or that the candidates that have been considered so far are not the good ones. In particular, according to the results presented above, small/medium-sized PAHs are not likely to survive in their normal hydrogenation state. One would like to search for carbon clusters (graphene-type or others?) and partially hydrogenated PAH species. Using the PIRENEA set-up, we can measure the spectral signatures of such species isolated in the cold ion trap and submitted to multiphoton dissociation with a tunable laser [10]. I will show some results and discuss current effort to record the spectra of cold ions.

Perspectives

The results that have been obtained so far open many perspectives on the evolution and nature of interstellar PAHs, and the possible connection with carbon clusters and graphene-like species. I will present some of the perspectives that will be addressed in the frame of the project GASPARIM (ANR-2010-BLAN-0501).

Acknowledgements

This work was supported by the European Research Training Network "Molecular Universe" (MRTN-CT- 2004-512302), the French National Program "Physique et Chimie du Milieu Interstellaire" (PCMI), the CNRS PICS 4260 and the PPF of the Toulouse University "Molécules et Grains: du laboratoire à l'Univers". The technical team of the PIRENEA set-up is also especially acknowledged.

References

- [1] C. Joblin and A.G.G.M. Tielens eds, "*PAHs and the Universe*", EAS Publications Series, vol. **46** (2011)
- [2] C. Joblin, P. Boissel, C. Pech, M. Armengaud, P. Frabel, in : *Infrared and Submillimeter Space Astronomy*, M. Giard et al. ed., EDP Sciences, EAS Publications Series, vol. **4**, 73-77 (2002)
- [3] P. Boissel, P. de Parseval, P. Marty, G. Lefèvre, *J. Chem. Phys.* **106**, 4973–4984 (1997)
- [4] C. Joblin, D. Toublanc, C. Pech, D. Toublanc, M. Armengaud, P. Frabel, P. Boissel, in prep.
- [5] A. Simon and C. Joblin, *The Journal of Physical Chemistry A* **113**, 4878 (2009)

- [6] J. Montillaud, C. Joblin, D. Toublanc, in : *PAHs and the Universe*, C. Joblin and A.G.G.M Tielens Eds, EAS Publications Series vol. 46, p. 447-452 (2011); J. Montillaud, C. Joblin, D. Toublanc, in prep.
- [7] K. Sellgren, M. W. Werner, J. G. Ingalls, J. D. T. Smith, T. M. Carleton, C. Joblin, *Astrophys. J. Lett.* **722**, L54-L57 (2010)
- [8] P. Sarre, *Journal of Molecular Spectroscopy* **238**, 1-10 (2006)
- [9] F. Salama, G. A. Galazutdinov, J. Krełowski, L. Biennier, Y. Beletsky, In-Ok Song, *The Astrophysical Journal* **728**, 154 (2011)
- [10] F. Useli-Bacchitta, A. Bonnamy, G. Mallocci, G. Mulas, D. Toublanc, C. Joblin, *Chemical Physics* **371**, 16-23 (2010)

State-to-state molecular collisions in astrophysics

Alexandre Faure

*Institut de Planétologie et d'Astrophysique de Grenoble, BP 53, Grenoble 38041 Cédex 9
France*

As the densities in astrophysical plasmas are very low ($n < 10^{10} \text{ cm}^{-3}$), the atomic and molecular levels are generally not in equilibrium with the kinetic temperature but rather they are determined by a complex competition between radiative and collisional processes. The accurate determination of molecular column densities therefore relies on radiative transfer modeling which, in turn, requires a very good knowledge of rate coefficients for the collisional (de)excitation of interstellar species by the dominant colliding partners, i.e. He, H, H₂ and free electrons. As it is extremely difficult to determine these coefficients experimentally, radiative transfer models rely heavily on theoretical predictions.

We will review the recent theoretical advances made in the computation of collisional state-to-state rate coefficients for interstellar molecules. Comparisons with experimental data will be presented. Examples of the impact of these coefficients on radiative transfer calculations will be also reported. Finally, state-to-state *reactive* processes involving hydrogen molecules will be discussed, with a special emphasis on the importance of the H₂ internal energy, including *ortho/para* effects.

Spectroscopy of chiral molecules

Jürgen Stohner

Zürich University of Applied Science (ZHAW), Institute of Chemistry and Biological Chemistry (ICBC),
Campus Reidbach RC E0.40, Einsiedlerstrasse 31, CH 8820 Wädenswil, Switzerland,
Email: sthj@zhaw.ch

Chiral molecules are very important in chemical and pharmaceutical research. Here we focus on their role at the border between chemistry and physics, particularly in relation to the current attempts to measure parity violating effects in molecular spectroscopy [1, 2].

In 1975, Vladimir Prelog formulated in his Nobel Lecture that '...although most compounds involved in fundamental life processes, such as sugars and amino acids, are chiral and although the energy of both enantiomers ... are equal, only one enantiomer occurs in Nature; the enantiomers involved in life processes are the same in men, animals, plants and microorganisms, independent on their place and time on Earth'. [3] Therefore, the heat of reaction for interconversion between isolated (R)- and (S)-enantiomers at $T = 0$ K would be exactly zero [4].

However, about a decade earlier, parity violation in particle physics was first predicted and shortly thereafter experimentally verified by various research groups [5-7]. It was realized with some delay that parity violation discovered in nuclear physics has an immediate consequence in chemistry, namely that it introduces a tiny energy difference between enantiomers isolated in the gas phase [8, 9]. Therefore, the heat of reaction for interconversion is different from zero, although very small, e.g. $\Delta_r H^0 \approx 10^{-14}$ kJ/mol in case of CHBrClF [10]. The energy difference between two enantiomers results in slightly different spectra with small shifts, independent of the spectral region considered. Various early attempts to measure those shifts in NMR [11] and Mössbauer [12] spectra have been reported, however, none of those with success. Optical spectroscopy in the infrared (and microwave) region are considered to be more suited for measuring frequency shifts because the molecular system can be investigated under nearly isolated conditions; recent reviews summarize our current understanding of the role of molecular parity violation [1, 2].

Prerequisites of most attempts to measure the effect of parity violation in chiral molecules can be divided into four categories, namely, (i) the synthesis of suitable chemical compounds, (ii) the separation into enantiomers with high enantiomeric excess, (iii) the measurement of high-

resolution rovibrational spectra including the assignment of the rovibrational transitions, and finally (iv) the determination of the absolute configuration. We will outline how we have contributed and will contribute in the future to those four steps just described [13, 14].

References

- [1] M. Quack and J. Stohner, *Chimia*, **59**, 530-538 (2005).
- [2] M. Quack, J. Stohner, and M. Willeke, *Annu. Rev. Phys. Chem.*, **59**, 741-769 (2008).
- [3] V. Prelog in: T. Frangsmyr and S. Forsen, editors, *Nobel Lectures, Chemistry 1971-1980*, Singapore, (1993). World Scientific Publ. Co.
- [4] M. Quack and J. Stohner, *CHIRALITY*, **13**, 745-753 (2001).
- [5] C. S. Wu, E. Ambler, R. W. Hayward, D. D. Hoppes, and R. P. Hudson, *Phys. Rev.*, **105**, 1413-1414 (1957).
- [6] R. L. Garwin, L. M. Lederman, and M. Weinrich, *Phys. Rev.*, **105**, 1415-1417 (1957).
- [7] J. I. Friedman and V. L. Telegdi, *Phys. Rev.*, **105**, 1681-1682 (1957).
- [8] Y. Yamagata, *J. Theoret. Biol.*, **11**, 495-498 (1966).
- [9] D. Rein, *J. Mol. Evol.*, **4**, 15 (1974).
- [10] M. Quack and J. Stohner, *Phys. Rev. Lett.*, **84**, 3807-3810 (2000).
- [11] A. Barra, J. Robert, and L. Wiesenfeld, *Phys. Lett. A*, **115**, 443-447 (1986).
- [12] A. Lahamer, S. Mahurin, R. Compton, D. House, J. Laerdahl, M. Lein, and P. Schwerdtfeger, *Phys. Rev. Lett.*, **85**, 4470-4473 (2000).
- [13] F. Hobi, *MSc Thesis*, ZHAW Wädenswil (2011).
- [14] B. Spenger, *BSc Thesis*, ZHAW Wädenswil (2011).

Chiral photochemistry and anisotropy in the solid phase

Jan Hendrik Bredehöft

University of Bremen, Institute of Applied and Physical Chemistry, Leobener Str. NW2, 28359 Bremen, Germany, jhbredehoef@uni-bremen.de

Molecules with an asymmetrically substituted atom, a chiral centre, come in two distinct forms called enantiomers. These enantiomers are nonsuperimposable mirror-images of each other. They are called L-form and D-form, which is short for left-handed and right-handed. The chemical properties of these enantiomers are identical. The only way to distinguish between enantiomers is by comparing them to something which is also chiral. This can be other chiral molecules as in enantioselective chromatography, but also chiral fields can act as a means of distinguishing between enantiomers. The kind of chiral field most often used is circularly polarized light (CPL). The absorption cross section of a given enantiomer will be different for *right*-CPL than for *left*-CPL. This effect of differential absorption is called circular dichroism (CD). CD is wavelength-dependant and the plot of CD versus wavelength is called a CD spectrum. CD spectroscopy is available for the wavelength region between VUV and IR.

A CD spectrum gives information at which wavelengths chiral photochemistry is possible. Whenever there is a differential absorption of CPL between L- and D-enantiomers, CPL could be used to break racemic symmetry by inducing a photochemical process leading to the preferential use of one enantiomer over the other. As Kagan pointed out in the 1970s^[1], the absolute magnitude of this symmetry-breaking effect does not only depend on the CD, the differential absorption, but rather on the ratio between differential absorption and total absorption, which he called the anisotropy factor g . To determine the anisotropy factor both the CD and the total absorption coefficient for any given wavelength need to be known. Usually this is achieved by measuring the absorption coefficient ϵ and the CD $\Delta\epsilon$ at the target wavelength and by then dividing $\Delta\epsilon$ by ϵ to give the anisotropy factor g . In order to achieve this, the optical density of the sample needs to be known. For samples in solution this is easily calculated from pathlength and concentration using the Lambert-Beer Law. For solid phase samples this is much less straight forward. The optical density depends on the number and orientation of the molecules in the sample and thus on the degree crystallinity and on the exact nature of the crystal phase. These are usually only known for single-crystals. Single crystals or indeed any crystals at all are however generally not suitable for CD measurements since other effects like linear dichroism, birefringence and dichroic scattering make the CD very difficult to observe. The only way of determining both $\Delta\epsilon$ and ϵ and thus g is by

performing the measurements at the same spot of the same sample, so that the optical density of the sample is identical in both measurements.

Experimental

The instrument used in this study is the CD1 beamline^[2,3] of ASTRID at the Institute for Storage Ring Facilities, University of Aarhus, Denmark. It utilizes synchrotron radiation as a high flux source of linearly polarized light (LPL). This instrument enables high UV and VUV fluxes down from the visible range to 120 nm/10.3 eV. The light is passed first through a monochromator grating and then a photomodulating CaF piezo crystal, which produces alternating beams of *left*-CPL and *right*-CPL from the monochromatic LPL at 50 KHz. This light is transmitted to the sample and from there onto a photomultiplier tube (see Figure 1).

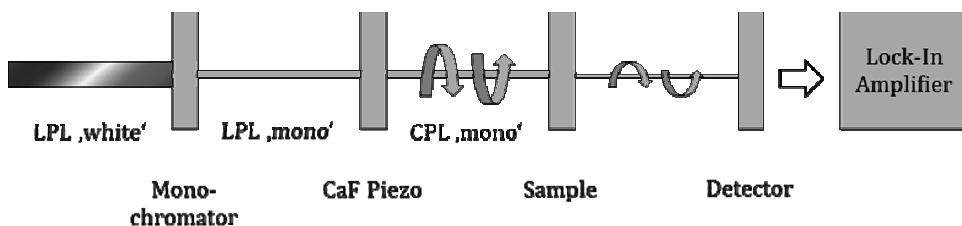


Figure 1: Schematic of a CD spectrometer

During the measurement of both absorption and CD spectra it became apparent that recording the spectra one after the other led to data which were difficult to interpret. This could be traced back to the fact that the intensity of the light source, the synchrotron ring, was not constant, due to a slow decrease of the electron current in the ring. Since recording time for spectra is in the order of magnitude of some few hours, this effect is non negligible. It thus became desirable to measure both absorption and CD at the same time. This is however not easily achieved: For measurements of absorption spectra the photomodulator is not used and the detector is used with a constant gain voltage. The output signal of the detector is then directly proportional to the absorption. The CD signal on the other hand is very small compared to the total absorption (about 10^{-5} of the absorption signal), so the signal is not detected right away but rather fed to a Lock-In amplifier where it is used to tune the detector gain, to achieve a constant detector output. The amplification voltage is then used to determine the CD signal. The absorption cannot be measured in this way, because the detector output is constant. We overcame this problem by taking the detector gain voltage and deriving the absorption signal from it. To this end we compared the absorption spectra recorded both on a calibrated commercial UV-spectrometer and at the beamline and worked

out the gain function of the detector. By this method we could use the CD1 beamline to record both absorption and CD spectra from a solid sample at the same time. The samples used were amorphous films of various amino acids. These were prepared by vapour deposition in a vacuum. Sample thickness was in the order of magnitude of about 500 nm, as measured with a quartz microbalance during deposition.

Results

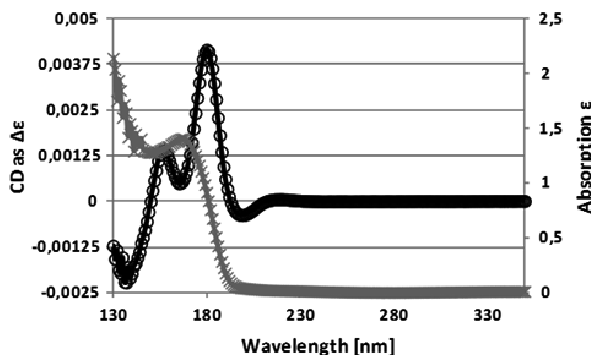


Figure 2: Circular Dichroism spectrum of a 600 nm amorphous film of L-Alanine (black circles and line) and Absorption spectrum (grey crosses and line).

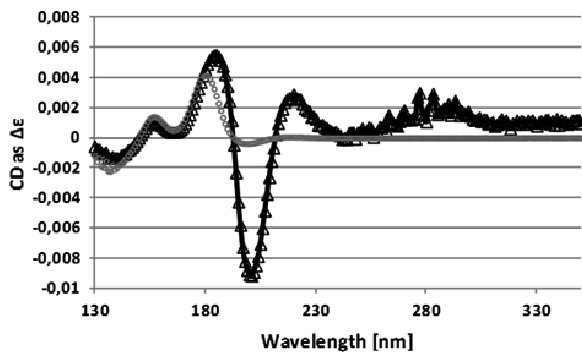


Figure 3: Anisotropy spectrum of a 600 nm amorphous film of L-Alanine (black triangles and line) and CD spectrum (grey circles).

Figure 2 shows both the CD absorption spectra of a 600 nm thick amorphous film of L-Alanine. The CD spectrum agrees well with previously recorded spectra of the compound at the same beamline^[4]. The maximum of the CD signal lies at 180 nm. By dividing the CD spectrum by the absorption spectrum, the anisotropy factor g was determined for every wavelength, yielding the Anisotropy spectrum (see Figure 3) The position of maxima and minima naturally does not change, the magnitude however is changed drastically. The majority of strong signals now lie in the UV range rather than the VUV, which is a lot better accessible experimentally. The strongest effect of photochemical symmetry breaking is expected in the region around 200 nm^[5].

Implications

Amino acids were used as sample because they are connected to a very puzzling scientific phenomenon, namely the origin of biomolecular homochirality. Biopolymers like proteins and RNA/DNA are made from homochiral monomers, meaning all the sugars and amino acids used in biological systems are of one handedness. The origin of this homochirality is not yet fully understood. It is known that amino acids found in meteorites, which were formed well outside the influence of the Earth's biosphere, show an excess of some L-amino acids over their D-counterparts. One of the models explaining this excess involves the photochemical breaking of symmetry in the interstellar medium. This is achieved by irradiation of interstellar dust with circularly polarized UV-light. The findings presented here underpin this explanation, since so far it has been assumed that VUV radiation at around 160 to 180 nm was necessary to achieve successful discrimination between L- and D-amino acids. The fact that UV light with a wavelength around 200 nm can achieve a far greater enantiomeric excess makes this scenario more likely, since light of this wavelength is far more common in the interstellar medium.

References

- [1] G. Balavoine, A. Moradpour, H. B. Kagan, *J. Am. Chem. Soc.* **96**, 5152–5158 (1974)
- [2] A. J. Miles, R. W. Janes, A. Brown, D.T. Clarke, J. C. Sutherland, Y. Tao, B. A. Wallace, S. V. Hoffmann, *J. Synchrotron Rad.* **15**, 420– 422 (2008)
- [3] J. Miles, S. V. Hoffmann, Y. Tao, R. W. Janes, B. A. Wallace, *Spectroscopy* **21**, 245–255 (2007)
- [4] U. J. Meierhenrich, J.-J. Filippi, C. Meinert, J. H. Bredehöft, J. Takahashi, L. Nahon, N. C. Jones, S. V. Hoffmann, *Angew. Chem.* **122**, 7966–7970 (2010); *Angew. Chem. Int. Ed.* **49**, 7799–7802 (2010)
- [5] C. Meinert, J. H. Bredehöft, J.-J. Filippi, F. Wien, N. C. Jones, S. V. Hoffmann, U. J. Meierhenrich, *submitted to Angew. Chem. Int. Ed.*

Phase changes of supercooled water: from aerosol to freely suspended droplets

Sigurd Bauerecker¹ and Tillmann Buttersack¹

¹ *Institut fuer Physikalische und Theoretische Chemie, Technische Universitaet Braunschweig, Hans-Sommer-Strasse 10, 38106 Braunschweig, Germany, s.bauerecker@tu-bs.de*

The freezing process of supercooled liquid water droplets freely suspended in air (or another carrier gas) strongly depends on droplet size, supercooling temperature, kind and concentration of solved ions, and nucleation mode. For supercooling temperature differences of > 5 K, bigger water droplets in the millimeter size range show a splitting of the freezing transition into a fast part (milliseconds) where a spongy network-ice forms and a slow part (seconds) where the droplet completely freezes from outside to the interior [1]. The structure, fine-structure and density of this “stage-one ice” in turn depend on the parameters mentioned above. So the stage-one ice determines or at least influences the texture of the finally forming “stage-two ice” which for instance can be investigated by X-ray photoelectron spectroscopy (XPS) and near-edge X-ray absorption fine structure spectroscopy (NEXAFS) [2]. The reason for the freezing split is a thermodynamic one: the bigger droplets cannot get rid of the formation heat by cooling via the surface within the short formation time span. On the other hand, for smaller droplets there should be a transition in the 1000 to 10 micrometer size range where the freezing split disappears due to the increasing relative particle surface which enhances the heat transfer towards the surrounding gas.

First results of the nature and the formation dynamics of the spongy network-ice gained by use of high-resolution high-speed monitoring are presented. Especially an electrical phenomenon was observed during the stage-one ice formation time-span which could be interpreted as an analog to the Workman-Reynolds effect [3] for the spongy network-ice. The effect is in the order of ± 1 Volt and closely correlates with the (time) position of the freezing front within the droplet [4]. Evidence for atmospheric processes as thundercloud electrification can be assumed.

References

- [1] S. Bauerecker, P. Ulbig, V. Buch, L. Vrbka, P. Jungwirth, *J. Phys. Chem. C* **112** 7631 (2008)
- [2] A. Krepelova, T. Huthwelker, H. Bluhm, M. Ammann, *Chem. Phys. Chem.* **11** 3859 (2010)
- [3] E. J. Workman, S. E. Reynolds, *Phys. Rev.* **78** 254 (1950)
- [4] S. Bauerecker, T. Buttersack, (2012), in preparation

Near infrared absorption spectroscopy at ultra high sensitivity: the case of H₂ and CH₄.

Alain Campargue and Samir Kassi

Laboratoire Interdisciplinaire de Physique Univ. Grenoble 1 / CNRS, LIPhy UMR 5588, Grenoble, F-38041, France

The coupling of lasers with very high finesse cavities allows achieving much higher sensitivity than traditional techniques. In this talk, I will present the results of the investigation of the H₂ and CH₄ spectra by very high sensitivity Cavity Ring Down Spectroscopy (CRDS) in the 1.26-1.71 μm region. The typical noise equivalent absorption (NEA) of our spectra, $\alpha_{min} \approx 5 \times 10^{-11} \text{ cm}^{-1}$, corresponds to a 1 % decrease of the transmitted light intensity after a path length of 2000 km. With such sensitivity, extremely weak transition of H₂ and CH₄ could be detected. The H₂ and CH₄ results allow to test the most advanced theoretical calculations and to fulfil important needs in planetary science, respectively.

H₂, HD and D₂

The absorption spectrum of H₂ and D₂ consists of vibrational bands of very weak quadrupole transitions (E2) which are the only allowed transitions in homonuclear species. The HD species possesses a (weak) permanent dipole moment resulting from non adiabatic effects due to the difference of masses of the proton and the deuteron. Thus the absorption spectrum of HD exhibits weak electric dipole (E1) rovibrational transitions in addition to the even weaker E2 lines. Transitions of the first overtone band of H₂, HD and D₂ could be detected by CRDS between 5850 and 7920 cm⁻¹, at pressure values ranging from 10 to 950 Torr. They include the weakest hydrogen transitions reported so far by absorption spectroscopy. The achieved noise equivalent absorption allowed for the following measurements:

- (i) the *O*(2)-*O*(5) and *Q*(5) E2 transitions of H₂ [1],
- (ii) the *P*(1)-*P*(2) and *R*(0)-*R*(8) E1 transitions and the *Q*(1)-*Q*(4) and *S*(0)-*S*(4) E2 transitions of HD [2].
- (iii) the *Q*(1), *Q*(2) and *S*(0)-*S*(5) E2 transitions of D₂

The uncertainty on the line positions is on the order of 0.001 cm⁻¹. Line intensities were obtained with a 2% uncertainty from a fit of the line profile using a Galatry line shape. The minimum intensity reported is on the order of 1 × 10⁻³⁰ cm/molecule. The dipole and quadrupole transition moments were derived from the measured line strengths. The agreement with the most recent theoretical calculations from K. Pachucki (University of Warsaw) and J. Komasa (A. Mickiewicz University, Poznan) will be discussed [1].

Methane

Insufficient knowledge of the near infrared spectrum of methane is an important limitation for the analysis of the spectra of Titan and of the outer planetary atmospheres in general. We are involved in a long-term project [3-14] aiming to provide astronomers with a line by line list for precise calculations of the methane absorption in the near infrared region. I will present our best to date empirical line list between 5854 and 7919 cm^{-1} (1.71 - $1.26\text{ }\mu\text{m}$) and illustrate its capability to significantly improve planetary spectral analysis, in particular for Titan. (The atmosphere of Titan, the largest satellite of Saturn, is equivalent to a 20 km cell with 75 mbar of CH_4 in 1.5 bar of N_2 and at $T=85\text{ K}$). Transitions of $^{13}\text{CH}_4$ and CH_3D were systematically identified by comparison with spectra of highly enriched $^{13}\text{CH}_4$ and CH_3D , recorded at the same temperatures.

When we undertook this project, three years ago, the reference list for methane in our region of interest was the empirical line list at 296 K constructed in Brown (2005) and included in the HITRAN (Rothman et al. 2009) and GEISA (Jacquinet-Husson et al. 2011) databases. L. Brown retrieved the methane line parameters from spectra recorded at the Kitt Peak National Observatory by high resolution Fourier Transform Spectroscopy (FTS) with path lengths up to 433 meters (Brown 2005). This line list does not fulfil the needs for planetary applications for two main reasons: (i) it lacks in sensitivity especially in the transparency windows and (ii) it doesn't provide lower state energy levels except for a few strong lines.

Indeed, the methane spectrum is highly sensitive to the temperature as illustrated by the considerable change of the appearance of the spectrum in the $1.58\text{ }\mu\text{m}$ transparency window (Fig. 1).

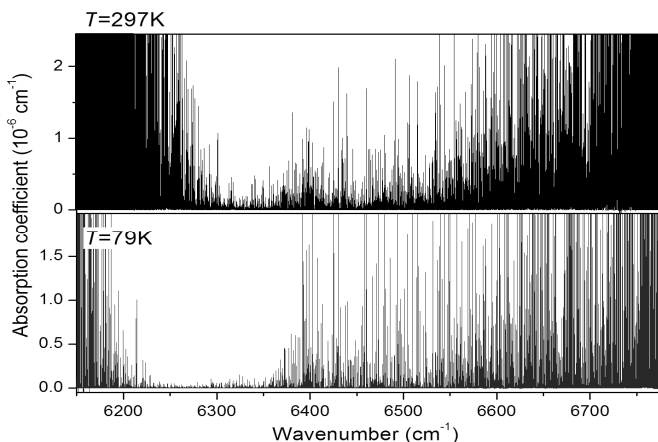


Figure 1. Comparison of the CW-CRDS spectra of methane recorded at room temperature (upper panel) and 79 K (lower panel) in the $1.58\text{ }\mu\text{m}$ transparency window (6150 – 6780 cm^{-1}). The room temperature and 79 K spectra correspond to 1.0 and 10.0 Torr , respectively.

The absorption spectrum of methane consists in a succession of strong absorption regions separated by intervals of weak opacity, called methane transparency windows. The overall appearance of the spectrum reflects the structure of the CH₄ vibrational levels which are organized in polyads of states in interaction. Due to approximate relations between stretching (ν_1, ν_3) and bending (ν_2, ν_4) vibrational frequencies, $\nu_1 \cong \nu_3 \cong 2\nu_2 \cong 2\nu_4$, a polyad is defined by the set of nearby levels with the same polyad number, $P = 2(\nu_1 + \nu_3) + \nu_2 + \nu_4$. Up to the octad region ($P = 3$) extending up to 4800 cm⁻¹, the room temperature spectrum of the main methane isotopologue, ¹²CH₄, has been theoretically modeled in the frame of the effective Hamiltonian and dipole moment approach. Based on the obtained rovibrational assignment and corresponding lower state energies, the ¹²CH₄ spectrum can then be accurately extrapolated to the temperature conditions of the studied planetary objects.

This is not the case for the higher polyads above 4800 cm⁻¹. The modelling of the ¹²CH₄ tetradecad ($P = 4$, 5000-6200 cm⁻¹ region) in the frame of the effective operator approach has been undertaken but the calculated spectrum does not reach the experimental accuracy. No accurate modelling is expected to be available in a near future for the next polyads, namely the icosad ($P = 5$, 6400-7500 cm⁻¹) and the triacontad ($P = 6$, 7600-8500 cm⁻¹). In this high energy region, the considerable spectral congestion and complexity of the methane spectrum resulting from many rovibrational interactions between the excited vibrational states hampers the application of the effective operator approach used for the lower polyads.

In the absence of exact lower state energies relying on a theoretical model, we adopted an alternative approach to determine the temperature dependence of the methane absorption in our region. It consists in deriving empirical values of the lower state energy values from the variation of the line intensities measured at two temperatures. This “two temperature method” requires the methane spectra acquisition at both very high sensitivity and low temperature which is particularly challenging in terms of experimental efforts. A specifically designed cryogenic cell was developed for CW-CRDS at liquid nitrogen temperature (about 80 K) [9] in order to characterize the 1.58 and 1.28 μm. transparency windows which are of high interest for planetary applications. This innovative experimental development allowed us to achieve the same sensitivity performances at 80 K as at room temperature ($\alpha_{min} \approx 1 \times 10^{-10}$ cm⁻¹) and then to record the methane spectra in temperature conditions close to those existing on Titan. From the room temperature and 80 K spectra, the line intensities were derived using a multiline fitting program and the lower state energy, E'' , could be obtained from the ratio of the line intensities.

The constructed WKMC (for Wang, Kassı, Mondelain, Campargue) empirical lists for methane have already proven to fulfill major needs in planetary science, allowing for an improved modeling of Titan, Pluto and Uranus spectra.

[1] A. Campargue, S. Kassı, K. Pachucki, and J. Komasa, *Phys. Chem. Chem. Phys.* 2011, DOI: 10.1039/c1cp22912e.

[2] S. Kassı and A. Campargue, *J. Mol. Spectrosc.*, 2011, **267**, 36-42.

- [3] S. Kassi, B. Gao, D. Romanini, A. Campargue, *Phys. Chem. Chem. Phys.* 10 (2008) 4410.
- [4]. B. Gao, S. Kassi, A. Campargue, *J. Mol. Spectrosc.* 253 (2009) 55.
- [5]. L. Wang, S. Kassi, A. Campargue, *J. Quant. Spectrosc. Radiat. Transfer.* 111 (2010) 1130
- [6] E. Sciamma-O'Brien, S. Kassi, B. Gao, A. Campargue, *J. Quant. Spectrosc. Radiat. Transfer.* 110 (2009) 951.
- [7] A. Campargue, Le Wang, S. Kassi, M. Mašát, O. Votava, *J. Quant. Spectrosc. Radiat. Transfer.* 111 (2010) 1141.
- [8] O. Votava, M. Mašát, P. Pracna, S. Kassi, A. Campargue, *Phys. Chem. Chem. Phys.* 12 (2010) 3145.
- [9] S. Kassi, D. Romanini, A. Campargue, *Chem. Phys. Lett.* 477 (2009) 17.
- [10] L. Wang, S. Kassi, A. W. Liu, S. M. Hu, A. Campargue, *J. Mol. Spectrosc.* 261 (2010) 41-52
- [11] A. Campargue, L. Wang, A. W. Liu, S. M. Hu, S. Kassi, *Chem. Phys.* 373(2010) 203–101
- [12] D. Mondelain S. Kassi L.Wang , A. Campargue. *Phys Chem Chem Phys.*17 (2011) 7985-96.
- [13] Y. Lu, D. Mondelain, S. Kassi, A. Campargue, *J. Quant. Spectrosc. Radiat. Transfer.* (2011) submitted.
- [14] C. De Bergh et al *Planet Space Sci* 2011 in press

Understanding surface adsorption through theoretical vibrational spectroscopy

David M. Benoit¹

¹ Department of Chemistry, The University of Hull, Cottingham Road, Kingston upon Hull, HU6 7RX United Kingdom, d.benoit@hull.ac.uk

The accurate description of interactions occurring at the interface between solids and the gas phase currently remains a significant challenge for computational chemistry. The difficulty arises due to the transition from an ordered periodic solid, which description requires techniques from solid-state physics, to the discrete molecular domain of adsorbates, which mostly needs quantum chemical methods to obtain a suitable accuracy. Over the years, there has been a constant improvement of the periodic density functional approaches so that it is nowadays possible to use gradient-corrected functionals to describe both metals and adsorbates alike. In particular, the functional proposed by Perdew, Burke and Ernzerhof (PBE)¹ has proved to be both reliable and accurate enough for most surface science work², and nowadays it is used routinely to provide a description of numerous processes on surfaces.

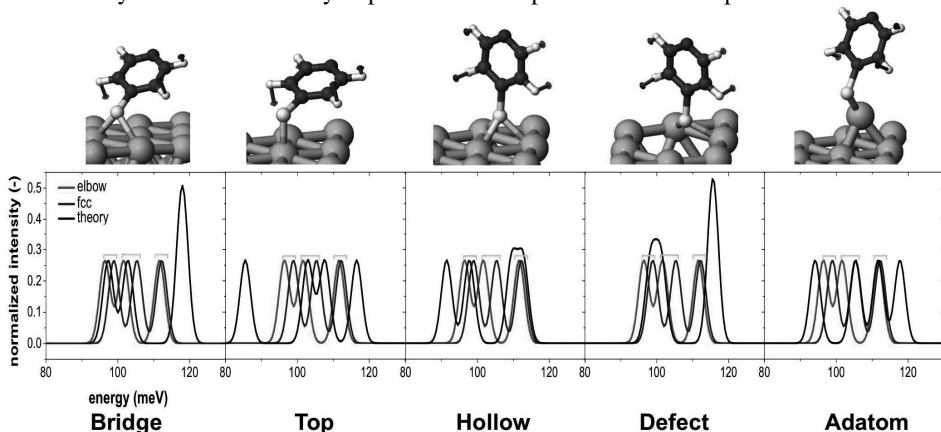


Figure 1: Measured and simulated vibrational IETS signal for a single 4-mercaptopyridine molecule deposited on a Au(111) surface. The simulations explore a number of possible adsorption sites and identify the bridge and defect sites as likely matches for the experimental data.

In this contribution, we compare vibrational spectroscopy measurements from single-molecule inelastic electron tunnelling (IETS) experiments and high-resolution electron energy loss spectroscopy (HREELS) obtained for adsorbed molecules on metal surfaces to an accurate first-principle theory of vibrational anharmonicity implemented in our laboratory³.

This enables us first to assess the accuracy of the model used to describe the adsorbate–metal interaction by performing a direct comparison between theory and experimentally observable quantities (vibrational transition frequencies). Secondly, by comparing the predicted spectra for a number of situations, we are able to determine the possible adsorption sites of molecules at the surface of a solid⁴ (see Figure 1 for details).

We also present a critical examination of the performances of PBE for acetylene on a Cu(100) surface and introduce a hybrid model that addresses some of the weaknesses of the existing density-functional-based methods. Our model combines an accurate quantum chemical description of the adsorbate with the efficiency of density functional theory for the solid (see Figure 2).

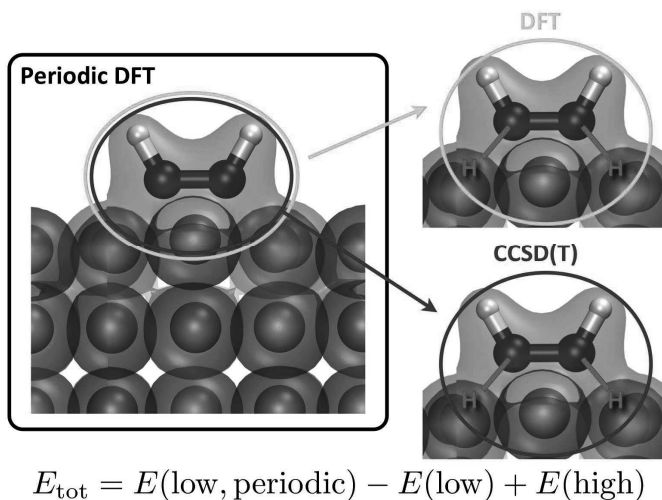


Figure 2: Hybrid scheme for the determination of the total energy of a composite adsorbate–metal system.

References

- [1] J.P. Perdew, K. Burke, M. Ernzerhof, Phys. Rev. Lett. **77**, 3865 (1996)
- [2] M. Ropo, K. Kokko, L. Vitos, Phys. Rev. B **77**, 195445 (2008)
- [3] D. M. Benoit, B. Madebene, I. Ulusoy, L. Mancera, Y. Scribano, S. Chulkov, Beilstein J. Nanotechnol. **2**, 427 (2011)
- [4] I. S. Ulusoy, Y. Scribano, D. M. Benoit, A. Tschetschetkin, N. Maurer, B. Koslowski, P. Ziemann, Phys. Chem. Chem. Phys. **13**, 612 (2011)

Formation of small molecules on substrates of astrochemical interest

Kousik Giri, Benjamin J. Irving and Anthony J. H. M. Meijer¹

Department of Chemistry, University of Sheffield, Sheffield S3 7HF, United Kingdom.

H₂ is one of the most important molecules in the interstellar medium. It plays a pivotal role in interstellar chemistry through reactions with ions and radicals. Furthermore, the energetics of the H₂ formation reaction directly affect the thermal balance of the interstellar medium. It is widely accepted that the dominant mechanism for the formation of H₂ in interstellar clouds is through surface-catalysed reactions on dust-grains.¹ One of the possible mechanisms for this gas-surface reaction is the Eley-Rideal² reaction mechanism in which an atom from the gas-phase reacts directly with an atom adsorbed on the surface. The key step in this reaction is the adsorption of the first H atom on the dust grains, which in our studies are taken to be graphitic or siliceous in origin.

Absorption of Hydrogen Atoms on Graphitic surfaces

It is well-established that the first absorption of H on single-crystal graphite is an activated process.³ However, much less is known about the modulation of its adsorption in the presence of defects, except in the presence of an already absorbed hydrogen atom. If we define the absorption positions as ‘ortho’, ‘meta’, and ‘para’ as in Figure 1, then it is clear from Figure 2 that pre-absorption of hydrogen atoms has a significant effect.

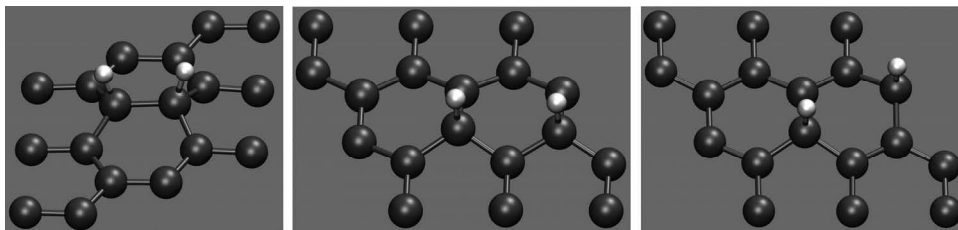


Figure 1: Different absorption configurations. From left to right: ortho, meta and para.

¹ Email address: a.meijer@sheffield.ac.uk

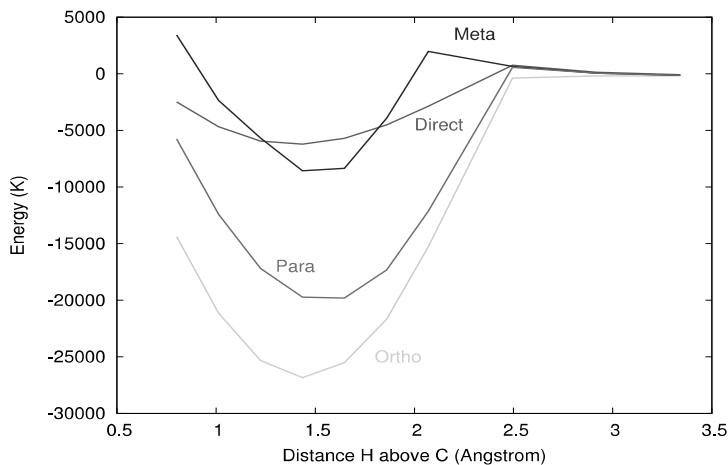


Figure 2: Absorption of hydrogen atoms on graphite with a pre-chemisorbed hydrogen atom.

In particular, it is found that absorption in either an ortho or para position is significantly more favourable than absorption in the meta position. In addition, it should be noted that even in such cases small barriers to adsorption still may exist. Moreover, this cooperative effect does not survive the adsorption of additional hydrogen atoms.⁴ The adsorption of *e.g.* a fourth atom in a small hydrogen cluster on a graphite surface is again an activated process.

Most studies so far have concentrated on crystalline graphitic materials and as a consequence little is known about the role dopants or defects other than pre-chemisorbed hydrogen could play in the formation of H_2 and other small molecules in the interstellar medium. Therefore, in this talk we will discuss the formation of H_2 with a particular emphasis on the adsorption of the first H atom and its consequences for the formation of H_2 by introducing defects and dopants into the graphite lattice.

References

- [1] H. C. van der Hulst, *Rec. Astron. Obs.* **XI(II)** (1949).
- [2] D. D. Eley and E. K. Rideal, *Nature* **146**, 401 (1940).
- [3] See *e.g.* (a) S. Morisset, F. Aguillon, M. Sizun, V. Sidis, *J. Chem. Phys.* **122**, 194702, (2005). (b) X. Sha and B. Jackson, *Surf. Sci.* **318**, 496, (2002). (c) S. Morisset, F. Aguillon, M. Sizun, and V. Sidis, *J. Phys. Chem. A*, **108**, 8571 (2004). (d) X. Sha, B. Jackson, and D. Lemoine, *J. Chem. Phys.*, **116**, 7158 (2002). (e) L. Jeloica and V. Sidis, *Chem. Phys. Lett.*, **300**, 157 (1999) and references therein.
- [4] B. J. Irving, A. J. H. M. Meijer, and D. Morgan *Phys. Scr.*, **84**, 028108 (2011).

Hydrogen chemistry on cold grain surfaces

**Naoki Watanabe¹, Hiroshi Hidaka¹, Tetsuya Hama¹, Yasuhiro Oba¹,
Akira Kouchi¹, Takeshi Chigai¹, Yuki Kimura²**

¹ Institute of Low Temperature Science, Hokkaido University, Sapporo, Hokkaido 060-0819, JAPAN
watanabe@lowtem.hokudai.ac.jp

² Department of Earth & Planetary Materials Science, Tohoku University, Sendai 980-8578, JAPAN

Surface reactions on cosmic ice grains play an important role in chemical evolution in space. Among the many kinds of interstellar molecules observed, the abundances of some major species such as H₂, H₂O, and organic molecules cannot be explained by gas-phase synthesis; therefore, surface reactions on cosmic ice grains are considered for the synthesis of such molecules. In an interstellar molecular cloud where the temperature is as low as 10 K and the radiation field is very weak, the energetic processes in/on ice grains is inefficient and thus tunneling surface reactions involving hydrogen atom would become important for chemical evolution [1]. When the reduced and/or effective mass of reaction system is very small, reaction having a significant activation barrier may occur even at very low temperatures by the transmission through the barrier due to the wave nature of particle. Theoretical approach to the surface tunneling reaction is not easy because the tunneling is very sensitive to the reaction potential surface which strongly depends on the composition and structure of the surfaces. Therefore, the quantitative experiments are desirable to understand the surface tunneling reactions relevant to chemical evolution in space.

We have experimentally studied various tunneling reactions and physicochemical processes of hydrogen on cryogenic surfaces, especially, amorphous solid water (ASW) which is an ice grain analogue, relevant to astrochemistry [1]. The topics which we have recently worked on are as follows.

1. Tunneling reaction of hydrogen and deuterium atoms on ASW to produce water, formaldehyde, methanol and those deuterad species [2-7] .
2. Diffusion process of hydrogen and deuterium atoms on ASW at very low temperatures [8,9] .
3. Reactions of cold OH radical with CO to produce CO₂ and H₂CO₃ [10,11] .
4. Spin temperatures of H₂ and H₂O molecules on ASW [8,9,12] .
5. Reaction of hydrogen and nitrogen atoms to produce NH₃ [13] .

In the present talk, I will introduce the results of above experiments briefly, and especially focus on the topic 2 and 4. The topics 3 and 4 will be presented by Oba and Hama in their posters.

We have three similar types of apparatus. One of them, the apparatus named RASCAL is shown in Figure 1. The apparatus consists of an atomic source and a main chamber. A cold substrate is located at the center of the chamber. Substrate area is surrounded by the cold

shroud connected to a liquid nitrogen reservoir to make a good pumping speed for water. Atoms and radicals are produced in the microwave-induced plasma from gases and led into a cold aluminum pipe to reduce the kinetic and internal energies and impinge the target surface. A beam chopper can be installed when it is necessary. The sample surface is monitored insitu by a reflection-type FTIR. Infrared-inactive and trace species such as atoms and radicals on the surface are photodesorbed and subsequently detected following selective ionization by resonance enhanced multiphoton ionization technique.

Diffusion of hydrogen atom is the most fundamental process on ice grains. Therefore, the measurement of activation energy for the diffusion is essential. There have been two reports on the activation energy with the different values of about 22meV[14] and 45 meV [15] on the basis of TPD experiments to detect the recombined H_2 (D_2). To resolve this controversy, we directly detected H atoms on ice and measured the attenuation of number density. It was found that there are at least two potential site having the activation energies of 18 and 50meV which cover the previous results [8]. No isotope effect on the diffusion was observed indicating that the diffusion is thermal hopping rather than tunneling [9].

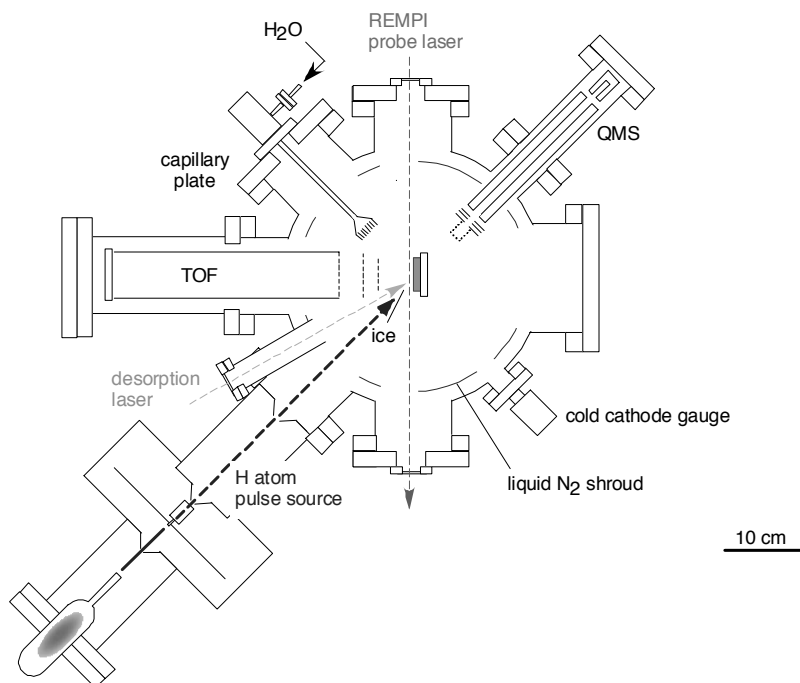


Figure 1: Schematic diagram of apparatus named RASCAL at ILTS, Hokkaido Univ.

References

- [1] e.g. N. Watanabe, A. Kouchi, *Prog. Surf. Sci.* **83**, 439 (2008)
- [2] N. Watanabe *et al.* *Astrophys. J.* **616**, 638 (2004)
- [3] H. Hidaka, A. Kouchi, N. Watanabe, *J. Chem. Phys.* **126**, 204707 (2007)
- [4] A. Nagaoka, N. Watanabe, A. Kouchi, *Astrophys. J.* **624**, L29 (2005)
- [5] H. Hidaka, M. Watanabe, A. Kouchi, N. Watanabe, *Astrophys. J.* **702**, 291 (2009)
- [6] N. Miyauchi *et al.* *Chem. Phys. Lett.* **456**, 27 (2008)
- [7] Y. Oba *et al.* *Astrophys. J.* **701**, 464 (2009)
- [8] N. Watanabe *et al.* *Astrophys. J.* **714**, L233 (2010)
- [9] Hama *et al.*, in preparation.
- [10] Y. Oba, N. Watanabe, A. Kouchi, T. Hama, V. Pirronello, *Astrophys. J.* **722**, 1598 (2010)
- [11] Y. Oba, N. Watanabe, A. Kouchi, T. Hama, V. Pirronello, *Phys. Chem. Chem. Phys.* **13**, 15792 (2011)
- [12] T. Hama, N. Watanabe, A. Kouchi, M. Yokoyama, *Astrophys. J.* **738**, L15 (2011)
- [13] H. Hidaka, M. Watanabe, A. Kouchi, N. Watanabe, *Phys. Chem. Chem. Phys.* **13**, 15798 (2011)
- [14] Matar, E. *et al.* *Astron. Astrophys.*, **492**, L17 (2008)
- [15] Perets, H. B. *et al.*, *Astrophys. J.*, **627**, 850 (2005)

Don't forget friction: theoretical perspectives on the laser control of adsorbate vibrations at metallic surfaces.

Jean Christophe Tremblay¹, Serge Monturet² and Peter Saalfrank³

¹ University of Potsdam, Karl-Liebknecht-str. 24-25, 14476 Potsdam (Germany), tremblay@uni-potsdam.de

² Institution Nanoscience Group & MANA Satellite CEMES/CNRS, 29 rue J. Marvig, Bp 4347, 31055 Toulouse Cedex (France)

³ University of Potsdam, Karl-Liebknecht-str. 24-25, 14476 Potsdam (Germany)

In this communication, we investigate laser-driven vibrational dynamics at metallic surfaces. Due to the interaction with the environment, the adsorbate vibrational states have finite lifetimes, which is responsible for line broadening in spectroscopy and which can further affect the chemical reactivity of the species. A brief overview of perturbative rate models will be given, as well as ideas to include important effects such as anharmonicity and corrugation using electronic friction theory.

Perturbative electronic friction theory

Energy relaxation is an ubiquitous problem when dealing with molecular dynamics in dissipative environments. For molecules in the vicinity of metallic surfaces, non-adiabatic coupling is known to play a dominant role in the transfer of energy from the system to the surroundings [1]. A current explanation of the phenomenon is based on the creation of electron-hole pairs in the metal conduction band to account for the finite speed at which the electrons react to nuclear displacements. During a vibrational period, the electrons at the surface try to adapt to their new local environment and eventually lag behind the molecular motion. An electron-hole pair is created when the charge separation is sufficiently large and part of the vibrational energy is transferred to the electronic degrees of freedom, slowing down the molecular motion in the process. This phenomenon is sometimes called “electronic friction”. Several authors proposed perturbative expressions for treating the effects of electron-hole pair coupling on excited states lifetime ($\tau_{m \rightarrow n}$) [2-6]. In most cases, the relaxation rate ($\Gamma_{m \rightarrow n}$) can be derived from or related to Fermi's Golden rule

$$\Gamma_{m \rightarrow n} = 1/\tau_{m \rightarrow n} = \frac{2\pi}{\hbar} \sum_{if} |\langle i, m | \hat{W} | f, n \rangle|^2 \delta(E_{f,n} - E_{i,m})$$

where $\{i, f\}$ are the initial and final electronic states, $\{m, n\}$ denote the vibrational states, and the delta function ensures energy conservation. The multidimensional coupling operator \hat{W} mediates the exchange of energy between the adsorbate and the surface.

To evaluate the expression, usual theoretical treatments resort to the harmonic approximation and only the first excited state along each given mode is considered. When performing dissipative vibrational dynamics, lifetimes for all states need to be considered. Typically, the lifetime of higher excited states is derived using a single-mode, site-local, harmonic approximation, and scales linearly with the vibrational quantum number. For strongly coupled systems where the quantum numbers are not well defined, and for corrugated potential energy surfaces with multiple minima, this approximation fails. To palliate these limitations, we recently introduced a perturbative rate model based on electronic friction theory [9-10]

$$\Gamma_{m \rightarrow n} = \sum_q \mathcal{Y}^{(q)} |\langle m | \rho_{embd}^{1/3} \frac{\partial}{\partial q} | n \rangle|^2$$

where the constant $\mathcal{Y}^{(q)}$ is the sum of the non-adiabatic contributions from all electronic states to the relaxation along mode q . Anharmonicity and intermode coupling are treated explicitly by integration of the gradient operator $\partial/\partial q$ over the multidimensional wave function. The effects of surface corrugation are accounted for by embedding the adsorbate in the electronic density of the metal substrate, ρ_{embd} , which thwarts the vibrational motion. These ideas were extended recently to polyatomic molecules [11].

Adsorbate-surface dynamics

In the following, we apply our position-dependent anharmonic rate model to evaluate the state-to-state lifetimes and to study the relaxation dynamics of different adsorbates (H, NO, CO) on metallic surfaces (Pd, Au, Cu). It is shown that, although the simple harmonic scaling law provides a good estimate of the overtones lifetime, the state-resolved mechanism for energy dissipation can be qualitatively incorrect. These results demonstrate the importance of including intermode coupling and anharmonicity for a reliable microscopic characterization of relaxation at metallic surfaces.

The selective excitation of carbon monoxide on a copper (100) surface is used as a prototypical example of dissipative dynamics. The time evolution of the system is studied using the reduced density matrix approach in its Lindblad form [12]. To investigate the diffusion dynamics of the adsorbate, a four-dimensional model Hamiltonian obtained by fixing the bond length r_0 and the Y coordinate at their equilibrium value is used

$$\hat{H}_{4d} = \frac{-\hbar^2}{2M} \left(\frac{\partial^2}{\partial X^2} + \frac{\partial^2}{\partial Z^2} \right) + \frac{1}{2\mu r^2} \hat{J}(\theta, \phi) + V(X, Z, \theta, \phi)$$

Here, $\hat{J}(\theta, \phi)$ is the well-known angular momentum operator, $\{X, Z\}$ denote the position of the adsorbate and $\{\theta, \phi\}$ its orientation, while M and μ are its total and reduced mass, respectively. This reduced-dimension model appears suitable to study diffusion along the X -axis. Different laser control strategies [13-17] are presented for the selective population of desired excited states. It is shown that short, intense laser pulses can be used to efficiently counter the effects of energy relaxation in strongly coupled systems.

References

- [1] Wodtke, Matsiev, and Auerbach, *Prog. Surf. Sci.* **83**, 167 (2008).
- [2] Persson and Hellsing, *Phys. Rev. Lett.* **49**, 662 (1982).
- [3] Puska and Nieminen, *Phys. Rev. B* **27**, 6121 (1983).
- [4] Rantala and Rosen, *Phys. Rev. B* **34**, 837 (1986).
- [5] Head-Gordon and Tully, *J. Chem. Phys.* **96**, 3939 (1992).
- [6] Krishna and Tully, *J. Chem. Phys.* **125**, 054706 (2005).
- [7] Winter, Juaristi, Nagy, Arnau, and Echenique, *Phys. Rev. B* **67**, 245201 (2003).
- [8] Juaristi, Alducin, Diez-Muino, Busnengo, and Salin, *Phys. Rev. Lett.* **100**, 116102 (2008).
- [9] Tremblay and Saalfrank, *J. Chem. Phys.* **131**, 084716 (2009).
- [10] Tremblay, Monturet, and Saalfrank, *Phys. Rev. B* **81**, 125428 (2010).
- [11] Tremblay, Monturet, and Saalfrank, *J. Phys. Chem. A* **115**, 10698 (2011).
- [12] Lindblad, *Comm. Math. Phys.* **48**, 119 (1976).
- [13] Brumer and Shapiro *Principles of the Quantum Control of Molecular Processes*, Wiley (Hoboken) 2003.
- [14] Ohtsuki, Yahata, Kono, and Fujimura, *Chem. Phys. Lett.* **287**, 627 (1998).
- [15] Shi and Rabitz, *J. Chem. Phys.* **92**, 364 (1990).
- [16] Tremblay and Saalfrank, *Phys. Rev. A* **78**, 063408 (2008).
- [17] Tremblay, *J. Chem. Phys.* **134**, 174111 (2011).

Reactive force fields for surface chemical reactions

W. Dong¹, **Y. Xiao**², **H. F. Busnengo**³, **X. J. Shen**^{1,2} and **X. H. Yan**²

¹ *Laboratoire de Chimie, UMR 5182 CNRS, Ecole Normale Supérieure de Lyon, 46, Allée d'Italie, 69364 Lyon Cedex 07, France, email: wei.dong@ens-lyon.fr*

² *College of Science, Nanjing University of Aeronautics and Astronautics, Nanjing 210016, China*

³ *Instituto de Física de Rosario (CONICET-UNR) and Facultad de Ciencias Exactas, Ingeniería y Agrimensura, Universidad Nacional de Rosario, Av. Pellegrini 250, 2000 Rosario, Argentina*

The two prerequisites of any reliable study on the dynamics of chemical reactions are: i) an accurate potential energy surface (PES), ii) an efficient method for performing dynamics calculations. Thanks to the steady increase of the power of computer hardware, the density functional theory (DFT) and other ab initio methods can provide nowadays accurate results on energetics for systems with moderate sizes. In this case, one can carry out ab initio molecular dynamics simulations (AIMD) to study reaction dynamics with the calculation of inter-atomic forces performed on the fly by using an ab initio method. For more complex systems of large scale, in particular, in the presence of condensed phase, the AIMD simulation becomes computationally prohibitive. Since the calculation of the inter-atomic forces is the bottleneck, one has to resort to computationally more efficient methods and for this there are several possibilities. For a system with a relatively small number of degrees of freedom, many methods have been proposed for constructing potential energy surfaces, e.g., method based on the interpolation of 2 dimensional cuts of PES. Nevertheless, the weak point of such an approach is that it becomes non tractable when the number of degrees of freedom is large, e.g., reactions between large molecules in gas phase, surface reactions with polyatomic adsorbates (in particular, when the motion of surface atoms have to be taken into account), etc.

The approach based on force fields has been very extensively used to study various properties of non reacting systems. Nowadays, a variety of accurate force fields are available which allow for investigating quite complex systems, e.g., large bio-molecules. The simulation of the processes involving chemical reactions (i.e., breaking and forming some chemical bonds) is more challenging because the modification of electronic structure due to the reactions has to be taken into account which requires a quantum-mechanics consideration. Reactive force field (RFF) follows the same spirit of the traditional force fields (i.e., the non reactive ones) but takes into account the modification of electronic structure in an approximate way. This is why it allows, in principle, for describing chemical reactions. The functional forms of many reactive force fields are inspired by an approximate relation between the density of states (DOS) and the bond energy. As all the force fields, a reactive

force field contains a certain number of parameters which have to be determined first (i.e., the so-called parameterization). Historically, the reactive force fields have been developed first by the solid physics and material science communities. It is only quite recently that they have attracted the attention of physical chemistry community and have been adapted to study some chemical reactions. Recently, we have developed RFF for some chemical reactions on solid surfaces [1-3]. Our results show that reliable information on reaction dynamics can be obtained from molecular dynamics (MD) simulations based on RFF. The most attractive feature of such an approach is its considerable gain in computational efficiency by 105 compared to AIMD. The demonstrated reliability and the computational performance of reactive force fields open very attractive perspectives for large-scale simulations of complex surface reactions.

References

- [1] Y. Xiao, W. Dong and H.F. Busnengo, *J. Chem. Phys.* **132**, 014704, (2010).
- [2] Y. Xiao and W. Dong, *Phys. Rev. B* **83**, 125418 (2011).
- [3] X.J. Shen, W. Dong, Y. Xiao and X.H. Yan, *J. Chem. Phys.* **135**, 167101, (2011).

Hydrogen interaction with polycyclic aromatic carbon systems - from graphene to PAHs

Liv Hornekaer

*Institut for Fysik og Astronomi ,Aarhus Universitet, Ny Munkegade 120, 8000 Aarhus C,
Denmark*

Multiquantum vibrational excitation of NO scattered from Au(111): benchmark data and comparison to theories of nonadiabatic molecule-surface interactions

Russell Cooper¹, Christof Bartels¹, Alexander Kandratsenka^{1,2}, Igor Rahinov³, Neil Shenvi⁴, Kai Golibrzuch¹, Zhisheng Li⁵, Daniel J. Auerbach⁶, John C. Tully⁷, Alec M. Wodtke^{1,2,6}

¹Institute for Physical Chemistry, Georg-August University of Göttingen, Göttingen, Germany

²Max Planck Institute for Biophysical Chemistry, Göttingen, Germany

³Department of Natural Sciences, The Open University of Israel

⁴Department of Chemistry, Duke University

⁵Department of Chemistry, Columbia University

⁶Department of Chemistry and Biochemistry, University of California Santa Barbara

⁷Department of Chemistry, Yale University

It is now well established that the adiabatic (Born-Oppenheimer) approximation¹, the foundation of conventional theories of chemical dynamics, is not always valid for describing atomic motions at metal surfaces². Electron-hole pair (EHP) transitions can provide a significant pathway for energy flow, particularly for processes involving high frequency molecular vibrations that do not couple efficiently to phonons³. Exoergic chemical bond formation can also involve nonadiabatic electronic transitions resulting from nuclear motion⁴. A striking example demonstrating Born-Oppenheimer break down involved multiquantum vibrational de-excitation of vibrationally excited NO($v=15$) molecules scattered from the (111) surface of a single crystal of gold^{3b}. This study revealed very efficient transfer of molecular vibrational energy to the surface, in contrast to the predominantly vibrationally elastic scattering observed for the same molecule scattered from the surface of an insulator.

These striking results stimulated several attempts⁵ to develop better approaches to the theory of nonadiabatic molecular motion at metal surfaces, a theory which is crucial for predicting the dynamics of chemical transformations that underlie such processes as catalytic reactions, etching, and corrosion. Two quite different theoretical approaches have been employed: electronic friction^{5f, 6}, which involves weak, perturbative coupling to EHP excitations, and independent electron surface hopping (IESH), which involves non-perturbative coupling to EHP excitations based on an electron transfer mechanism forming a transient negative ion (NO^-)^{5b-d}. Both of these approaches, with interaction parameters obtained from first principles density functional theory (DFT), were in fact able to adequately reproduce the major features of the NO($v=15$) de-excitation experiment.

Despite this impressive progress, important open questions remain. Based on the success of a perturbative (electronic friction) approach in modelling de-excitation data, it is not clear whether a strong coupling approach like IESH is required. As electronic friction theory is much simpler to implement, this question carries significant practical implications. Furthermore transient negative ion formation is only important in the IESH approach. Hence, the fundamental mechanism of the molecule surface interaction remains unclear.

Comparison of theory with experiment for both multiquantum vibrational *excitation* as well as de-excitation over a wide range of surface temperatures, T_s , and incidence energies, E_i , on

the same molecule-surface collision system would provide a very stringent test of theoretical models. Such a test would more easily distinguish competing theories based on different physical assumptions.

In this work, we present experimentally determined *absolute* excitation probabilities for $\text{NO}(v=0 \rightarrow 1)$ and $\text{NO}(v=0 \rightarrow 2)$ scattering from a $\text{Au}(111)$ surface, complementing data already available for de-excitation of $\text{NO}(v=15)^{3b}$. We report over eighty excitation probabilities for $300\text{K} \leq T_s \leq 1000\text{K}$ and $0.11\text{ eV} \leq E_i \leq 1.05\text{ eV}$. These comprehensive and quantitative experimental results inspired us to carry out new IESH calculations of the vibrational *excitation* of NO. Remarkably, we find that the IESH theory used to model vibrational de-excitation of $\text{NO}(v=15)$ on $\text{Au}(111)$ is in good agreement with absolute experimental excitation probabilities for $\text{NO}(v=0 \rightarrow 1,2)$. We emphasize that both IESH calculations of excitation and de-excitation employed the identical DFT-derived Newns-Anderson Hamiltonian. On the other hand, an electronic friction model based on the same many-electron Hamiltonian used in the IESH calculations is not consistent with the data. These calculations demonstrate that transient negative ion formation plays an important role in the nonadiabatic vibrational energy transfer process as well as the need to go beyond perturbative (electronic friction) approaches to molecule-surface interactions.

The equipment and procedures used to make these measurements have been previously described in detail⁷. Supersonic molecular beams of NO are produced with variable translational energy. The molecular beam scatters from an $\text{Au}(111)$ crystal in UHV at near normal incidence. The surface temperature is varied by resistive heating of tungsten wires to which the gold crystal is mounted. The scattered NO molecules are state-selectively ionized with UV laser light used for (1+1) REMPI via the $A^2\Sigma^+$ state⁸. The ions are detected by a dual micro-channel plate detector.

Absolute excitation probabilities were extracted by comparing the signal of inelastically scattered NO molecules in $v=1$ and 2 to the signal of vibrationally elastically scattered NO molecules in $v=0$. To make this comparison, the entire rotational spectrum was integrated giving the spectral intensity in each vibrational band, and the integrated signal was corrected for various factors such as MCP gain, angular and temporal dilution, and laser power. Angular, temporal, and rotational distributions indicate a direct scattering mechanism for vibrational excitation under all conditions of this work.

To model the nonadiabatic dynamics of NO molecules scattering from a $\text{Au}(111)$ surface, we used the recently developed IESH method^{5b, 5c}. The IESH approach has several advantages. First, one may calculate nonadiabatic dynamics based on potential energy surfaces and nonadiabatic coupling strengths obtained from DFT calculations. Second, all electrons are assumed to be non-interacting. Hence, we can independently propagate many one-electron orbitals instead of a single many-electron wave function increasing the algorithm efficiency. Third, motion of the nuclear degrees of freedom is modeled classically and the coupled electron-nuclear dynamics is calculated within the framework of the surface hopping theory⁹. Thus we can perform high dimensional dynamics calculations including both the NO molecule as well as the Au lattice degrees of freedom.

We calculated excitation probabilities each from 100,000 trajectories at several values of T_S and E_i . The initial states of the NO molecules were chosen to be randomly oriented and non-rotating with initial center-of-mass velocities directed normal to the surface and corresponding to a given incidence energy. The initial vibrational energy of NO was set to 0.12 eV, representing the vibrational zero point energy. A detailed description of the construction of the many-electron system Hamiltonian and implementation of the IESH algorithm can be found in Refs. 5b, 5c.

The results of both theory (open symbols) and experiment (closed symbols) are presented in Fig. 1, where the vibrational excitation probabilities for NO($v=0 \rightarrow 1$) (black symbols) and NO($v=0 \rightarrow 2$) (blue symbols) are plotted as a function of T_S at six values of E_i . The experimental vibrational excitation probability is always much larger for NO($v=0 \rightarrow 1$) than for NO($v=0 \rightarrow 2$) and for both, higher incidence energy leads to an increase in excitation probability. At all incidence energies and for both vibrational channels, the experimental data follow an Arrhenius dependence on surface temperature with the activation energy equal to the change of vibrational energy (dashed lines).

The absolute excitation probabilities are reproduced by the IESH theory to within a factor of five over the entire range of conditions for both vibrational channels. The Arrhenius T_S dependence, which has so often been attributed to vibrational excitation occurring via coupling to EHPs in the solid, is also found in the IESH calculations. This is the first time that this characteristic T_S behaviour is accurately reproduced in a first principles theory of molecule surface interactions. Remarkably, this characteristic of vibrational excitation is derived from a theory that was originally developed for modelling de-excitation, using an identical parameterization of the Hamiltonian. This unifies our physical picture of energy transfer for NO on Au over a wide range of vibrational states, surface temperatures and incidence energies.

Calculations for NO/Au(111) scattering were also performed using an electronic-friction model⁶ applied with the same many-electron Hamiltonian that was used in the IESH calculations. The extent of vibrational excitation is substantially lower in the electronic friction calculation in comparison to that of IESH. In fact, no trajectory is found, out of the

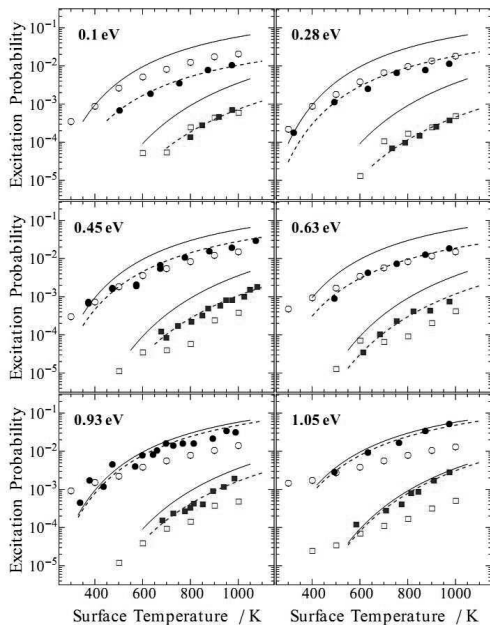


Figure 1: Excitation probabilities for NO/Au(111) as a function of surface temperature for six different incidence energies of translation.

100,000 calculated, that would be binned as $v=1$ or higher. This absence of vibrational excitation shows that the friction model is insufficient to explain nonadiabatic vibrational excitation in this system. Moreover, its results are very close to ones obtained from the adiabatic model, when surface hopping and electronic friction mechanisms are switched off.

This failure of friction theory arises from the theory's weak coupling assumption. A weak coupling description of a direct scattering process cannot produce vibrational excitation probabilities that approach the thermal limit. Thermalization with the surface is an upper limit to the vibrational excitation probability when excitation occurs via an electron mediated process neglecting translation-vibration coupling^{3d, 10}, shown as solid lines in Fig. 1.

The observed vibrational excitation probabilities range between 0.1 and 0.85 of the thermal limit indicating the need to go beyond the perturbative (electron friction) approach. In contrast, the IESH theory, which describes the strong coupling induced by an electron transfer event, leads to good agreement with experiment.

Finally, having demonstrated a successful theoretical approach that goes beyond the perturbative assumptions of electronic friction theory, we emphasize that IESH is also capable of dealing with the weak coupling case, making it a potentially widely applicable approach to the treatment of BOA breakdown.

References

- [1] M Born *et al.*, *Ann. der Phys.* **84**, 0457 (1927).
- [2] (a) AM Wodtke *et al.*, *Int. Rev. Phys. Chem.* **23**, 513 (2004); (b) AM Wodtke *et al.*, *Prog. Surf. Sci.* **83**, 167 (2008); (c) I Rahinov *et al.*, *PCCP* **13**, 12680 (2011); (d) C Bartels *et al.*, *Chem. Sci.* **2**, 1647 (2011); (e) E Hasselbrink, *Surf. Sci.* **603**, 1564 (2009); (f) GJ Kroes, *Science* **321**, 794 (2008).
- [3] (a) CT Rettner *et al.*, *Phys. Rev. Lett.* **55**, 1904 (1985); (b) Y Huang *et al.*, *Science* **290**, 111 (2000); (c) JD White *et al.*, *Nature* **433**, 503 (2005); (d) R Cooper *et al.*, *Chem. Sci.*, 55 (2010).
- [4] (a) B Gergen *et al.*, *Science* **294**, 2521 (2001); (b) JR Trail *et al.*, *Phys. Rev. Lett.* **88**, (2002).
- [5] (a) G Katz *et al.*, *J. Phys. Chem. B* **109**, 18876 (2005); (b) N Shenvi *et al.*, *J. Chem. Phys.* **130**, 174107 (2009); (c) S Roy *et al.*, *J. Chem. Phys.* **130**, 174716 (2009); (d) N Shenvi *et al.*, *Science* **326**, 829 (2009); (e) N Shenvi *et al.*, *J. Chem. Phys.* **125**, 154703 (2006); (f) S Monturet *et al.*, *Phys. Rev. B* **82**, 075404 (2010).
- [6] M Head-Gordon *et al.*, *J. Chem. Phys.* **103**, 10137 (1995).
- [7] (a) Q Ran *et al.*, *Rev. Sci. Instrum.* **78**, 104104 (2007); (b) I Rahinov *et al.*, *J. Chem. Phys.* **129**, 214708 (2008).
- [8] J Luque *et al.*, *J. Chem. Phys.* **111**, 7405 (1999).
- [9] JC Tully, *J. Chem. Phys.* **93**, 1061 (1990).
- [10] (a) DM Newns, *Surf. Sci.* **171**, 600 (1986); (b) D Matsiev *et al.*, *PCCP* **13**, 8153 (2011).

Energy Production and Storage

Photon harvesting and charge carrier collection in mesoscopic solar energy conversion systems

Michael Grätzel

Laboratoire de Photonique et Interfaces, Institut des Sciences et Ingénierie Chimiques, Ecole Polytechnique Fédérale de Lausanne, Station 6, CH-1015 Lausanne, Switzerland

Patrick Sanglan

AXANE - 2, rue de Clémencière - BP 15 - 38360 Sassenage - France

Schrödinger Medal Award Session

Astrochemistry in Ion Traps: From Cold Hydrogen to Hot Carbon

Dieter Gerlich

Faculty of Natural Science, Technical University, 09107 Chemnitz, Germany, gerlich@physik.tu-chemnitz.de, also Faculty of Mathematics and Physics, Charles University, 180 00 Prague

Astrochemistry deals with the formation and destruction of matter in various environments including the early universe, cold dense interstellar clouds, hot circumstellar regions, planetary atmospheres etc. In this contribution I try to summarize previous, present and planned experimental activities in this field using radio frequency (rf) traps for ions and nanoparticles. After a more technological retrospect with selected applications, new results for reactions of slow H atoms with stored CH^+ and H^- ions are presented as well as decay rates for C_{60}^+ ions, heated with a CW CO_2 laser to temperatures up to 2200 K.

Experimental

The eighties have seen several innovative experiments developed for exploring gas phase chemistry at low temperatures. An early summary can be found in Ref. [1] which also refers to the pioneering work of G. Dunn. His group used a l-He cooled Penning ion trap for studying collision between ions and neutrals. Alternative approaches started with rf ion traps where confinement is achieved with the so-called effective potential. Fig. 1 shows the first trap which could be operated down to 80 K but also up to 500 K. It was presented at the SASP 1988 [2]. Meanwhile, using closed cycle refrigerators, the temperature range down to 4 K has been opened up. From the various multi-electrode arrangements, the 22-pole is probably the most common ion trap used to cool ions for reaction dynamics and spectroscopy.

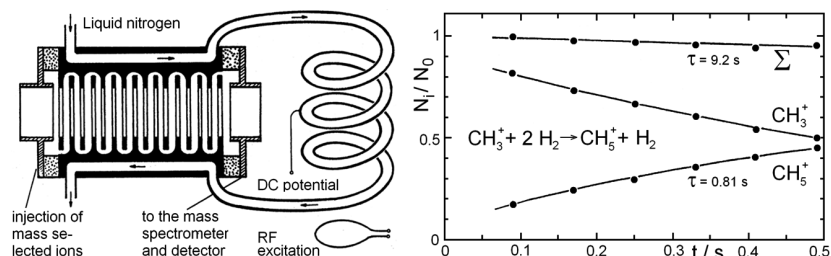


Figure 1: *Left: first rf trap which can be cooled with l-N₂. Right: CH₃⁺ ions reacting to CH₅⁺ with H₂ at a number density of 10¹³ cm⁻³. For details see SASP 1988 (La Plagne) [2].*

However, already in 1993, during the Faraday Symposium 28 on *Chemistry in the Interstellar Medium*, Alec Dalgarno emphasized, that also detailed experiments at high temperatures are needed for understanding the complex interaction between gas phase, grains, ice layers and photons in the universe. For ions, translational energies of several eV are easy to obtain; however, e.g. for understanding the chemistry in the outflow of stars, all degrees of freedom have to be heated. Also for this purpose traps are well suited. One technical realization is the Split Ring Electrode Trap (SRET), a stack of specially shaped electrodes with integrated high precision parabolic mirrors for focusing a continuous CO₂ laser into its center [3].

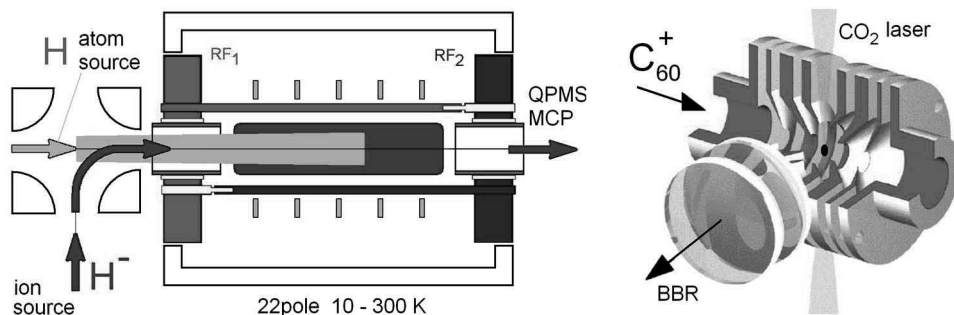


Figure 2: Left: 22-pole ion trap combined with an H-atom beam. Right: Split Ring Electrode Trap for heating and monitoring high temperature particles confined in the center.

The stored particles are characterized *in situ* by imaging their thermal emission (BBR) onto an ICCD camera or by counting the emitted photons in various spectral regions. In this way the total number of stored objects can be monitored as well as their spatial distribution in the trap, and, especially important, their internal temperature. For calibration and consistency checks, the ions can be extracted, mass selected and counted using a Daly detector. Besides thermal decay of hot interstellar grain equivalents, the method allows one to explore their growth in specific gaseous environments. Successful tests with C₆₀⁺ are mentioned below.

Results

Many gas phase processes involving ions have been studied in rf traps, including bi- and termolecular reactions, radiative association, clustering, isomerization, and isotope fractionation. For applications in spectroscopy and anion chemistry see the contributions from J. Maier, S. Schlemmer and R. Wester to this SASP conference. One of our recent activities has concentrated on the formation and destruction of small hydrocarbons in collisions with H₂ and H atoms. Of fundamental importance are the results for CH⁺(*v*=0,*J*) + H → C⁺ + H₂(*J*). As shown in Fig. 3 and discussed in [4], CH⁺ in the rotational ground state does not react! So far there is no convincing explanations.

The primordial chemistry and the formation of the first stars is determined by atomic and molecular processes involving mainly hydrogen (H, D), helium (^3He , ^4He), electrons, and radiation. One of the key question until recently was, how efficient is formation of H_2 molecules from H-atoms [5]. There are no grains, but also under early universe conditions this process requires a catalyst, the dominant one being the electron. The first step is the formation of H^- , followed by associative detachment with a second H atom. In our ion trap experiment (see Fig. 3 and Ref. [6]), the temperature of both reactants could be varied independently and a range between 10 and 135 K has been accessed experimentally, for the first time. The results are in good accordance with a simple capture model, using the long range potential.

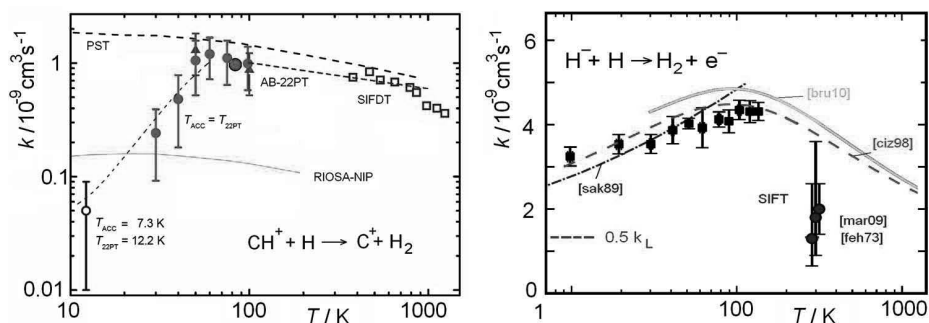


Figure 3: Low temperature collisions. Left: H-atom abstraction reaction, right: associative detachment. For more details see the references [4] and [6].

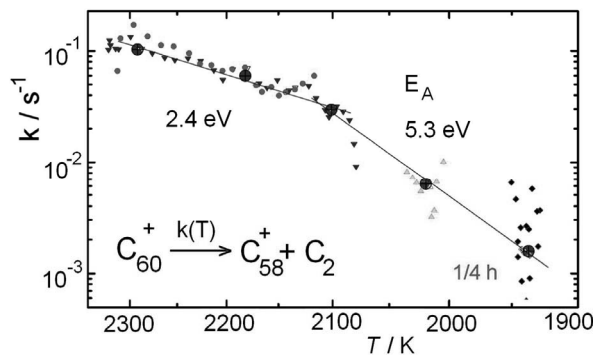


Figure 4: Decay rates of some thousand C_{60}^+ at temperatures above 1900 K [3].

So far, all experiments which monitored the decay of highly excited C_{60}^+ started with ions with rather undefined internal energies. In the SRET trap we succeeded, for the first time, to

maintain *stationary equilibria* over long periods, meaning that, in time average, the same energy is emitted as absorbed. With less than 10 W of CO₂ laser power, conditions have been reached which may be described by "temperatures" ranging from 1900 to 2300 K. Trapping times up to 15 min without any loss of ions allow us to follow very slow decay of C₆₀⁺ via C₂ ejection. In Fig. 4, rates between 10⁻¹ and 10⁻³ s⁻¹ are plotted. At 1850 K, *k* is as low as 1 h⁻¹. Evaluation of the results using an Arrhenius type function leads to "activation energies" E_A between 2 and 5 eV [3]. Although our experiment really monitors the thermal decay of C₆₀⁺ in a high temperature radiation field, it is not yet clear how to correlate E_A with the binding energy of C₂.

Conclusions, Outlook, Acknowledgement

Instruments, using inhomogeneous rf fields are very versatile. It started with W. Paul in the fifties and more than 40 years ago, the first guided ion beam apparatus has been developed. 25 years ago, the first cooled rf ion trap became operational. In combination with optical methods, beams of molecules and radicals, and using the variety of features the rf technique offers, many unique experiments have been performed. The long storage times allow one to detect extremely slow processes with high sensitivity. Activities in the near future (in Prague) will improve and extend our H⁻ + H results by using D⁺ + H → H⁺ + D for calibrating the H-atom beam and by measuring the competition between electron transfer and associative detachment in D⁻ + H collision. More state specific rate coefficients for primordial chemistry are on the list, e.g. the reaction HeH⁺(*J*) + H → H₂⁺(*v*,*J*) + He. By closing the trap with meV barriers, it will become possible to observe the exothermic reaction H⁺ + H₂(*J*=1) → H⁺ + H₂(*J*'=0). A real innovative experimental challenge is to superimpose a linear rf multipole with a suitable magnetic field guiding electrons in and out the trap. Trapping nanoparticles opens up a wide, still unexplored field including the very precise mass determination.

I thank all my coworkers who made the various developments possible. The activities have been supported by the DFG, the VW foundation, the EC and others sources. I am grateful for the hospitality of various groups who allow me to try to continue my ambitious plans and to dream from innovations, especially to J. Glosík, J. Roithova, and S. Schlemmer.

References

- [1] D. Gerlich, S. Horning, *Chemical Reviews* **92**, 1509-1539 (1992)
- [2] D. Gerlich and G. Kaefer in: *Symposium on Atomic and Surface Physics*, eds. A. Pesnelle et al., La Plangne, 115 (1988)
- [3] S. Decker, <http://nbn-resolving.de/urn:nbn:de:bsz:ch1-200901988>, PhD thesis TU Chemnitz (2009)
- [4] R. Plašil, T. Mehner, P. Dohnal, T. Kotrik, J. Glosík, D. Gerlich, *ApJ*, **737**, 60 (2011)
- [5] H. Kreckel, H. Bruhns, M. Čížek, S.C.O. Glover, K.A. Miller, X. Urbain, D.W. Savin, *Science* **329**, 69 (2010)
- [6] D. Gerlich, P. Jusko, Š. Roučka, I. Zymak, R. Plašil, J. Glosík, submitted to *ApJ*.

Schrödinger Medal Award Session

Electronic Spectroscopy of Astrophysically Relevant Molecules

John P. Maier

*Department of Chemistry, University of Basel, Klingelbergstrasse 80,
CH-4046 Basel, Switzerland, email: j.p.maier@unibas.ch*

The focus of our research is the measurement of the electronic spectra of carbon containing chains, rings and ions of astrophysical relevance. Initial information on the systems is often obtained by measuring the absorption in 6 K neon matrices using mass-selected ion beams. In the gas-phase the transient molecules are produced in discharges and laser vaporization sources coupled with supersonic free jets. The transitions are searched for with several laser-based spectroscopic techniques. For the studies of cations an instrument using ion trapping technology has been developed. Mass-selected ions are constrained in a 22-pole radio-frequency trap where they are cooled by collisions to around 20 K prior to the measurement of the electronic transitions by two color two photon approaches.

The availability of the laboratory gas-phase spectra enables a direct comparison with astronomical observations to be made and the implications for the potential carriers of the diffuse interstellar absorptions in the optical region are discussed.

Characterization of Clusters and Ultrafine Aerosols by Ultraviolet Photoionization

Bruce L. Yoder, Jessica H. Litman, and Ruth Signorell

University of British Columbia, Chemistry Department, 2036 Main Mall, Vancouver, BC, V6T 1Z1, Canada

Ultraviolet photoionization has been widely used to study many different types of molecular clusters. These investigations often focus on the characterization of size-dependent properties such as structure, vibrational frequencies, ionization energies, and dissociation energies.

We are investigating how these methods could be exploited for the characterization of ultrafine aerosols. For that purpose, we compare experimental results for small clusters with those of ultrafine aerosols and with commercial aerosol characterization methods. Where experimental information is not accessible we try to complete the picture by modeling.

References

- [1] B. L. Yoder, J. H. Litman, P. F. Forysinski, R. Signorell, *J. Chem. Lett.* **2**, 2623-2628 (2011)
- [2] P. F. Forysinski, P. Zielke, D. Luckhaus, R. Signorell, *J. Chem. Phys.* **134**, 094314 (2011)

Ice nanoparticles in molecular beam experiments: pick-up cross sections for atmospheric molecules and their photochemistry

Michal Fárník¹, Viktoriya Poterya¹, Andriy Pysanenko¹, Jozef Lengyel^{1,2}, Pavla Svrčková^{1,2}, Jaroslav Kočíšek^{1,3}, Juraj Fedor^{1,4}, Milan Ončák² and Petr Slaviček^{1,2}

¹ J. Heyrovský Institute of Physical Chemistry, Academy of Sciences of the Czech Republic, Dolejškova 3, 182 23 Prague 8, Czech Republic, michal.farnik@jh-inst.cas.cz

² Institute of Chemical Technology, Technická 5, Prague 6, Czech Republic

³ Charles University Prague, Faculty of Mathematics and Physics, Prague, Czech Republic

⁴ Department of Chemistry, University of Fribourg, CH-1700 Fribourg, Switzerland

Ice particles play a key role in many processes in atmospheric chemistry and also in chemistry of interstellar space. Many of the chemical reactions in the interstellar space take place on/in dust and ice particles of microscopic and nanoscopic sizes [1]. The reason is that the conditions, i.e., the temperatures and reactant densities are extremely low in the interstellar space, and thus unfavourable for any sort of neutral-neutral chemistry. The dust and ice particles can act as a “sponge” storing the reactant molecules for long enough times so that the chemistry can actually take place. Besides, the cosmic radiation can excite the species in the particles initiating the chemistry in the excited states.

In the atmosphere of our planet, the ice particles in the polar stratospheric clouds (PSCs) catalyze the reactions which lead to the ozone depletion process in the stratosphere above Antarctica [2]. Reservoir species such as hydrogen halides HX (X=Cl, Br) undergo chemical reactions on the ice particles in the PSCs converting them to the active species such as Cl₂ molecules, which are then readily photolyzed by the UV sun radiation to the ozone destroying Cl· radicals. Some recent models also suggest a direct dissociative electron attachment (DEA) to freon molecules (CFC) on PSC particles leading to the generation of Cl· radicals [3].

To mimic the atmospheric and interstellar space ice particles we generate large water clusters (H₂O)_n –*ice nanoparticles*– with the mean cluster sizes $n \approx 10^2$ – 10^3 in a molecular beam experiment in our laboratory in Prague [4], Fig. 1.

The clusters are generated in a supersonic expansion of water vapor through a 90 μm conical nozzle into a vacuum. Various experiments can be performed with the clusters in our versatile apparatus, e.g., they can be doped with foreign molecules in the pick-up cell. The pickup process is investigated by measuring the cluster velocities in the beam. From mass spectra of cluster fragments measured after ionization with electrons or UV-photons the cluster composition and its dynamics in ionized state can be learned. Most importantly the photodissociation of molecules in the clusters is studied with UV-lasers and time-of-flight and ion imaging techniques to determine the kinetic energy distribution of photofragments.

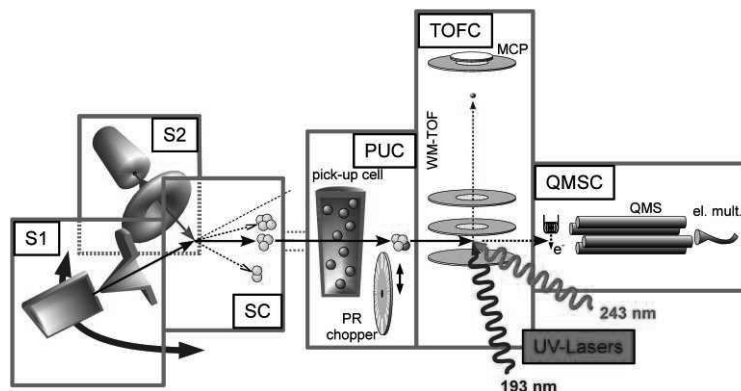


Figure 1: Cluster beam apparatus

Recently, we have critically investigated the pickup processes and cluster velocity measurements for determination of pickup cross sections of various molecules on large argon clusters [5]. In the present contribution we further employ this technique to obtain the pickup cross sections for various –especially atmospherically relevant- molecules on ice nanoparticles. One of the most striking results was an extremely small pickup cross section for freon CCl_2F_2 (CFC). The measured pickup cross section is several times smaller than the cluster geometrical cross section suggesting a sticking coefficient for CFC on ice nanoparticles significantly smaller than one, $s \approx 0.25$. This result has potentially a large atmospheric relevance, since the dissociative electron attachment of CFCs on ice particles in PSCs has been suggested as one of the mechanisms of Cl^- radical generation in the stratosphere.

We will also present the photochemistry of hydrogen halide molecules HX ($\text{X}=\text{Cl}, \text{Br}, \text{I}$) on ice nanoparticles which we have recently investigated in our laboratory [6-9]. In these experiments we have provided an evidence for H_3O neutral molecular radical generation by the UV excitation of the $\text{HX} \cdot (\text{H}_2\text{O})_n$ cluster. Besides, we have provided an experimental evidence for the H_3O generation in excited pure water clusters [10].

Further, the photochemistry of other atmospherically relevant species will be discussed, namely ice nanoparticles with the adsorbed CFC molecules, and mixed $\text{HNO}_3/\text{H}_2\text{O}$ ice nanoparticles

Acknowledgement: This work has been supported by the Grant Agency of the Czech Republic Project Nos. 203/09/0422 and P208/11/0161 and by young scientist (JK) grant by Vakuum Praha, Prague, CZ

References

- [1] D. J. Caruana, K. B. Holt, *Phys. Chem. Chem. Phys.* **12**, 3072 (2010).
- [2] S. Solomon, R.R. Garcia, F.S. Rowland, D.J. Wuebbles, *Nature* **321**, 755 (1986); M.J. Molina, T.L. Tso, L.T. Molina, F.C.Y. Wang, *Science* **238**, 1253 (1987).
- [3] Q.-B. Lu, L. Sanche, *Phys. Rev. Lett.* **87**, 078501 (2001).
- [4] M. Fárník, *Molecular Dynamics in Free Clusters and Nanoparticles Studied in Molecular Beams*, ICT Prague Press, Institute of Chemical Technology, Prague, (2011).
- [5] J. Fedor, V. Poterya, A. Pysanenko, and M. Fárník, *J. Chem. Phys.*, **135**, 104305 (2011).
- [6] M. Fárník, U. Buck, *Phys. Scr.* **76**, 73 (2007).
- [7] M. Ončák, P. Slavíček, V. Poterya, M. Fárník, U. Buck, *J. Phys. Chem. A* **122**, 5344 (2008).
- [8] V. Poterya, J. Fedor, A. Pysanenko, O. Tkáč, J. Lengyel, M. Ončák, P. Slavíček, and M. Fárník, *Phys. Chem. Chem. Phys.* **13**, 2250 (2011).
- [9] M. Ončák, P. Slavíček, M. Fárník, U. Buck, *J. Phys. Chem. A* **115**, 6155 (2011).
- [10] V. Poterya, M. Fárník, M. Ončák, P. Slavíček, *Phys. Chem. Chem. Phys.* **10**, 4835 (2008).

Ice processes relevant to astrophysics: radiation products, thermal and photodesorption

Guillermo Muñoz-Caro

*Centro de Astrobiología (CSIC/INTA), Instituto Nacional de Técnica Aeroespacial,
Ctra de Torrejón a Ajalvir, km 4, 28850 Torrejón de Ardoz, Madrid, Spain*

Theoretical Study of the insertion of small molecules inside clathrate hydrates using metadynamics

Anne Milet¹, Mircea Oltean¹, and Nevin Uras-Aytemiz²

¹ Université Joseph Fourier, Grenoble, CNRS DCM UMR 5250 Theoretical Chemistry DU BP53 38041 Grenoble cedex 9, France Anne.Milet@ujf-grenoble.fr

² Suleyman Demirel University, Department of Chemistry 32260 Isparta Turkey.

Introduction

Clathrate hydrates (CHs) are inclusion compounds composed of bonded H₂O, which form a crystalline host lattice composed of a periodic array of cages. The structure is stabilized by guest particles, which occupy the cages and interact with cages walls via van der Waals interactions. The clathrates structures may be various but they exist as two cubic structural types named structure cs-I and cs-II and one hexagonal structure named hs-III. The two cubic structures contained cages of different sizes: small and large. The smaller structure sc-I is a cubic unit cell of 46 water molecules and is composed of 8 cages: two small cages and 6 large cages. The larger structure sc-II contains 136 water molecules per unit cell and exhibits 16 small cages and 8 large cages. In both cases, stabilization of the crystal lattice is obtained thanks to guests molecules.^{1,2} These guests molecules could be H-bonding molecules (small ethers, H₂S, HCN, ...) as well as molecules as CO₂ or CH₄ which are commonly observed in natural environment in cs-I structure. There is no more than one molecule per cage and molecules larger than CO₂ occupy mainly large cages. Interest in CHs has been drawn by two facts: around 6.4 trillion tonnes of CH₄ is confined into CH deposits found beneath the sediment of deep ocean and in the permafrost, and the plugging of pipelines transporting natural gas by CHs is to be prevented. The interaction of these hosts with the CH has been studied by infra-red spectra³ and it was shown that motion of the guest between the cages can occur with different kinetics depending of the guests. For example, H₂S displacement of DME (dimethyl ether) in sc-I is very fast (half-life of 4 minutes at 120K) whereas CO₂ displacement of CH₄ is slow in sc-I (half-life of around 400 minutes at 122K).

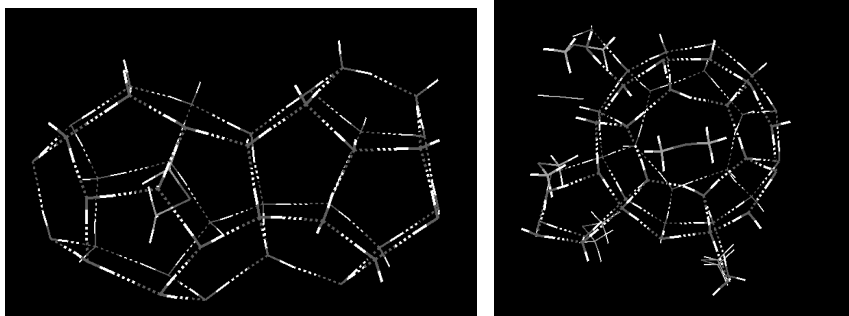


Figure 1 left) View of the cluster, right) View of unit cells-I clathrate cell unit with HCN and DME inside the cages,

Results

In this presentation, we will study the sc-I compounds and its interaction with the guests. First, we will study the cost of this kind of interactions. Indeed, this type of interactions involves dispersion terms and the adequacy of DFT to describe such systems will be discussed. Thus, we used the newly developed dispersion corrections termed DFT-D3 developed by Grimme and co-workers.⁴ We also compared the results obtained using different functionals with or without corrections for the dispersion to the widely used B3LYP⁵ functional and the newly functional developed by Truhlar⁶ and coworkers. We also compared the interaction energies for the periodic sc-I and with the two cages clusters (see Fig. 1).

We also study the displacement of dimethyl ether DME in the sc-I clathrate from one cage to the adjacent cage. Such process is definitively a dynamic process but it will not be possible to simulate it in the “normal” time of simulations. So metadynamics has been used to overcome this issue.^{5,6} The simulation shows that to move from cage to the other one, the DME has to displace one water molecule of the water pentamer, which defines the frontier between the two cages. This finding is in agreement with the belief that displacement of guests inside the CHs is eased by defects. To have insight into the thermodynamic cost of this process, we used the energy as a collective variable in the metadynamics framework in order to have an estimation of the entropic contribution coming along this process in addition to the free energy contribution given by the metadynamics.

Computational details

Ab initio simulations have been carried out using the CP2K/QuickStep of programs^{9,10} as well as the Gaussian09¹¹ for the calculations for the two cages clusters. We used different functionals as previously described with DZVP basis sets.

Metadynamics :

Metadynamics has been used to overcome the problem of observing rare events in conventional molecular dynamics and of finding the reaction coordinate. A series of small repulsive Gaussian potentials centered on the values of some collective variables are added during the dynamics, preventing the system from revisiting the same points in configurational space and creating a history-dependent multidimensional biasing potential. In the limit of a long metadynamics run, the free energy surface can be reconstructed as a function of the CV s : $F(s) < -V_G(s,t)$. A time step of 1 fs was used for the dynamics and the hills were added every 10 fs. We used one or two collective variables depending on the calculations. When two collective variables are used, one of them is the energy and the other one is the distance between the center of mass of the guest molecule and the center of mass of the water molecules forming the targeted cage.

Computing Entropic contributions:

We have shown that the potential energy E can also be used as a generalized coordinate for studying chemical reactions. During a chemical process, the potential energy E varies as the system explores new intermediate/transition states. Thus, it is a relevant collective variable. We have proposed to use E in combination with ordinary geometrical CVs. The advantages of such an extended set of CVs are the following: tracing the entropy along a reactive pathway and extrapolating the thermodynamic quantities at different temperatures. Using the potential energy E as a CV together with ordinary geometrical variables s in a metadynamics scheme allows reconstructing, at a temperature T_0 , the free energy as a function of E and s simultaneously. Remarkably $F_{T_0}(E, s)$ contains the relevant information for characterizing the thermodynamic properties of the system at *all the temperatures* T , including the probability to observe the reactants/products and the activation entropy. The internal energy profile and the free energy profile are also directly derived from $F_{T_0}(E, s)$ and so the entropic contribution can be deduced from these later contributions.¹²

References

- [1] D.W. Davidson, S.K. Garg, S.E. Gough, R.E. Hawkins, J.A. Ripmeester, *Inclusion Compounds II*, Ed. J.L. Atwood, J.E. Davies D.D. MacNicol, Academic, New York, **3**, 69-128, (1984).
- [2] E.D. Sloan, *Nature* **426**, 353 (2003).
- [3] V. Buch, J.P. Devlin, I.A. Monreal, B. Jagoda-Cwiklik, N. Uras-Aytemiz, L. Cwiklik, *Phys. Chem. Chem. Phys.* **11**, 10245 (2009).
- [4] S. Grimme, J. Antony, S. Ehrlich, H. Krieg ; *J. Chem. Phys.* **132**, 154104 (2010).
- [5] A.D. Becke, *J.Chem.Phys.* **98**, 5648 (1993)
- [6] Y. Zhao, D. G. Truhlar, *Theor. Chem. Acc.* **120**, 215 (2008).
- [7] A. Laio, M. Parrinello, *Proc. Natl. Acad. Sci. USA* **99**, 12562 (2002).
- [8] A. Laio, R. Rodriguez-Forteza, F.L. Gervasio, M. Ceccarelli, M. Parrinello, *J. Chem.Phys. B*, **109**, 6714 (2005).
- [9] CP2K, <http://cp2k.berlios.de>
- [10] J. VandeVondele, M. Krack, F. Mohamed, M. Parrinello, T. Chassaing, J. Hutter *J. Comp. Phys. Com.* **167**, 103 (2005).
- [11] Gaussian 09, Revision A.02, M. J. Frisch et al. Gaussian, Inc., Wallingford CT, 2009.
- [12] C. Michel, A. Laio, A. Milet *J. Chem. Theory Comput.* **5**, 2193 (2009).

Infrared and Raman Spectroscopy of Clathrate Hydrates

Bernard Schmitt¹

¹ Institut de Planétologie et Astrophysique de Grenoble, CNRS - University J. Fourier, Bâtiment D de Physique, B.P. 53, 38041 Grenoble Cedex 9, France. E-mail : Bernard.Schmitt@obs.ujf-grenoble.fr.

Clathrate hydrates are crystalline inclusion compounds in which small guest molecules are trapped in water cages (the host) formed by a regular H-bonded lattice. At least three types of clathrate hydrate structures are known which differ in the number, size and repartition of the different types of cages, and the molecules they can contain [1]. Although these compounds have been discovered as early as in the beginning of the 19th century the infrared and Raman spectroscopic properties of the molecules trapped in clathrate structures are still poorly known. However the growing interest for clathrate hydrate in the last decade, for fossil energy [2], environmental, astrophysical [3,4], industrial or fundamental aims [5], has restarted their spectroscopic studies. In particular the vibrations and rotations of the molecules in the different types of clathrate cages provide some insight in the interaction of individual molecules with the water cages, with some similarities and differences with molecules trapped in rare gases matrices. Their spectral signature in the near to far-infrared provides a means to determine the abundance and distribution of the molecules in the various cages (in pure and mixed clathrate hydrates) and should also be a potentially powerful remote sensing tool to identify these compounds in terrestrial, astrophysical and planetary environments. In this talk I will review the measurements and spectroscopic properties of the molecules trapped in clathrate hydrate structures, and outline some of their potential applications.

Clathrate structures

At least three types of clathrate hydrate structures are known. The two first types (I and II) contain 2 types of cages, one small and one large but in different proportion, while the last structure contain 3 types (Table and Figure 1) [5]. Several new clathrate phases have been discovered at high pressure but their structure are still unknown. The maximum amount of gas molecules that can be trapped relative to H₂O is 8/48 (17.4%) for structure I and 24/136 (17.65%) for structure II and H. But the filling of the cage is rarely 1. Clathrates are thus non-stoichiometric compounds.

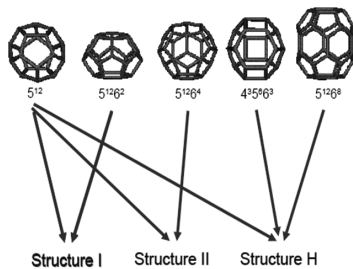


Figure 1: The different cage types of the three known structures of clathrate hydrates

The encaged molecules

The ability for one species to be included as a guest in one of these clathrate structures depends on many parameters: its size and shape relative to the cages, its type and interaction with H₂O, its partial pressure at the temperature of the system (should be above the equilibrium pressure of the corresponding clathrate hydrate), the presence of other clathrate-forming molecules, ... without speaking about formation kinetics which is frequently a strong limiting factor and a very complex and poorly known issue.

A strong ability to form H-bond (strong proton-donor species: NH₃, CH₃OH ?, ...) with H₂O precludes the formation of a clathrate structure in favour of stoichiometric hydrates. Proton acceptor molecules (H₂CO, C₂H₄O, ...) form a weak H-bond with the H₂O lattice and can be efficiently trapped inside clathrate cages. Non-polar and weak proton-donor species (Ar, Xe, CH₄, CO₂, C₃H₈, H₂S,...) easily form clathrates with Van der Waals intermolecular potentials inside the cage which are frequently approximated with the Lennard-Jones & Devonshire (spherical) or Kihara (asymmetric) potentials. Statistical mechanical models [6] allow us to predict the equilibrium pressure of mixed clathrate but use several poorly constrained hypotheses on size and shape of cages and cage-species interactions. But recent ab-initio molecular dynamics have strongly improved our understanding of the cage interactions [7].

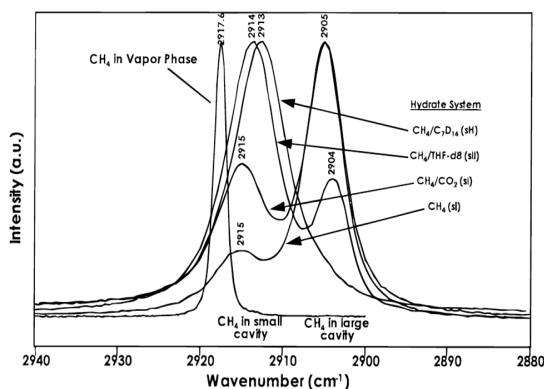
For single species clathrates the stable structure depends mostly on the species size. The smallest species (H₂, He, Ne) form structure I or II only at very high pressure, while small species (Ar, Kr, ...) form structure II by filling only the small cages, medium sized species (CH₄, Xe, ...) fill both cages of structure I and the larger species (CO₂, C₃H₈, ...) form either structure I or II by filling only their large cages. Even larger molecules they can only fit in the very large cage of structure H but additional smaller species are necessary to stabilize the structure by filling part of the other cages. Double clathrates (one species in the small cage and another in the large) or mixed clathrates (several species in the same cage type) can form in contact with a gas containing several species. The structure will depend on the relative species abundance. A « single clathrate » can also be stabilized by small amounts of other species or reversely can trap species that did not form clathrate at these T-P conditions (and thus form a mixed clathrate). The formation of mixed clathrates can lead to a strong gas fractionation in the clathrate cages. The structure of a mixed clathrate can also change depending on composition and temperature.

Cage occupancies by gas species depend on the encaged species, and on pressure and temperature. They can vary between 0 and 1 at low pressure. However at high pressure and for small molecules (H₂, N₂, ...) double occupancy of the large cages may occur. Small molecules can fill small and large cages, while medium sized ones may fill only part of the small cages and large molecules only fill fully or partly the large cages. In double and mixed clathrates it depends on the gas composition but the small cages are generally partly filled by the smaller molecule, if small enough to fit [8]. Taking into account cage filling the non-stoichiometric formula of clathrate is M.nH₂O, with n typically varying between 5.75 (full filling of structure I: CH₄, C₂H₂,...) to 17 (only filling of large cages of structure II: C₃H₈,...).

Depending on their size and shape and the cage in which they are trapped the molecules cannot rotate (most of the cases), or have some 1D rotation (e.g. CO₂ in large cages of structure II) or hindered libration, or have some free rotation (CH₄).

Clathrate spectroscopy

There are several interests to study the spectroscopic properties of clathrate hydrates. First the encaged molecules are isolated with a simple interaction potential within the cage (some being almost spherical) which is function of cage type and size. In such cages the almost free, limited or hindered rotations or librations can be studied by varying cage size with temperature. Some forbidden bands, such as in CO₂ can also be activated [2]. Some H-bond



interactions between proton-acceptor molecules and H₂O network are also of great interest. At very high pressure molecule-molecule interactions (dimers, ...) may be studied when double occupancy of large cages occurs. But one of the major advantage of the clathrate structure is to allow molecule trapping at much higher temperatures (up to 290 K!) than rare gas matrices. Hot bands may thus also possibly studied.

Figure 2: Raman spectra of CH₄ in double clathrate hydrates of structures I, II and H [9]

Spectral characteristics

The major characteristics of the infrared spectra of single clathrate relative to the spectrum of the pure gas or solid phases of the trapped species is a splitting of the vibration bands in two components corresponding to the molecules trapped in the two different cage types (if both occupied). The position of these bands are frequently shifted to lower frequency relative to the gas phase with a larger shift for the large cage. This is opposite to what was expected in a confined environment with more free space in the large than in the small cages. Recently ab-initio calculation for CH₄ have shown that the molecule-H₂O network interactions lead in fact to an elongation of the molecule bonds [7]. But in some cases the shift may be opposite, as for C₃H₈ in the large cages of structure II. These interactions are quite sensitive to thermal changes in cage size and induce very strong band width changes, generally linked to molecule hindered librations, and small band shifts with temperature [3,8,10,11]. Sometimes bands can

have some sub-structure due either to molecule rotation inside the cage or due to some symmetry lowering (several sites or orientations in the cage). More generally the sign and amplitude of the shifts as well as the temperature sensitivity of the bandwidth and rotational structure depend on the molecule, the vibration mode and on the structure and cage type [9].

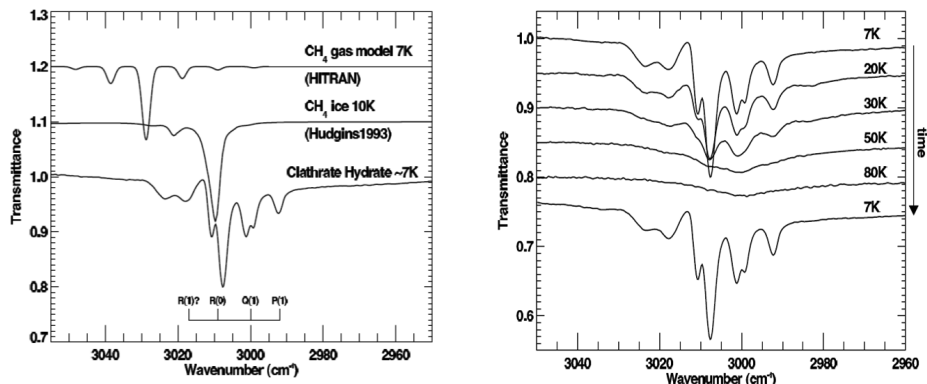


Figure 3: Infrared spectra of CH₄ clathrate hydrates: a) at 7K compared to gas and solid phases, showing its rotational structure in the both cages. b) as a function of temperature with strong temperature dependence [3].

In single clathrate the doubling of bands occurs only when the 2 cages are occupied. The band intensity ratio being then equal to the cage occupation ratio (assuming identical molecular band strength). For double clathrate, each species being in one type of cage there is only one band per species. But in mixed clathrate each species can be in one or two types of cage so band doubling occurs for at least one species [8,9].

References

- [1] P. Englezos, *Ind. Eng. Chem. Res.*, **32**, 1251-1274 (1993)
- [2] D. Mahajan, C.E. Taylor, G.A. Mansoori, *J. Petroleum Sci. Eng.*, **56**, 1–8 (2007)
- [3] E. Dartois, D. Deboffle, *Astron. Astrophys.*, **490**, L19-L22 (2008)
- [4] E. Dartois, B. Schmitt, *Astron. Astrophys.*, **504**, 869-873 (2009)
- [5] A. Koh, A.K. Sum, E.D. Sloan, *J. Appl. Phys.* **106**, 061101 (2009)
- [6] J.H. van der Waals, J.C. Platteeuw, *Adv. Chem. Phys.*, **2**, 1-56 (1959)
- [7] J.S. Tse, *J. Supramol. Chem.*, **2**, 429-433 (2002)
- [8] E. Dartois, D. Deboffle, M. Bouzit, *Astron. Astrophys.*, **514**, A49 (2010)
- [9] A.K. Sum, R.C. Burruss, E.D. Sloan, *J. Phys. Chem. B*, **101**, 7371-7377 (1997)
- [10] K. Consani, G.C. Pimentel, *J. Phys. Chem.*, **91**, 289-293 (1987)
- [11] E. Dartois, *Icarus*, **212**, 950-956 (2011).

Ultrafast Dynamics Following Photoionization in Water: From Clusters to the Aqueous Bulk

Ondřej Maršálek, Frank Uhlig, and Pavel Jungwirth

Institute of Organic Chemistry and Biochemistry, Academy of Sciences of the Czech Republic, Flemingovo nám. 2, 16610 Prague 6, Czech Republic, e-mail: pavel.jungwirth@uochb.cas.cz

Interaction of water with ionizing radiation is, in addition to direct DNA damage, causing radiation damage in living organisms and it is also important for nuclear waste treatment. Upon photoionization in water an electron and a cationic hole are formed. We present a computational study of the structure and dynamics of an excess electron in a medium-sized water cluster aimed at addressing the question of interior vs. exterior solvation, electron localization and its quenching with a hydrated proton leading to the formation of a hydrogen atom.¹⁻²

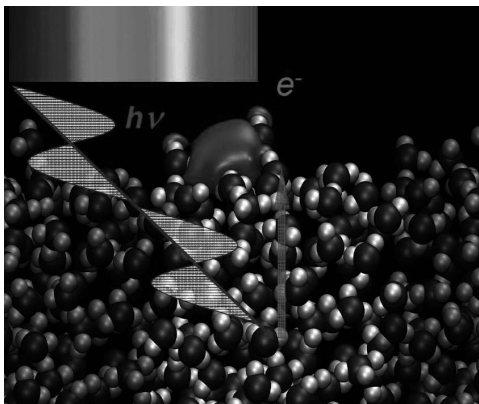


Figure 1: A schematic picture of photoionization in water leading to the formation of a solvated electron.

References

- [1] Marsalek, O.; Uhlig, F.; Frigato, T.; Schmidt, B.; Jungwirth, P.: Dynamics of Electron Localization in Warm versus Cold Water Clusters. *Physical Review Letters*, 2010, 114, 043002.
- [2] Marsalek, O.; Frigato, T.; VandeVondele J.; Bradforth, S. E.; Schmidt, B.; Schuette, C.; Jungwirth, P.: Hydrogen forms in water by proton transfer to a distorted electron. *Journal of Physical Chemistry B*, 2010, 114, 915.

Highest resolution Fourier transform infrared (FTIR) spectroscopy of polyatomic molecules with and without synchrotron radiation

Sieghard Albert¹, Karen Keppler Albert¹, Philippe Lerch² and Martin Quack¹

¹ *Physical Chemistry, ETH Zurich, CH-8093 Zurich, Switzerland, albert@ir.phys.chem.ethz.ch*

¹ *Swiss Light Source, PSI, CH-5232 Villigen, Switzerland*

Abstract

We discuss the analysis of the high resolution FTIR spectra of the bicyclic compounds naphthalene, azulene and indole measured with synchrotron radiation in the context of the identification of the unidentified infrared bands (UIB). The FTIR spectra of phenol and aniline have been analysed to get a deeper insight into the torsional dynamics of the OH and NH₂ groups. The analysis of the spectra of the chiral compounds CDBrClF and CHBrIF might be the starting point to conduct line shifts experiments using ultra-high resolution devices for the experimental detection of parity violation.

Introduction

Impressive progress has been made in the field of high resolution Fourier transform infrared (FTIR) spectroscopy regarding resolution and sensitivity over the last decade [1-3]. In particular, the rise and use of synchrotron sources [4] have overcome one of the strategic disadvantages of high resolution FTIR spectroscopy, the problem of noise due to broad band coverage. In particular, due to the application of synchrotron radiation the THz region becomes now accessible for high resolution studies. This state-of-the-art FTIR spectroscopy makes it now possible to investigate scientific question of fundamental physics and astrophysics. After a brief discussion of the different FTIR setups of the Zurich group we will review three examples on which we currently work in Zurich. One of the great challenges of astronomical infrared spectroscopy is the identification of the Unidentified Infrared Bands (UIBs) found in several interstellar objects. Polycyclic Aromatic Hydrocarbons (PAHs) have been proposed to be the carrier of the UIBs [5]. For that reason we have started to investigate the rotationally resolved FTIR spectrum of the bicyclic molecules naphthalene (C₁₀H₈) [4] and azulene (C₁₀H₈) as a simple prototypical spectrum for a PAH infrared spectrum and of indole (C₈H₆N) as a prototype of a bicyclic heteroaromatic system. The understanding of the dynamic behavior of functional groups like the hydroxyl (OH) [6], the amino (NH₂) [7] or the aldehyde (CHO) group in biomolecules is essential for a complete understanding of their biochemical processes. In particular, tunneling processes which are generally neglected in classical biomolecular dynamics modeling are in fact important and deserve study. For that reason we have investigated the torsional tunneling dynamics of phenol (C₆H₅OH), aniline (C₆H₅NH₂) and benzaldehyde (C₆H₅CHO) as benchmark molecules using high resolution ($\Delta\nu = 20$ MHz) FTIR spectroscopy with synchrotron radiation. In the last part, we illustrate, how high resolution FTIR spectroscopy might help to experimentally detect molecular parity

violation in chiral molecules [8,9]. The experimental detection of molecular parity violation $\Delta_{PV}E$ is of great interest because of its importance for the understanding of fundamental aspects of molecular dynamics and symmetries [9]. One possible method for this is measuring rovibrational or rotational frequency shifts predicted for the infrared or microwave spectra of enantiomers. A value of 50 mHz is predicted for vibrational frequency shifts in CHBrFI [10]. For that reason we have analysed the rovibrationally resolved spectra of CHBrCIF [11], CDBrCIF and CHBrFI.

Experimental setup

The Zurich group uses two high resolution FTIR spectrometer setups. The first setup, the Zurich prototype FTIR spectrometer 2001 consists of a Bruker IFS 120/125 nine chamber interferometer with an unapodized resolution of 0.00075 cm^{-1} and several external cells, in particular a collisional cooling cell [12] which makes measurements possible down to 5 K. This cooling cell was used to measure the FTIR spectra of different methane isotopomers in the range from 1200 to 12000 cm^{-1} [13]. Recently, we have extended our instrumentation with a new 2009 eleven chamber prototype Bruker spectrometer, the ETH-SLS spectrometer (max. res. = 0.00058 cm^{-1}) which is connected to a synchrotron, the Swiss Light Source (SLS), located at the Paul-Scherrer-Institute (PSI).

Analysis of the spectra

The out-of-plane mode ν_{46} of naphthalene at $12.78\text{ }\mu\text{m}$ was assigned using graphic pattern recognition methods. More than 2400 absorption lines have been used to determine the spectroscopic constants. Based on the rotational constants, we have simulated the band at resolutions which are used for the interstellar detection of the UIBs. We have found a coincidence between the ν_{46} fundamental of naphthalene and the UIB at $12.78\text{ }\mu\text{m}$. We propose a method for the identification of UIBs based on the band shapes of *a*-, *b*- and *c*-type bands. In addition, we have analysed in high resolution the ν_{35} band of indole and the first overtone band $2\nu_{40}$ of indole as well as the ν_{44} band of azulene. Recently, we have measured biphenyl in the range $650\text{ to }900\text{ cm}^{-1}$ with synchrotron radiation. A comparison of the biphenyl FTIR spectrum with the UIBs in the range $13\text{ to }15\text{ }\mu\text{m}$ illustrates a coincidence between the UIBs at $13.6\text{ and }14.2\text{ }\mu\text{m}$ with the major biphenyl bands. One should note that the shape of the biphenyl bands is different from that of the naphthalene band at $12.8\text{ }\mu\text{m}$.

We have investigated the torsional tunneling of phenol, $\text{C}_6\text{H}_5\text{OH}$, in the electronic ground state upon excitation of different vibrational modes describing phenol with effective C_{2v} symmetry. If the torsional splitting is considered, phenol belongs to the Longuet Higgins group M_{S4} group isomorphous to the C_{2v} point group which leads to a nuclear spin statistical weight of 10:10:6:6 for ee:eo:oo:oe and the torsional sublevel $\sigma=0$ and 6:6:10:10 for ee:eo:oo:oe and the torsional sublevel $\sigma=1$. The torsional splitting of the ground state is 56 MHz. The phenol spectra have been measured with the Zurich 2001 spectrometer and ETH-SLS spectrometer in the range $200\text{-}1300\text{ cm}^{-1}$ with a resolution up to 0.0007 cm^{-1} . It was possible to rovibrationally analyse the torsional fundamental ν_τ of phenol at 309.2 cm^{-1}

leading to a detection of a torsional splitting of the torsional excited state of 0.0896 cm^{-1} . As a further example of a THz spectrum of a large molecule we have analysed the rotationally resolved FTIR spectrum of aniline, $\text{C}_6\text{H}_5\text{NH}_2$, measured with the Swiss Light Source (SLS) in the range from 210 to 330 cm^{-1} . 40 scans have been averaged corresponding to a measuring time of 6 hours. This spectral range is the region of the NH_2 torsional mode of aniline which splits into two components due to the inversion splitting of the NH_2 group. The two inversion bands consist of b -type transitions and therefore the transitions are very weak. In addition, two other b -type bands have been identified.

We have analysed the spectrum of CDBrClF between 600 and 2300 cm^{-1} , which contains the ν_6 , ν_5 , ν_4 , ν_3 and $2\nu_4$ bands. CDBrClF is one of the simplest chiral molecules with C_1 point group symmetry. Due to the low symmetry of the molecule and the presence of four different isotopomers, CDBrClF has a highly congested spectrum. Different perturbations are observable in the spectra of the various isotopomers. In addition to the already known anharmonic resonance ν_2 , ν_3 and ν_4 , which can be neglected in the rovibrational spectra, we have found interesting local interactions in the ν_3 and $2\nu_4$ regions of the spectrum. We have assigned the spectra of the two major isotopomers $\text{CD}^{79}\text{Br}^{35}\text{ClF}$ and $\text{CD}^{81}\text{Br}^{35}\text{ClF}$. CDBrClF has been discussed as a prototype for demonstrating the importance of anharmonic vibrational interactions on parity violation [14].

The FTIR spectrum of CHBrFI was recorded at 190 K and 295 K in the regions 600 - 1300 cm^{-1} and 1800 - 2350 cm^{-1} with an instrumental resolution of better than 30 MHz and a pressure of 0.2 to 0.5 mbar . CHBrFI exists as a mixture of two major isotopomers $\text{CH}^{79}\text{BrFI}$ and $\text{CH}^{81}\text{BrFI}$. Due to the two heavy atoms the rotational structure of the bands is dense, extremely congested and complicated. Hybrid bands of a - and b -types have been observed. We were able to analyse the rovibrational spectra of $\text{CH}^{79}\text{BrFI}$ ($\nu_0 = 1060.8157\text{ cm}^{-1}$) and $\text{CH}^{81}\text{BrFI}$ ($\nu_0 = 1060.7786\text{ cm}^{-1}$) in the CF-stretching (ν_6) and its overtone region with band centers $\nu_0 = 2103.7573\text{ cm}^{-1}$ for $\text{CH}^{79}\text{BrFI}$ and $\nu_0 = 2103.6597\text{ cm}^{-1}$ for $\text{CH}^{81}\text{BrFI}$. The overtone region is important because Doppler-free quasi-resonant two photon transitions can be conducted on these bands. In addition, we have measured the 600 to 900 cm^{-1} region with our synchrotron source at a resolution of 20 MHz . The bright synchrotron radiation improves the signal-to-noise ratio compared to classical thermal source-based FTIR spectroscopy by a factor up to 20 and is now comparable to laser sources. These advantages, better signal-to-noise ratio and higher resolution, made it possible to analyse the FTIR spectrum of CHBrFI in the ν_5 region.

Conclusion

The use of new bright light sources like synchrotron radiation overcomes the resolution and noise limitations of thermal sources and opens the route for more highly resolving interferometers by extending the maximum optical path difference to new dimensions. We were able to resolve the rovibrational structure of bands of naphthalene, azulene and indole at

room temperature. We have determined the spectroscopic constants of these bands and based on these constants we have been able to simulate the spectrum. Considering the biphenyl spectra we have found three coincidences with UIB bands, the 12.8 μm naphthalene band and the 13.6 μm and 14.2 μm biphenyl bands. We have probed the torsional tunneling dynamics of phenol in the first torsional excited state and upon excitation of other OH modes and detect large changes of the tunneling time up to a factor of 40. The torsional dynamics in aniline is complicated due to the inversion dynamics. We have identified the two inversion components rovibrationally resolved due to inversion splitting in the torsional fundamental of aniline and have detected within each inversion-torsional component two bands. Based on our rovibrational analysis of the overtone region of CHBrFI we propose to use ultra-high resolution frequency comb laser spectroscopy around 2100 cm^{-1} to measure the predicted frequency shifts of 50 mHz due to parity violation.

Acknowledgement

Our work is supported financially by the Schweizerischer Nationalfonds, ETH Zürich and the Paul-Scherrer-Institute.

References

- [1] S. Albert, K. K. Albert, and M. Quack, *Trends in Optics and Photonics* **84**, 177 (2003).
- [2] S. Albert and M. Quack. *ChemPhysChem* **8**, 1271 (2007).
- [3] S. Albert, K. K. Albert and M. Quack, *High Resolution Fourier Transform Infrared Spectroscopy*, in *Handbook of High-Resolution Spectroscopy*, (Eds. M Quack and F Merkt), Wiley, Chichester (2011), 965-1021.
- [4] S. Albert, K.K. Albert, Ph. Lerch, M. Quack, *Faraday Discussions* **150**, 71-99 (2011).
- [5] A.G.G.M. Tielens, *Annu. Rev. Astron. Astrophys.* **46**, 289 (2008).
- [6] S. Albert, K.K. Albert, Ph. Lerch, M. Quack, *Faraday Discuss.* (2011) , **150**, 517-519.
- [7] B. Fehrensen, D. Luckhaus and M. Quack, *Chem. Phys.* **338**, 90 (2007).
- [8] M. Quack, J. Stohner and M. Willeke, *Annu. Rev. Phys. Chem.* (2008) **59**, 741.
- [9] M. Quack, *Fundamental Symmetries and Symmetry Violations from High Resolution Spectroscopy*, in *Handbook of High-Resolution Spectroscopy*, (Eds. M Quack and F Merkt), Wiley, Chichester (2011).
- [10] J.K. Laerdahl, P. Schwerdtfeger and H.M. Quiney, *Phys. Rev. Lett* **84**, 3811 (2000).
- [11] A. Bauder, A. Beil, D. Luckhaus, F. Müller and M. Quack, *J. Chem. Phys.* **106**, 7558 (1997).
- [12] S. Albert, S. Bauerecker, M. Quack, and A. Steinlin, *Mol. Phys.* **105**, 541 (2007).
- [13] S. Albert, S. Bauerecker, V. Boudon, L.R. Brown, J.P. Champion, M. Loete, A. Nikitin, and M. Quack, *Chem Phys* **356**, 131 (2009).
- [14] M. Quack and J. Stohner *J. Chem. Phys.* **119**, 11228 (2003).

IR and THz spectroscopy of cold molecular ions

Stephan Schlemmer, Oskar Asvany and Sandra Brünken

I. Physikalisches Institut, Universität zu Köln, Zùlpicher Strasse 77, 50937 Köln, Germany

Molecular ions play an important role in a wide variety of environments. They are identified by their spectra in particular in the IR and FIR range where molecular vibrations are characteristic for their specific bonds and the rotational or ro-vibrational spectra can be used to reveal the molecular structure. Traditional spectroscopic methods are often not sensitive enough to record spectra of these elusive species. Due to the production mechanisms, a discharge in most cases, a large variety of species with similar spectra is generated, see e.g. [1]. Relatively high-temperatures are also associated with the production process. These effects lead to spectral congestion and to limitations in spectral resolution.

Mass selection of the ion of interest combined with long time storage in higher order multipole ion traps along with buffer gas cooling is nowadays widely used to overcome all of the above limitations. Various ways of action spectroscopy have been employed to record the excitation process of the stored ion. In favorable cases one photon carries enough energy to eventually dissociate the parent ion. A spectrum is obtained by recording the number of photo-products as a function of excitation wavelength. Examples of this technique will be presented in John Maier's contribution with examples of electronic spectra. In order to record vibrational spectra of molecular ions often absorption of several photons (IRMPD, see e.g. [2]) also leads to fragmentation. Alternatively an additional IR photon is used to deplete the fragmentation signal which has been generated by the dissociating laser, see e.g. [3]. Another alternative is the use of a messenger atom or molecule which detaches from the parent ion upon excitation, a method pioneered already in the late 1980s in Y.T. Lee's group.

All these methods make use of a unimolecular decay of the parent molecule or a cluster containing this ion. In our method bimolecular reactions are studied in a 22-pole ion trap at cold temperatures. Endothermicities or barriers to reaction can often be overcome by excitation of the parent molecular ions. In our experiments excitation of ro-vibrational and even pure rotational transitions are used to promote the formation of ionic reaction products. Due to the very efficient ion detection this method employs an ultra-sensitive technique of action spectroscopy of cold, mass selected ions when recording the number of products as a function of the excitation wavelength. Employing bimolecular reactions allows for the investigation of a large set of molecular ions which otherwise are hard to address.

Proton transfer reactions and deuterium exchange reactions are two prominent classes of reactions which have been used for our light induced reaction (LIR) technique. Example molecules studied to-date are N_2^+ [4], C_2H_2^+ [5], H_2D^+ [6], CH_2D^+ [7] and CH_5^+ [8]. High-resolution spectra for those molecules are obtained using a home-built cw IR OPO system

and THz radiation sources. Due to the low temperatures in the trap the Doppler width can be reduced substantially. As a result accuracies of present IR spectra are high enough ($\Delta\nu \leq 1$ MHz) to make predictions for astronomical searches of molecular ions. The use of a frequency comb in combination with an atomic clock and a wavemeter will further improve the accuracy of the observed transitions and replace the cumbersome use of calibration lines and etalon fringes.

The molecular collision is an inherent part of the experimental method. At low temperatures only a few states of the ion and the neutral collision partner are populated. As a result state-specific processes start to govern the reactivity and can be unraveled in our experiments. One interesting example concerns the near thermoneutral proton transfer from H_2 to O_2 . Current technical developments for a further generalization and improvement of the method will be discussed. Two new instruments are built in our laboratory, one of which will be available as an instrument at the free electron laser facility (FELIX) in Nijmegen. Collaborations making use of this new instrument are welcome.

References

- [1] M. Jagod, M. Rösslein, C. M. Gabrys, B. D. Rehfuss, F. Scappini, M. W. Crofton, and T. Oka, *J. Chem. Phys.* **97**, 7111 (1992).
- [2] J. Oomens, A.G.G.M. Tielens, B.G. Sartakov, G. von Helden and G. Meijer, *Astrophysical Journal* **591** 968–85 (2003).
- [3] J.A. Stearns, M. Guidi, O.V. Boyarkin, and T.R. Rizzo, *J. Chem.Phys.* **127**, 154322 (2007).
- [4] S. Schlemmer, T. Kuhn, E. Lescop, and D. Gerlich, *Int. J. Mass Spectrometry and Ion Processes*, **185-187**, 589-602, (1999).
- [5] S. Schlemmer, E. Lescop, J. von Richthofen, D. Gerlich, and M. Smith, *J. Chem. Phys.* **117**, 2068-2075 (2002).
- [6] O. Asvany, E. Hugo, F. Müller, J. Tennyson F. Kühnemann, S. Schiller, and S. Schlemmer, *J. Chem. Phys.* **127** 154317 (2007). O. Asvany, O. Ricken, H.S.P. Müller, M.C. Wiedner, T.F. Giesen, and S. Schlemmer, *Phys. Rev. Lett.* **100**, 233004 (2008)
- [7] S. Gaertner, J. Krieg, A. Klemann, O. Asvany and S. Schlemmer, *Astron. Astrophys.*, 516 (2010) L3.
- [8] O. Asvany, P. Kumar, I. Hegemann, B. Redlich, S. Schlemmer and D. Marx, *SCIENCE* **309**, 1219-1222 (2005), S.D. Ivanov, O. Asvany, A. Witt, E. Hugo, G. Mathias, B. Redlich, D. Marx and S. Schlemmer, *Nature Chemistry*, **2**, 298–302 (2010).

Electron driven reactions in doped He nanodroplets

Christian Leidlmair¹, Peter Bartl¹, Harald Schöbel¹, Lukas an der Lan¹, Samuel Zöttl¹, Matthias Daxner¹, Odin Mack¹, Benjamin Puschnigg¹, Violaine Vizcaino¹, David Gschliesser¹, Johannes Postler¹, Michaela Hager¹, Stephan Denifl¹, Andrew M. Ellis², Olof Echt³ and Paul Scheier¹

¹ *Institut für Ionenphysik und Angewandte Physik, Universität Innsbruck, Technikerstr. 25, A-6020 Innsbruck, Austria, paul.scheier@uibk.ac.at*

² *Department of Chemistry University of Leicester, Leicester LE1 7RH, UK*

³ *Department of Physics, University of New Hampshire, Durham NH 03824, USA*

Ultra-cold molecular complexes are formed via sophisticated pickup experiments inside He nanodroplets that provide an isothermal matrix at 0.38K. During the growth of these complexes, the evaporation of He atoms removes excess energy, released by the adsorption of each species, and cools the complex before the next atom or molecule arrives. The resulting complexes are expected to be very similar to those formed in cold interstellar clouds. Ionization of these complexes is achieved via electron collisions and high-resolution mass spectrometry is utilized to measure their properties, such as binding energy and structure. Furthermore, various ionization pathways are identified and studied in detail. Novel mechanisms such as sequential Penning ionization lead to efficient energy harvesting of ionic dopants. Competition between energy deposition and efficient cooling by the superfluid He droplet leads to interesting reaction products. The results are relevant to fundamental aspects of low-temperature physics, chemistry, and surface chemistry and are expected to find application in astrophysics and astrochemistry.

Experimental

Helium droplets are produced by expanding ultra-pure ⁴He (99.9999%) at a stagnation pressure of 1-3 MPa through a 5 μm diameter aperture into vacuum. The nozzle is mounted on a copper cylinder which is cooled to 6-15 K by a closed-cycle cryostat (Sumitomo RDK-415 F50H). The stagnation pressure and temperature determine the size of the resulting helium droplets that can range from 10⁴ to several 10⁶ atoms [1,2]. A few millimeters downstream of the nozzle, the helium droplets pass through a conical skimmer and enter a series of pickup chambers. Up to four of these differentially pumped pickup regions can be attached where doping of the He droplets by atoms or molecules from a stagnant gas target is achieved. The doped droplets are ionized subsequently by interaction with an electron beam. Depending on the electron energy anions or cations can be formed. The resulting ions are analyzed in various mass spectrometer systems having resolving power up to $m/\Delta m=10000$ (FWHM). Detailed information can be found in [3-5].

Results and Discussion

Submersion of alkali clusters in He droplets²

Small alkali clusters do not submerge in liquid helium nanodroplets. Instead they preferentially form in high spin states that reside on the surface of the nanodroplet. However, a recent theoretical prediction by Stark and Kresin [6], based on a classical description of the energetics of bubble formation for a fully submerged alkali cluster, suggests that the alkali clusters will submerge when they exceed a critical size. Ion efficiency curves for mass selected cluster ions reveal a distinct change when moving from small clusters to large clusters. This switch is attributed to cluster submersion, which is found to occur at $n > 20$ for Na_n [7] and $n > 70$ for K_n clusters. These values are in good agreement with the prediction by Stark and Kresin [6].

Multiply charged ion formation

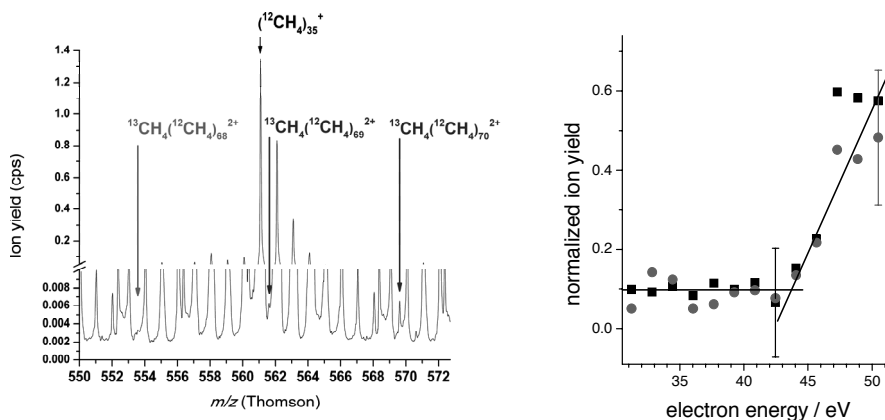


Figure 1: Left diagram: mass spectrum showing methane cluster dication formation near the threshold cluster size. The dications show a sudden onset at $n = 70$ carbon units. Right diagram: ion efficiency curves for $(\text{CH}_4)_{75}^{2+}$ and $(\text{CH}_4)_{77}^{2+}$ dications.

The dominant ionization mechanisms upon electron collisions with doped He droplets are charge transfer ionization from an initially formed He^+ or Penning ionization when an electronically excited He^* collides with the dopant. Whereas a second He^+ will be repelled by

² See contribution by M. Daxner et al.

the positive charge of a cationic dopant, metastable He^* , which is highly polarizable, will be dragged to the ion where it deposits almost 20eV of electronic energy. For atomic or molecular dopants with a second ionization energy lower than 19.8eV double ionization is observed [3]. The sum of the first and second ionization energy of a cluster is twice the ionization energy of the corresponding monomer plus the Coulomb repulsion of the two charges minus the solvation energy of the ion in the neighboring neutral monomers. This is much lower than the energy required to form a doubly charged monomer and thus double ionization of a cluster dopant is expected to be an efficient process. Depending on the stability of the multiply charged cluster, Coulomb explosion of the dopant will lead to the formation of lower-mass singly charged ions, or stable cluster dications for larger sizes. Figure 1 shows a section of a mass spectrum of methane doped He nanodroplets close to the critical size of $(\text{CH}_4)_n^{2+}$ together with the ion efficiency curves of two cluster dications. The threshold energy of the dications being about 44eV indicates that these ions are formed by a sequential process that involves charge transfer from He^+ and Penning ionization by He^* , which has a predicted threshold of about 44.5eV.

Decoration of fullerenes

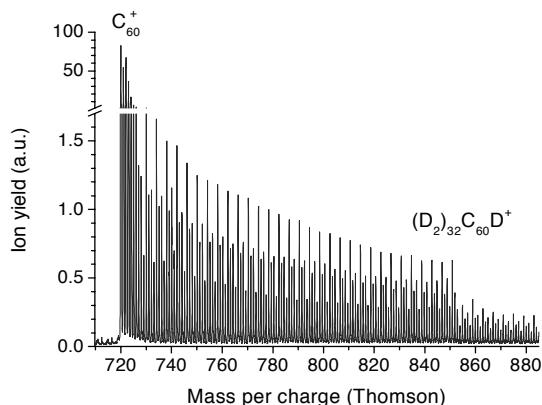


Figure 2: Mass spectrum of ions formed upon electron ionization of He nano-droplets doped with C_{60} and deuterium. Two ion series can be identified: $(\text{D}_2)_n\text{C}_{60}^+$ and, with higher intensity, $(\text{D}_2)_n\text{C}_{60}\text{D}^+$.

Mass spectra obtained via electron ionization of helium nanodroplets doped with C_{60} or C_{70} and various molecules clearly indicate that fullerene ions are easily decorated with other molecules and atoms including molecular hydrogen and helium [8-10]. Polar molecules such as water and ammonia form hydrogen bridged clusters attached to the fullerene cation [8,9]. In the case of non-polar molecules such as hydrogen, methane or CO_2 co-doped with

fullerenes a uniform decoration of the fullerene faces is observed [10], leading to pronounced shell closures at $n=32$ and $n=37$ for C_{60} and C_{70} , respectively (see Figure 2). According to DFT calculations [11] the binding energy of H_2 physisorbed to C_{60}^+ is roughly 50 meV which suggests that neutral and charged fullerenes may very well be decorated with hydrogen in cold (10-15K) molecular clouds. Molecules with a stronger interaction to fullerenes will form complexes also at higher temperatures. Unexplained absorption lines observed in space could be a result of these decorated fullerenes. Additionally, chemical reactions in molecular adlayers can be expected analogous to molecular films on dust particles.

Acknowledgement

This work was supported by the Austrian Science Fund, Wien (FWF, projects P19073, L633, and I200 N29) and the European Commission (Cost action CM0601). C.L. and P.B. gratefully acknowledge a dissertation grant from the University of Innsbruck.

References

- [1] J.P. Toennies, A.F. Vilesov, *Angew. Chem. Int. Ed.* **43**, 2622 (2004)
- [2] F. Stienkemeier and K. K. Lehmann, *J. Phys. B: At., Mol. Opt. Phys.* **39**, R127 (2006)
- [3] H. Schöbel, P. Bartl, C. Leidlmair, M. Daxner, S. Zöttl, S. Denifl, T. D. Märk, P. Scheier, D. Spånberg, A. Mauracher, D. K. Bohme, *Phys. Rev. Lett.* **105**, 243402 (2010)
- [4] F. Ferreira da Silva, S. Ptasinska, S. Denifl, D. Gschliesser, J. Postler, C. Matias, T.D. Märk, P. Limao-Vieira, P. Scheier, *J. Chem. Phys.* **135**, 174504 (2011)
- [5] S. Denifl, F. Zappa, I. Mähr, J. Lecointre, M. Probst, T. D. Märk, P. Scheier, *Phys. Rev. Lett.* **97**, 043201 (2006)
- [6] C. Stark, V. V. Kresin, *Phys. Rev. B* **81**, 085401 (2010)
- [7] L. An der Lan, P. Bartl, C. Leidlmair, H. Schöbel, R. Jochum, S. Denifl, T. D. Märk, A. M. Ellis, P. Scheier, *J. Chem. Phys.* **135**, 044309 (2011)
- [8] S. Denifl, F. Zappa, I. Mähr, F. Ferreira da Silva, A. Aleem, A. Mauracher, M. Probst, J. Urban, P. Mach, A. Bacher, O. Echt, T. D. Märk, P. Scheier, *Angew. Chem. Int. Ed.* **48**, 8940 (2009)
- [9] H. Schöbel, C. Leidlmair, P. Bartl, A. Aleem, M. Hager, O. Echt, T.D. Märk, P. Scheier, *Phys. Chem. Chem. Phys.* **13**, 1092 (2011)
- [10] C. Leidlmair, P. Bartl, H. Schöbel, S. Denifl, M. Probst, P. Scheier, O. Echt, *ApJ* **738**, L4 (2011)
- [11] P.A. Denis, *J. Phys. Chem. C* **112**, 2791 (2008)

Mixed quantum classical dynamics including laser interactions and spin-orbit coupling

Philipp Marquetand¹, Martin Richter², Jesús González-Vázquez³, Juan José Bajo³, Ignacio Sola³, Jesus Santamaria³ and Leticia González¹

¹ *Institut für Theoretische Chemie, Universität Wien, Währinger Str. 17, 1090 Wien, Austria, philipp.marquetand@univie.ac.at*

² *Institut für Physikalische Chemie, Universität Jena, Helmholtzweg 4, 07743 Jena, Germany*

³ *Departamento de Química Física I, Universidad Complutense, 28040 Madrid, Spain*

Introduction

A prominent aim in cutting-edge science is to unravel ultrafast processes in systems of increasing complexity. Experiments are nowadays possible using laser pulses in the femto- or attosecond regime on molecules consisting of thousands of atoms. New theoretical techniques are necessary to keep pace and to study the interaction of electrons and nuclei with strong laser fields in multiple molecular states including also relativistic effects.

The SHARC method

We have recently developed a mixed quantum-classical dynamics (MQCD) code including arbitrary couplings as a general tool for studying excited-state processes in full dimensionality [1]. In our approach, the quantum and the classical parts are linked via a modified version of Tully’s surface hopping (SH) scheme [2]. Similar approaches [3–8] also rely on SH and are able to treat either dipole couplings or spin-orbit couplings in addition to the nonadiabatic couplings originally handled by Tully. However, to our knowledge, we treat explicitly spin-orbit coupling and dipole couplings simultaneously for the first time in MD. Up to now, spin-orbit couplings are not included in standard ab initio MD packages and the description of laser interactions in MD is in its infancy [9]. In our new method, termed SHARC (surface-hopping-in-the-adiabatic-representation-including-arbitrary-couplings), we treat all couplings on the same footing using a unitary transformation [1]. The central equation in the original surface hopping scheme describes the probability $P_{\beta\alpha}$ for a hop from one potential surface to another one:

$$P_{\beta\alpha} = \frac{2\Re \left\{ c_{\beta}^*(t)c_{\alpha}(t) \left[\frac{i}{\hbar} H_{\beta\alpha} + K_{\beta\alpha} \right] \right\}}{c_{\beta}^*(t)c_{\beta}(t)} \Delta t \quad (1)$$

Here, \Re denotes the real part, $c_{\alpha,\beta}$ are the amplitudes of the respective basis function corresponding to state α, β , H is the Hamiltonian matrix, K contains the kinetic

couplings, and Δt is the time step. A very important point in the surface hopping scheme is the choice of the basis functions. Tully [2] demonstrated that surface hopping is not invariant with respect to the representation and he recommended to work in the adiabatic basis. In this case, the potential matrix H is always diagonal and the coupling between the surfaces is included in the kinetic part K . Note that in contrast, it is desirable to work in the diabatic regime in quantum dynamics (QD), where the K matrix is always zero and the coupling between the different electronic basis functions is included in the off-diagonal elements of the potential matrix H . Most *ab initio* quantum chemistry programs yield potential energies in the adiabatic representation. However, as the spin-orbit coupling and the electric-field interaction entering through the dipole moment matrix (permanent and transition ones) are not included when obtaining the electronic wave functions, they are usually incorporated *a posteriori* in the potential part of the Hamiltonian. The resulting Hamiltonian matrix cannot be called adiabatic anymore although the so-called “adiabatic” potential surfaces are employed. In order to include the effect of the spin-orbit coupling and the electric field interaction in the classical motion, we proposed in Ref. [1] to “fully” adiabaticize (denoted by the index a) the Hamiltonian matrix with respect to any arising coupling. We employ a unitary transformation U which leads to a modified equation for the hopping probability:

$$P_{\beta\alpha} = \frac{2\Re \left\{ c_{\beta}^a(t)^* c_{\alpha}^a(t) \left[\frac{i}{\hbar} H_{\beta\alpha}^a + K_{\beta\alpha}^a \right] \right\}}{c_{\beta}^a(t)^* c_{\beta}^a(t)} \Delta t. \quad (2)$$

The new matrix K^a contains two different terms, one due to the previous K matrix rotates to the new representation and the other due to the time variation of the U matrix.

Numerical applications

In order to test the method, IBr is taken as a model system, since spin-orbit coupling plays an important role in its dissociation dynamics. Additionally, the influence of laser control via the non-resonant dynamic Stark effect (NRDSE) is investigated [10], motivated by the recent experiment of Stolow and coworkers [11].

The IBr molecule initially in the electronic ground state (black, see Fig. 1a) is excited to the $1^3\Pi_{0+}$ excited electronic state (red) and can undergo dissociation into two different channels due to SOC with the $1^3\Sigma_{0+}^-$ excited state (turquoise). Excited state dissociation in these two states results in $I + Br$ and $I + Br^*$ (the asterisk indicates the spin-excited state), respectively.

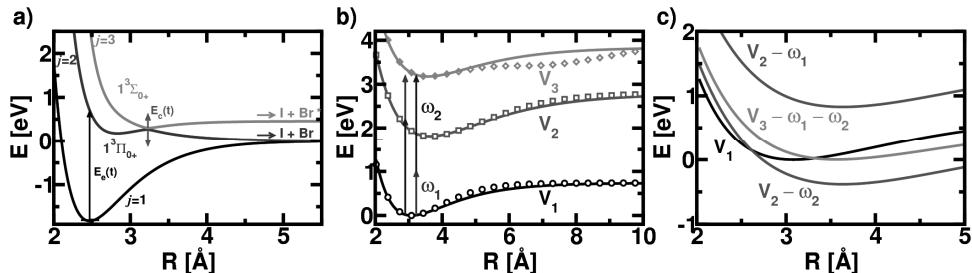


Figure 1: Selected model systems: a) Potential energy curves of the IBr molecule and excitation scheme. b) Potential energy curves of the Na_2 molecule. The curves for the electronic states $1^1\Sigma_g^+$ ($3s$) (circles), $1^1\Sigma_u$ ($3p$) (squares) and $1^3\Sigma_g^+$ ($4s$) (diamonds) are fitted by the potentials V_1 , V_2 and V_3 , and the frequencies of the two laser fields employed in the APLIP control scheme (ω_1 and ω_2) are indicated. c) Floquet representation constructed with the original V_1 , V_2 and V_3 , where laser pulses are included in the different potentials.

After simulating an electronic excitation of the IBr molecule with a resonant laser, the branching ratio in the two channels is influenced with a second, nonresonant laser. We illustrate how this NRDSE process can be modeled within SHARC. Fig. 2 reveals that identical processes are described by exact QD and SHARC calculations.

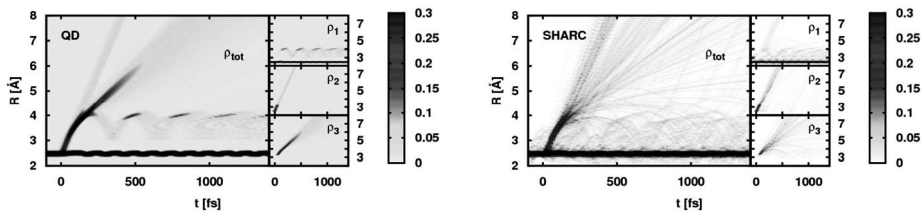


Figure 2: Probability density in the IBr molecule for a time delay of 90 fs between excitation and NRDSE control pulse. Results from SHARC are shown on the right, output from QD on the left. The respective large panel shows the total probability density and the small panels show the fractions of the same density belonging to the adiabatic states j as indicated.

A further study has applied SHARC, where the APLIP (Adiabatic Passage by Light-Induced Potential) scheme [12] is simulated in Na_2 using the Floquet formalism (see Fig. 1b, c). The nuclear motion is influenced by the gradients of the laser-modified potentials and nonadiabatic couplings are seen as transitions between the light-induced potentials [13].

As MD allows for the handling of many atoms, the photo-induced dynamics including the interplay between triplet and singlet states of large molecular systems will be accessible. Current applications of the SHARC method to multidimensional molecular systems include the relaxation of DNA nucleobases via triplet states after photoexcitation.

Conclusion

To conclude, we have shown that our new SHARC algorithm is able to describe photophysical processes even at intermediate field strengths. Several scenarios have been modelled by our semiclassical method, where the surface hopping probabilities are calculated in terms of a unitary transformation matrix. Thus, SHARC is able to treat all kinds of couplings in molecular systems including all degrees of freedom on the same footing.

References

- [1] M. Richter, P. Marquetand, J. González-Vázquez, I. Sola, and L. González, *J. Chem. Theory Comput.* **7**, 1253 (2011).
- [2] J. C. Tully, *J. Chem. Phys.* **93**, 1061 (1990).
- [3] M. Thachuk, M. Y. Ivanov, and D. M. Wardlaw, *J. Chem. Phys.* **105**, 4094 (1996).
- [4] B. Maiti, G. C. Schatz, and G. Lendvay, *J. Phys. Chem. A* **108**, 8772 (2004).
- [5] G. A. Jones, A. Acocella, and F. Zerbetto, *J. Phys. Chem. A* **112**, 9650 (2008).
- [6] R. Mitrić, J. Petersen, and V. Bonacić-Koutecký, *Phys. Rev. A* **79**, 053416 (2009).
- [7] N. Shenvi, *J. Chem. Phys.* **130**, 124117 (2009).
- [8] I. Tavernelli, B. F. E. Curchod, and U. Rothlisberger, *Phys. Rev. A* **81**, 052508 (2010).
- [9] M. Barbatti, *WIREs Comput. Mol. Sci.* **1**, 620 (2011).
- [10] P. Marquetand, M. Richter, J. González-Vázquez, I. Sola, and L. González, *Faraday Discuss.* **153**, 261 (2011).
- [11] B. J. Sussman, D. Townsend, M. Y. Ivanov, and A. Stolow, *Science* **314**, 278 (2006).
- [12] B. M. Garraway and K. Suominen, *Phys. Rev. Lett.* **80**, 932 (1998).
- [13] J. J. Bajo, J. González-Vázquez, I. Sola, J. Santamaria, M. Richter, P. Marquetand, and L. González, *J. Phys. Chem. A* **submitted** (2011).

Crossed beam imaging of ion-molecule reactions

Roland Wester¹

¹ *Institute for Ion Physics and Applied Physics, University of Innsbruck, Technikerstr. 25/3
6020 Innsbruck, Austria, roland.wester@uibk.ac.at*

In this talk I will discuss experimental investigations of the dynamics of negative-ion reactions [1]. We employ crossed-beam ion imaging to measure energy- and angle-differential reactive scattering cross sections. Recently we introduced cryogenic ion trapping as a means to prepare translationally and internally cold reactant ions and ion clusters [2].

At the focus of our work is the nucleophilic substitution reaction [3], an important class of reactions in organic and synthetic chemistry. Results will be reported for the exothermic reactions of Cl^- , F^- and OH^- anions with CH_3I [4,5]. By analyzing the differential scattering cross sections for these systems, we have found several distinct and system-dependent reaction mechanisms that govern the dynamics at different collision energies. These results are compared with direct dynamics simulations.

Recently we have extended this work to reactions of small water cluster anions to investigate the influence of micro-solvation on chemical reaction dynamics. Many different dynamical features are observed that are also found to depend on the reactant cluster temperature. Comparison with unsolvated reactants hints at steric hindrance as an important motif for the observed differences in the reaction dynamics.

References

- [1] J. Mikosch, M. Weidemüller, R. Wester, *Int. Rev. Phys. Chem.* **29**, 589 (2010)
- [2] R. Wester, *J. Phys. B* **42**, 154001 (2009)
- [3] M. L. Chabinyc; S. L. Craig; C. K. Regan, J. I. Brauman, *Science* **279**, 1882 (1998)
- [4] J. Mikosch, S. Trippel, C. Eichhorn, R. Otto, U. Lourderaj, J. X. Zhang, W. L. Hase, M. Weidemüller, R. Wester, *Science* **319**, 183 (2008)
- [5] J. Zhang, J. Mikosch, S. Trippel, R. Otto, M. Weidemüller, R. Wester, W. L. Hase, *J. Phys. Chem. Lett.* **1**, 2747 (2010)

Molecular growth via ion-molecule and radical reactions. From planetary atmospheres to plasma reforming

Paolo Tosi and Daniela Ascenzi

Department of Physics University of Trento, Via Sommarive 14 38123 Trento Italy, paolo.tosi@unitn.it

Studies on the chemistry of planetary atmospheres and the interstellar medium have been historically focussed mainly on small molecules (see Ref. [1] as an example). Due to advances in infrared/ microwave astronomy and the settlement of space missions to outer planets, in more recent years the attention has shifted towards larger molecules, mostly of organic nature. A great research effort is focussed on the modelling of the hydrocarbon atmosphere of Titan, the second largest moon in the Solar system. Heavy ions with masses over 100 a.m.u. have been detected in significant amounts into Titan's ionosphere below 1200 km [2-4]. Possible chemical structures include PAHs, nitrile aromatic polymers, fullerenes and polyphenyls, and such heavy particles have been proposed to act as seeds for aerosols formations. In spite of several laboratory investigations, new experimental and theoretical data are still required to provide a quantitative comparison between the *in situ* observations of the Cassini orbiter and the proposed models [5]. Several mechanisms have been suggested for the growth of large organic molecules under extraterrestrial conditions and in the higher atmosphere of Titan, and the idea is put forward that complex molecules build up by association of pre-formed building blocks. To shed light on the growth mechanisms of aromatic hydrocarbons initiated by charged particles, we are investigating association processes affording covalently bound species, in particular C-C coupling reactions involving phenyl $C_6H_5^+$ [6], ethyl $C_2H_5^+$ [7], naphthyl $C_{10}H_7^+$ [8] and biphenyl $C_{12}H_8^+$ cations with neutral arenes.

Ion-molecule reactivity is investigated using tandem mass spectrometric techniques, which allow mass selection and manipulation of both reactant and product ions. The molecular ion under study is generated by dissociative ionization of an adequate precursor, either in an electron impact ion source or in an atmospheric pressure chemical ionization APCI source. The latter source allows the generation of molecular ions with a lower degree of internal excitation than the former. We can estimate absolute values of reactive cross sections as a function of the collision energy and branching ratios (from which rate constant values can be inferred). When carried out on large molecules, such studies pose several experimental and computational problems related to the increased number of degrees of freedom, and a complementary experimental and theoretical approach is the key to obtain reliable information on reaction mechanisms. We use DFT methods to calculate energy and structures of the most relevant points on the reactive potential hypersurface. Knowledge of the

chemistry following VUV ionization of nitriles is also necessary for interpreting astrophysical and astrochemical observations. We have investigated the photoinduced ion chemistry of acetonitrile by injecting tuneable VUV synchrotron radiation into an octupolar ion trap and detecting primary photoions and secondary ionic products deriving from self-reactions at thermal collision energies [9].

The growth of molecular systems initiated by charged particles or electrons is also of relevance for the chemistry occurring in non thermal plasma [10]. In addition to the already established applications of plasma in the field of material deposition, recently the plasma reforming of hydrocarbon feedstock begins to attract increasing interest for its potentially important contribution to the next generation of green technologies. This is mainly due to the ability of non-equilibrium plasma to generate reactive species at a much lower temperature than normal thermochemical reactions. An important example is the conversion of the greenhouse gases CO_2 and CH_4 in chemical fuels. Although this conversion is energy costly, it can be a promising way to store and transport sustainable energy if an energy efficient dissociation of CO_2 and CH_4 is achieved. By treating methane with argon or carbon dioxide in a dielectric barrier discharge at atmospheric pressure, we have observed the formation of a liquid, consisting of a mixture of branched hydrocarbons (C15-C25) and oxygenates [11]. This means that CO_2 and CH_4 are dissociated into the plasma producing radicals that undergo C-C bond coupling reactions.

References

- [1] P. Tosi, O. Dmitriev, D. Bassi, O. Wick, D. Gerlich, *J. Chem. Phys.* **100**, 4300 (1994).
- [2] J.-E. Wahlund, M. Galand, I. Müller-Wodarg, J. Cui, R.V. Yelle, F.J. Crary, K. Mandt, B. A. Magee, J.H. Waite Jr., D.T. Young, A.J. Coates, P. Garnier, K. Agren, M. Andre, A.I. Eriksson, T.E. Cravens, V. Vuitton, D.A. Gurnett, W.S. Kurth, *Plan. Space Sci.* **57**, 1857 (2009).
- [3] F.J. Crary, B.A. Magee, K. Mandt, J.H. Waite Jr., J. Westlake, D.T. Young, *Plan. Space Sci.* **57**, 1847 (2009).
- [4] M.L. Delitsky, C.P. McKay, *Icarus* **207**, 477 (2010).
- [5] I.P. Robertson, T.E. Cravens, J.H. Waite Jr., R.V. Yelle, V. Vuitton, A.J. Coates, J.E. Wahlund, K. Agren, K. Mandt, B.A. Magee, M.S. Richard, E. Fating, *Plan. Space Sci.* **57**, 1834 (2009).
- [6] D. Ascenzi, N. Cont, G. Guella, P. Franceschi, P. Tosi, *J. Phys. Chem. A* **111**, 12513 (2007).
- [7] J. Zabka, M. Polasek, D. Ascenzi, P. Tosi, J. Roithová, D. Schröder, *J. Phys. Chem. A* **113** 11153 (2009).

-
- [8] D. Ascenzi, J. Aysina, P. Tosi, A. Maranzana, G. Tonachini, *J. Chem. Phys.* **133**, 184308 (2010).
- [9] D. Ascenzi, P. Tosi, P. Franceschi, D. Catone, S. Turchini, K. C. Prince, *Chem. Phys.* in press (2011).
- [10] P. Tosi, D. Ascenzi, P. Franceschi, G. Guella, *Plasma Sources Sci. Technol.* **18**, 034005 (2009).
- [11] G. Scarduelli, G. Guella, D. Ascenzi, P. Tosi, *Plasma Process. Polym.* **8**, 25 (2011).

Deceleration and Velocity Filtering of Neutral Molecules in Electric Fields

Andreas Osterwalder¹

¹ *Institute of Chemical Sciences and Engineering, Ecole Polytechnique Fédérale de Lausanne, 1015 Lausanne, Switzerland, email: andreas.osterwalder@epfl.ch*

I will present recent developments in the deceleration and velocity filtering of polar neutral molecules in electric fields. By making use of the Stark effect, electric fields can be used to produce forces on neutral molecules. If these forces can be perpendicular to the translational motion of the molecule they provide access to guiding structures. If they are along the direction of translation, they allow for the acceleration or deceleration of the molecules.

The latter has led to a method called Stark-deceleration that has proven extremely powerful in applications to the investigation of both the spectroscopy and dynamics of polar molecules. We have recently developed a new Stark decelerator where the molecules are picked up and confined in moving three-dimensional electrostatic traps. The velocity of these traps can be modified, allowing the deceleration of the trapped molecules. Advantages of the new technique over traditional (switched) decelerators will be discussed.

As an alternative to decelerators, electrostatic guides can be used to extract the slow molecules from a thermal sample, resulting in a technically simpler approach than most deceleration methods. Since the Stark effect depends on the rotational state of a molecule, the guiding probability will also depend on the rotational quantum numbers. We have studied the state-dependent guiding probabilities in ammonia by recording REMPI spectra of the guided and filtered molecules and found only moderate change in the rotational temperature during the filtering procedure.

Optimal control by using parametrically polarization shaped laser pulses

Albrecht Lindinger

Institut für Experimentalphysik, Freie Universität Berlin, Arnimallee 14, D-14195 Berlin, Germany

e-mail: lindin@physik.fu-berlin.de

Abstract

Polarization pulse shaping is presented for coherent control of molecular systems. Moreover, in a parametric sub pulse encoding the physically intuitive sub pulse parameters including the polarization state are individually controlled. The application of such tailored pulses for coherent control is demonstrated in a feedback loop optimization of the multi-photon ionization of alkali dimers. This is also performed by transmitting the shaped pulses through a hollow core photonic crystal fiber which can be valuable for endoscopic applications.

Introduction

Optimal control of photo-induced molecular processes has attained considerable success in recent years. It became most exciting when self-learning feedback loop algorithms were employed where tailored laser pulses can be generated, which drive the induced processes at a maximum yield along desired paths. An important issue in this regard is the information coded in the optimized laser pulse shape which supplies insight about the underlying processes [1]. Small alkali systems are suitable since they exhibit bound states available for resonant transitions with weak fields which aids the theoretical description and thus the interpretation.

In the last years pulse shaping including polarization was explored in order to consider the vectorial character of the light field. Novel pulse shaper schemes for simultaneous phase, amplitude, and polarization pulse control were designed in our group, and a parametric sub pulse encoding was developed [2] (see Fig. 1). In this approach, the physically intuitive parameters energies, distances, and chirps, as well as the states of polarization of the sub pulses can be controlled. The application of such tailored pulses for coherent control was demonstrated in feedback loop optimizations of the multi-photon ionization of alkali dimers. The results show the perspectives of adding the polarization and hence utilizing all properties of the light field in the pulse modulation.

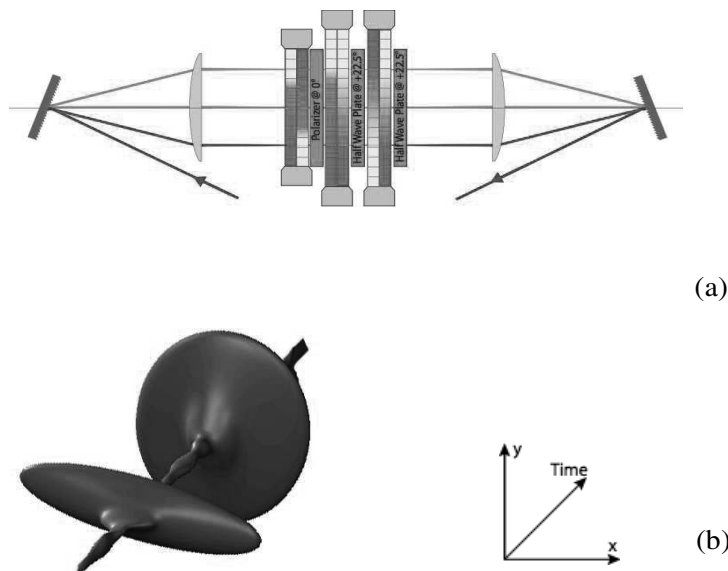


Figure 3. (a) Pulse shaper design for simultaneous modulation of phase, amplitude, and polarization. (b) 3-dimensional representation of a parametric polarization shaped laser pulse with sub pulses.

Results

Recently, we applied laser pulse shaping to optical fibers. Polarization shaped laser pulses were guided through photonic crystal hollow core fibers, and predetermined parametrically shaped laser pulses in phase, amplitude and polarization were achieved after the fiber by considering the linear, nonlinear, and polarization fiber properties [3]. This enabled us to steer molecular processes by utilizing these pulses for optimization processes in molecular systems. The application of these pulses for coherent control is demonstrated for feedback loop optimization of the multi-photon ionization of potassium dimers [4]. Fig. 2 shows the experimental sketch including the optimized pulse shape in a 3-dimensional representation and the ionization path via specific electronically excited states. Hence, even after optical fibers the optimized wave packet dynamics with the involved oscillations is revealed and the advantage of polarization shaping can be demonstrated leading to higher optimization factors due to the increased control dimension.

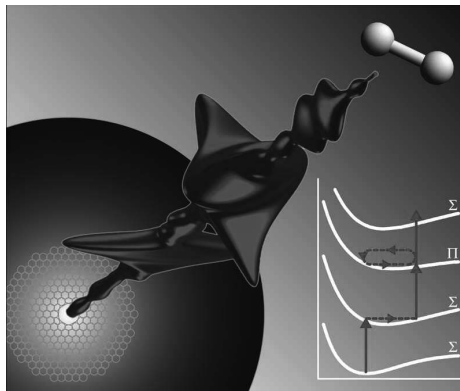


Figure 2. Schematic illustration of the experimental principle including the pulse shape for optimizing a 3-photon ionization process on K_2 molecules after transmission through a hollow core photonic crystal fiber. The inset displays the ionization path via the involved potential energy curves.

Moreover, a method was introduced to reconstruct the pulse shape at the distal end of the fiber by reflecting a part of the laser beam back through the fiber and detecting it [5]. This allows to characterize the pulse shape in endoscopic applications even if there is no space to place a detector at the distal end of the fiber. The presented endoscopic pulse shaping method will be particularly relevant for medical and near-field applications.

References

- [1] B. Schäfer-Bung, R. Mitrić, V. Bonačić-Koutecký, A. Bartelt, C. Lupulescu, A. Lindinger, Š. Vajda, S. M. Weber, and L. Wöste, *J. Phys. Chem. A* **108**, 4175 (2004).
- [2] F. Weise and A. Lindinger, *Appl. Phys. B* **101**, 79 (2010).
- [3] F. Weise, G. Achazi, and A. Lindinger, *Phys. Rev A* **82**, 053827 (2010).
- [4] F. Weise, G. Achazi, and A. Lindinger, *Phys. Chem. Chem. Phys.* **13**, 8621 (2011).
- [5] G. Achazi, A. Patas, F. Weise, M. Pawłowska, and A. Lindinger, *Appl. Opt.* **50**, 915 (2011).

Ion-Molecule Reaction Processes in a Molecular Beam-Ring Electrode Trap

Mark A. Smith^{1,2}, Bing Yuan¹ and Andrei Sanov¹

¹ *Department of Chemistry and Biochemistry, University of Arizona, Tucson, AZ 85721 USA*

² *Department of Chemistry, 216 Science and Research Bldg. 1, University of Houston, Houston TX 77204 USA*

Ion-Molecule Chemistry in the new Coaxial Molecular Beam-Radiofrequency Ring Electrode Trap (CoMB-RET)

We describe a new coaxial molecular beam radiofrequency ring electrode trap (CoMB-RET) for the study of ion-molecule reaction rates over a broad temperature range. This instrument is capable of delivering molecular beams from equilibrated effusive nozzles at temperatures ranging from 20-500K into a trapped ion cloud equilibrated via buffer gas cooling with an independently temperature tunable rf trap at temperatures between 20 and 500K. Extensive differential pumping allows for very long trap times even at high temperature and the chopped molecular beam allows for selective ion-molecule exposure times between 10 μ s and 1 s or longer. In this manner, it is possible to study the separate internal energy effects of both neutral and ionic reactants on reaction rate coefficients.

In this contribution, we will discuss the properties and capabilities of this instrument and present initial reaction studies. Following a discussion of the calibration reaction[1];



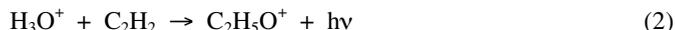
we will discuss two studies investigating oxygenation of organics, or oxygen fixation, in the system of H_3O^+ with acetylene.

Simple oxygenation of organics via H_3O^+ : Radiative association with C_2H_2 vs. reaction of C_2H_2 dimers

Production of oxygenated organics in the interstellar medium (ISM) possibly represents the first step towards the abiotic generation of molecules critical to life. Understanding their production mechanisms is important if we are to begin to understand the plethora of complex organics now known to exist in the ISM as well as on other planetary bodies beyond Earth. Acetaldehyde, CH_3CHO , is ubiquitous in interstellar environments and has been detected in a

variety of environments since it was first detected in 1973. These environments include hot cores, dark clouds, and regions of star formation [2,3].

Radiative association plays a significant role in gas phase molecular ion synthesis in dense interstellar clouds and planetary atmospheres [4-8]. The radiative association reaction between H_3O^+ and C_2H_2 monomer is considered as one of the most important steps for acetaldehyde production in the interstellar medium:



This is followed by recombination of an electron to produce CH_3CHO [7]. Protonated water is one of the most stable forms of oxygen containing molecular ions and understanding its reactive potential with small hydrocarbons present in natural environments is critical.

The independent neutral molecule and ion temperature dependence of the rate coefficient for reactions between H_3O^+ and $(\text{C}_2\text{H}_2)_2$ producing $\text{C}_2\text{H}_5\text{O}^+$ is determined using the coaxial molecular beam radiofrequency ring electrode ion trap (CoMB-RET). The rate coefficient for radiative association reaction between H_3O^+ and C_2H_2 monomer forming $\text{C}_2\text{H}_5\text{O}^+$ is also studied in this system. The temperature of the H_3O^+ was varied from 25 K to 170 K while the neutral molecule $\text{C}_2\text{H}_2/(\text{C}_2\text{H}_2)_2$ beam temperature was maintained at 160 K, 170 K, 175 K, 180 K and 200 K independently. For acetylene monomer study, the beam temperature was maintained above 300K to ensure the percent of acetylene dimer is less than 0.01%. The result demonstrates that acetylene dimer can be easily formed in the cold effusive molecular beam and its rate coefficient with H_3O^+ ions is close to the capture rate. The rate coefficient decreases as the collision pair translational center-of-mass, or effective, temperature increases. The binding energy of acetylene dimer deduced from the experimental data is $436 \pm 19 \text{ cm}^{-1}$. The rate coefficient of the H_3O^+ - C_2H_2 radiative association reaction is below $1 \times 10^{-13} \text{ molecule} \cdot \text{cm}^3$ when the effective temperature is 173K, consistent with the determination of Herbst[8].

Acknowledgements

We wish to thank Prof. Dr. Dieter Gerlich for his invaluable assistance with this project.

References

- [1] B. Yuan, Z. Scott, G. Tikhonov, D. Gerlich, and M. A. Smith, *J. Phys. Chem. A* **115**, 25–29 (2011)
- [2] Vigren, E.; Hamberg, M.; Zhaunerchyk, V.; Kaminska, M.; Thomas, R.D.; Trippel, S.; Zhang, M.; Kashperka, I.; Ugglas, M.; Walsh, C.; Wester, R.; Semaniak, J.; Larsson, M.; Geppert, W.D. *Phys. Chem. Chem. Phys.* **2010**, *12*, 11670-11673.

- [3] Fairly, D.A.; Scott, G.B.; Freeman, C.G.; Maclagan, R.G.A.R.; McEwan, M. *J. Chem. Soc., Faraday Trans.* **1996**, 92, 1305-1309.
- [4] Gerlich, D.; Horning, S. *Chem Rev.* **1992**, 92, 1509-1539.
- [5] Ryzhov, V.; Dunbar, R. C. *Int. J. Mass Spectrom. Ion Proc.* 1997, 167/168, 627-635.
- [6] Dunbar, R.C. *Int. J. Mass Spectrom. Ion Proc.* **1997**, 160, 1-16.
- [7] Herbst, E. *Astrophys. J.* **1976**, 205, 94-102.
- [8] Herbst, E. *J. Chem. Soc., Faraday Trans.* **1989**, 85, 1655-1664.

Ion-Neutral Reactive Collisions at sub-Kelvin Temperatures

Stefan Willitsch, Xin Tong and Felix H.J. Hall

Department of Chemistry, University of Basel, Klingelbergstrasse 80, 4056 Basel, Switzerland

The study of chemical processes at extremely low temperatures $T \ll 1$ K has recently received considerable attention [1,2,3,4]. The reasons for this interest lie in the intriguing features of reactive collisions at ultralow energies. In this regime, molecular collisions are dominated by only a few partial waves. These conditions are ideal for studying quantum effects which depend on the collisional angular momentum such as reactive scattering resonances and tunnelling through centrifugal barriers. Moreover, the dynamics of ultralow-energy collisions is often dominated by long-range forces such as charge-dipole or dipole-dipole interactions enabling the characterisation of the role of these “universal” forces in chemical reactions. Finally, the experimental methods developed in this context not only allow for cooling, but also for the precise control of the collision energy and the internal quantum state of the reaction partners. Thus, prospects open up to study and control chemical processes at a level of accuracy which has not been possible before [5,6].

In the talk, recent progress in the study of ion-neutral reactions at sub-Kelvin temperatures will be reviewed. The presentation will begin with a brief overview over experimental approaches for the preparation of translationally cold trapped ions and neutral molecules. The combination of these methods for the investigation of ion-neutral processes down to millikelvin temperatures will be discussed [4].

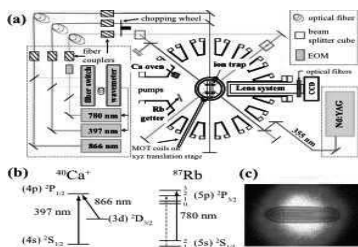


Figure 1: False-colour fluorescence image of a Coulomb crystal of laser-cooled Ca^+ ions (blue) in a cloud of ultracold Rb atoms.

A brief overview over a series of first-generation experiments will be given in which an ion trap for the laser- and sympathetic cooling of ions was combined with a velocity selector for the generation of cold neutrals [7]. These experiments enabled the study of ion-molecule reactive collisions down to energies corresponding to a few Kelvin and helped to elucidate low-temperature dynamical effects in ion-molecule reactions such as arising from submerged potential barriers.

Subsequently, two recent developments in the field will be discussed. First, new methods will be highlighted which simultaneously allow for the cooling of the translational motion and for the accurate preparation of the rovibrational quantum state of trapped molecular ions. In particular, focus will be placed on recent

experiments which relied on threshold photoionization for the preparation of molecular ions in a single rovibrational quantum state followed by the sympathetic cooling of their translational motion [8]. These advances now pave the way for ion-neutral reaction experiments with an unprecedented control over both, the kinetic energy and the internal quantum state of the reaction partners.

Second, recent experiments will be presented in which cold trapped ions were immersed in a bath of ultracold atoms in an ion-atom hybrid trap (see Fig. 1) [9]. This development has enabled to push the study of ion-neutral reactions into the millikelvin regime. First results on reactive collisions between laser-cooled Ca^+ ions and Rb atoms will be presented. This model system will serve to illustrate the rich chemical dynamics exhibited even by simple atomic-ion neutral-atom collision systems in the sub-Kelvin domain. In particular, the role of light-assisted processes such as radiative association and charge exchange as well as non-adiabatic processes will be discussed.

References

- [1] O. Dulieu, R.V. Krems, M. Weidemüller and S. Willitsch, *Phys. Chem. Chem. Phys.*, **42**, 18703 (2011)
- [2] R.V. Krems, *Phys. Chem. Chem. Phys.* **10**, 4079 (2008)
- [3] M.T. Bell and T.P. Softley, *Mol. Phys.* **107**, 99 (2009)
- [4] S. Willitsch, M.T. Bell, A.D. Gingell, and T.P. Softley, *Phys. Chem. Chem. Phys.* **10**, 7200 (2008)
- [5] S. Ospelkaus et al., *Science* **327**, 853 (2010)
- [6] M.H.G. de Miranda et al., *Nat. Phys.* **7**, 502 (2011)
- [7] S. Willitsch, M. T. Bell, A. D. Gingell, S. R. Procter and T. P. Softley, *Phys. Rev. Lett.* **100**, 043203 (2008)
- [8] X. Tong, A.H. Winney and S. Willitsch, *Phys. Rev. Lett.* **105**, 143001 (2010)
- [9] F.H.J. Hall, M. Aymar, N. Bouloufa-Maafa, O. Dulieu and S. Willitsch, *Phys. Rev. Lett.* (in press, *arXiv preprint* 1108.3739)

Hot Topic Papers

Low temperature reactions on interstellar dust grains: new surface chemistry for the interstellar medium

Stephen D Price¹, Rona E Watson¹ and Michael D Ward¹

¹ Chemistry Department, University College London, 20 Gordon Street, London, WC1H 0AJ, UK.

Summary

We report a series of new experimental results from an apparatus designed to probe the low temperature (12 K-80 K) reactivity of atoms on molecular ices under conditions relevant to the interstellar medium. Many, but not all, previous investigations of such reactivity have concentrated on *non-thermal* chemistry, the chemistry induced in the ices following energetic particle impact. In contrast, our experiment probes the *thermal* reactivity, where atoms and molecules react on the grain surface without any external activation from a charged particle or photon. We focus on the reactions of O and H atoms with molecules representative of the icy mantles that coat interstellar dust grains in denser interstellar clouds. Significant reactivity is observed for a variety of systems at low temperatures comparable to those found in interstellar clouds. Our experimental technique allows the determination of the kinetic parameters characterizing the reactions and identifies the product species. Indeed, in some cases, the precise identification of the structural isomers formed is possible. The results will be illustrated with a study of the reactions of O atoms with alkenes. Here we see that epoxides are the dominant product, a selectivity in stark contrast to the non-thermal chemistry, and that we can clearly differentiate the Eley-Rideal and Langmuir Hinshelwood

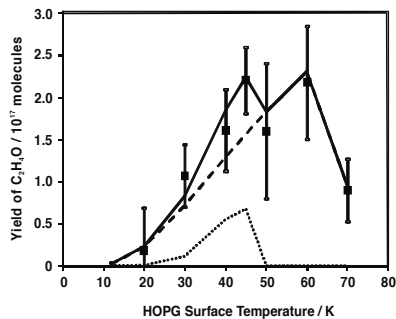


Figure 1: The temperature dependence of the yield of C_2H_4O molecules following co-deposition of C_2H_4 and O atoms. Squares = Experiment, Solid line = Model [1].

processes on the surface. Secondly, we present an investigation of the reactions of sulfur containing molecules on interstellar surfaces, a topic of considerable current interest. Indeed, our experiments represent the first investigation of the thermal surface astrochemistry of sulfur containing molecules. In these studies, for example, we clearly see that CS_2 reacts efficiently with O and H atoms and thus CS_2 may not act as a solid-state sulfur reservoir, as has been proposed.

Background and motivation

The composition of the interstellar medium is dominated by hydrogen and helium with other atoms (C,N,O) being four or five orders of magnitude less abundant than hydrogen [2].

However, these chemical building blocks are not uniformly distributed across interstellar space but accumulate in a variety of environments such as diffuse and dense interstellar clouds [3-5]. In these interstellar clouds atoms and molecules are accompanied by dust grains of sizes comparable with the wavelengths of visible light [6]. In the denser clouds, these cold (10-20K) dust grains accumulate mantles of molecular ices. Despite the overwhelming abundance of hydrogen, interstellar clouds have a rich and complex chemistry, as evidenced by the over 150 molecules detected to date in the interstellar medium (ISM) [7-8]. The abundances of many of these interstellar molecules cannot be explained solely by chemical synthesis in the gas-phase, and it is now widely accepted that reactions on the surfaces of interstellar dust grains play an important role in the formation of many interstellar molecules [3,6,8-10]. However, due to the low temperatures of these interstellar dust grains [5] chemical reactions of thermalised surface species, so called “thermal” synthetic routes, can only proceed *via* pathways with very low or non-existent reaction barriers.

An alternative to the above *thermal* processes, for the synthesis of molecules on grain surfaces, involves the energetic processing of the molecules in the icy mantles which accumulate on the dust grains in the cooler interstellar clouds [6]. This processing of the molecular ices can occur via their interaction with ultra-violet photons and cosmic rays [11]. This irradiation allows the generation of energized species within the ices which are sufficiently activated to overcome reaction barriers. There have been a number of investigations of this *non-thermal* processing of interstellar ices, whilst investigations of thermal heterogeneous reactions at interstellar temperatures have been much rarer.

Here we report a study of the thermal reactions of O atoms with alkenes on a prototypical interstellar surface at 12-90 K. From our results we can identify the reaction products and extract binding energies and reaction barriers. Our results show that these reactions are likely to be efficient in the interstellar medium and provide a specific route to the formation of epoxides [1].

The discrepancy between the elemental abundance of sulfur and the gas phase abundances of sulfur bearing molecules has prompted interest in the chemistry of sulfur on interstellar dust grains. The elemental abundance of sulfur relative to hydrogen has been calculated to be in the region of 10^{-5} [12-14]. However, the elemental sulfur abundances required to explain the gas-phase abundances of sulfur containing species in dense interstellar clouds are typically $10^{-7} - 10^{-9}$ [15-17]. An obvious conclusion is thus that a significant proportion of sulfur in dense interstellar clouds must be contained in the icy mantles of interstellar dust grains [18]. However, to date, only two sulfur containing molecules have been definitively identified in interstellar ices: sulfur dioxide (SO₂) and carbonyl sulfide (OCS)[19-22]. The presence of hydrogen sulphide (H₂S) in grain mantles has been suggested, via observations of W33A [23], but the definitive detection of H₂S is complicated by the overlap of its main infrared band with an infrared feature of methanol [18]. The above deduction of a significant

abundance of sulfur containing molecules in the icy mantles on interstellar grains indicates there is potentially a rich sulfur chemistry in this environment, a conclusion reached, for example in accounting for the abundance of OCS [24-25] in hot cores.

Given the above interest, we report here an investigation of the chemistry of CS₂ on a highly oriented pyrolytic graphite (HOPG) surface under astrophysically relevant conditions. CS₂ has been proposed as a reservoir of sulfur in the molecular ices present in interstellar clouds. Thus, understanding the fate of CS₂ on interstellar dust grain surfaces is vital for developing a complete picture of the chemistry of sulfur in the ISM. Our experiments reveal that CS₂ reacts efficiently with H and O atoms and thus CS₂ may not act as a solid-state sulfur reservoir, as has previously been proposed.

Experimental

In our experiments, which have been described in the literature [1], we can co-deposit atoms and molecules onto an HOPG substrate at a range of different surface temperatures between 15 and 100 K, in a UHV target chamber. Following this dosing period we slowly heat the surface and monitor the molecules desorbed as a function of surface temperature, using mass spectrometry, a temperature programmed desorption (TPD) experiment. In order to derive the rate constants and energetics for any reactions observed we fit our product yields with a simple kinetic model.

In some cases the mass of the product molecule, given by our TPD signals, is not sufficient to allow us to determine the chemical connectivity of the product species. In these cases we have the facility to selectively ionize the products using laser radiation. This approach, for example, allows us to show that the epoxide (I) (not the aldehyde [II] or alcohol [III], Figure 2) is the product form the reaction of C₂H₄ with O atoms.

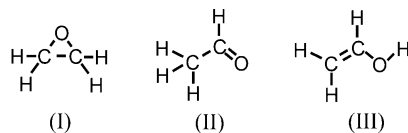


Figure 2. The possible isomeric forms of the C₂H₄O product from the reaction of O atoms with C₂H₄.

Results

Representative results will be presented for the reactions of O atoms with alkenes and the reactions of O and H atoms with CS₂. In brief, we see that O atoms react efficiently with alkenes at low temperature to form epoxides. By modelling the yields we observe (Figure 1) we can extract activation and binding energies for these reactive systems. We also see that O atoms react efficiently with CS₂ to form OCS and a variety of other oxygenated products. A brief overview of other systems studied will be included. Such recent data includes the reaction of NO with H atoms which we will show does, as previously speculated, provide a

route to hydroxylamine. The formation of hydroxylamine on dust grain surfaces has been proposed as the first step in the interstellar synthesis of simple amino acids.

References

- [1] M.D. Ward and S.D. Price *Astrophys. J.* (2011) in press
- [2] E. Herbst *Annual Review of Physical Chemistry* **46** (1995) 27
- [3] A.G.G.M. Tielens (2005) *The Physics and Chemistry of the Interstellar Medium*. Cambridge University Press, Cambridge
- [4] T.W. Hartquist in (1990), Cambridge University Press, Cambridge
- [5] T.P. Snow and B.J. McCall *Annual Review of Astronomy and Astrophysics* **44** (2006) 367
- [6] D.A. Williams and E. Herbst *Surface Science* **500** (2002) 823
- [7] M. Lattalais, F. Pauzat, Y. Ellinger and C. Ceccarelli *Astron. Astrophys.* **519** (2010) 7
- [8] D.J. Burke and W.A. Brown *Physical Chemistry Chemical Physics* **12** (2010) 5947
- [9] D.A. Williams and T.W. Hartquist *Accounts Chem. Res.* **32** (1999) 334
- [10] H.M. Cuppen and E. Herbst *Astrophys. J.* **668** (2007) 294
- [11] M. Garozzo, L. La Rosa, Z. Kanuchova, S. Ioppolo, G.A. Baratta, M.E. Palumbo and G. Strazzulla *Astron. Astrophys.* **528** (2011) A118
- [12] K. Lodders *Astrophysical Journal* **591** (2003) 1220
- [13] M.E. van Steenbergen and J.M. Shull *Astrophysical Journal* **330** (1988) 942
- [14] U.J. Sofia, J.A. Cardelli and B.D. Savage *Astrophysical Journal* **430** (1994) 650
- [15] R.T. Garrod, V. Wakelam and E. Herbst *Astronomy & Astrophysics* **467** (2007) 1103
- [16] T.J. Millar and E. Herbst *Astronomy and Astrophysics* **231** (1990) 466
- [17] S.D. Doty, E.F. van Dishoeck, F.F.S. van der Tak and A.M.S. Boonman *Astronomy & Astrophysics* **389** (2002) 446
- [18] M. Garozzo, D. Fulvio, Z. Kanuchova, M.E. Palumbo and G. Strazzulla *Astronomy & Astrophysics* **509** (2010) 9
- [19] A.C.A. Boogert, W.A. Schutte, F.P. Helmich, A. Tielens and D.H. Wooden *Astronomy and Astrophysics* **317** (1997) 929
- [20] M.E. Palumbo, T.R. Geballe and A. Tielens *Astrophysical Journal* **479** (1997) 839
- [21] M.E. Palumbo, A. Tielens and A.T. Tokunaga *Astrophysical Journal* **449** (1995) 674
- [22] G. Zasowski, F. Kemper, D.M. Watson, E. Furlan, C.J. Bohac, C. Hull and J.D. Green *Astrophysical Journal* **694** (2009) 459
- [23] T.R. Geballe, F. Baas, J.M. Greenberg and W. Schutte *Astronomy & Astrophysics* **146** (1985) L6
- [24] S.B. Charnley *Astrophysical Journal* **481** (1997) 396
- [25] S.B. Charnley, P. Ehrenfreund, T.J. Millar, A.C.A. Boogert, A.J. Markwick, H.M. Butner, R. Ruitkamp and S.D. Rodgers *Mon. Not. Roy. Astron. Soc.* **347** (2004) 157

New concepts for on-line monitoring of complex gas mixtures using photo ionisation mass spectrometry

R. Zimmermann, R. Hertz, A. Fendt, Eschner, T. Streibel

Joint Mass Spectrometry Centre of the Helmholtz Zentrum München, Neuherberg, D

and the University of Rostock, Analytical Chemistry, Rostock, D.

* ralf.zimmermann@uni-rostock.de

Photo ionisation mass spectrometry (PIMS) is an interesting approach for direct on-line monitoring of mixtures of organic gases and vapours. In addition to laser based photo ionisation methods, such as resonance-enhanced multiphoton ionization (REMPI) techniques, in particular the application of innovative incoherent VUV-light sources (electron beam pumped rare gas excimer light source – EBEL) for photo ionisation made new applications accessible. However, innovative analytical concepts for PIMS were developed in the fields of sampling technology, fast pre-separation approaches as well in mass spectrometric couplings in order to further increase versatility, selectivity and sensitivity.

For example, a micro probe technology was developed to sample within small, confined objects. This approach e.g. was used to study the time-resolved formation of flavour compounds during coffee roasting process within individual coffee beans. In order to reach higher detection sensitivity as well the possibility to separate interfering isobaric compounds a rapidly modulated gas chromatographic technique was developed and hyphenated to PIMS for quasi-on-line analyses. This latter technology was used e.g. to record the concentration of several isobaric/isomeric compounds puff-by-puff in cigarette smoke. The detection of traces of target compounds in complex mixtures requires a further increase of sensitivity and selectivity. In a recent application for PIMS-detection of harmful and illegal compounds, such as explosives or drugs of abuse, a tandem MS approach was realised (PI-MS/MS). The strong prevalence of the molecular ions predestines PIMS method for MS/MS applications. The PI-MS/MS approach was demonstrated in a field measurement in a former clandestine drug laboratory. Finally the further development potential of PIMS is discussed.

Properties of small TiC clusters: Implications for dust nucleation studies under the conditions of C-rich AGB stars

A. B. C. Patzer¹, Ch. Chang¹ and D. Sülzle¹

¹ *Zentrum für Astronomie und Astrophysik, Technische Universität Berlin, Hardenbergstr. 36, 10623 Berlin, Germany*

Abstract.

Dust particles formed in circumstellar outflows of carbon-rich AGB stars are a mixture of several chemical elements such as silicon or titanium in addition to the main component carbon as verified by many studies of pre-solar grains enclosed in meteorites. In this contribution we focus on the investigation of the properties of small molecular titanium carbide clusters, which have been estimated within density functional theory (DFT) approaches. The molecular properties, thus obtained, are necessary prerequisites for the study of phase transitions in astrophysical environments such as the surroundings of cool, late-type stars on the asymptotic giant branch (AGB). First implications on the homogenous nucleation of TiC are discussed for conditions considered to be representative for circumstellar dust shells around typical carbon-rich AGB stars.

Introduction

In circumstellar environments around cool, late-type stars on the asymptotic giant branch (AGB) dust particles are effectively formed via the formation and subsequent growth of small molecular clusters in the gas phase. The details of the dust formation process and the nature of the condensed material depend decisively on the chemical composition as determined by the elemental mixtures of the circumstellar envelopes. Carbon-rich situations are thereby characterised by an overabundance of carbon in comparison to oxygen (i.e. $\epsilon_C > \epsilon_O$), which results in carbonaceous dust materials.

As revealed by many studies of pre-solar grains enclosed in meteorites, dust particles with characteristic isotopic signatures, which originate from AGB stars as dust sources (e.g. Bernatowicz et al. 2005, Croat et al. 2005), contain also e.g. silicon or titanium carbides in addition to the main component carbon. The detection of central inclusions of such TiC particles in carbon material implicates titanium carbide condensation before carbon dust formation, thus constraining the so-called dust condensation sequence. Phase stability lines

($S=1$) of different carbon materials have been analysed by Bernatowicz et al. (2005) especially in view of this sequence. They conclude that TiC before C dust formation is in principle possible at high temperatures (ca. 1570K - 1780K) but low C/O ratios ($\sim C/O < 1.2$) depending only weakly on the pressure. Other studies on the theoretical condensation sequence made to constrain the physical parameters of the dust condensation regimes show also, that the phase stability lines depend notably on the C/O ratio (e.g. Lodders & Fegley 1995, Sharp & Wasserburg 1995). However, these considerations are not taking any details of the nucleation process of titanium carbide itself into account.

Molecular properties of small titanium carbide clusters and implications for nucleation under the conditions of C-rich AGB stars

The transition from a gas to solid particles takes place via the formation and growth of small molecular clusters in the gas phase. Therefore, the investigation of the properties of molecular clusters is essential for the understanding of dust nucleation in circumstellar environments of AGB stars. They can be obtained theoretically by electronic structure techniques to determine the required data of the microphysical processes involved, which are often not at hand (see also Patzer 2007). Here, we focus on the properties of small titanium carbide clusters of mainly stoichiometric composition, which have been studied within the density functional approach (DFT) (cf. e.g. Paar & Yang 1989) employing the bpl local, non-gradient corrected exchange correlation functional in conjunction with the standard medium sized all-electron split valence 6-31G(d) basis set (Frisch et al. 1984). In view of a consistent level of description for even much larger cluster sizes this theoretical level of approximation is a reasonable compromise between computational effort and desired numerical accuracy (cf. Wendt 2008). Since no general building principles or schemes are known for small carbide clusters in contrast to e.g. polyaromatic hydrocarbons (PAHs), the potential energy surface (PES) of each molecular system determined by the solution of the Schrödinger equation for given configurations of atoms has to be searched thoroughly for minima representing stable cluster configurations. Thus, all titanium carbide clusters are treated within the DFT approach by full optimisation and characterisation of the stationary points. The calculated molecular properties of the clusters (e.g. dissociation energy, harmonic frequencies, geometrical structure parameters) can then be used to set up the partition functions applying the RRHO approximation, which is generally applied in thermodynamic studies of polyatomic molecules. The thermochemical cluster properties (e.g. the molar Gibbs free energies of formation) can be obtained from the partition functions by standard statistics (see e.g. Patzer et al. 2005).

The small titanium carbide cluster systems with mainly stoichiometric composition investigated so far show structural motives of the bulk TiC lattice (fcc). The calculated positions of the main active IR modes around $15.7\mu\text{m}$ and $\sim 21\mu\text{m}$ of these titanium carbide clusters, which are caused by vibrating carbon atoms in a 'grid' of titanium atoms as illustrated by Figure 1, are in very good agreement³ with the results of the TiC cluster measurements of von Helden et al. (2000) (cf. also Patzer et al. 2011).

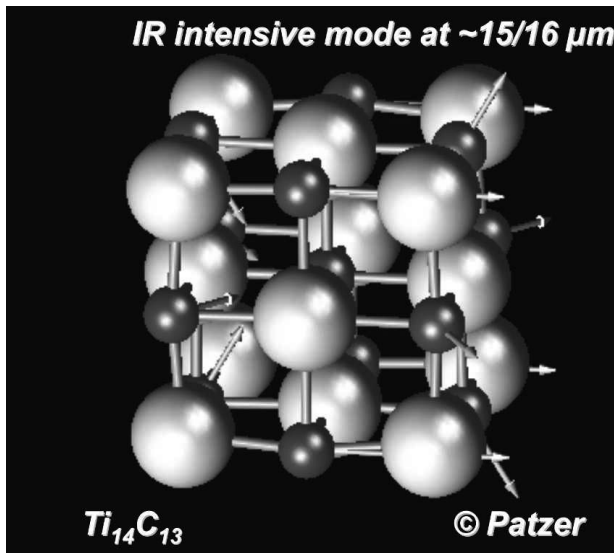


Figure 1: DFT/BPL/6-31G(d) IR active mode at $\sim 15.7\mu\text{m}$ of the energetically lowest $\text{Ti}_{14}\text{C}_{13}$ isomer (Ti - light grey; C - grey) caused by vibrating C atoms in a 'grid' of Ti atoms.

Chigai et al. (1999), for example, investigated previously the nucleation of titanium carbide in AGB winds by using a special key species⁴ concept, since important data on titanium carbide clusters were not available. Studying first implications we apply here our findings on the properties of small titanium carbide clusters to the most simple nucleation process, to determine an upper limit on the stationary homogeneous TiC nucleation rate (see e.g. Patzer 2004 for more details on nucleation theory). Only the addition of monomers is, therefore,

³ This does not necessarily imply, that the $21\mu\text{m}$ feature, which has been discovered in carbon-rich stars in the post-AGB phase of evolution is caused by TiC dust particles. Strong objections are given by e.g. Henning & Mutschke (2001), Chigai et al. (2003).

⁴ Ti atoms were considered as key species.

taken into account and depletion effects are not yet considered. It turns out, that effective TiC nucleation is possible at high temperatures (see also above), but high supersaturation ratios are absolutely necessary.

Summary

The key to the understanding of dust nucleation in circumstellar environments of AGB stars is the investigation of the properties of molecular clusters to determine the required data of the microphysical processes involved. In this study properties of small titanium carbide clusters have been obtained from DFT/BPL/6-31G(d) calculations. A simple application of these findings to the homogeneous nucleation process reveals, that in cool and expanding outflows of carbon—rich AGB stars effective TiC nucleation is in principle possible at high temperatures, but highly supersaturated conditions are required. Ti_xC_y clusters in further, chemically more complex TiC nucleation studies have to be considered to address the formation of titanium carbide dust under such conditions in greater detail.

Acknowledgements

This work has been partly supported by the *Deutsche Forschungsgemeinschaft* (DFG) in the framework of the Schwerpunktprogramm **SPP 1573** - grant PA 1648. The authors are very grateful to H. Bauer for his achievements in data processing.

References

- [1] T.J. Bernatowicz, O.W. Akande, T.K. Croat, R. Cowsik, *ApJ* **631**, 988 (2005)
- [2] T. Chigai, T. Yamamoto, T. Kozasa, *ApJ* **510**, 999 (1999)
- [3] T. Chigai, T. Yamamoto, C. Kaito, Y. Kimura, *ApJ* **587**, 771 (2003)
- [4] T.K. Croat, F. Stadermann, T.J. Bernatowicz, *ApJ* **631**, 976 (2005)
- [5] M.J. Frisch, J.A. Pople, J.S. Binkley, *J. Chem. Phys.* **80**, 3265 (1984)
- [6] T. Henning, H. Mutschke, *Spectrochim. Acta* **57**, 815 (2001)
- [7] K. Lodders, B. Fegley Jr., *Meteoritics* **30**, 661 (1995)
- [8] R.G. Paar, W. Yang, *DFT of atoms and molecules*, Oxford Univ. Press (1989)
- [9] A.B.C. Patzer, *ASPC Series* **309**, 301 (2004)
- [10] A.B.C. Patzer, *ASPC Series* **378**, 181 (2007)
- [11] A.B.C. Patzer, Ch. Chang, E. Sedlmayr, D. Sülzle, *EPJ D* **32**, 329 (2005)
- [12] A.B.C. Patzer, M. Wendt, Ch. Chang, D. Sülzle, *ASPC Series* **445**, 361 (2011)
- [13] C.M. Sharp, G.J. Wasserburg, *Geochim. et Cosmochim. Acta* **59**, 1633 (1995)
- [14] G. von Helden, A.G.G.M. Tielens, D. van Heijnsbergen et al., *Science* **288**, 313 (2000)
- [15] M. Wendt, *Diploma Thesis*, Technische Universität Berlin, Germany (2008)

Anion Chemistry on Titan: A possible route to large N-bearing hydrocarbons

J. Zabka¹, M. Polasek¹, C. Romanzin², and C. Alcaraz²

¹ *J. Heyrovsky Institute of Physical Chemistry of the ASCR, v. v. i. Dolejškova 2155/3, 182 23 Prague 8, Czech Republic (jan.zabka@jh-inst.cas.cz, miroslav.polasek@jh-inst.cas.cz)*

² *Lab. de Chimie Physique, Bât 350, UMR 8000 CNRS-Université Paris-Sud 11, 91405 Orsay, France (claire.romanzin@u-psud.fr, christian.alcaraz@u-psud.fr)*

Abstract

The $\text{CN}^- + \text{HC}_3\text{N}$ reaction has been studied in a tandem mass spectrometer as a function of the HC_3N target molecule going from a single to a multiple collision regime. The primary and secondary reactions with HC_3N were found to be extremely efficient, resulting in anionic products of rapidly growing size through a simple mechanism [1]. Comparison of the experimental mass spectra with the spectrum observed on board of CASSINI with the CAPS-ELS instrument by Coates et al [2,3] suggests that the proposed mechanism may be of interest to describe the growth of negatively charged hydrocarbons in Titan's ionosphere [1].

1. Introduction

Among the numerous negative ions observed in Titan's upper atmosphere [2,3], CN^- is believed to play a key role in the formation of larger species [4]. In this context, the reaction of CN^- with cyanoacetylene (HC_3N) whose concentration is not negligible in Titan's upper atmosphere, is of particular interest. The kinetic of the $\text{CN}^- + \text{HC}_3\text{N}$ reaction has recently been experimentally investigated by Carles et al. [5] under single collision conditions. The rate constant is $k = 4.8 \times 10^{-9} \text{ cm}^3/\text{s}$ and C_3N^- could be identified as the main reaction product following the proton transfer $\text{CN}^- + \text{HC}_3\text{N} \rightarrow \text{C}_3\text{N}^- + \text{HCN}$.

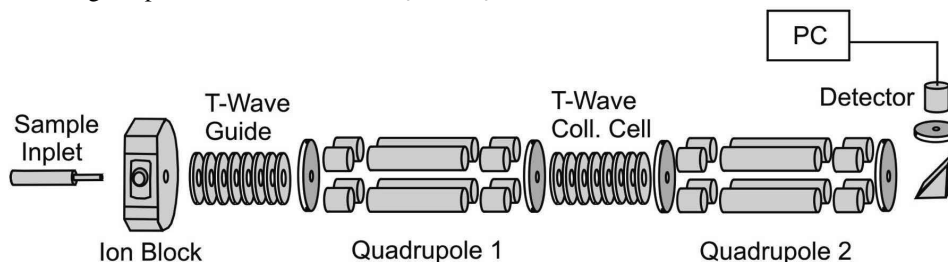


Figure 1: Experimental setup

2. Experimental section

In this work, the same reaction has been studied as a function of the HC_3N target pressure on a tandem mass spectrometer shown in Fig. 1. CN^- parent anions were produced from acetonitrile in an APCI (Atmospheric Pressure Chemical Ionisation) source. They are selected in mass in a 1st quadrupole mass filter and react with HC_3N in a RF travelling-wave collision cell. Synthesis of the HC_3N molecule was performed following [6]. Parent and product anions are analyzed in mass up to $m/z = 400$ in a 2nd quadrupole mass filter before their detection.

3. Results

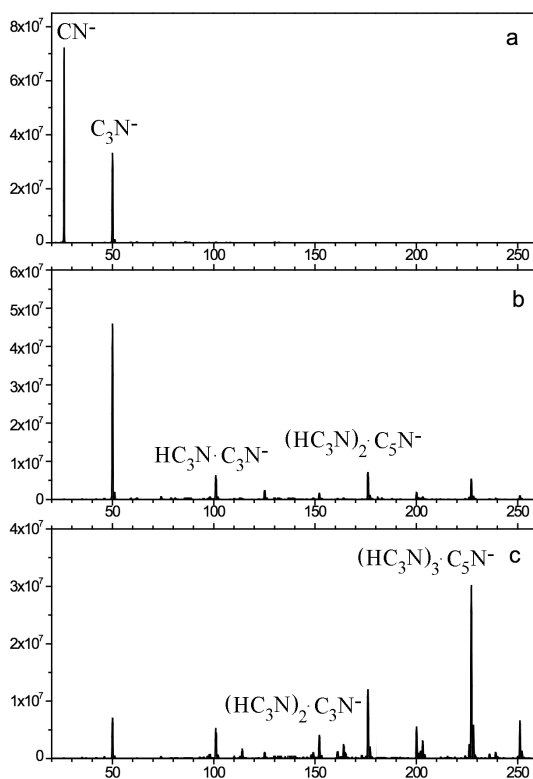


Figure 2: Mass spectra recorded at a HC_3N target gas pressure of 0.02 (a), 0.3 (b), and 0.5 Pa (c).

Typical mass spectra shown in Fig. 2 reveal the fast decrease of the CN^- parent and appearance of larger anions of rapidly growing size. Most of the masses observed were found to belong only to two series of products: $(\text{HC}_3\text{N})_x \cdot \text{C}_{2p+1}\text{N}^-$ and $(\text{HC}_3\text{N})_x \cdot \text{C}_{2p}\text{N}^-$ resulting from the sequential additions of HC_3N molecules and loss of HCN or HCCN molecules. The intensity of each product has been followed as a function of the HC_3N pressure [1].

For a comparison with the spectrum recorded on Titan ionosphere [2-4], we have convoluted our measured spectra with the mass resolution ($\Delta m/m$ of 16.7 %) of the CAPS-ELS spectrometer and summed up in a similar histogram as shown in Fig. 3. Similarities can be found between the laboratory and observed spectra, in particular for the first peaks due to CN^- and C_3N^- , at $m/z = 26$ and 50, and the beginning of the broad structure at higher masses.

Extended measurements at higher

masses would be needed for a better comparison. To extrapolate these results to Titan, we will also discuss the effect of temperature and pressure which are different in Titan's ionosphere.

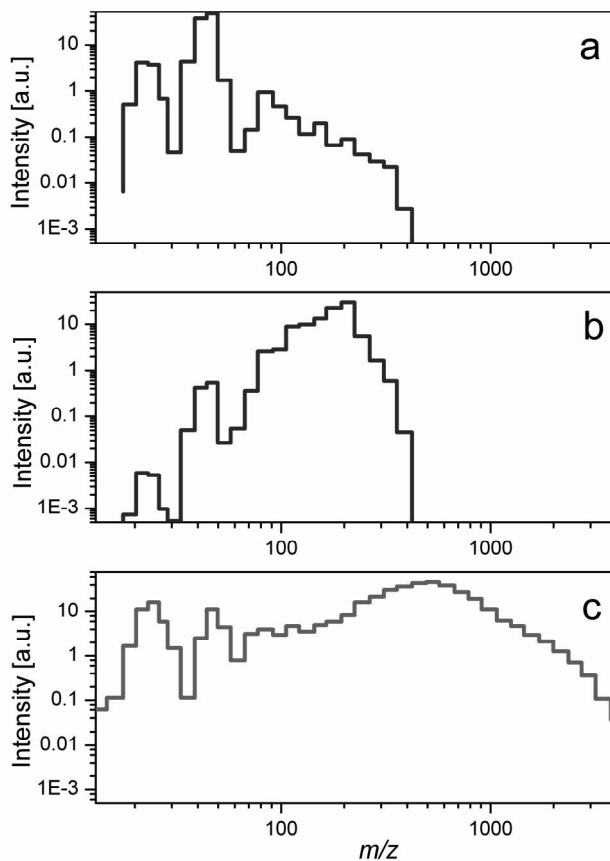


Figure 3: Convolution of mass spectra recorded at a HC_3N target gas pressure of 0.05 (a) and 0.5 Pa (b) with a gaussian apparatus function representing the resolution ($\Delta m/m$ of 16.7 %) of the CAPS-ELS spectrometer of CASSINI [2-4], and observed spectrum (c) by CASSINI / CAPS-ELS.

Conclusion

A growth mechanism of anions in Titan's ionosphere based on ion-molecule reactions is proposed for the first time. Apart from the $\text{CN}^- + \text{HC}_3\text{N}$ reaction studied here, any anion that could abstract a proton from HC_3N would lead to C_3N^- first, and then to the production of the same series of anions. Reactions with HCN , C_2N_2 or HC_5N should also be considered to account for large anion formation. Decay processes would also be important to characterize for a complete modeling of anions in Titan's ionosphere. In particular, almost nothing is known on photodetachment processes for these anions.

Acknowledgments

Programme National de Planétologie (PNP), Pôle Planétologie du PRES Universud (contract 2008-53), COST (Action CM0805 « The Chemical Cosmos »), France-Czech Republic Program CNRS-AVCR (n°20201) and Czech Science Foundation (P208/11/0446).

References

- [1] J. Žabka, M. Polášek, C. Romanzin, C. Alcaraz, "Anion Chemistry on Titan: A possible route to large N-bearing hydrocarbons" (submitted to Icarus).
- [2] A.J. Coates, F.J. Crary, G.R. Lewis, D.T. Young, J.H. Waite, E.C. Sittler, "Discovery of heavy negative ions in Titan's ionosphere", *Geophys. Res. Lett.* **34**(22) (2007).
- [3] A.J. Coates, A. Wellbrock, G.R. Lewis, G.H. Jones, D.T. Young, F.J. Crary, J.H. Waite, R.E. Johnson, T.W. Hill, E.C. Sittler, "Negative ions at Titan and Enceladus: recent results", *Farad. Discuss.* **147**, 293-305 (2010).
- [4] V. Vuitton, P. Lavvas, R.V. Yelle, M. Galand, A. Wellbrock, G.R. Lewis, A.J. Coates, J.E. Wahlund, "Negative ion chemistry in Titan's upper atmosphere", *Planet. Space Sci.* **57**(13), 1558-72 (2009).
- [5] S. Carles, F.A., C. Monnerie, J.-C. Guillemin, J.-L. Le Garrec, *Kinetic studies at room temperature of the cyanide anion CN^- with cyanoacetylene (HC_3N) reaction.* *Icarus*, **211**(1), 901-905 (2011).
- [6] Miller, F.A., Lemmon, D.H., *The infrared and Raman spectra of dicyanodiacetylene (NCCCCCN).* *Spectrochim. Acta Part A – Mol. Spectrosc.* **A 23**, 1415 (1967)

Laboratory data needs for modeling Titan's atmospheric chemistry

Y ronique Vuitton¹, Nadia Balucani², Odile Dutuit^{1,3}, Axel Bazin¹ and Roger V. Yelle⁴

¹ *Institut de Plan tologie et d'Astrophysique de Grenoble, UJF-CNRS, Grenoble, France.*

(veronique.vuitton@obs.ujf-grenoble.fr)

² *Dipartimento di Chimica, Universita degli Studi di Perugia, Perugia, Italy.*

³ *Space Research Institute, Austrian Academy of Sciences, Graz, Austria.*

⁴ *Lunar & Planetary Laboratory, University of Arizona, Tucson AZ, USA.*

Titan, the largest moon of Saturn, is the only satellite in the Solar System with a massive atmosphere. Titan's atmospheric chemistry is extremely complex because of the multiplicity of chemical as well as physical processes involved. Chemical processes begin with the dissociation and/or ionization of the most abundant species, N₂ and CH₄, by a variety of energy sources, i.e. solar ultraviolet and X-ray photons, suprathermal electrons (<100 eV) and ions (H⁺, O⁺, <1 keV) trapped in Saturn's magnetosphere and cosmic rays [1, 2]. The energetic species produced further react to generate a plethora of gaseous molecules that will eventually become heavy enough to become organic aerosols. Thus, molecular growth is driven by gas phase reactions involving radicals as well as positive and negative ions, all possibly in some excited electronic and vibrational state [3, 4]. Heterogeneous chemistry at the surface of the aerosols could also play a significant role [5]. The efficiency and outcome of these reactions depends strongly on the physical characteristics of the atmosphere, namely pressure and temperature, ranging from 1.5×10³ to 10⁻¹⁰ mbar and from 70 to 200 K, respectively. Moreover, the distribution of the species is affected by molecular diffusion, vertical and horizontal winds as well as escape from the top of the atmosphere and condensation in the lower stratosphere [5, 6]. A cartoon illustrating Titan's atmospheric chemistry is presented in Figure 1.

Photochemical models are the keystone of our understanding of Titan's atmospheric chemistry. Their main objective is to compute the altitude density profile of the minor chemical species (typically containing up to 6 carbon atoms) resulting from the irradiation of a N₂/CH₄ background atmosphere. These profiles can be compared to the available observations, allowing the refinement of the description of the chemical as well as physical processes considered in the models. State-of-the-art models include hundreds of species (neutrals, positive and negative ions) and thousands of reactions [6, 7]. Different classes of reactions included in photochemical models can be found in Table 1. They can be divided into 2 main categories:

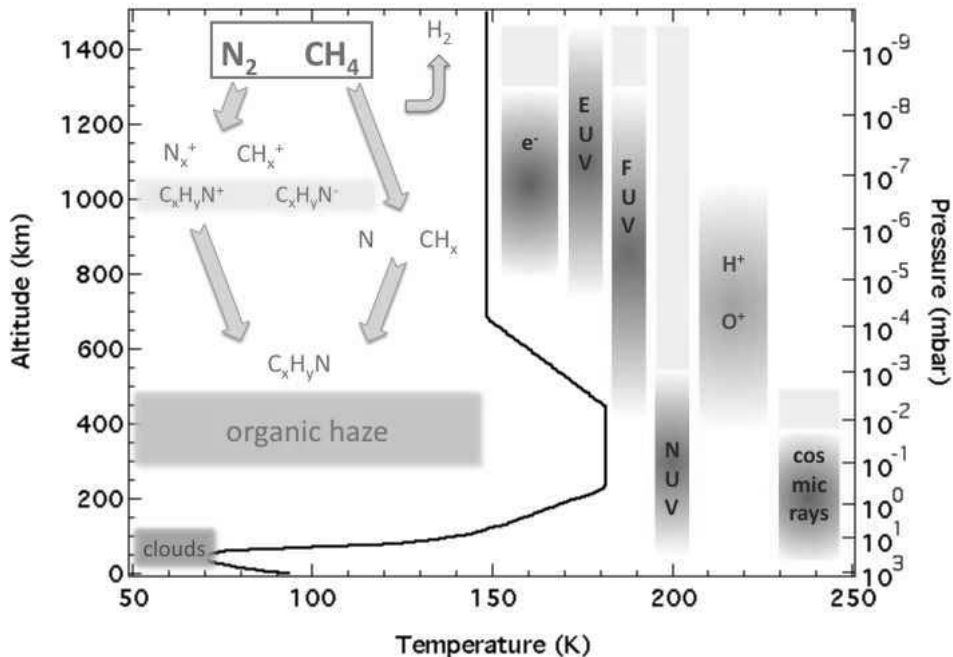


Figure 1: Summary of our current understanding of Titan's atmospheric chemistry, from N_2 and CH_4 to minor gas species, then to macromolecules and organic aerosols.

- Reactions that are initiated by impact of a photon or an energetic electron on a chemical species that break it apart into smaller but usually more reactive fragments, such as a radical, a positive or a negative ion. These reactions include dissociation, (dissociative) ionization, ion-pair formation, and dissociative attachment. They are characterized by their absorption/ionization cross-section and products branching ratio, which depend strongly on wavelength and to a lesser degree on temperature.
- Reactions between molecules, ions and thermal (<1000 K) electrons. Some, such as radiative attachment, charge transfer and radiative recombination simply modify the degree of ionization of a given species. Association reactions lead to some molecular growth as well as atoms transfer and ion recombination reactions (except if the atom transferred is an H). Dissociative recombination leads to the fragmentation of the initial ion. These reactions are characterized by their rate coefficient and products branching ratio that can be strongly temperature dependent.

Reaction class	Chemical equation
Photochemical reactions	
Dissociation ^a	$AB + h\nu \rightarrow A + B$
Ionization	$AB + h\nu \rightarrow AB^+ + e^-$
Dissociative ionization ^a	$AB + h\nu \rightarrow A^+ + B + e^-$
Ion-pair formation ^a	$AB + h\nu \rightarrow A^+ + B^-$
Photodetachment ^a	$A^- + h\nu \rightarrow A + e^-$
Electron induced reactions	
Dissociative attachment	$AB + e^- \rightarrow A^- + B$
Radiative attachment	$A + e^- \rightarrow A^- + h\nu$
Neutral-neutral reactions	
Atoms transfer	$A + BC \rightarrow AB + C$
3-body association	$A + B + M \rightarrow AB + M$
Radiative association	$A + B \rightarrow AB + h\nu$
Positive ion-neutral reactions	
Charge transfer	$A^+ + B \rightarrow B^+ + A$
Atoms transfer	$A^+ + BC \rightarrow AB^+ + C$
3-body association	$A^+ + B + M \rightarrow AB^+ + M$
Radiative association	$A^+ + B \rightarrow AB^+ + h\nu$
Negative ion-neutral reactions	
Atoms transfer	$A^- + BC \rightarrow AB^- + C$
Associative detachment	$A^- + B \rightarrow AB + e^-$
Recombination reactions	
Dissociative recombination	$AB^+ + e^- \rightarrow A + B$
Radiative recombination	$A^+ + e^- \rightarrow A + h\nu$
Ion recombination	$A^+ + BC^- \rightarrow AB + C$

Table 1: Classes of gas phase reactions included in Titan photochemical models.

^aThese processes can be initiated by a suprathermal electron as well.

Cross sections, rate coefficients and branching ratios are measured in laboratory experiments or computed from theoretical principles. Determining these parameters is a daunting task and only a fraction of them are available for the low pressure and temperature conditions relevant to Titan. This lack of critical chemical data deeply alters the predictivity of the models [8, 9].

We will review Titan's atmospheric chemistry, especially focusing on those missing laboratory data that are crucial from the modeler's point of view. Of highest interest are radical-radical and ion-radical association reactions (both collisional and radiative), electron recombination reactions as well as negative ion chemistry in general. Special attention should

be paid to product branching ratios at low temperature and isomers identification. Both experimental and theoretical investigations should be pursued. Beyond gas phase reactions, the impact of aerosols on the chemistry has been almost neglected so far. Solid particles could attach electrons and/or adsorb molecules that would then be simply removed from the gas phase or further react on the surface, producing some new species. These processes are highly uncharacterized and specific studies are highly desirable.

Acknowledgements

This work was performed in the framework of the Marie Curie International Research Staff Exchange Scheme PIRSES-GA-2009-247509. V. V. is grateful to the European Commission for the Marie Curie International Reintegration Grant No. 231013.

References

- [1] Cravens, T.E., et al., *Geophys. Res. Lett.*, **35**, L03103 (2008).
- [2] Lavvas, P., R.V. Yelle, and V. Vuitton, *Icarus*, **201**, 626-633 (2009).
- [3] Vuitton, V., R.V. Yelle, and P. Lavvas, *Phil. Trans. R. Soc. A*, **367**, 729-741 (2009).
- [4] Vuitton, V., et al., *Planet. Space Sci.*, **57**, 1558-1572 (2009).
- [5] Lavvas, P., A. Coustenis, and I.M. Vardavas, *Planet. Space Sci.*, **56**, 27-66 (2008).
- [6] Krasnopolsky, V.A., *Icarus*, **201**, 226-256 (2009).
- [7] Yelle, R.V., et al., *Faraday Discuss.*, **147**, 31-49 (2010).
- [8] Hébrard, E., et al., *J. Phys. Chem. A*, **113**, 11227-11237 (2009).
- [9] Peng, Z., et al., *Faraday Discuss.*, **147**, 137-153 (2010).

Equipment for ionic cluster formation based on ion drift-tube with selected-ion injection

Yoichi Nakai¹, Hiroshi Hidaka², Naoki Watanabe² and Takao M. Kojima³

¹ *RIKEN Nishina Center, Wako, Saitama 351-1098, Japan, nakaiy@riken.jp*

² *Institute of Low Temperature Science, Hokkaido University, Sapporo 060-0819, Japan*

³ *RIKEN Advanced Science Institute, Wako, Saitama 351-0198, Japan*

Ion-induced nucleation recently attracts attentions as one of important processes of fine particles, especially for aerosol particle formation in the atmosphere.[1,2] The ion-induced nucleation is expected to proceed more rapidly than neutral nucleation since attractive polarization forces between an ion and molecules is stronger compared with forces between neutral molecules. Ionic cluster formation, early stages of the ion-induced nucleation, is one of important research subjects when we consider the role of the ion-induced nucleation.

In the past, the ionic cluster formation in thermal chemical processes has widely been studied from various points of view. However, in many of the studies, the ionic cluster formation was triggered in gas including reactant molecules by ionization with discharge, a pulsed electron beam, radiation sources, and so on. Therefore, initial ionic reactions are not well defined, generally. Here, we report our developing equipment for the study of the ionic cluster formation. It is based on a method using an ion drift-tube with selected-ion injection [3-5] to limit the initial ionic reactions.

A schematic drawing of the equipment is shown in Fig. 1. Atomic or molecular ions are extracted from an ion source and mass-selected using a Q-pole mass analyzer. Then, they are focused on the entrance aperture of a drift tube. The ions with their kinetic energy of 5-10eV are injected into gas with its total pressure of several tens Pa filled in the drift tube. Since a uniform electric field is applied in the drift tube, the injected ions are decelerated by collisions with gas molecules down to the region of the drift velocity, which is defined by the electric field and the number densities of the molecules. Then, they react with the molecules. The product ions drift and the ionic clusters are grown via attachment processes of molecules. Finally, produced ionic clusters are extracted from the drift tube. The masses of the extracted ionic clusters are analyzed with another Q-pole mass analyzer. The temperature of the drift tube is controlled using a refrigerator system and ceramic heaters as seen in Fig. 1. It is also monitored with semiconductor temperature sensors. The drift tube has two sets of ion shutter for measurement of the drift time inside the drift tube.

We have been measuring free energy changes in the attachment processes of a water molecule for hydrated H_3O^+ ions. Currently, obtained values are in reasonably agreement with the values of the previous studies [6].

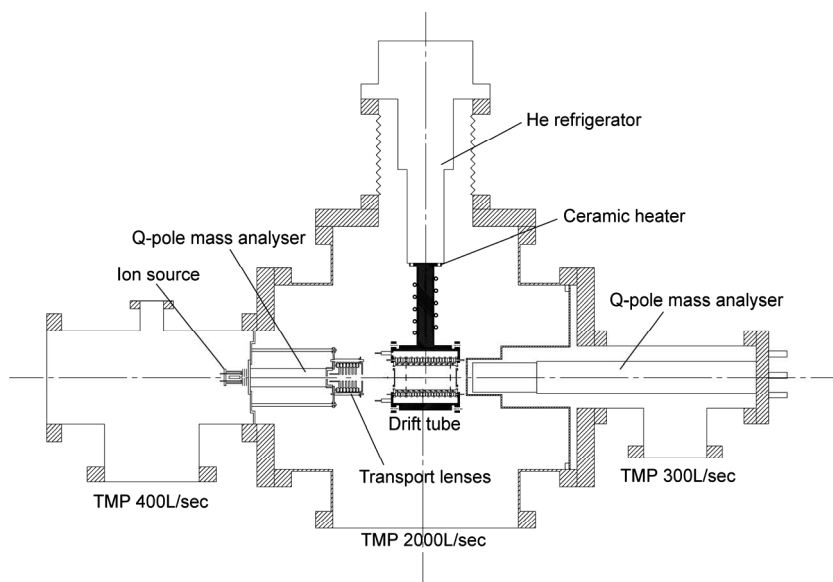


Figure 1: A schematic drawing of the equipment.

References

- [1] M. B. Enghoff and H. Svensmark, *Atmos. Chem. Phys.*, **8**, 4911(2008).
- [2] J. Kirkby *et al.*, *Nature* **476**, 429 (2011).
- [3] H. Böhringer and F. Arnold, *Int. J. Mass Spectrom. and Ion Phys.*, **49**, 61 (1983).
- [4] T. M. Kojima *et al.*, *Z. Phys. D: At., Mol. Clusters* **22**, 645 (1992).
- [5] H. Tanuma *et al.*, *Rev. Sci. Instrum.* **71**, 2019 (2000).
- [6] *NIST Chemistry WebBook*, <http://webbook.nist.gov/chemistry/>.

Low energy electron induced resonant processes in terphenyl-thiol SAMs

Lionel Amiaud¹, Vincent Humblot², Roger Azria¹, Claire-Marie Pradier² and Anne Lafosse¹

¹ Institut des Sciences Moléculaires d'Orsay (ISMO, UMR8214), CNRS – Univ. Paris-Sud, Bât. 351, 91405 Orsay, France, anne.lafosse@u-psud.fr

² Laboratoire de Réactivité de Surface (LRS, UMR7197), Université Pierre et Marie Curie, Paris 6, France.

Stability improvement or surface chemical composition adjustment of Self-Assembled Monolayers (SAMs) may be mandatory for their applications. It has been shown that aromatic thiol SAMs deposited on gold can be stabilized by irradiation through cross-linking within the spacer layer [1]. Such irradiations might simultaneously induce chemical changes at the level of the SAM's terminal functions [2], since many processes are competing at high energy. By contrast, selective and efficient dissociative processes can be induced by low-energy electron (LEE) irradiation at sub-excitation energies, though dissociative electron attachment (DEA) [3]. By optimizing an appropriate LEE irradiation sequence at adapted energies, chemical modifications of the SAMs could be driven specifically at the level of the spacer chains and/or of the terminal groups.

SAMs of terphenyl-thiol (TPT) deposited on gold were characterized by polarization modulation reflection absorption infra-red spectroscopy (PM-RAIRS) and XPS at the LRS. A complete study of their vibrational excitation by LEE was performed at the ISMO by recording electron energy loss spectra and vibrational excitation functions using high resolution electron energy loss spectroscopy (HREELS). An electron attachment resonance was identified at 6 eV through enhanced vibrational excitation of the C-H stretching modes alone, as opposed to ring modes. Scanning the LEE irradiation energy through this resonance, the chemical changes induced within the TPT SAMs were investigated by following the resulting modifications of the vibrational spectra.

References

- [1] Turchanin et al., *Langmuir* **25** (2009) 7342
- [2] Eck et al., *Adv. Mater.* **12** (2000) 805; Ballav et al., *Angew. Chem.* **47** (2008) 1421
- [3] Review. I. Bald et al., *Int. J. Mass Spectrometry* **277** (2008) 4

An ionizing time-domain matter-wave interferometer

Philipp Haslinger¹, Nadine Dörre¹, Philipp Geyer¹, Jonas Rodewald¹, Stefan Nimmrichter¹, Klaus Hornberger² and Markus Arndt¹

¹*Universität Wien; Boltzmannngasse 5, A-1090 Wien, Austria, philipp.haslinger@univie.ac.at*

²*Universität Duisburg; Duisburg, Germany*

In the past century quantum physics has developed from an intriguing theory with daring Gedanken experiments to one of the most precisely studied and verified theories of nature. Yet, it is highly discussed whether there exists a mass or complexity limit to the predictions of quantum theory, a question famously formulated in Schrödinger's cat paradox. Here we present an ionizing time-domain matter-wave interferometer which will allow us to probe quantum mechanics on an increasingly large mass scale.

Our setup combines absorptive single-photon-ionization gratings [1] with the advantages of interferometry in the time-domain [2]. The interferometer uses pulsed standing laser light waves as diffracting structures. These can act as absorptive gratings for matter waves, as soon as the wavelength and laser intensity suffice to photo-ionize each particle with almost certainty in the vicinity of an anti-node of the standing wave. We use 157 nm F₂ lasers which allow us to realize the shortest optical diffraction gratings for complex matter waves to date. In contrast to material absorptive masks, such gratings allow to be operated in a pulsed mode, which makes the longitudinal motion of the particles negligible. This establishes a new kind of universal de Broglie interferometry for molecules or clusters, with two complementary goals:

On the one hand, we can explore the limits of quantum physics, specifically the de Broglie wave nature of massive particles, potentially up to 10⁶ amu or more. This is required for a recently proposed test of spontaneous quantum localization models [3].

On the other hand, matter-wave near-field interferometry [4,5] in combination with deflectometry [8] or spectroscopy [9] provides a molecular ruler on the nanoscale. This can be exploited to determine molecular properties, such as polarizabilities [6], electric and magnetic moments, susceptibilities, absorption and ionization cross sections among others [7] with high precision.

Near-field interferometry of the Talbot-Lau (TL) type [10] is particularly suitable for the coherent manipulation of mesoscopic matter, such as clusters, since it is compatible with rather moderate source requirements, i.e. with finite velocity spread and with a finite cluster beam width and divergence.

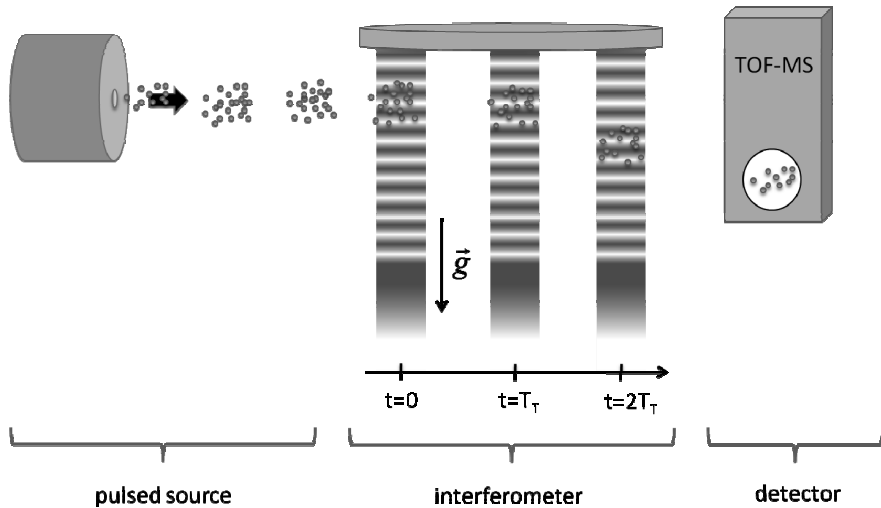


Figure 4: Optical Time-Domain Ionizing Matter Wave (OTIMA) Interferometer. A pulsed bunch of clusters is prepared and sent to interact with three subsequent UV standing light waves. The first one prepares the cluster coherence, the second realizes the diffraction process and the third grating probes the interferogram. Afterwards the clusters are photo-ionized and detected in a time-of-flight mass spectrometer.

TL-matter-wave interferometry usually requires three gratings: the first prepares transversal coherence in the particle beam by acting as an array of point sources. At the second grating the diffraction process takes place and the third grating is used to probe the matter wave interferogram that forms behind the second grating. In a material grating setup, the required spacing between gratings is proportional to the particle velocity. This concept can be translated into the time-domain by shifting the reference frame from the gratings to the particles. The role of the grating separation is then transformed into a delay in time. Our present implementation focuses on this temporal version and therefore offers a fundamental and decisive gain in precision.

The interferometer is sketched in Figure 1. It consists of three vacuum-ultra violet laser pulses with a variable pulse delay that are retro-reflected by the same mirror, thus realizing three standing light wave gratings. All three lasers have the same wavelength λ and create gratings of the same period $d = \lambda/2$, with a relative accuracy of $\Delta d/d = 10^{-6}$.

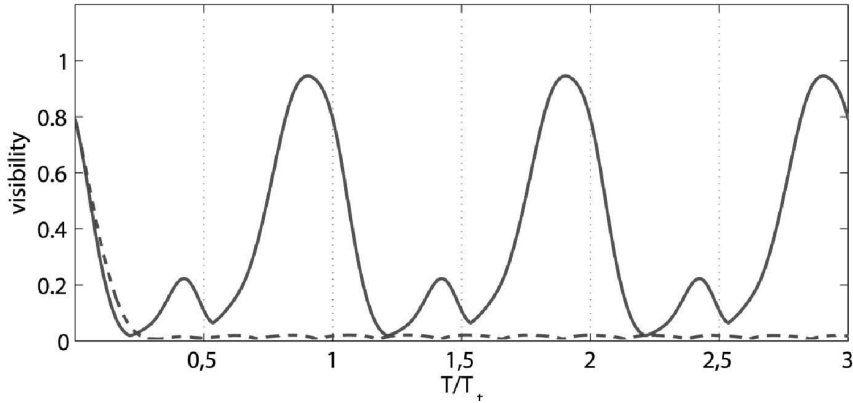


Figure 5: Simulated quantum fringe visibility (red) and classical fringe visibility (green dotted) for Au50 (ca. 10,000 amu) as a function of the pulse separation time T in relation to the Talbot time (see text). The classical density modulation is mainly produced by shadow effects of the grating and disappears for longer pulse separation times. We notice that a high fringe contrast is expected for a large variety of pulse separation times. This calculation was made under the assumption that the passing clusters absorb on average 8 photons in the antinode of the standing light field.

A short bunch of neutral particles is emitted by a pulsed source. While passing the mirror the particles are subjected to the three gratings which are separated in time by the Talbot time $T_T = md^2/h$. This is the delay after which the cluster de Broglie waves rephase and interfere. For our F_2 -lasers, the Talbot time scales with mass as 15 ns/amu, reaching up to 15 ms for a cluster of $m=10^6$ amu. It is important to note that the particle velocity does not enter in this consideration. Instead, the time between the grating pulses determines the evolution of the matter wave. Time-domain interferometry thus offers the appreciable advantage over fixed-length setups to eliminate many velocity-dispersive phase shifts and it introduces the precision of time and frequency measurements into complex matter-wave physics.

The laser light field interacts with the particles in two ways: Firstly, it applies a phase modulation $\phi \propto \alpha_{\text{opt}} E^2$ which is related to the interaction between the electric field E and the particle's optical dipole polarizability α_{opt} . Secondly, the wave function of each cluster becomes amplitude modulated through the single-photon ionization process that occurs at the antinodes of the standing light wave. The ionization and subsequent extraction of clusters from the antinodes realizes an absorptive light grating, similar in effect to a nanomechanical mask as used in other matter wave experiments [4]. The remaining neutral particles are effectively confined to regions close to the nodes of the field and seem to emerge from a grating of 'slits'. After their passage through all three gratings the clusters are detected by single photon post-ionization and time-of-flight mass spectrometry. Compared to material absorptive gratings the standing light waves offer a perfect sinusoidal grating structure

without any dispersive van-der-Waals forces [4]. This leads to a high visibility over a broad range of pulse separation times [Fig. 2].

TL interferometry expects the clusters to form a nanosized density pattern with the same period as the optical standing light wave. This has been proposed to be a suitable ruler for absorption spectroscopy [4] and it has been experimentally applied to determine molecular polarizabilities in quantum-enhanced deflectometry [5, 6] at longer scales, before. Our refined setup offers the possibility to extract additional information about photo-ionization and photo-dissociation probabilities, as well. Fragmentation or fluorescence between the first and third laser grating will also influence the visibility of the interference pattern because dissociated particles or emitted photons will carry ‘which-path’ information about the initially delocalized propagating matter wave into the environment.

The proposed OTIMA-interferometer is unique in the sense that it allows to work with a large class of nanoparticles, such as metal clusters, semiconductor nanocrystals and biomolecular complexes. It may act on objects as small as single atoms up to cold giant clusters, as long as ionization is the dominant response to the absorption of a single photon. The time-of-flight mass spectrometer allows to sort different cluster types and to record interference for different masses under identical conditions, independent of the particle velocities. This renders the instrument insensitive to common mode noise and systematic phase shifts.

References

- [1] Reiger E., et al., *Opt. Comm.*, **264**, 326-332 (2006)
- [2] Nimmrichter S., et al., *New J Phys.*, **13**, 075002 (2011)
- [3] Nimmrichter S., et al., *Phys. Rev. A*, **83**, 043621 (2011)
- [4] Brezger B., et al., *Phys. Rev. Lett.*, **88**, 100404 (2002)
- [5] Gerlich S., et al., *Nature Physics*, **3**, 711-715 (2007)
- [6] Berninger M., et al., *Phys. Rev. A*, **76**, 013607 (2007)
- [7] Hornberger K., et al., *Rev. Mod. Phys.*, (2011) accepted, in print
- [8] Tüxen J., et al., *Chem. Comm.*, **46**, 4145-4147 (2010)
- [9] Nimmrichter S., et al., *Phys. Rev. A*, **78**, 063607 (2008)
- [10] Clauser J.F., Li S., *Phys. Rev. A*, **49**, R2213 (1994)

Contributed Papers (Poster)

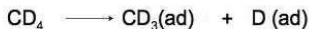
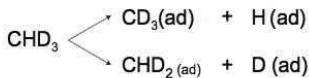
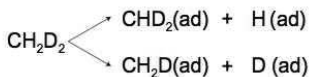
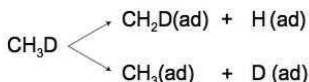
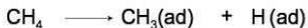
Vibrational Bond-Selectivity in Methane Chemisorption

Li Chen¹, Hirokazu Ueta¹, Régis Bisson², and Rainer D. Beck¹

¹ *Laboratoire de Chimie Physique Moléculaire, Ecole Polytechnique Fédérale de Lausanne, Switzerland. Corresponding author : Rainer.Beck@epfl.ch*

² *Aix-Marseille Univ, PIIM, 13397, Marseille, France.*

The contribution presents a study of vibrationally mediated bond-selective chemisorption of five different methane isotopologues on a Pt(111) surface. Vibrationally excited methane molecules are prepared by infrared laser pumping of a C-H stretch vibration in a molecular beam incident on a clean single crystal Pt(111) surface in ultra-high vacuum. Products of the dissociative chemisorption of methane are detected in-situ and online during the deposition by reflection absorption infrared spectroscopy (RAIRS). RAIRS detection enables us to distinguish the different surface bound methyl species $-\text{CH}_x\text{D}_y$ resulting from C-H and C-D cleavage reaction of the incident methane isotopologues according to Table 1.



While incident kinetic energy and/or thermal vibrational excitation produce a nearly statistical distribution of C-H and C-D bond cleavage products, we observe that laser excitation of an infrared active C-H stretch vibration leads to highly selective dissociation of a C-H bond for CHD_3 , CH_2D_2 , and CH_3D . Our results show that vibrational energy redistribution (IVR) between C-H and C-D stretch modes due to methane/surface interactions is negligible during the sub-picosecond collision time which indicates that vibrational bond-selectivity may be the rule rather than the exception in heterogeneous reactions of small polyatomic molecules.

Table 1: C-H and C-D cleavage channels in methane chemisorption.

Reactivity of Carbon Dioxide Radical Anions in Water Clusters

Robert F. Höckendorf,¹ O. Petru Balaj,¹ Kirsten Fischmann,¹ Amou Akhgarnusch,¹ Christian van der Linde,¹ K. Philip Jäger,¹ Qiang Hao,² Chi-Kit Siu² and Martin K. Beyer¹

¹Institut für Physikalische Chemie, Christian-Albrechts-Universität zu Kiel, Olshausenstraße 40, 24098 Kiel, Germany, beyer@phc.uni-kiel.de

²Department of Biology and Chemistry, City University of Hong Kong, 83 Tat Chee Avenue, Kowloon Tong, Hong Kong, PR China, email: chiksiu@cityu.edu.hk

While bare carbon dioxide forms a metastable anion [1], $\text{CO}_2^-(\text{H}_2\text{O})_n$ is stable [2], and its chemistry can be investigated by Fourier transform ion cyclotron resonance (FT-ICR) mass spectrometry. Among the studied reactions, proton transfer from CF_3COOH leads to removal of $[\text{H},\text{CO}_2]$ from the cluster, presumably in the form of $\text{OH} + \text{CO}$, while solvated $\text{CF}_3\text{COO}^-(\text{CF}_3\text{COOH})_n$ remain as the charged species. Neutral H atom transfer from CH_3SH , on the other hand, results in $\text{HCOO}^-(\text{H}_2\text{O})_n$, effectively synthesizing formic acid from CO_2 and CH_3SH [3]. CO_2^- also attacks disulfide bonds. DFT calculations show that formation of a C-S bond in CH_3SCOO^- explains the experimentally observed loss of the CH_3S radical in reactions with dimethyl disulfide. Besides C-H and C-S bond formation, also addition of the carbon dioxide radical anion to C-C double bonds is observed. Again, experiment and theory gives a concise picture of the reactivity of CO_2^- with allyl alcohol. In all cases, nanocalorimetry [4] provides additional insight into thermochemistry and reaction dynamics.

References

- [1] M. Knapp, O. Echt, D. Kreisle, T. D. Märk, E. Recknagel, *Chem. Phys. Lett.* **126**, 225-231 (1986)
- [2] C. E. Klots, *J. Chem. Phys.* **71**, 4172 (1979)
- [3] R. F. Höckendorf, C.-K. Siu, C. van der Linde, O. P. Balaj, M. K. Beyer, *Angew. Chem. Int. Edit.* **49**, 8257-8259 (2010)
- [4] R. F. Höckendorf, C. van der Linde, O. P. Balaj, M. K. Beyer, *Phys. Chem. Chem. Phys.* **12**, 3772-3779 (2010)

Low-energy electron-induced synthesis of formamide

E. Böhler, J. H. Bredehöft, P. Swiderek

Universität Bremen, Fachbereich 2 (Chemie/Biologie), Institute of Applied and Physical Chemistry, Leobener Straße / NW 2, Postfach 330440, 28334 Bremen, Germany

Formamide (HCONH_2) is the smallest molecule which contains a peptide bond and thus represents an important building block of biologically relevant substances. This contribution shows that exposure to low-energy electrons induces the production of formamide in condensed mixtures of ammonia (NH_3) and carbon monoxide (CO). Previous experiments on mixtures of NH_3 and ethylene (C_2H_4) have revealed that ethylamine ($\text{C}_2\text{H}_5\text{NH}_2$) is formed under low-energy electron exposure^[1]. This reaction is driven by electron impact ionization while dissociative electron attachment (DEA) is not involved as seen from the negligible formation of $\text{C}_2\text{H}_5\text{NH}_2$ at energies where DEA is prominent in NH_3 (around 5 eV and 9 eV^[2,3]). The reaction is initiated by ionization of either C_2H_4 (IE = 10.1 eV) or NH_3 (IE = 10.5 eV). In the analogous reaction between CO (IE = 14.0 eV) and NH_3 , however, a first maximum in the production of formamide around 9 eV coincides with a known DEA process in NH_3 ^[3]. This suggests that the production of formamide involves both electron impact ionization and DEA.

Experimental approach

Reactions in thin condensed films of mixtures of CO and NH_3 (1:1) were induced by exposure to a low-energy electron beam with tunable energy (E_0) and current density of a few $\mu\text{A}/\text{cm}^2$. All experiments took place under UHV conditions (10^{-10} mbar). Multilayer molecular films were deposited onto a polycrystalline gold substrate at 35 K. The formation of products was monitored after electron exposure by use of thermal desorption spectrometry (TDS). In these experiments, characteristic positive fragment ions of the desorbing molecules were monitored by mass spectrometry (electron impact ionisation at 70 eV) upon heating the Au foil with a rate of 1 K/s.

Identification of formamide

After irradiation of condensed mixtures of CO and NH_3 a product is observed that gives rise to a desorption signal in the 45 amu TDS curve (see Figure 1). As this mass corresponds to

the sum of the molecular masses of CO and NH₃, this leads to the assumption that an addition reaction has taken place. The most stable molecule, which could be formed from CO and NH₃ is formamide (HCONH₂). Other isomers include nitrosomethane (CH₃NO), formaldehyde oxime (H₂C=NOH), which both are known to be reactive compounds in the condensed phase, as well as several other high-energy species^[4]. Apart from formamide, all other isomers require extensive bond reorganisation if formed from CO and NH₃. In accord with the fact that 45 amu dominates the mass spectrum of formamide^[5], desorption signals recorded at other masses are much less pronounced. Furthermore, formation of nitrosomethane can be excluded because its characteristic fragment with mass 30 amu was not observed in the TDS experiments^[5]. To further support the assignment of the observed 45 amu desorption signal to formamide, thickness dependent TDS experiments on pure formamide were performed for comparison. They show a strong shift of the desorption temperature from 210 K at multilayer coverage to 230 K for a coverage of 0.2 monolayers (ML). The maximum desorption temperature of the 45 amu product is typically somewhat higher (240-260 K). However, the low intensity of the desorption peak points to an even smaller amount of product formed under electron exposure for which a desorption temperature of more than 230 K is not unexpected.

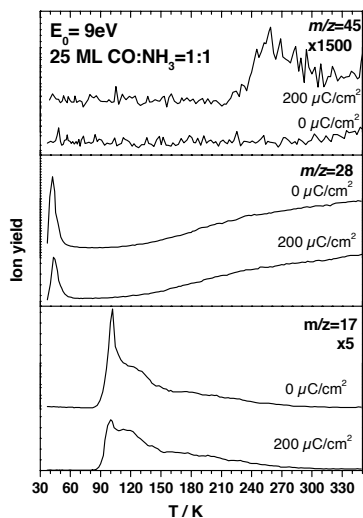


Figure 1: TDS results showing decay of NH₃ (17 amu) and CO (28 amu) as well as formation of formamide (45 amu) in mixed condensed multilayers of CO and NH₃ upon electron exposure.

Dependence of formamide production on electron exposure

The amount of produced formamide increases linearly with increasing electron exposure up to about 400 $\mu\text{C}/\text{cm}^2$ as deduced from the plot of the integrated desorption peaks in the

45 amu TDS data (see Figure 2). Therefore it can be assumed that the amount of product formed during an exposure of $200 \mu\text{C}/\text{cm}^2$ reflects the initial rates of the reaction between NH_3 and CO.

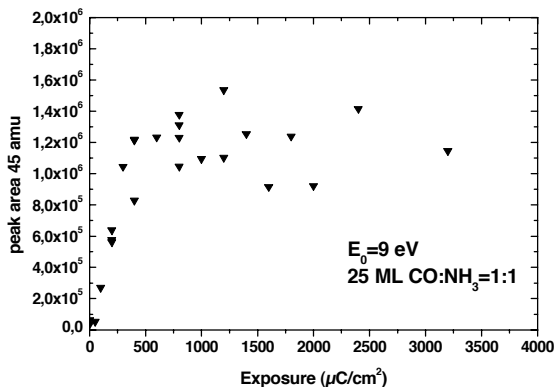


Figure 2: Integrated desorption peaks in the 45 amu TDS curves obtained after increasing electron exposure at 35 K of mixed condensed multilayers of CO and NH_3 .

Energy dependence of the formation of formamide

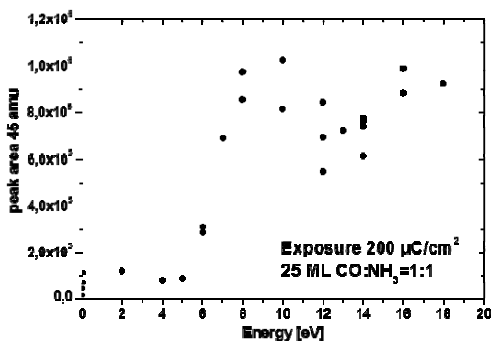


Figure 3: Integrated desorption peaks in the 45 amu TDS curves obtained at E_0 between 2 and 18 eV from mixed condensed multilayers of CO and NH_3 after an electron exposure of $200 \mu\text{C}/\text{cm}^2$ at 35 K.

Formation of formamide is observed at and above $E_0 = 6 \text{ eV}$. Above 13 eV, the amount of product increases with E_0 similar to the previous case of formation of ethylamine from NH_3 and C_2H_4 ^[1]. Therefore, an ionization-driven reaction mechanism can again be assumed.

However, in the present experiment, ionization of NH_3 is more likely responsible because its ionization energy (IE) is considerably smaller (IE = 10.4 eV)^[5] than for CO (IE = 14.0 eV)^[5]. In addition, a maximum around 8 – 10 eV is observed in the energy dependence of formamide production. This hints at a second independent formation pathway for formamide, which cannot be due to impact ionization.

Proposed mechanism of formamide production

An ionization-driven addition reaction has been suggested previously to explain the formation of ethylamine in condensed mixtures of NH_3 and C_2H_4 ^[1]. We suggest that in the present experiments an analogous mechanism also leads to the formation of formamide. This can explain product formation at E_0 above the ionization threshold of NH_3 (IE = 10.4 eV) (see Figure 4).

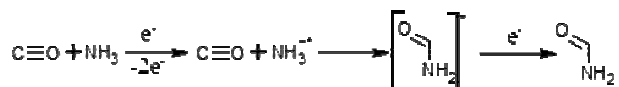


Figure 4: Reaction schematic for the electron impact induced condensation of carbon monoxide and ammonia.

However, the additional maximum in the rate of formamide production around 9 eV gives evidence for an additional reaction channel via DEA. Condensed-phase measurements on electron-stimulated desorption have shown that NH bond dissociation via DEA occurs in NH_3 within this range of E_0 ^[3].

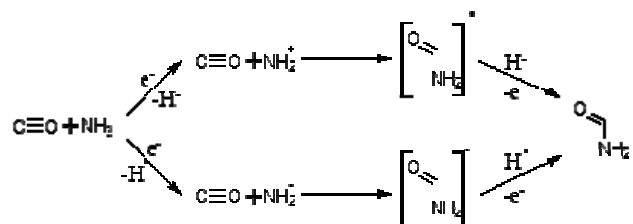


Figure 5: Reaction schematic for the DEA induced condensation of carbon monoxide and ammonia.

Judged from the respective heights of the desorption peaks, the production of formamide in the present experiments appears to be slower than that of ethylamine in condensed mixtures of NH_3 and C_2H_4 ^[1]. This difference in reactivity can be explained by the higher ionization threshold for carbon monoxide (IE = 14.0 eV) compared with that of ethylene

(IE = 10.1 eV)^[5], so that the alternative reaction channel involving ionization of CO only becomes accessible at higher E_0 . Therefore, a DEA-driven reaction may not be visible due to the dominance of ionization-driven reaction in NH_3 and C_2H_4 but become more obvious in the reaction between CO and NH_3 (see Figure 5).

References

- [1] T. Hamann, E. Böhler, P. Swiderek, *Angew. Chem. Int. Ed.* **48**, 4643 (2009).
- [2] M. Tronc, R. Azria, M. Ben Arfa, *J. Phys. Chem.B* **21**, 2497 (1988).
- [3] M. Tronc, R. Azria, Y. LeCoat, E. Illenberger, *J. Phys. Chem.* **100**, 14745 (1996).
- [4] A.Schulz, H.Brand, A.Villinger, *The chemistry of hydroxylamines, oximes and hydroxamic acids, Part 1*, Z.Rappoport, J.F.Liebman (Editors), Wiley, Chichester, (2009), p. 655.
- [5] NIST Chemistry WebBook, NIST Standard Reference Database Number 69, Eds. P. J. Linstrom and W. G. Mallard, June 2005, National Institute of Standards and Technology, Gaithersburg MD, 20899 (<http://webbook.nist.gov>).

Effect of organic ligands on electron-induced reactions of Si compounds

E. Böhler^{1,2}, D.Gschliesser¹, J.Postler¹, P. Swiderek², P.Scheier¹

¹ Universität Innsbruck, Institute for Ion Physics and Applied Physics, Technikerstr.25/3, A-6020 Innsbruck, Austria

² Universität Bremen, Fachbereich 2 (Chemie/Biologie), Institute of Applied and Physical Chemistry, Leobener Straße / NW 2, Postfach 330440, 28334 Bremen, Germany

Similar to carbon, also compounds of its heavier analogue silicon have been found in the interstellar medium. In this low-density environment where intermolecular encounters are very rare, reactive low-valent compounds like HSi^+ , SiO or SiCN can exist^[1,2]. Due to their reactivity, however, such molecules are difficult to investigate under laboratory conditions. Isolating such species in a matrix of inert gases is a strategy to stabilise them and make them accessible to spectroscopic investigation. Another strategy is to synthesize derivatives carrying suitable sterically hindering ligands which shield the reactive molecular sites from collisions with reaction partners^[1,2]. However, it must be questioned if the ligands do not also alter the behaviour of the molecules of interest towards reaction.

This project aims at investigating the effect of a variation of the organic ligands attached to a small silane on the reactivity of this molecule towards low-energy electrons. As a model system we investigated two different chlorosilanes, namely trimethylchlorosilane ($(\text{CH}_3)_3\text{SiCl}$) and phenyldimethylchlorosilane ($(\text{C}_6\text{H}_5)(\text{CH}_3)_2\text{SiCl}$). In interstellar environments slow electrons can be produced by ionising radiation. Their energies typically fall within the range of values where dissociative electron attachment (DEA) takes place, a process that can lead to dissociation and initiates molecular reactions with particularly large cross sections.

Due to the large electron affinity of Cl, dissociative electron attachment to trimethylchlorosilane and phenyldimethylchlorosilane should lead to dissociation of the SiCl bond producing Cl^- (see Figure 1)



Figure 1: Reaction schematic showing the dissociation of two different silanes into radicals and chloride upon electron attachment.

However, a phenyl group possesses low-lying unoccupied energy levels (electron attachment into the π^* orbitals of benzene takes place at energies of 1.15 eV and 4.8 eV^[3]) while methyl substituents do not. The specific aim of this project was to clarify if these low-lying orbitals can act as additional entrance pathways in dissociative electron attachment leading to abstraction of Cl⁻.

Crossed electron-molecular beam experiments on DEA of the two silanes were performed in Innsbruck using the apparatus VG ZAB-2SEQ. The details of this apparatus have been described elsewhere^[4]. Negative ion mass scans were performed for both silanes to find the anions produced by DEA during low-energy electron irradiation. For the anions found in mass scans, energy scans in the range from 0-50 eV were performed. The inlet pressure was 10^{-5} mbar for trimethylchlorosilane and $8 \cdot 10^{-6}$ mbar for phenyldimethylchlorosilane.

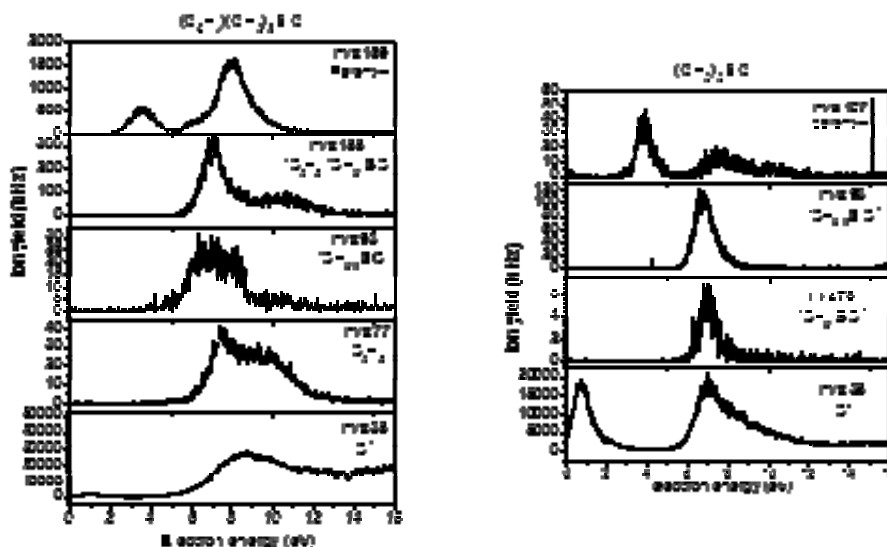


Figure 2: Energy scans for anion formation by DEA from trimethylchlorosilane and phenyldimethylchlorosilane

As expected the strongest signal found in the negative mass scans is from Cl⁻ for both molecules (see Figure 2). In the experiment on phenyldimethylchlorosilane energy scans were also performed for the anions C₆H₅⁻, (CH₃)₂SiCl⁻, (C₆H₅)(CH₃)SiCl⁻ and [M-H]⁻. In the case of trimethylchlorosilane, negative ion energy scans were performed for the anions Cl⁻, Si(CH₃)₃⁻, Si(CH₃)₂Cl⁻, SiCH₃Cl⁻ and [M-H]⁻ as well as for CH₃⁻ and CH₃Cl⁻ (not shown). For Cl⁻ two signals were found at about 1 eV and 8-9 eV. [M-H]⁻ signals appear at about 3-4 eV

and 8 eV . Signals of all other anions are located in the range between 7 and 11 eV. Anions formed by electron irradiation of SiH_4 ^[5] and Si_2H_6 ^[6] had been found in a similar energy range. In contrast to the initial hypothesis, the phenyl resonance at 4.8 eV does not lead to anion formation.

References

- [1] P.Jutzi, A.Mix, B.Rummel, W.W.Schoeller, B.Neumann, H.-G.Stammler, *Science* **305**, 849 (2004)
- [2] S.K.Mandal, H.W.Roesky, *Chem. Commun.* **46**, 6016 (2010)
- [3] M.Allan, *J.Electron Spectrosc.* **48**, 219 (1989)
- [4] D.Huber, M.Beikircher, S.Denifl, F.Zappa, S.Matejcik, A Bacher, V.Grill, T.D.Märk, P.Scheier, *J. Chem. Phys.* **125**, (2006)
- [5] P. Haaland *J. Chem. Phys.* **93**,4066 (2006)
- [6] E. Krishnakumar, S.K.Srivatava, I.Iga *Int J Mass Spectrom.* **103**, 107 (1991)

A Combined Crossed-Beam and Theoretical Study of Radical-Radical Reaction Dynamics of $O(^3P) + C_2H_3$

Min-Jin Park and Jong-Ho Choi

Department of Chemistry and Research Institute for Natural Sciences,
Korea University, 1, Anam-dong, Seoul 136-701, E-mail: jhc@korea.ac.kr

Herein, we present an overview of our recent studies of the gas-phase reaction dynamics of $O(^3P)$ with an iso-propyl radical [C_2H_3] as prototypical radical-radical oxidation reactions. High-resolution laser spectroscopy in a crossed-beam configuration was applied to examine the nascent rovibrational state distributions and Doppler profiles of the reactive scattering products. The analyses of the product energy and population distributions demonstrated the existence of unusual dynamic characteristics and competition between the addition and abstraction reaction mechanisms at the molecular level. These features, which are in sharp contrast with those of the oxidation reactions of closed-shell hydrocarbon molecules, are discussed with the aid of the *ab initio* and quantum statistical calculations.

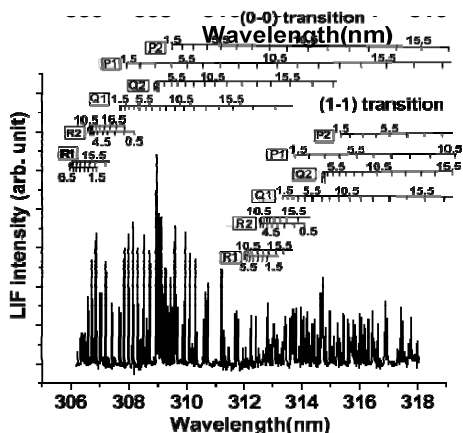


Figure 1: A typical LIF spectrum in the (0-0) diagonal band region of the nascent OH ($A \ ^2\Sigma^- \leftarrow X \ ^2\Pi$) produced from the reaction: $O(^3P) + C_2H_3 \rightarrow C_2H_2$ (acetylene) + OH

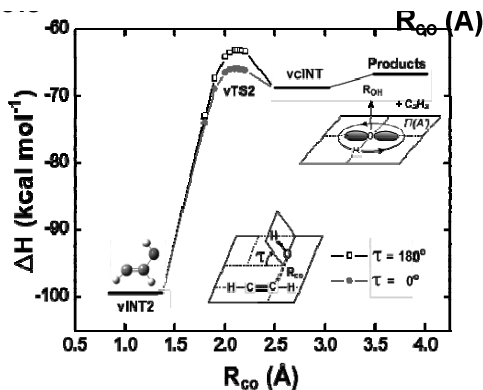


Figure 2: Comparison of two computed pathways of vINT2 showing the dependence on the dihedral angles (τ) of 0° and 180° along the $O(^3P) + C_2H_3 \rightarrow C_2H_2$ (acetylene) + OH reaction coordinates at the CBS-QB3 level of theory.

References

- [1] Jong-Ho Choi, *Int. Rev. Phys. Chem.* **25**, 613 (2006), and references therein.
- [2] Min-Jin Park, Kyoo-Weon Kang, Gi Woo Lee, Jong-Ho Choi, *Chem. Eur. J.* **17**, 11410 (2011).

Toward a new global potential energy surface for the $\text{H}_2\text{O}\cdots\text{HF}$ complex

Yann Cornaton, Roberto Marquardt

Laboratoire de Chimie Quantique

Institut de Chimie UMR 7177 CNRS/Université de Strasbourg

4 rue Blaise Pascal - CS90032 - 67081 Strasbourg cedex - France

ycornaton@unistra.fr

Abstract

The reaction between a water molecule and an hydrogen fluoride molecule is a prototype system for the study of the hydrogen bond up to the proton transfer within the current capacities of carrying out calculations of full-space (here 9-dimensional) molecular quantum dynamics [1, 2]. The study of this system is relevant in astrochemistry for understanding the $\text{H}_2\text{O}/\text{HF}$ ratio in the galactic sources [3], the chemistry of ices [4], and the proton transfer in the interstellar space [5]. Following previous work [6], we aim at determining a global and yet spectroscopically accurate representation of the ground state potential energy surface (PES) of the $\text{H}_2\text{O}\cdots\text{HF}$ complex to be used in these calculations. A new analytical function based on the physical angular dependency of induction and dispersion potentials is used in addition to covalent potential terms. It is fitted to electronic energies of the complex under constraints taken from spectroscopic [7] and thermodynamic data. In this contribution, preliminary results on our first model will be presented.

Introduction

To carry out molecular quantum dynamics calculations, one has first to investigate the dependency of the energy with the geometry of the complex so as to define the potential energy surface (PES). In this study, the approach of representing the PES by a non-polynomial compact expression has been chosen.

Usually, multivariate polynomials are used to represent PES. Such an approach has been used also for the $\text{H}_2\text{O}\cdots\text{HF}$ complex [8]. Although these models are rather simple to use and to be fitted to energies, they exhibit some drawbacks which will be dispensed with by using a non-polynomial compact expression. Such an expression reduces the number of parameters to be fitted from several hundreds to a few tens, typically [9]. The global character of the PES is also more easily reachable with such an expression. Often, it is possible to give a physical meaning to the parameters and it is possible to fit them under spectroscopic and thermodynamic constraints.

To describe the interactions in the 9-dimensional space of the $\text{H}_2\text{O}\cdots\text{HF}$ complex, the following 9-coordinates set is defined (see Figure 1) :

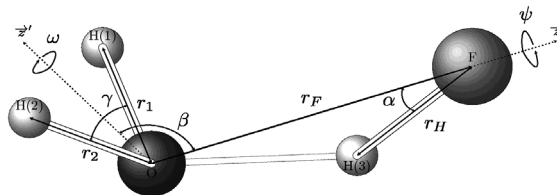


Figure 1 :
Coordinate set
defining the
 $H_2O \cdots HF$ complex

This coordinate set is composed by 4 lengths (r_F , r_H , r_1 , r_2), 3 polar angles (γ , β , α) and 2 azimuthal angles (ω , ψ).

Model

$$V = V_0 + V_{H_2O} + V_{HF} + V_{xc} + V_{dd} + V_{ind} + V_{dis} \quad (1)$$

The model presented in this study is based on the sum of different physical terms :
where :

V_0 is an additive constant,

V_{H_2O} is the internat potential of the H_2O monomer (2 OH 2-body potentials and 1 HOH 3-body potential),

V_{HF} is the internal potential of the HF monomer (1 FH 2-body potential),

V_{xc} is a repulsive exchange potential between the monomers (simple decreasing exponential),

V_{dd} is the dipole-dipole interaction potential,

V_{ind} is the induction potential,

V_{dis} is the dispersion potential.

The analytical expressions used for the dipole-dipole interaction, induction and dispersion potentials are the physical ones taken from the litterature [10] :

$$V_{dd} = - \sum_{tu} \mu_t^{(HF)} T_{tu} \mu_u^{(H_2O)} \quad (2)$$

$$V_{ind} = \frac{-1}{2} \sum_{tt'uu'} (\mu_t^{(HF)} T_{tt'} \alpha_{t'u'}^{(H_2O)}(0) T_{u'u} \mu_u^{(HF)} + \mu_t^{(H_2O)} T_{tt'} \alpha_{t'u'}^{(HF)}(0) T_{u'u} \mu_u^{(H_2O)}) \quad (3)$$

$$V_{dis} = \frac{-\hbar}{2\pi} \sum_{tt'uu'} T_{tu} T_{t'u'} \int_0^\infty \alpha_{tu}^{(HF)}(i\nu) \alpha_{t'u'}^{(H_2O)}(i\nu) d\nu \quad (4)$$

where $\underline{\mu}$ is the dipole moment, $\underline{\alpha}$ is the polarisability tensor (static and dynamic) and \underline{T} is the tensor defined by :

$$T_{iu} = \frac{1}{4\pi\epsilon_0} \nabla_i \nabla_u \frac{1}{r} \quad (5)$$

All the vectors and tensors have been expressed in the same cartesian reference frame as functions of the inter-monomer coordinates (r_F , β , ω , α , ψ). Developing equations (2), (3)

$$V_{\text{ind}} = \frac{-1}{r_F^3} M^2 \mathcal{D} \quad (6)$$

$$V_{\text{ind}} = \frac{-1}{r_F^3} \left(A_o^{(s)} \mathcal{A}_o^{(s)} + A_p^{(s)} \mathcal{A}_p^{(s)} + A_x^{(s)} \mathcal{A}_x^{(s)} + A_y^{(s)} \mathcal{A}_y^{(s)} + A_z^{(s)} \mathcal{A}_z^{(s)} \right) \quad (7)$$

$$V_{\text{dis}} = \frac{-1}{r_F^6} \left(A_{\text{ox}}^{(d)} \mathcal{A}_{\text{ox}}^{(d)} + A_{\text{oy}}^{(d)} \mathcal{A}_{\text{oy}}^{(d)} + A_{\text{oz}}^{(d)} \mathcal{A}_{\text{oz}}^{(d)} + A_{\text{pxx}}^{(d)} \mathcal{A}_{\text{pxx}}^{(d)} + A_{\text{pyx}}^{(d)} \mathcal{A}_{\text{pyx}}^{(d)} + A_{\text{pzz}}^{(d)} \mathcal{A}_{\text{pzz}}^{(d)} \right) \quad (8)$$

and (4) using these expressions leads to the following ones :

where \mathcal{D} , the $\mathcal{A}_i^{(s)}$ and the $\mathcal{A}_{ij}^{(d)}$ are more complicated functions of the inter-monomer orientation angles (β , ω , α , ψ) and M^2 , the $A_i^{(s)}$ and the $A_{ij}^{(d)}$ are effective fit parameters which can be related to some physical quantities (dipole moments, polarisabilities).

Methods

Series of electronic energies have been calculated *ab initio* at the CCSD(T) level of theory using an aug-cc-pVTZ basis set and taking into account the basis superposition error (BSSE) using the Molpro 2009.1 program [11] covering a large part of the 9D space of the geometries for the $\text{H}_2\text{O}\cdots\text{HF}$ complex.

Effective parameters of the analytical model potential have been fitted to these energies under spectroscopic and thermodynamic data. The algorithm used for this fit is an extended Levenberg-Marquardt algorithm [12].

Results

Figure 2 shows a first comparison between calculated energies (stars) and the fitted analytical model (line) for 1-dimensional cuts of the PES along inter-monomer coordinates around the equilibrium geometry of the complex ($r_F = 2.651\text{\AA}$, $r_H = 0.938\text{\AA}$, $r_l = r_2 = 0.961\text{\AA}$, $\gamma = 105.1^\circ$, $\beta = 131.1^\circ$, $\omega = 0.0^\circ$, $\alpha = 1.6^\circ$, $\psi = 180.0^\circ$) [8].

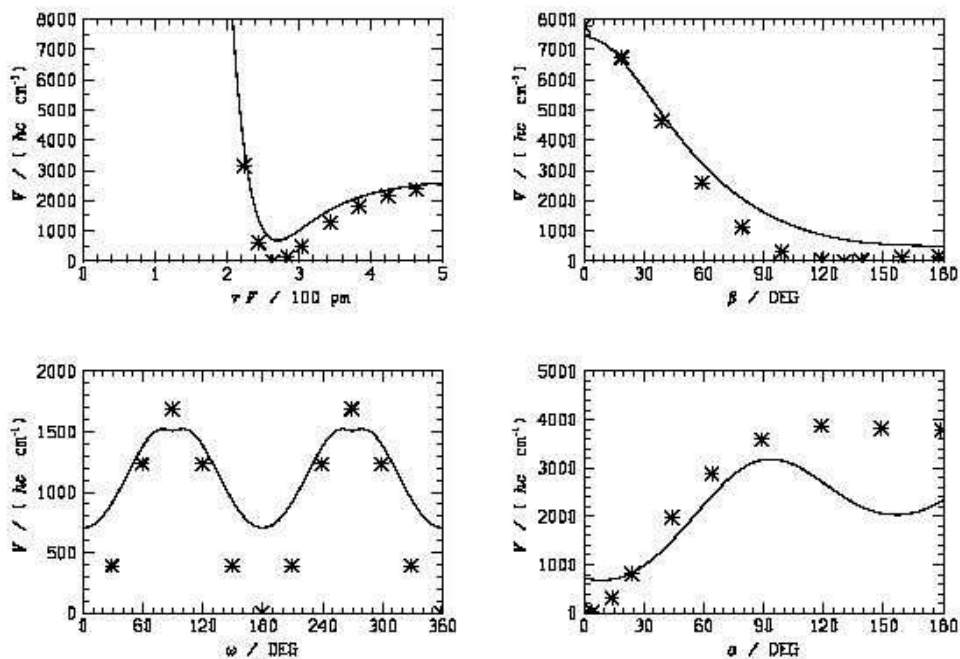


Figure 2 : 1D cuts of the PES of $\text{H}_2\text{O}\cdots\text{HF}$ around the equilibrium geometry along r_F (top left), β (top right), ω (bottom left) and α (bottom right)

Conclusions

In this contribution, a preliminary work on a new analytical model for the global potential energy surface of the $\text{H}_2\text{O}\cdots\text{HF}$ complex is reported. This first simple model fits rather well the shape of calculated energies but more work remains to be done to improve the model.

Acknowledgment

The authors thank N. Loëte for valuable contributions to this paper, and M. Lewerenz for very fruitful discussions

References

- [1] O. Vendrell, F. Gatti, H.-D. Meyer, *J. Chem. Phys.* **127**, 184303 (2007)
- [2] X.-G. Wang, T. Carrington Jr., *J. Chem. Phys.* **119**, 101 (2003)

-
- [3] R.R. Monje, M. Emprechtinger, T.G. Phillips, D.C. Lis, P.F. Goldsmith, E.A. Bergin, T.A. Bell, D.A. Neufeld, P. Sonnentrucker, *Astrophys. J. Lett.* **734**, L23 (2011)
- [4] K.I. Oumlberg, E.F. Van Dishoeck, H. Linnartz, S. Andersson, *Astrophys. J.* **718**, 832 (2010)
- [5] S.-C. Xu, L.-Y. Ma, F.-Y. Bian, Q. Shi, M.-F. Ge, X.-K. Zhang, *Acta Physico-Chimica Sinica* **25**, 2312 (2009)
- [6] R. Marquardt, K. Sagui, W. Klopper, M. Quack, *J. Phys. Chem. B* **109**, 8439 (2005)
- [7] V.P. Bulytchev, I.M. Grigoriev, E.I. Gromova, K.G. Tokhadze, *Phys. Chem. Chem. Phys.* **7**, 2266 (2005)
- [8] J. Demaison, J. Liévin, *Mol. Phys.* **109**, 1249 (2008)
- [9] R. Marquardt, M. Quack, "Global Analytical Potential Energy Surface for High-resolution Molecular Spectroscopy and Reaction Dynamics" in *Handbook of High-resolution Spectroscopy*, John Wiley, Chichester, UK (2011)
- [10] A. Stone, *The Theory of Intermolecular Forces*, Oxford University Press, Oxford, UK (1996)
- [11] Molcas, a package of *ab initio* programs designed by H.-J. Werner and P.-J. Knowles, version 2009.1, Cardiff, UK
- [12] R. Marquardt, *J. Math. Chem.*, DOI 10.1007/s10910-011-9819-2 (2011)

The submersion of sodium clusters in helium nanodroplets: Identification of the surface → interior transition

Matthias Daxner¹, Lukas An der Lan¹, Peter Bartl¹, Christian Leidlmair¹, Harald Schöbel¹, Roland Jochum¹, Stephan Denifl, Tilmann D. Märk¹, Andrew M. Ellis² and Paul Scheier¹

¹ *Institut für Ionenphysik und Angewandte Physik und Research Platform Advanced Materials, Universität Innsbruck, Technikerstr. 25, A-6020 Innsbruck, Austria*

² *Department of Chemistry, University of Leicester, University Road, Leicester LE1 7RH, United Kingdom*

We recently reported ^[1] the submersion of sodium clusters beyond a critical size in helium nanodroplets, which had been predicted on theoretical grounds in 2010 ^[2] but had not been hitherto demonstrated experimentally. Confirmation of a clear transition from a surface location, which occurs for alkali atoms and small clusters, to full immersion for larger clusters, is provided by identifying the threshold electron energy required to initiate Na_n cluster ionization. On the basis of these measurements, a lower limit for the cluster size required for submersion, $n \geq 21$, has been determined. This finding is consistent with the recent theoretical prediction.

Experimental Setup

A cluster source generates the helium cluster beam by supersonic expansion (Conditions: 25 bar helium pressure, 5.7 K nozzle temperature and 5 μm nozzle diameter). The beam is doped with sodium in a 6 cm long pick-up chamber. The beam is then ionized by electron impact and the mass spectrum is recorded with an orthogonal time-of-flight mass spectrometer with high mass resolution (>5000 FWHM). Sodium vapour was generated by oven evaporation and both the oven and

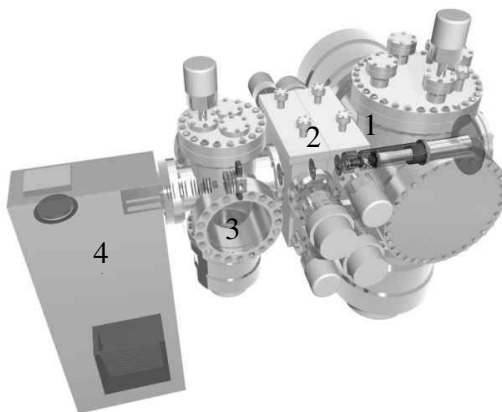


Figure 6: *Experimental setup of the CLUSTOF-Experiment. The helium nanodroplets are generated by supersonic expansion in the cluster source (1) then pass the pick-up region (2) before they are ionized (3) and finally are detected with a Reflecton-TOF (4)*

the pick-up cell were heated to 270 C°, which should correspond to a sodium vapour pressure of approximately 5×10^{-3} mbar. Due to the additional pumping in the pick-up region the local sodium pressure encountered by the helium droplet beam is expected to be significantly lower but was not measured. Electrons emitted from a tungsten filament and accelerated up to 150 eV are used for ionization. The energy resolution was about 1 eV and the achieved accuracy of the ionization energies lies in the range of ± 0.3 eV.

Results and Discussion

Magic Numbers

Cluster ions with up to ~ 100 Na were easily seen in this work. These are much larger than in previous studies^[3], which yielded maximum sizes of 25 atoms. The odd-even oscillation and the observed magic numbers (9, 21, 41, 59, and 93) are well known and can be explained by a model similar to electron shells.

One should note that we would not expect to see any magic number features if the ions were efficiently cooled by the helium.

The cooling of the Na_n^+ clusters in our work will be suppressed by the fact that the formation of neutral Na_n clusters will remove most of the helium. The binding energy per atom in a sodium cluster has been calculated to be 0.6 eV. Each sodium atom attached will remove about 1000 helium atoms and 100 more because of their thermal energy (assuming the binding energy of a helium atom in cluster is about 0.6 meV). The assumed helium mean cluster size in this work is 10^5 atoms, so for the key Na_n ($n < 30$) cluster sizes interrogated in the next section the majority of them should be in/on helium droplets of several thousand helium atoms.

There are two options for ionisation: charge transfer from He^+ (delivers 24.6eV) or Penning ionisation via He^* (19.8eV). The low ionisation energy of sodium clusters ($< 5\text{eV}$) shows that there is a huge amount of energy to dissipate, i.e. hot Na_n^+ clusters are formed. Fragmentation of the hot Na_n^+ leads to the size distribution seen in Fig. 2, because more stable clusters are more likely formed.

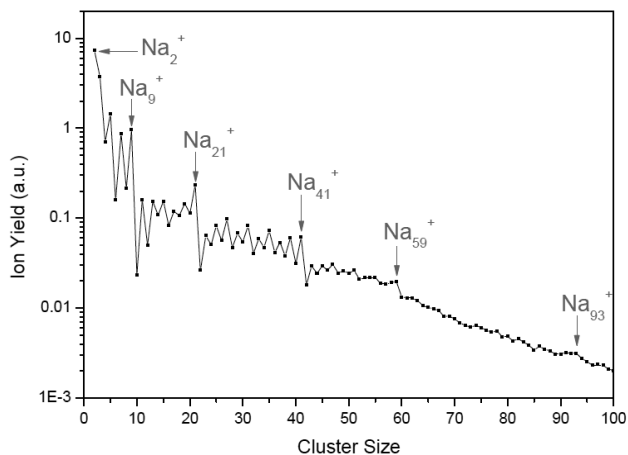


Figure 7: Plot of the measured abundance of Na_n^+ cluster ions as a function of n , obtained at an electron impact energy of 77eV

Sodium cluster immersion

The two possible ionisation processes differ not only by their energy onsets, but also the location where ionisation takes place is different. He^+ transfers its charge by charge hopping. For a positive hole the energy is progressively lowered as it moves to the centre of the droplet, so the charge hopping route will more likely point to the centre^[4]. On the other hand the metastable 2^3S state will favour a surface location. Consequently, it is expected that Penning ionisation will primarily ionize dopants on the surface, while a positive hole will more likely ionize a dopant in the interior of the droplet. These two processes make it possible to distinguish between surface and interior locations for the neutral sodium cluster.

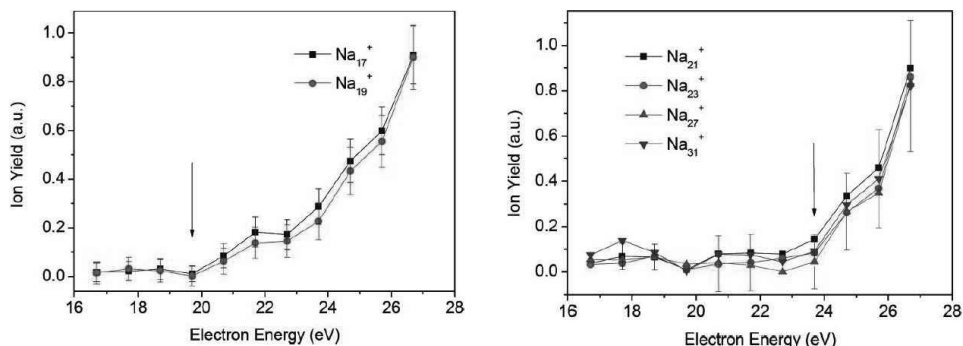


Figure 8: Ion yield as a function of energy for Na_{17}^+ and Na_{19}^+ (left) and Na_{21}^+ , Na_{23}^+ , Na_{27}^+ and Na_{31}^+ (right). The error bars were obtained from Poisson statistics. The arrows mark the point where the ion yield begins to rise above background level.

In Figure 3 we can see a clear difference between the ion yield of clusters smaller than 20 atoms, with a first energy onset at 20 eV and clusters with more than 20 atoms. For these small clusters there is no detectable rise of ion yield at 20 eV, which suggests that Penning ionisation is unimportant in the production of these ions. Both curves show an onset close to 24 eV, which is explained by ion production by charge transfer from He^+ . The ion yield curves for Na_{19}^+ and smaller clusters are consistent with a surface location of the corresponding neutral clusters, whereas those for Na_{21}^+ and larger clusters are consistent with an interior location. However, establishing the precise size at which the surface-interior transition occurs is complicated by ion fragmentation, which can arise because of the considerable excess energy released regardless of whether ionization is mediated via He^* or He^+ . Thus we only can establish a lower limit of $n \geq 21$ for sodium submersion in ^4He droplets. Nevertheless, this lower limit is in excellent agreement with a recent theoretical

prediction made by Stark and Kresin, whose model suggested that the minimum Na_n cluster size for submersion in ^4He droplets occurs at $n = 21$ [2].

Acknowledgment

The work was supported by the FWF, Wien (P19073) and the European Commission, Brussels. A.M.E. is grateful to the University of Innsbruck for financial support. S.D. gratefully acknowledges an APART grant from the Austrian Academy of Sciences. L.A.d.L., P.B., and C.L. thank the University of Innsbruck for support via the Doktoratsstipendium aus der Nachwuchsförderung.

References

- [1] L. An der Lan, P. Bartl, C. Leidlmair, H. Schöbel, R. Jochum, S. Denifl, T.D. Märk, A. Ellis, P. Scheier, *J. Chem. Phys.* **135**, 044309 (2011)
- [2] Stark and V. V. Kresin, *Phys. Rev. B* **81**, 085401 (2010)
- [3] J. Tiggesbäumker and F. Stienkemeier, *Phys. Chem. Chem. Phys.* **9**, 4748 (2007).
- [4] A. M. Ellis and S. Yang, *Phys. Rev. A* **76**, 032714 (2007).

Excited alkali atoms in He_n : influence of the dimer potential energy curves

David Dell'Angelo¹, Grégoire Guillon² and Alexandra Viel¹

¹ *Institut de Physique de Rennes, UMR 6251, CNRS et Université de Rennes 1, F-35042 Rennes, France*

² *Departement of Chemistry, University of Waterloo, Waterloo, N2L 3G1, Canada*

These last two decades, helium clusters¹ have attracted considerable attention in many experimental and theoretical groups. These finite systems present unique and peculiar properties, like for example superfluidity. Various dopants, from atoms to large biological molecules, have been used to probe at the molecular scale, the interior and the surface properties of these liquid droplets.

Helium nano-droplets also offer a quite unique and weakly perturbing environment, with cold temperature, quantum nature, high thermal conductivity and superfluidity, for the spectroscopic study of diverse species including unstable and transient systems.

In this perspective, the HENDI spectroscopy and its usage within electronic spectroscopy is an advantageous alternative to cryogenic matrix isolation spectroscopy in crystalline phase.

Alkali atoms appear to be among the best candidates for the study of electronic excitation due to the simple electronic configuration and the optically accessible electronic transitions.

In their electronic ground state, they reside on the surface of the helium clusters because the alkali-helium interaction is several times weaker than the helium - helium van der Waals attraction.

Our work

With the aim of studying Li^*He_n and Na^*He_n clusters, a systematic study of two global potential energy surfaces based on a DIM modeling and including the spin orbit coupling term has been performed.²

The surfaces differ by the $A^2\Pi$ and $B^2\Sigma$ diatomic energies used for building the DIM matrix, either Pascale's or our *ab initio* curves. In addition to the smaller well depths obtained with our *ab initio* curves, more subtle effects induced by the non-pair additive model used are obtained. The classical analysis is extended by IS-DMC computations of energetics and structural properties of Li^*He_n and Na^*He_n clusters in the first electronic excited state and with $n \leq 5$.

Globally the results are independent of the diatomic curves used, since in both cases clusters are found stable with up to 5 helium atoms in the first shell for Li and Na.

The Li doped cluster helium densities show more dependences on the diatomic curves used than the Na doped clusters. Concerning energetics, the largest difference is obtained for the chemical potential of Li^+He_5 cluster.

One can easily conceive that a larger difference in the diatomic curves could have led to a more visible difference in the clusters, like for example, pushing this fifth helium atom in the second solvation shell. Keeping in mind that the current study does not test the validity of the DIM modeling used to represent the interaction potential, the physical conclusions obtained with Pascale's curves seem quite reasonable.

A systematic study of the alkali series including larger cluster sizes using these curves is in progress.

References

- [1] J. P. Toennies and A. F. Vilesov, *Angew. Chem. Int. Ed.*, **43**, 2622 (2004)
- [2] D. Dell'Angelo, G. Guillon and A. Viel, *J. Chem. Phys.*, (submitted)

State selective study of the recombination of D_3^+ ions with electrons

Petr Dohnal, Michal Hejduk, Jozef Varju, Peter Rubovič, Sergii Opanasiuk, Radek Plašil and Juraj Glosík

Charles University, Faculty of Mathematics and Physics, Department of Surface and Plasma Science, V Holesovickach 2, Praha 8, 180 00, Czech Republic, pr.dohnal@seznam.cz

Introduction

Recombination of D_3^+ ions (and its isotopologue H_3^+ ions) with electrons has been one of the most important problems in recombination studies for over fifty years [1,2]. For many years there were significant differences between recombination rate coefficients obtained in different types of experiments [3,4,5,6] and the difference between the experimental values and the theoretical ones was of several orders of magnitude [7]. In 2001 a new theory of fast dissociative recombination emerged [8] and after further improvement [9] a very good agreement with storage ring experiments [3] was achieved. The main differences in magnitude between recombination rate coefficients of D_3^+ (H_3^+) obtained in plasmatic experiments and in storage rings was explained by existence of fast helium assisted ternary recombination channel [10]. Recombination of H_3^+ ions with electrons was also studied by means of absorption spectroscopy [11,12] but to our best knowledge there is no such study for D_3^+ . In presented study we measure the binary recombination rate coefficient α_{bin} and helium assisted ternary recombination rate coefficient K_{He} of D_3^+ recombination with electrons: $D_3^+ + e^- \xrightarrow{\alpha_{\text{eff}}} \text{products}$, $\alpha_{\text{eff}} = \alpha_{\text{bin}} + K_{\text{He}}[\text{He}]$, where $[\text{He}]$ is number density of helium buffer gas. We monitor plasma parameters (ion number density, rotational temperature T_{Rot} , kinetic temperature T_{Kin}) in D_3^+ dominated plasma during the discharge and afterglow.

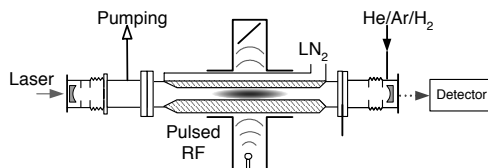


Figure 1: Discharge tube equipped with an optical resonator (not in scale). A discharge is ignited in the middle part of the glass discharge tube in a He/Ar/ D_2 gas mixture. Light signal passing through the cavity is measured by an InGaAs avalanche photodiode.

Experiment

A cavity ring down spectroscopy in a continuous wave modification (cw-CRDS) [13] is used as a main diagnostics tool to measure number densities of ions of interest. A schematic picture of the apparatus is shown in Figure 1. Microwave discharge is periodically ignited in a glass discharge tube cooled by liquid nitrogen and an evolution of ion number densities in discharge and early afterglow is measured. The lowest rotational levels of the vibrational ground state of the D_3^+ ion are shown in Figure 2. The arrows indicate the rotational levels probed in this study (we used transitions at 5793.92 cm^{-1} and 5792.68 cm^{-1} for ortho- D_3^+ (0,0) and meta- D_3^+ (4,2) respectively).

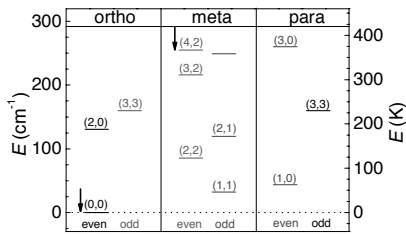


Figure 2: The lowest rotational levels of the ground vibrational state. Each rotational level is indicated by corresponding quantum numbers (J,G). The energy levels were taken from [14]. For details on notation see [15]. Arrows indicate the rotational states observed in the present study.

Results

Example of measured ion number density evolutions in discharge and early afterglow is shown in the upper panel of Figure 3. Dashed vertical line indicates end of the discharge region. The evolution of the ratio of the number density of the meta- D_3^+ (4,2) to the number density of the ortho- D_3^+ (0,0) is shown in the lower panel of Figure 3. The horizontal dashed line indicates ratio of these two states according to the thermodynamic equilibrium at 80 K.

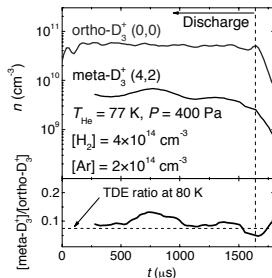


Figure 3: **Upper panel:** Measured number densities of the ions in ortho (1,0) and meta (4,2) states of D_3^+ in discharge and early afterglow. **Lower panel:** Ratio of the number densities of the states shown in the upper panel. Dashed line indicates value of this ratio corresponding to the thermodynamic equilibrium (TDE) at 80 K.

The mean value of rotational temperature evaluated from populations of these two states is (84 ± 7) K. This is in agreement with previous measurements in H_3^+ dominated plasma when rotational temperature of the ions in discharge was also close to the temperature of the wall and to the measured kinetic temperature of the ions $T_{Rot} = T_{Kin} = T_{He}$ [16]. The detailed calculation of electron energy relaxation leads to the conclusion that plasma in afterglow is in local thermodynamic equilibrium (for details see [17]).

An example of the time decay of overall D_3^+ ion number density ($[D_3^+] = n_e$) in afterglow is plotted in log-log scale in Figure 4 together with data from the previous flowing afterglow experiment [10]. The full line indicates the evolution of the electron number density n_e with losses by effective binary recombination without other loss channels:

$$n_e = 1/(\alpha_{eff}(t-t_0) + 1/n_{e0}) \quad (1)$$

where $\alpha_{eff} = 1.5 \times 10^{-7} \text{ cm}^3 \text{ s}^{-1}$ is the effective binary recombination rate coefficient, t is time and $n_{e0} = 2 \times 10^{11} \text{ cm}^{-3}$ is electron number density in time $t_0 = 0 \text{ } \mu\text{s}$. The dashed line indicates the calculated decay due to the ternary collisional radiative recombination [18] (for details see equation (5) in ref. [19]):

$$n_e = 1/\sqrt{2K_{CRR}(t-t_1) + 1/n_{e0}^2} \quad (2)$$

where $K_{CRR} = 1 \times 10^{-17} \text{ cm}^6 \text{ s}^{-1}$ is the ternary recombination rate coefficient taken from [19], the calculation was normalized to fit the CRDS data at $t_1 = 16 \text{ } \mu\text{s}$. From this figure it is clearly visible that the decay of the plasma is governed by dissociative recombination rather than by collisional radiative recombination. Deviation of the CRDS data from the full line is due to the diffusion losses. Note large extend of the timescale and of the electron number densities where is dependence (1) a very good approximation of electron number density decay.

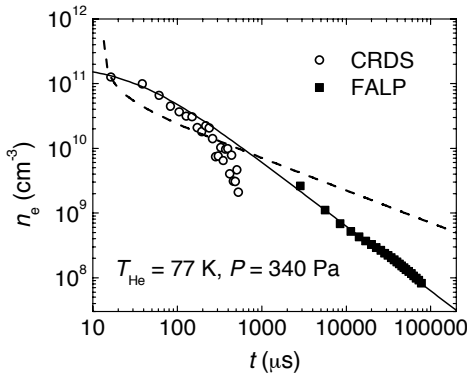


Figure 4: Time evolution of the electron number density in D_3^+ dominated He/Ar/ D_2 plasma obtained in presented stationary afterglow experiment (open circles) and in flowing afterglow experiment (squares) [10] at the same temperature and pressure. Full line corresponds to electron number density decay due to effective binary recombination ($\alpha_{eff} = 1.5 \times 10^{-7} \text{ cm}^3 \text{ s}^{-1}$) only. Dashed line corresponds to electron number density decay due to collisional radiative recombination only (see in text).

Conclusion

We have presented the first preliminary results of our spectroscopic study of the recombination of the D_3^+ ions with electrons. By probing two rotational states of the D_3^+ ion we evaluated the rotational temperature of the D_3^+ ions in discharge to be (84 ± 7) K. We concluded that plasma in afterglow is in local thermodynamic equilibrium. Results from previous FALP experiment [10] and current stationary afterglow data measured at the same temperature and pressure are in good agreement with each other. To our best knowledge this is the first spectroscopic study of D_3^+ recombination. Further measurements are in progress.

Acknowledgement

This work is a part of the research plan MSM 0021620834 and grant OC10046 financed by the Ministry of Education of the Czech Republic and was partly supported by GACR (202/07/0495, 202/08/H057, 205/09/1183, 202/09/0642), by GAUK 92410, GAUK 353811, GAUK 54010 and by COST Action CM0805 (The Chemical Cosmos).

References

- [1] M. Larsson, A. E. Orel, *Dissociative Recombination of Molecular Ions* (Cambridge University Press, New York, 2008)
- [2] M. Larsson, B. McCall, A. E. Orel, *Chem. Phys. Lett.* **462**, 145 (2008)
- [3] A. Le Padellac, et al., *Physica Scripta* **57**, 215 (1998)
- [4] S. Laube et al., *J. Phys. B: At. Mol. Opt. Phys.* **31**, 2111 (1998)
- [5] V. Poterya et al., *Phys. Rev. Lett.* **88(4)**, 044802 (2002)
- [6] O. Novotný et al., *J. Phys. B: At. Mol. Opt. Phys.* **39**, 2561 (2006)
- [7] A. E. Orel et al., *Philos. Trans. R. Soc. London, Ser. A* **358**, 2445 (2000)
- [8] V. Kokoouline, C. H. Greene, B. D. Esry, *Nature* **412**, 891 (2001)
- [9] V. Kokoouline, C. H. Greene, *Phys. Rev. A* **68(1)**, 012703 (2003)
- [10] J. Glosík, I. Korolov, R. Plašil, et al., *Phys. Rev. A* **80(4)**, 042706 (2009)
- [11] T. Amano, *J. Chem. Phys.* **92**, 6492 (1990)
- [12] J. Varju et al., *Phys. Rev. Lett.* **106(20)**, 203201 (2011)
- [13] D. Romanini et al., *Chemical Physics Letters* **264(3-4)**, 316 (1997)
- [14] J. Tennyson, *private communication*
- [15] J. Ramanlal, J. Tennyson, *Mon. Not. R. Astron. Soc.* **354**, 161 - 168 (2004)
- [16] M. Hejduk et al., *Plasma Sources Sci. Technol.* in print.
- [17] P. Dohnal et al., to be submitted to *Phil. Trans. R. Soc.* (2012)
- [18] J. Stevefelt, J. Boulmer, and J. Delpech, *Phys. Rev. A* **12**, 1246 (1975)
- [19] T. Kotrík et al., *Phys. Rev. A* **83**, 032720 (2011)

Photochemistry of essential building blocks of biomolecules in clusters

Michal Fárník¹, Viktoriya Poterya¹, Lukáš Šišťák² and Petr Slavíček^{1,2}

¹ *J. Heyrovský Institute of Physical Chemistry, Academy of Sciences of the Czech Republic, Dolejškova 3, 182 23 Prague 8, Czech Republic, michal.farnik@jh-inst.cas.cz*

² *Institute of Chemical Technology, Technická 5, Prague 6, Czech Republic*

It is surprising how the great diversity of life is based on a relatively restricted number of essential molecular units which represent the basis for all biomolecules. The examples can be the four nucleic acid bases adenine, cytosine, guanine and thymine which encode the entire genetic information of life in DNA. It has been proposed that the essential building blocks for biomolecules were selected by nature due to their stability with respect to the ultraviolet (UV) radiation, which was striking the early Earth surface intensely before the protective ozone layer was generated [1].

Under the action of the UV light the molecule can get electronically excited. In the excited state the molecules can undergo conformational changes, decay or chemical reactions with the surrounding species. All these processes can potentially harm the biological functioning of the molecules. Thus the necessary condition for a molecule to be photostable is that the excited state quenches on a very short time scale (~100 fs) to the ground state. Besides, the excess energy has to be dissipated in the quenching process to stabilize the ground state of the molecule [2].

It has been suggested [3] that the stabilization can be provided by a conical intersection of a repulsive excited state of $\pi\sigma^*$ character with the ground state. The system evolving along this essentially dissociative state can quench via the conical intersection into the ground state and if the excess energy is dissipated by, e.g., the solvating molecules the system can be stabilized in the ground state. This rather general mechanism has been proposed and observed for numerous molecules.

In our laboratory, we investigate the photodissociation of small molecular units which are the essential building blocks of larger biomolecules. We study their photodynamics in clusters of various complexities. By changing the clusters size we can observe how the photostability of a molecule depends on the solvation.

A recent description of our experiment can be found elsewhere [4]. Briefly, we generate clusters by coexpansion of evaporated molecules (either from liquid or solid phase) with a buffer gas (Ar or He) into the vacuum through a 50 μm conical nozzle. Clusters of various mean sizes and compositions can be generated by changing the expansion conditions. The neutral cluster size and composition is established in a scattering experiment combined with

mass spectrometry after electron or a nonresonant multiphoton ionization. In the photodissociation experiment the clusters are photolyzed by a UV laser pulse (193 or 243 nm), and the escaping H-fragments are REMPI ionized at 243 nm and their kinetic energy distributions are measured.

Probably the most important bond in biology is the hydrogen bond. Therefore by probing the hydrogens dissociated from the hydrogen bonds between the molecules in the cluster we can learn the molecular details of the bond breaking in these species which are the model systems for the more complicated biological systems.

Our experimental data are complemented and interpreted by theoretical calculations.

Five-membered heterocyclic molecules

Recently, we have studied the photochemistry of five-membered nitrogen containing heterocycles (pyrrole, imidazole and pyrazole) in clusters [5-9]. These heterocycles represent paradigmatic structures for larger biologically active heterocyclic molecules and complexes. The dimers of the three molecules are also archetypes of different bonding patterns: N–H... π interaction, N–H...N hydrogen bond and double hydrogen bond. Based on *ab initio* calculations we discuss various possible reactions in the excited states of the clusters (illustrated for imidazole dimer in Fig. 1): (1) hydrogen dissociation, (2) hydrogen transfer between the heterocyclic units, (3) molecular ring distortion, and (4) coupled electron–proton transfer. The increasing photostability with complexity of the system can be inferred from experiments with photodissociation in these clusters. Even though the different deactivation channels are energetically possible for the complexed heterocycles, in most cases the major result is a fast reconstruction of the ground state. The complexed or solvated heterocycles are thus inherently photostable although the stability can in principle be achieved via different reaction routes.

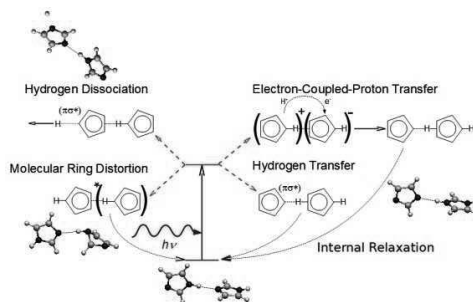


Figure 1: Possible reaction channels in the photodissociation of imidazole dimer

Phenol in clusters

Photochemistry of phenol molecule has received a great attention due to its relevance to biology [10-12]. Here we present our study of phenol photochemistry in clusters. We compare the kinetic energy spectra of H-atoms released from the O-H bond in phenol obtained for bare molecules, small clusters (mean size $N < 5$), and large species ($N \geq 10$). Two major conclusions arise: (i) At the photodissociation wavelength 243 nm, the kinetic energy spectra from bare molecules are almost identical with the spectra from clusters, i.e., the solvation of the molecule in the cluster does not influence the photodissociation dynamics. (ii) At 193 nm on the other hand the spectra change significantly upon clustering; the fast fragment contribution is suppressed in clusters (see Fig. 2), suggesting a stabilization of the molecule in clusters (similar to the case of five membered heterocycles discussed above).

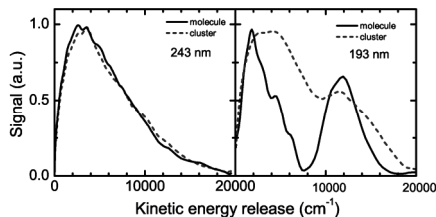


Figure 2: H-fragment kinetic energy distribution from O-H bond in phenol for bare molecules and large clusters ($N \geq 10$).

In addition, we have performed mass spectrometric study of phenol clusters. Mass spectra after electron ionization as well as after nonresonant multiphoton ionization were recorded at various expansion conditions. A very interesting feature is the observation phenol cluster peaks with additional water molecule $[(C_6H_5OH)_k \cdot H_2O]^+$ generated in the ionization process of pure phenol clusters $(C_6H_5OH)_n$.

Both the photodissociation and the ionization processes will be discussed in our contribution based on theoretical calculations

Acknowledgement: This work has been supported by the Grant Agency of the Czech Republic Project Nos. 203/09/0422 and P208/11/0161

References

- [1] C. Sagan, *J. Theor. Biol.* **39**, 195 (1973).
- [2] J.-E. A. Otterstedt, *J. Chem. Phys.* **58**, 5716 (1973).
- [3] A. L. Sobolewski, W. Domcke, C. Dedonder-Lardeux and C. Jouvet, *Pys. Chem. Chem Phys.* **4**, 1093 (2002).
- [4] M. Fárník, *Molecular Dynamics in Free Clusters and Nanoparticles Studied in Molecular Beams*, ICT Prague Press, Institute of Chemical Technology, Prague, (2011).
- [5] V. Poterya, V. Profant, M. Fárník, P. Slavíček, and U. Buck, *J. Chem. Phys.*, **127**, 064307 (2007).
- [6] V. Profant, V. Poterya, M. Fárník, P. Slavíček, and U. Buck, *J. Phys. Chem. A*, **111**, 12477 (2007).
- [7] V. Poterya, V. Profant, M. Fárník, L. Šištík, P. Slavíček, and U. Buck, *J. Phys. Chem. A*, **113**, 14583 (2009).
- [8] V. Poterya, O. Tkáč, J. Fedor, M. Fárník, P. Slavíček, and U. Buck, *Int. J. Mass Spectrometry*, **290**, 85 (2010).
- [9] P. Slavíček and M. Fárník, *Phys. Chem. Chem. Phys.*, **13**, 12123 (2011).
- [10] M. N. R. Ashfold, A. L. Devine, R. N. Dixon, G. A. King, M. G. D. Nix and T. A. A. Oliver, *Proc. Nat. Acad. Sci. USA*, **105**, 12701 (2008); M. G. D. Nix, A. L. Devine, B. Cronin and M. N. R. Ashfold, *J. Chem. Phys.* **125**, 133318 (2006).
- [11] M. L. Hause, Y. H. Yoon, A. S. Case and F. F. Crim, *J. Chem. Phys.* **128**, 104307 (2008).
- [12] A. Iqbal, M. S. Y. Cheung, M. G. D. Nix and V. G. Stavros, *J. Phys. Chem. A*, **113**, 8157 (2009).

Toward the quantum dynamics of the frustrated translation of $\text{H}_2/\text{Cu}(100)$

Thiago Firmino and Roberto Marquardt

Laboratoire de Chimie Quantique

Institut de Chimie UMR 7177 CNRS/Université de Strasbourg

4 rue Blaise Pascal - CS90032 - 67081 Strasbourg cedex - France

thiago.firmino@etu.unistra.fr

Abstract

We discuss the importance for the investigation of the frustrated translation of adsorbed molecules and the development of a global potential energy surface (PES) for that.

Introduction

Theoretical studies of molecule-surface reactions have the main objective to determine in detail how molecules react on surfaces. Here, several important physical and chemical processes may occur such as reaction (dissociation), or the back scattering (diffraction) into the gas phase in a vibrationally or rotationally excited state, or with a quantized change in the momentum parallel to the surface. In addition, coupling to the phonons and to electron-hole pair excitations may be important [1, 2]. The dissociative chemisorption of molecules on surface has a significant number of industrial applications. We can highlight the hydrogen storage in metals, in corrosion and in heterogeneous catalysis. The understanding at the microscopic level of the catalytic synthesis of ammonia from the elements ($\text{N}_2 + 3\text{H}_2 \rightarrow 2\text{NH}_3$) was crucial to understand the fundamental mechanism of the Haber-Boch process, by which vast amounts of ammonia, a raw material for fertilizer, are produced[3].

Few techniques are capable to detail the mechanism of lateral diffusion of molecules on a surface. Ellis *et al* [4] used the ^3He Spin-Echo Spectroscopy to study the motion of CO on Cu(001) and observed both along the $\langle 110 \rangle$ and $\langle 100 \rangle$ directions an oscillatory dependence of the quasi-elastic broadening as a function of momentum transfer. This was modelled by a jump diffusion mechanism which allowed them to conclude that the ratio between the hollow and bridge site energy barrier is approximately, $E_H/E_B \simeq 1$. While this result is in disagreement with current available data from electronic structure calculation [5], it shows how relevant is a true quantum dynamical calculations for the description of the frustrated translational motion of adsorbed molecules. In this project, we aim at achieving such a description.

Methods

We focus here on the dissociative adsorption system (100). We use the representation PES5 from [6] which is based on DFT calculations, using a two-layer slab for the copper surface and employing the experimental Cu bulk lattice constant. Here, the Cu-Cu nearest distance becomes $4.824a_0$. For the hydrogen molecule, the PES of molecule-surface interaction is a six-dimensional one if a rigid surface model is considered, where phonons are neglected. The hamiltonian for nuclear motion is written a

$$\hat{H}_{6d} = -\frac{1}{2M}\nabla_{\mathbf{R}}^2 - \frac{1}{2\mu}\nabla_{\mathbf{r}}^2 + V_{6d}(\mathbf{R},\mathbf{r}), \quad (1)$$

where \mathbf{R} is the vector of the center-of-mass (COM) coordinates (X,Y,Z) of the molecule, X and Y being coordinates for the motion parallel to the substrate, the “frustrated translation” (see figure 1), and M is the mass of the molecule. Furthermore, \mathbf{r} is the vector of the internal coordinates of the molecule, which are usually taken as (r, θ, ϕ) where θ is the polar and ϕ the azimuthal angle of orientation of the molecular axis and μ is the reduced mass of the molecule. The first term of equation 1 represents the kinetic energy in the COM frame, the second term represents the kinetic energy in the internal (vibrational or dissociative and rotational) motion of the molecule and the third term is the potential energy of the molecule interacting with the surface. The diffusion dynamics is planned to be studied with in the MCTDH approach, as implemented in the Heidelberg program package [7].

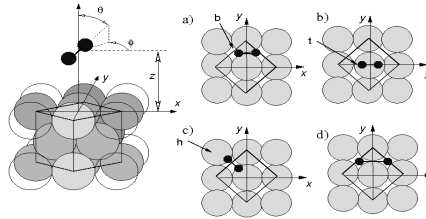


Figure 1: Schematic representation of the grid model chosen to describe the $H_2/Cu(100)$ system. The inserts show the a) bridge, b) top and c) hollow high-symmetry sites of saddle points; insert d) shows the bridge site minimum.

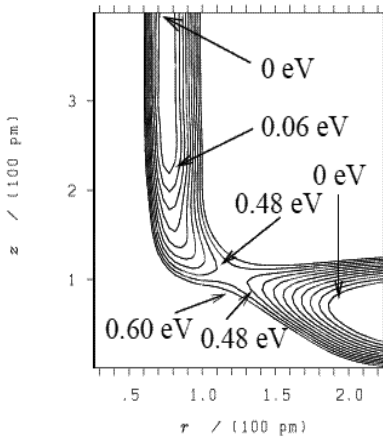


Figure 2: Two dimensional cut of the PES in Z and r at $X = 0.00 \text{ pm}$, $Y = 0.00 \text{ pm}$, $q = 90^\circ$ and $f = 0^\circ$; contour line differences are 0.06 eV

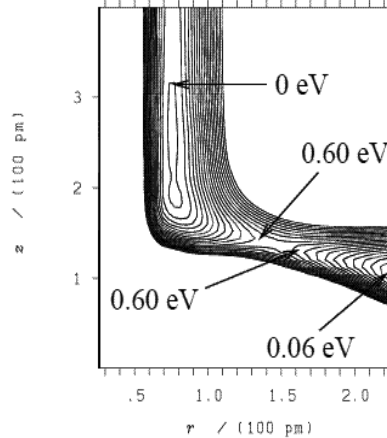


Figure 3: As figure 2 but $X = 0.00 \text{ pm}$, $Y = 128 \text{ pm}$.

Results

We first need to analyse the PES from [6]. Figures 2, 3 show the dependence of PES5 on r and Z for the two high-symmetry sites with molecular orientation parallel to the substrate (see also figure 1). Note that for the two configurations in which the H_2 molecule is parallel to the substrate ($\theta = 90^\circ$) at the bridge and top high-symmetry sites, the PES has energy barriers to dissociation $H_2 \rightarrow 2H$ of 0.48 and 0.54 respectively. For the two configurations, the energy barrier is 0.54 eV. These barriers fall within the domain of barriers described in [4].

Figures 2 and 3 are essentially reproductions from [6]. In fact, they do not allow to see the behaviour of the one dimensional potential $V(r)$ beyond the potential "minimum", which is reached when the two H atoms are at the bridge site, and the distance between them is $r_c \simeq 4.8 a_0 \simeq 256$ pm, the nearest neighbour distance on the Cu substrate (see the insert d in figure 1). Such a one-dimensional section is shown in figure 4. We see that the potential becomes constant after 250 pm, roughly. When the molecule centre is at a "bridge" site, as depicted in figure 4, the PES should increase, as the hydrogen atoms approach the copper atoms. The potential energy should be maximal (a barrier), as the H atoms are closest to the Cu atoms. But figure 4 leads us to understand that beyond r_c atoms behave as free-particles. This is most likely a technical artefact of the representation (the apparent well at $r \simeq 4.8 a_0$ is also artificial).

In this figure, the expected function is indicated by the hand drawn dashed line. Here, the PES should increase, when the H atoms are separated beyond r_c , with modulations governed by the H-Cu interaction and the periodicity of the lattice.

It becomes obvious that the PES5 representation from [6] is not global. In the subsequent quantum dynamical simulation carried out in [6], H_2 molecules were scattered at the Cu substrate and the wave packet was absorbed for r beyond r_c by an optical potential. Such a trick cannot be applied in the context of the present investigation of the frustrated translation.

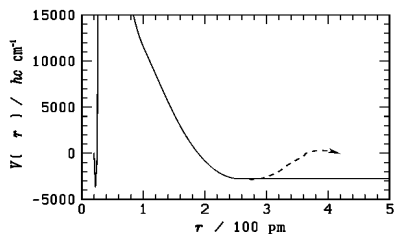


Figure 4: One dimensional section of the PES as function of the coordinate r ($X=0.00$ pm, $Y=128$ pm, $Z=60$ pm, and $\theta = 90^\circ$ and $\phi = 0^\circ$). The hand-drawn dashed line represents the expected function, the maximum of the barrier beyond r_c being essentially unknown at present.

Conclusions

An extension of PES5 to include large positions of the configuration space in X and Y is needed before the MCTDH approach can be applied here to study the frustrated translation.

Acknowledgment

The present work is supported financially by the Agence Nationale de la Recherche, ANR-blanc project "DYQUMA". We thank F. Gatti and D. Zanuttini for help as well as H. F. Busnengo, M. F. Somers and R. A. Olsen for discussions.

References

- [1] S. Holloway, *Surf. Sci.*, **299/300**, 656–666 (1994).
- [2] G. J. Kroes, A. Gross, E. J. Baerends, M. Scheffler and D. A. McCormack, *Acc. Chem. Res.*, **35**, 193–200 (2002).
- [3] G. Ertl, *J. Vac. Sci. Technol. A.*, **1**, 1247–1253 (1983).
- [4] G. Alexandrowicz, A. P. Jardine, P. Fouquet, S. Dworski, W. Allison, J. Ellis, *Phys. Rev. Lett.*, **93**, 156103-1–156103-4 (2004)
- [5] R. Marquardt, F. Cuvelier, R. A. Olsen, E. J. Baerends, J. C. Tremblay, and P. Saalfrank, *J. Chem. Phys.*, **132**, 074108 (2010).
- [6] M. F. Somers, R. A. Olsen, H. F. Busnengo, E. J. Baerends, G. J. Kroes, *J. Chem. Phys.*, **121**, 11379–11387 (2004)
- [7] G. A. Worth, M. H. Beck, A. Jäckle, and H. -D. Meyer, the MCTDH package, version 8.4 (2007). See <http://mctdh.uni-hd.de/>.

The (Ca, N₂O) reactive system on helium clusters

Marc-André Gaveau¹, Marc Briant¹, Gloria Spighi¹ and Jean-Michel Mestdagh¹

¹ *Laboratoire Francis Perrin, CNRS URA 2453, DSM/DRECAM/SPAM, CEA Saclay, 91191 Gif-sur-Yvette Cedex, FRANCE*

A convenient way to study physical or chemical process at an atomic scale which allows determining its exact stoichiometry, is to use clusters as a medium. Two variants exist whether van der Waals clusters (argon, neon,...) or quantum clusters (helium nanodroplets) are used. This leads to the Cluster Isolated Chemical Reaction (CICR) technique developed in our laboratory in the former case [1] and to the Helium Nanodroplet Isolation (HENDI) technique, first developed in the group of Scoles [2]. Both techniques are currently used in our laboratory. The subject of the present contribution is the reactivity of N₂O molecules with the calcium aggregate Ca_n which is formed on helium clusters by the sequential pick up of n Ca atoms.

Helium clusters are grown by condensation in a supersonic beam (stagnation conditions: T₀=10°K, P₀=9 bar, D* =5 μm). The average size of the cluster is estimated to a few thousands [3]. After extraction by a skimmer, the helium clusters beam passes through a heated calcium vapour cell. Here, Ca atoms are picked-up by the helium clusters. They are believed to stay at the surface of the clusters [4]. When two of them are present on the same cluster, they migrate and associate together as the Ca₂ molecule since their association energy is higher [5] than the cluster temperature (0.4 K). Moreover, successive pick-up of n calcium atoms leads to the formation of a small calcium aggregate on the helium cluster.

A N₂O effusive beam is crossed with the helium cluster beam, after the Ca pick-up region. Hence clusters carrying Ca atoms and N₂O molecules are generated. The N₂O molecules and Ca atoms which are present on the same cluster can migrate relative to each other and react. No chemiluminescence signal is observed when a single Ca atom and a single N₂O molecule are present on the cluster. This is surprising given the reaction Ca+N₂O→CaO+N₂ is exoenergetic by 2.4 eV, *i.e.* enough for opening a chemiluminescence channel. Moreover, such a channel was observed in the gas phase [6,7]. This might be due to the existence of a yet unsuspected reaction barrier which cannot be overcome at the low temperature of the helium clusters. In contrast, a chemiluminescent reaction is observed when at least two Ca atoms and two N₂O molecules are present on the same cluster. A typical chemiluminescence spectrum is shown in figure 1. It associates an intense band to small sidebands. It has some resemblance with a spectrum observed in argon matrix and assigned to the d³Δ, D¹Δ → A¹Π, C³Σ⁺ → a³Π transitions of CaO [8] but substantial differences exist between the two spectra. This suggests that other electronic states contribute to the

chemiluminescence. This will be discussed at the conference in the light of recent calculations of the electronic states of the CaO molecule [9].

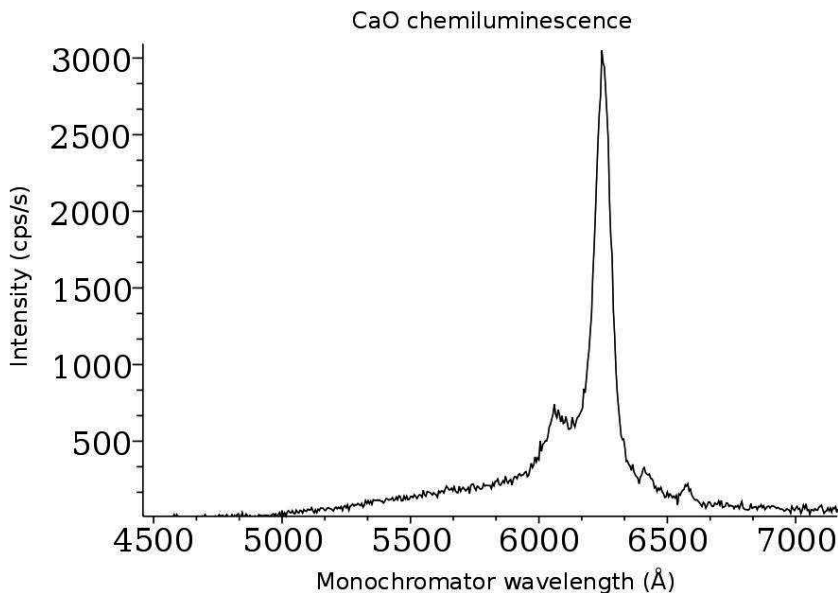


Figure 1 : Chemiluminescence observed from helium clusters carrying at least two Ca atoms and two N_2O molecules

References

- [1] J.M. Mestdagh, M.A. Gaveau, C. Gée, O. Sublemontier, J.P. Visticot, *Int. Rev. Phys. Chem.* **16**, 215 (1997)
- [2] F. Stienkemeier, J. Higgins, W. E. Ernst, G. Scoles, *Phys. Rev. Lett.* **74**, 3592 (1995)
- [3] F. Stienkemeier, K.K. Lehmann, *J. Phys.* **B 39**, R127 (2006)
- [4] F. Stienkemeier, F. Meier, H. O. Lutz, *J. Chem. Phys.* **107**, 10816 (1997)
- [5] T. Bouissou, G. Durand, M.-C. Heitz, F. Spiegelman, *J. Chem. Phys.* **113**, 164317 (2010)
- [6] J.A. Irvin, P.J. Dagdigian, *J. Chem. Phys.* **74**, 6178 (1981)
- [7] J.A. Irvin, P.J. Dagdigian, *J. Chem. Phys.* **73**, 176 (1980)
- [8] C.S. Wei, S.W. Guo, Y.P. Lee, *J. Chem. Phys.* **82**, 2942 (1985)
- [9] H. Khalil, V. Brites, F. Le Quéré and C. Léonard, *Chem. Phys.* **386**, 50 (2011).

Recombination of spin-polarised Hydrogen Atoms on non-porous Water Ice at 3.5K

Thomas R. Govers

Aecono Consulting, 59 rue de Prony, 75017 Paris, France. thomas.govers@wanadoo.fr

1. Introduction

Physisorption and recombination of atomic hydrogen on non-porous water ice depends critically on the presence of pre-adsorbed molecular hydrogen [1-3]. This results from two opposing effects: preadsorbed molecular hydrogen "cushions" the impinging atoms and thus enhances kinetic energy accommodation and sticking; increasing molecular coverage, however, decreases the physisorption energy of the atoms, so that even atoms that do stick re-evaporate before recombining. The optimum compromise occurs at a molecular coverage of about $2 \times 10^{14} \text{ cm}^{-2}$ [2].

In dense interstellar clouds such opposing effects may lead to self-regulation of hydrogen recombination on interstellar dust. In the laboratory, it affects the outcome and interpretation of molecular-beam experiments, since the atomic beam almost invariably contains residual molecular hydrogen which deposits on the low-temperature surface in preference to atomic hydrogen. Separating atoms and molecules using an inhomogeneous magnetic field, provides a means to minimise this difficulty. The results of such experiments [4], as recalled in section 2 below, suggest that in the absence of molecular hydrogen, atomic hydrogen does not recombine on non-porous water ice. Section 3 addresses the importance of electron spin in regard to the recombination of physisorbed atomic hydrogen.

2. Bolometer experiments with a beam of spin-polarised H atoms

In the experiments depicted in Fig.1, a liquid-helium cooled bolometer constitutes both the target surface and the detector of energy transferred by the incident beam particles or by surface recombination [1,2,4]. Its surface accumulates non-porous water ice during cool-down of the cryostat. The bolometer temperature was 3.45 ± 0.05 K in the present experiments. The RF source produces an effusive beam flux containing about 80% atomic hydrogen. A secondary beam source is used to deposit controlled amounts of H_2 , which can be removed by raising the bolometer temperature to 20 K by increasing the bias current.

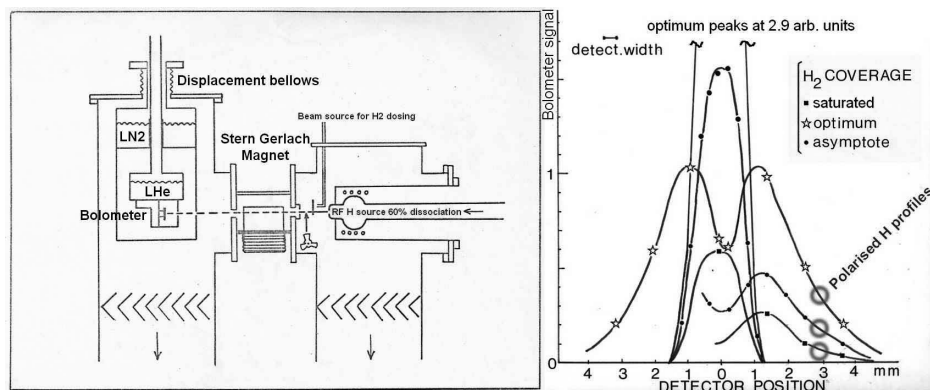


Figure 1: Schematic of apparatus and beam profiles obtained for three pre-dosed H_2 coverages.

When moving the bolometer across the atomic beam with no magnetic field applied, one obtains the profiles shown in the centre of the RHS picture in Fig.1. These signals vary with the amount of pre-adsorbed H_2 largely because of its strong influence on H recombination, as discussed in detail in [1,2]. With a molecular coverage of about $2 \times 10^{14} \text{cm}^{-2}$, one obtains an optimum signal nearly 5 times higher than on a surface saturated with H_2 . An intermediate value is obtained with an asymptotic H_2 coverage, corresponding to a long-time exposure to the atomic beam (balance between H_2 removal by H recombination and deposition by residual H_2 in the beam and by background gas).

With the inhomogeneous magnetic field applied, one obtains the winged Stern-Gerlach profiles indicated as "polarised" in Fig. 1. Symmetry corresponding to opposite deflections of the $M_S = \pm 1/2$ components was verified at optimum H_2 coverage. The profiles are widened by the velocity distribution of the thermal beam. By positioning the bolometer 2 mm off-axis, one exposes the surface to H atoms with an average velocity of $4.5 \times 10^5 \text{ cm/s}$, while avoiding the simultaneous deposition of molecular H_2 from the beam.

After raising the bolometer temperature to 20 K until time $t=0$ to remove all adsorbed hydrogen, such a pure H beam produces the signal illustrated in Fig. 2. The surface temperature and detection electronics take about one minute to recover from the temperature rise. When opening the beam flag at that moment, one observes a small signal which slowly rises to an asymptote corresponding to an equilibrium between H_2 deposition from the background gas, which "cushions" the incident atoms, and H_2 removal by H recombination.

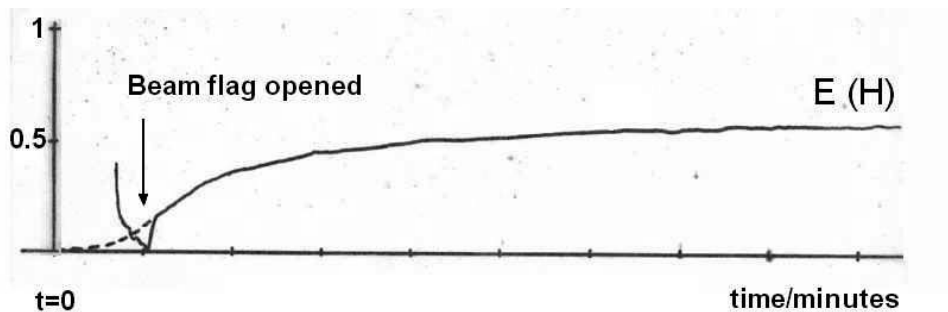


Figure 2: Time dependence of the bolometer signal when exposed to a beam of spin-polarised H. Removal of molecular H_2 is interrupted at $t=0$

Extrapolating to $t=0$ the signal is estimated to be vanishingly small, leading to the conclusion that in the absence of any pre-adsorbed molecular hydrogen, the H atoms are reflected from the ice surface without transferring significant amounts of kinetic energy and without recombining to any measurable extent. Molecular H_2 , even at coverages much smaller than the $2 \times 10^{14} \text{cm}^{-2}$ optimum, significantly increases energy accommodation and sticking, thus promoting atomic recombination in proportion to the fraction of adsorption sites occupied by H_2 . As adsorption of molecular hydrogen varies considerably when the surface temperature is modified from a few K to a few tens of K, experiments investigating temperature effects on surface recombination, e.g., should critically examine the possibility of misinterpretation due to uncontrolled changes in H_2 coverage.

3. The influence of electronic spin on atomic recombination

When electronic spin polarised hydrogen atoms are weakly physisorbed on a neutral surface, and if electron spin alignment is preserved, their interaction should be described by the repulsive triplet potential, inhibiting recombination into the bound singlet well.

The experiments summarised in section 2 above do not show significant differences that can be attributed to the electron spin polarisation of the atomic beam, the only distinction being the possibility eliminate H_2 co-deposition with a polarised beam. The latter also allows some velocity section depending on the position of the bolometer. Presumably, spin alignment is lost when atoms impact on the surface [5], so that the spin of physisorbed atoms is randomly oriented up or down with respect to each other or with respect to H atoms in the beam, even if the latter is spin polarised. This does not mean that electronic spin should not be taken into consideration, however.

In an Eley-Rideal (ER) model, where recombination is the result of a direct encounter between a physisorbed atom and an incoming gas-phase atom, only 1 out of 4 encounters could possibly lead to recombination, as 3 out of 4 collisions are governed by the repulsive triplet potential. In the Langmuir-Hinshelwood (LH) picture, the incoming H atom, once trapped or thermalised, will "explore" the surface until it encounters a pre-adsorbed atom, and recombine with high probability if the electron spins are opposite. Again, only one out of four of such individual encounters will be able to form stable singlet H₂, as explicitly taken into account in the theoretical study by Morisset et al. [6]. But if the timescale for exploring different surface sites is short compared to the residence time of a physisorbed atom, all atoms that do stick to the surface will ultimately recombine even though spin statistics prolong the average time lag before recombination occurs. When compared to beam experiments or astrophysical observations, models based on an ER recombination mechanism should thus incorporate a ¼ weighing factor, whereas LH models should not. We note that H₂ formation by ER recombination is expected to vary quadratically with incident H flux, which is not the case in beam experiments as those reported here. On non-porous water ice, LH recombination involving highly mobile physisorbed H atoms dominates, even at surface temperatures as low as 3.5 K.

References

- [1] A. Schutte, D. Bassi, F. Tommasini, A. Turelli, G. Scoles, and L.J.F. Hermans, *J.Chem. Phys.* 64 (1976) 4135
- [2] T. R. Govers, <http://arxiv.org/ftp/physics/papers/0502/0502101.pdf>
- [3] L. Amiaud, F. Dulieu, J.-H. Fillion, A. Momeni, and J.L. Lemaire, *J. Chem. Phys.* 127 (2007) 144709
- [4] Unpublished data from the work carried out at the University of Waterloo in the late 1970's. Details on physisorption of H₂ and D₂ can be found in: T.R. Govers, L. Mattera, and G. Scoles, *J. Chem. Phys.* 72 (1980) 5446
- [5] J.T.M. Walraven, E.R. Eliël, and I.F. Silvera, *Phys. Letters*, 66A (1978) 247
- [6] S. Morisset, F. Aguillon, M. Sizun, and V. Sidis, *J. Chem. Phys.* 122 (2005) 194702

Monte-Carlo modeling of hot O, C, and N particles in the upper atmosphere of Mars and Venus

H. Gröller¹, H. I. M. Lichtenegger¹, H. Lammer¹, O. Dutuit^{2,1}, M. Pflieger¹, V. I. Shematovich³, Yu. N. Kulikov⁴

¹ *Space Research Institute, Austrian Academy of Sciences, Graz, Austria, hannes.groeller@oeaw.ac.at*

² *Institut de Planétologie et d' Astrophysique de Grenoble, CNRS-UJF, Grenoble, France*

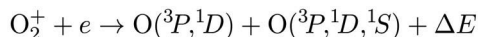
³ *Polar Geophysical Institute, Russian Academy of Science, Murmansk, Russian Federation*

⁴ *INASAN, Russian Academy of Sciences, Moscow, Russian Federation*

A thorough understanding of atmospheric escape processes of terrestrial planets is crucial in order to predict the time evolution of their atmospheres. Suprathermal O, C, and N atoms produced by means of photochemical reactions in planetary thermospheres can play an important role for the escape of atmospheric species by direct and indirect processes. These hot atoms attain enough energy to overcome the gravity at Mars and may directly escape. In the case of Venus due to its higher gravity the released energy is not sufficient for direct escape, thus indirect escape processes, like e.g. ion escape, are relevant. In either case the non-thermal energy distribution functions at the exobase (separates the collision dominated from the collision less region) must be known in order to estimate the hot exosphere density profiles. For this purpose, hot particles generated via photochemical processes are traced along their stochastic way through the thermosphere of the planet by using a 3D Monte-Carlo model and the kinetics and transport characteristics of these particles are determined. Elastic, inelastic, and quenching collisions between the traced hot particle and the ambient neutral atmosphere are simulated by using a total and differential collision cross sections. The energy and mass dependent cross sections as well as the collisional redistribution of the inner energies are listed in [1]. Rotational and vibrational excitation energies for the calculation of the initial energy of the produced hot oxygen atoms are also included in the simulation. The exosphere density is obtained from the corresponding energy and angular distribution at the exobase altitude by using a test particle model which traces the ballistic trajectories of hot O, C, and N atoms in the exosphere.

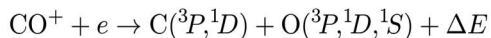
Sources of Hot Atoms

The main source of hot oxygen atoms is the dissociative recombination of O_2^+



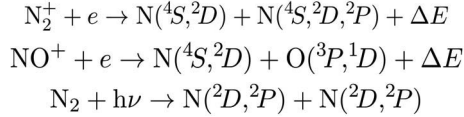
as shown for instance in [1], [2], and [3].

For hot carbon atoms, both dissociative recombination of CO^+ and photodissociation of CO are important sources





According to [4] the photodissociation of CO is the most important source of hot C atoms. The dissociative recombination of N_2^+ as well as of NO^+ and the photodissociation of N_2 are the sources of hot nitrogen atoms



Results

The used solar spectra for high and low solar activity are taken from Solar Irradiance Platform (SIP), version 2.36, and the needed photo cross sections from the AMOP database. Energy distribution functions (EDFs) are calculated at an altitude of 240 km for the dayside of Mars and shown for O and C in Figure 1 and the corresponding hot exosphere densities in Figure 2. By integrating the EDFs over energies greater than the escape energy, one can calculate the escape flux and therefore the loss rate (Table 1).

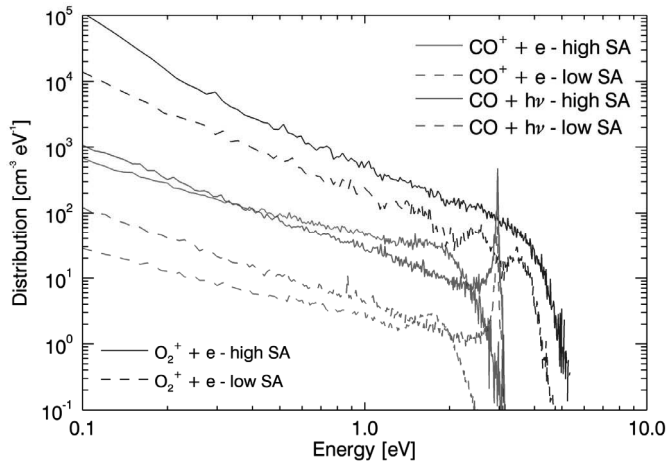


Figure 1: Energy distribution functions for high (solid) and low (dashed) solar activity at present Mars for hot O and hot C atoms.

For the Venus dayside the exosphere densities of the hot O atoms are shown in Figure 3 for high and low solar activity. To illustrate the effect of the vibrational energy of the O_2^+ ions on

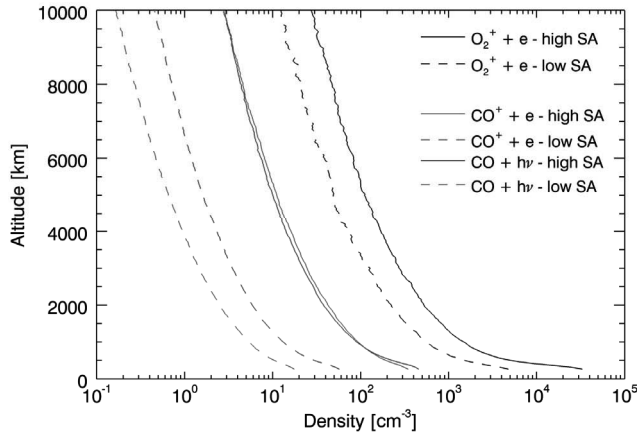


Figure 2: Hot O and hot C exosphere densities for high (solid) and low (dashed) solar activity.

Table 1: Loss rates (dayside) and escape fluxes for hot O, C, and N atoms for high solar activity at present Mars.

Solar activity	Element	Reaction	Loss rate [s^{-1}]	Escape flux [$cm^{-2} s^{-1}$]
High solar activity (240 km altitude)	O	$O_2^+ + e$	8.9×10^{23}	1.1×10^8
	C	$CO^+ + e$	1.1×10^{25}	1.3×10^7
	N	$N_2^+ + e$	6.8×10^{23}	8.2×10^5
		$NO^+ + e$	1.9×10^{23}	2.3×10^5

the initial energy of the suprathermal O particles, two density profiles, one including and one excluding the vibrational states are displayed. For comparison the densities derived from the PVO observations [5] and the hot O profile from [6] for high solar activity are also illustrated.

Conclusion

Our results indicate that the cross sections and the fraction between elastic, inelastic and quenching collisions are the most sensitive parameters affecting the corona density. Due to the low gravity on Mars, direct escape of hot particles appears to be one of the main loss processes.

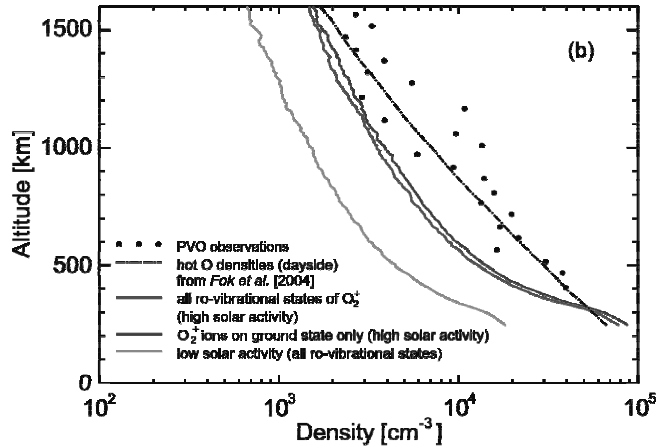


Figure 3: Hot O exosphere density at the Venus dayside for high and low solar activity as well as the density profile for high solar activity with all O₂⁺ ions in the vibrational ground state are shown.

Acknowledgements

This research has been supported by the Helmholtz Association through the research alliance “Planetary Evolution and Life” and through the joined Russian-Austrian project under the RFBR grant 09-02-91002-215-ANF-a and the FWF grant I199-N16. V. I. S. is supported by the RFBR grant 11-02-00479. H. G. thanks Dr. Michel Vervloet for very helpful discussions.

References

- [1] Gröller, H., V. I. Shematovich, H. I. M. Lichtenegger, H. Lammer, M. Pflieger, Yu. N. Kulikov, W. Macher, U. V. Amerstorfer, and H. K. Biernat, *JGR* **115**, E12017, 2010
- [2] Gröller, H., H. Lammer, H. I. M. Lichtenegger, M. Pflieger, O. Dutuit, V. I. Shematovich, Yu. N. Kulikov, and H. K. Biernat, 2011 (submitted to GRL)
- [3] Fox, J. L., and A. B. Hać, *Icarus* **204**, 527 – 544, 2009
- [4] Fox, J. L., and L. J. Paxton, *JGR* **110**, A01311, 2005
- [5] Nagy, A. F., T. E. Cravens, J.-H. Yee, and A. I. F. Stewart, *GRL* **8**, 629 – 632, 1981
- [6] Fok, M.-C., *JGR* **109**, A01206, 2004

Spin temperature measurement of thermally desorbed water molecules from water ice prepared at 8K

Tetsuya Hama¹, Naoki Watanabe¹ and Akira Kouchi¹

¹ *Institute of Low Temperature Science, Hokkaido University, Sapporo, Hokkaido, Japan*
hama@lowtem.hokudai.ac.jp

The nuclear-spin temperatures of interstellar molecules are often observed, because they are indicators of these molecules' physical and chemical histories (See subsection for details). In cometary coma, for example, spin temperatures of H₂O have been derived in the range from 21 to greater than 50 K, typically ~30 K [1]. Nuclear-spin conversion is unlikely to occur for isolated molecules in the gas phase. Thus, it has been interpreted as the temperature of cold grains at molecular condensation or formation in a molecular cloud, or in the solar nebula, whereas the real meaning of the observed spin temperatures of molecular species remains a topic of continuing debate [2]. For a proper interpretation of spin temperatures of molecules observed in interstellar space or cometary coma, the correlation between spin temperatures and temperatures of ice at condensation, formation, and desorption needs to be investigated.

In the present study, we measured the spin temperatures of H₂O thermally desorbed from pure amorphous solid water (ASW) deposited at 8 K by employing a combination of temperature-programmed desorption and resonance-enhanced multiphoton ionization (REMPI). We used various sample solids; *i.e.*, H₂O/O₂ mixed ice, vacuum-ultraviolet (VUV) photo-irradiated ASW, and ASW produced at 8 K by VUV irradiation of a CH₄/O₂ mixture (photoproduct ASW) for the idea that spin temperature of H₂O molecules formed at a low temperature relates to the formation environment. The prepared ice samples were heated to ~150 K to sublime H₂O from the solid samples at a heating rate of typically 4 K minute⁻¹. After the surface temperature reached at ~140 K, the desorbed H₂O molecules were subsequently analyzed ro-vibrationally by 2 + 1 REMPI through the C ¹B₁(000) ← X ¹A₁(000) transition in the wavelength range of 248.1 – 248.6 nm. H₂O⁺ ions were detected using a time-of-flight mass analyzer.

As a result, thermally desorbed H₂O molecules from all ice samples prepared at 8K show T_{spin} almost at the statistical high-temperature limit ($\geq \sim 30$ K) [3]. For example, Figure 1 shows a REMPI spectrum of thermally desorbed H₂O from photoproduct ASW. The REMPI spectrum was best reproduced by the simulation with $T_{\text{rot}} = T_{\text{spin}} = 150$ K, where T_{rot} and T_{spin} represent nuclear spin and rotational temperatures, respectively.

These results suggest that the spin temperatures of gaseous H₂O molecules thermally desorbed from ice do not necessarily reflect the surface temperature at which H₂O molecules condensed or formed. We discuss the possibility of nuclear-spin conversion of H₂O in water

ice [4]. The present study advocates the importance of further studies to give an interpretation of spin temperatures of molecules observed in interstellar space or cometary coma.

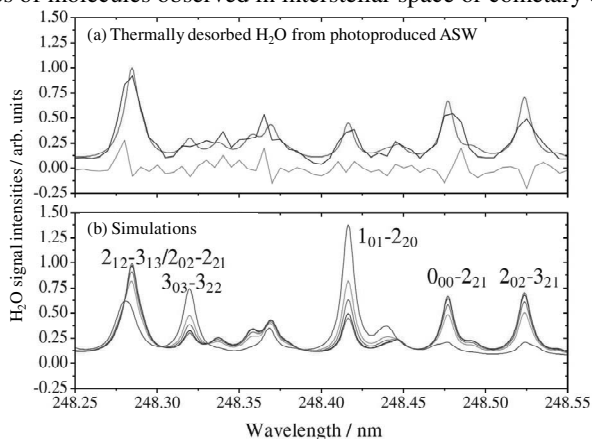


Figure 1: (a) $(2 + 1)$ REMPI spectra of the thermally desorbed H_2O from photoproduced ASW at 8 K. The red line is the best-fitting simulations with $T_{\text{rot}} = T_{\text{spin}} = 150$ K. The gray line is the residual spectra of (experiment – simulation). (b) Reference simulations with $T_{\text{spin}} = 150$ (red), 30 (black), 20 (green), 15 (orange), and 8 (blue) K. T_{rot} is fixed at 150 K. T_{spin} and T_{rot} represent nuclear spin and rotational temperatures, respectively. Indications ($J'_{K_a', K_c'} - J_{K_a, K_c}$) are rotational assignments of the $C-X$ transition in H_2O .

Nuclear-spin temperature of H_2O molecule

Nuclear-spin temperature is derived from the ortho-to-para ratio (OPR) of H_2O . H_2O contains two protons with spin of $1/2$; thus, its total spin state can be either 0 (singlet, para) or 1 (triplet, ortho). The rotational levels of H_2O (an asymmetric top molecule with C_{2v} point-group symmetry) can be represented by J_{K_a, K_c} , and H_2O molecules with ($K_a + K_c = \text{odd}$) are ortho, while those with ($K_a + K_c = \text{even}$) are para species. J is the total rotational angular momentum. K_a and K_c are the projections of J on the molecular a and c axes, respectively, where the former is oriented perpendicular to the molecular plane and the latter lies in the plane, perpendicular to the C_2 rotation axis. In statistical equilibrium, the OPR of H_2O is equal to 3, which is achieved at temperatures above ~ 50 K [1].

References

- [1] Bonev et al. 2007, ApJ, 661, L97
- [2] Kawakita & Kobayashi 2009, ApJ, 693, 388
- [3] Hama et al. 2011, ApJ, 738, L15
- [4] Buntkowsky et al. 2008, Z. Phys. Chem., 222, 1049

Collisions of slow N_2^+ ions with room temperature and heated fusion relevant surfaces

Martina Harnisch¹, Alan Keim¹, Samuel Zöttl¹, Paul Scheier¹, Tilmann D. Märk¹, Zdenek Herman²

¹*Institute for Ion Physics and Applied Physics, University of Innsbruck, EURATOM ÖAW, Technikerstraße 25b, 6020 Innsbruck, Austria*

²*J. Heyrovský Institute of Physical Chemistry, Academy of Sciences of the Czech Republic, EURATOM IPP.CR, Dolejškova 3, 18223 Prague 8, Czech Republic*

Interactions of N_2^+ projectile ions at incident energies from a few eV up to 100eV with different fusion relevant surfaces (W and CFC) were investigated at temperatures ranging from room temperature up to 600°C. Besides various hydrocarbon contributions also an abundance of alkali ions Na^+ and K^+ was found in the mass spectra. To ensure the cleanliness of the surface samples X-ray photoelectron spectroscopy was carried out, indicating that the alkalis are not present on the surface, but originate as contamination of the surface from different sources.

Introduction

Research and development of feasible fusion reactors require reliable fundamental data quantifying plasma-wall interactions. Modelling and computational science for the pioneering project ITER depend on the determination of erosion and deposition interactions of the involved plasma constituents with the materials used in the plasma facing components, i.e., beryllium, tungsten and carbon, in the form of carbon fibre composite (CFC). Extensive studies have been carried out in the past, investigating interactions of small hydrocarbon molecules with these surface materials [1], [2], [3].

Recently the attention of material studies in fusion science has shifted towards another issue. The divertor region in fusion reactors is planned to be cooled by impurity seeding with gases such as argon or nitrogen. Therefore, profound knowledge on interactions between these possible projectiles and the tiles of the inner wall is essential.

Experimental setup

The experimental setup BESTOF in Innsbruck is described in large detail in previous publications [4]. It consists of two mass spectrometers arranged in tandem geometry (Figure 1).

Ions are produced in a Nier-type electron ionization source and extracted into the first mass analyzer, a reverse-geometry two-sector-field mass spectrometer. Subsequently, the beam of m/z -selected N_2^+ ions is focused on a surface sample, which can be heated up to 600°C . There the projectile ions interact with the target surface at the incident angle of 45° and at well-defined incident energies ranging from a few eV up to 100eV . Ions produced during this interaction are extracted into a linear time-of-flight mass analyzer and recorded with a multi-channel-plate detector.

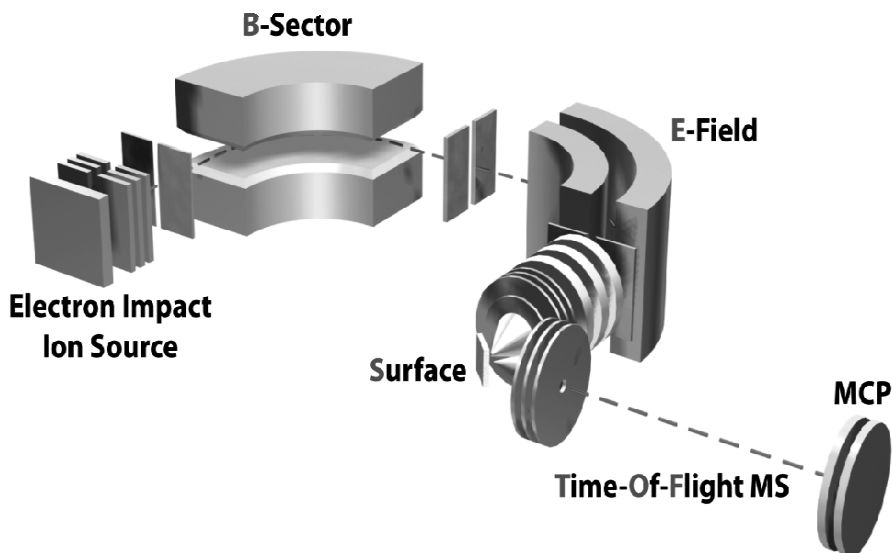


Figure 9: Schematics of the tandem mass spectrometer BESTOF. A mass and energy analyzed N_2^+ ion beam interacts with a surface, the product ions are detected by a TOF mass spectrometer.

Results and discussion

Interactions of N_2^+ with carbon fibre composite

Starting at room temperature ion-surface interactions of N_2^+ with CFC were investigated for different incident energies from $15\text{--}100\text{eV}$. The spectra showed contributions of sputtered products from a hydrocarbon layer adsorbed on the surface and from alkali contaminants Na^+ and K^+ much like spectra measured with Ar^+ as a projectile ion [2]. At higher surface

temperatures the alkali contributions are very dominant. The exact origin of the alkali contamination was not clear and was subsequently a subject of more thorough investigation. Hence these impurity signals were excluded from the discussion below (Figure 2).

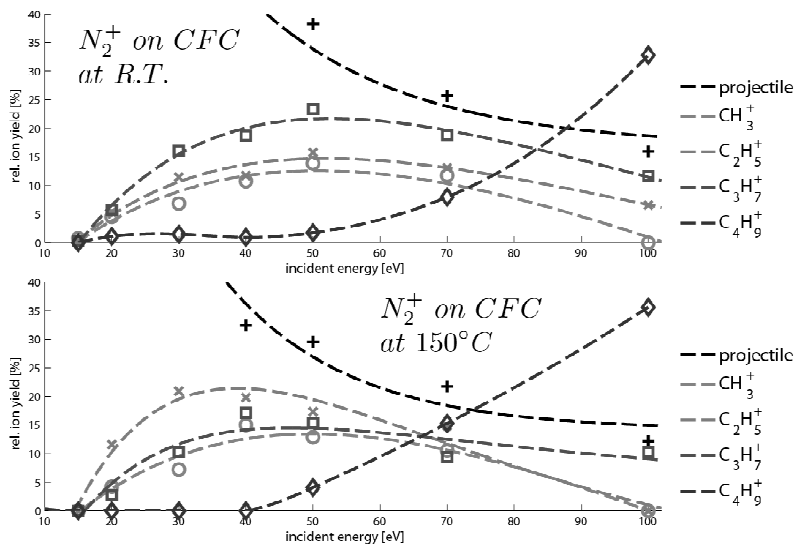


Figure 2: Collision energy resolved mass spectra showing contributions from the projectile ion (black, +) and selected surface hydrocarbons CH_3^+ (blue, o), C_2H_5^+ (green, x), C_3H_7^+ (red, □) and C_4H_9^+ (purple, ◇) at room temperature and at a surface temperature of 150°C, respectively. Lines between data points are guides for the eye.

Interactions of N_2^+ with tungsten

Room temperature measurements of N_2^+ with clean, pristine tungsten surface show almost no alkali contamination (see Figure 3, $m/z=23$, blue line).

Only with increasing temperature the Na^+ and K^+ contributions begin to show and become very dominant at 300°C. This leads to the conclusion that the alkali contaminants are not situated on the surface, but rather originate from some other part of the machine inside the vacuum chamber or from the bulk of the surface sample.

At higher temperatures around 600°C also a substantial amount of calcium can be detected at $m/z = 40$. At this point it was reasonable to analyse the surface sample composition by X-ray photoelectron spectroscopy (XPS).

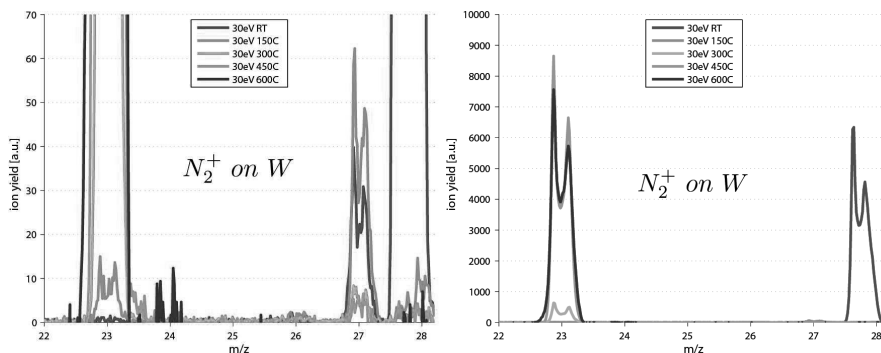


Figure 3: Product ion spectrum of interactions of N_2^+ with W at 30eV projectile incident energy and at different surface temperature, showing Na^+ ($m/z = 23$), $C_2H_3^+$ ($m/z = 27$) and the projectile N_2^+ ($m/z = 28$) in detailed view (left) and as overview (right).

XPS analyses of surface samples

In cooperation with A. Menzel, Institute of Physical Chemistry, University of Innsbruck, XPS analyses of several samples were performed. The result was very similar for all samples, used or pristine, polished or cleaned-only W-surfaces as well as those originating from a different production batch.

On all samples a thin hydrocarbon and carbide layer was observed. The carbon traces as well as the signal of Calcium vanish in the XPS spectrum after sputtering off the upmost layers. However, the XPS-profile did not show traces of Na and K in any of the investigated W-surfaces.

Acknowledgement: This work was supported by the KKKÖ and the EU (EURATOM).

References

- [1] Z. Herman, *J. Am. Soc. Mass. Spectrom.*, **14**, 1360 (2003)
- [2] A. Keim, B. Rasul, N. Endstrasser, P. Scheier, T. D. Märk, Z. Herman, *Int. J. Mass Spectrom.*, **306**, 204 (2011)
- [3] L. Feketeova, J. Žabka, F. Zappa, V. Grill, P. Scheier, T. D. Märk, Z. Herman, *J. Am. Soc. Mass Spectrom.*, **20**, 927 (2009)
- [4] C. Mair, T. Fiegele, F. Biasioli, Z. Herman, T. D. Märk, *J. Chem. Phys.*, **111**, 2770 (1999)

Scattering of T and He at graphite (0001) surfaces: a 3D time-dependent wave packet study

Stefan E. Huber¹, Tobias Hell², Michael Probst¹ and Alexander Ostermann²

¹ *Institute for Ion Physics and Applied Physics, Innsbruck University, Technikerstrasse 25, A-6020 Innsbruck, Austria, electronic mail: s.huber@uibk.ac.at*

² *Department of Mathematics, Innsbruck University, Technikerstrasse 13, A-6020 Innsbruck, Austria*

We performed simulations of the elastic scattering of atomic tritium and helium beams at graphite (0001) surfaces in an energy range of 1 to 4 eV. For this we solve the time-dependent Schrödinger equation numerically using a split-step Fourier method. The T- and the He-graphite potentials were derived from density functional theory calculations on a cluster model for the graphite surface. We observe that the elastic interaction of T with graphite differs fundamentally from the one of He. Whereas the Helium wavepackets are directed to the centres of the aromatic cycles constituting the graphite hexagonal lattice, they are directed towards the carbon atoms and carbon-carbon bonds for the T-beam.

1. Introduction

The interaction of carbon-based materials with low-Z atoms such as hydrogen isotopes and helium is of great interest in nuclear fusion reactors since carbon composites are frequently used as wall material, at least in regions where the highest heat loads are expected. Present fusion experiments have shown that the divertor is significantly eroded by incoming hydrogen (isotopes) due to sputtering of hydrocarbon molecules already at low plasma temperatures of about 1 to 10 eV. To complement experiments and illuminate underlying mechanisms, a variety of molecular dynamics (MD) simulations have been carried out revealing several fascinating aspects of this chemical erosion [1-3]. Swift chemical sputtering has been proposed [1] as one of the main mechanisms leading to significant erosion at low impact energies. The sputtering proceeds as impinging hydrogen atoms penetrate the region between C-C bonds and, if their energy is in a certain range, subsequently break the bond. Moreover, MD studies have shown that the addition of noble gases (in small concentration less than 10 per cent) to the usual impact species hydrogen (isotopes) does not significantly alter the erosion yields [2]. Furthermore, MD studies involving pure perfect hexagonal graphite revealed the interesting sputtering mechanism known as graphite peeling, i.e. as the graphite layers are bombarded they are peeled off one after the other [3].

We approach the interaction of tritium and helium with graphite in a different way. We derive H-graphite and He-graphite potentials from quantum chemical cluster calculations and use them to describe these atoms as appropriate wave packets colliding with graphite. We

simulate elastic scattering of T- and He-beams at a graphite (0001) surface in an energy range of 1 to 4 eV. Though only elastic scattering can be studied in this way, our results can be related to the physics underlying the phenomena mentioned above.

2. Methodology

2.1 Numerical method

In appropriate units, the linear time-dependent Schrödinger equation is

$$i\partial_t \psi(t, x) = -\Delta \psi(t, x) + V(x) \psi(t, x), \quad t > 0, \quad (1)$$

with initial value $\psi(0, x) = \psi_0(x)$, $x \in \mathbb{R}^3$, where $\psi: [0, \infty) \times \mathbb{R}^3 \rightarrow \mathbb{C}$ denotes the wave function and V the potential described in section 2.2. To numerically solve equation (1), we use a splitting method. In our situation, the underlying idea of splitting is to first solve the free Schrödinger equation

$$i\partial_t \psi(t, x) = -\Delta \psi(t, x) \quad (2)$$

and then to use the result as the initial value for solving

$$i\partial_t \psi(t, x) = V(x) \psi(t, x). \quad (3)$$

By choosing an appropriately large domain, we can artificially impose periodic boundary conditions. As a result, equation (2) can be solved very efficiently by a Fourier spectral method. Note that equation (3) is easily solved by pointwise multiplication. Using the Strang splitting, this yields the split-step Fourier method described and investigated in reference [4].

2.2 Construction of the potentials

The determination of energy barriers is discussed in detail in [5]. In short, the permeation of an atom through a graphite (0001) surface, is modelled by quantum chemical calculations where graphite is replaced by PAH molecules. Technically, the distance between a contaminant atom (here T or He) and a sufficiently large PAH molecule, i.e. coronene, is varied in 30 steps, each having the size of 0.15 Å. Thus, the atom is moved perpendicularly to the molecular plane of the undisturbed hydrocarbon from 3 Å in front of the PAH molecule to 3 Å behind the PAH molecule. At each position the energy $E(\text{A-PAH})$ of the total system is calculated after relaxation of the PAH molecule, i.e. the adiabatic energy barrier $E(z)$ at the respective position z of the contaminant atom is then given as the difference $E(z) = E(\text{A-PAH}) - (E(\text{A}) + E(\text{PAH}))$. The geometry optimizations and energy calculations have been performed in the framework of density functional theory using the well-established B3LYP functional [6]. All quantum chemical computations have been carried out with the Gaussian 09 software [7]. Energy curves for the approach of and the permeation through coronene have

been calculated at 21 distinct sites in a quarter of the central aromatic cycle. The potentials used for the 3D time-dependent wave-packet method have then been constructed by interpolation and periodic continuation of the numerical data.

3. Results and discussion

In figure 1, the results for the time evolution of an initial wave packet are shown for the scattering of T and He at the graphite surface. Plotted is a slice resulting from a cut through the computational domain parallel to the graphite surface at $z=3$ Å. In case of normal incidence, like here, the slice is also perpendicular to the motion of the impinging wave-packet. The wave-packet first passes the slice as it approaches the interaction region, i.e. the region where the potential is nonzero. Then, the wave-packet is scattered at the graphite surface and the reflected wave-packet passes the slice again, now from the opposite direction. Both the T- and the He-wave-packets, were constructed to interact with the graphite surface at top site, i.e. such that their center of mass is directed precisely onto a carbon constituent of the hexagonal lattice. The energies have been 4 eV in both cases.

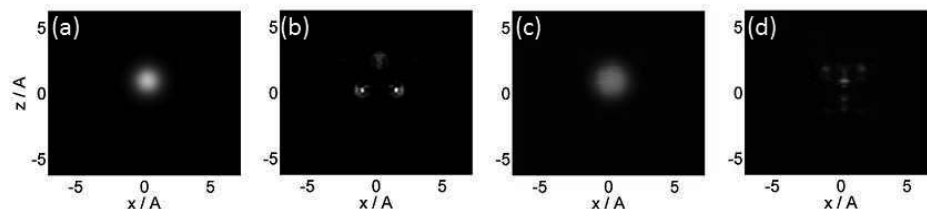


Figure 10. Wave-packet passing through the window. (a) He-wave-packet passing the window before being scattered, (b) reflection pattern of He after scattering, (c) T-wave-packet before scattering, (d) reflection pattern of T after scattering.

In figure 1, a remarkable difference between T- and He-scattering can be observed. Whereas the reflection pattern for He yields a strong repulsion at top site, the T-wave-packet is diffracted towards the aromatic cycle, i.e. towards the carbon constituents and C-C bonds forming the hexagonal lattice of the graphite surface. The hexagonal pattern can be recognized in figure 1d. Although not shown here, also the reflection patterns for beams directed initially towards bridge site (onto a C-C bond) and hollow site (towards the centre of an aromatic cycle) behave in the same way.

This difference in the scattering behaviour of T and He has several consequences for the chemical erosion of graphite. First, it underlines the role of swift chemical sputtering. This means that not only if a hydrogen (isotope) enters the region between two carbon atoms, it contributes to the erosion by bond breaking, but in fact hydrogen always interacts with the

surface exactly in this relevant region of the aromatic cycle. Second, the same effect of deflecting tritium towards the carbon hexagon serves as fundamental explanation for the graphite peeling mechanism. Though hydrogen atoms are small enough to permeate through the hole of one hexagon, the H-graphite potential directs them towards the layer skeleton. Thus, the layers are ablated one by one. Third, since the interaction of He with graphite is prototypical for the interaction with other closed-shell noble gases, the results for He-scattering serve as an explanation for the negligibility of noble gas concentrations in the constitution of the impact particles. The deflection towards the centre of the aromatic cycles simply suppresses the effect of swift chemical sputtering for these impact particle species.

4. Conclusion

As a complement to beam experiments and molecular dynamics simulations, we present a 3D time-dependent wave-packet simulation to investigate elastic scattering of tritium and helium on graphite (0001) surfaces. We believe that our method gives valuable insight into the physics underlying important mechanisms for chemical erosion of carbon-based materials exposed to hot plasma or gas. In particular, it underlines the importance of swift chemical sputtering for the chemical erosion of carbon-based materials and it yields a first-principle explanation for the observed graphite peeling during particle bombardment.

Acknowledgements

This work was supported by the Austrian Ministry of Science BMWF as part of the university infrastructure program of the scientific computing platform at LFU Innsbruck. Support from the DK+ on computational interdisciplinary modelling is gratefully acknowledged.

References

- [1] K. Nordlund, E. Salonen, S. Krasheninnikov, J. Keinonen, *Pure Appl. Chem.*, **78** (2006) 1203-1211.
- [2] P. Traeskelin, K. Nordlund, J. Keinonen, *J. Nucl. Mat.*, **357** (2006) 1-8.
- [3] A. Ito, H. Nakamura, *Comm. Comput. Phys.*, **4** (2008) 592-610.
- [4] T. Jahnke, C. Lubich, *BIT*, **40** (2000) 735-744.
- [5] S.E. Huber, M. Probst, in preparation.
- [6] A. Becke, *J. Chem. Phys.*, **98** (1993) 5648-5652.
- [7] M.J. Frisch, G.W. Trucks, et al., Gaussian 09, Revision A.1, Gaussian, Inc., Wallingford CT, 2009.

Melting behaviour of pure and coated gold nanowires: Molecular dynamics simulations

Stefan E. Huber¹, Chompunuch Warakulwit^{2,3}, Jumras Limtrakul^{2,3}, Tatsuya Tsukuda⁴ and Michael Probst¹

¹*Institute of Ion Physics and Applied Physics, Innsbruck University, Technikerstraße 25, A-6020 Innsbruck, Austria, electronic mail: s.huber@uibk.ac.at*

²*Chemistry Department, Center of Nanotechnology, and Center for Advanced Studies in Nanotechnology and Its Applications in Chemical, Food and Agricultural Industries, Kasetsart University, Bangkok 10900, Thailand*

³*NANOTEC Center of Excellence, National Nanotechnology Center, Kasetsart University, Bangkok 10900, Thailand*

⁴*Catalysis Research Center, Hokkaido University, Nishi 10, Kita 21, 5 Sapporo 001-0021, Japan*

The thermal stabilization of thin gold nanowires with a diameter of about 2 nm by surfactants is investigated by means of classical molecular dynamics simulations. While the well-known melting point depression leads to a much lower melting of gold nanowires compared to bulk gold, coating the nanowires with surfactants can reverse this, given that the attractive interaction between surfactant molecules and gold atoms lies beyond a certain threshold. The suppression of the melting by surfactants is explained by the isotropic pressure acting on the gold surface (due to the attractive interaction) which successfully suppresses large-amplitude thermal motions of the gold atoms.

1. Introduction and Methodology

We use an atomistic model to investigate the melting process of thin Au nanowires (AuNWs) by means of molecular dynamics (MD) simulation. Furthermore, we propose a model of the physical mechanism responsible for their thermal stabilization by coating them with surfactant molecules. We discuss the results for the melting of a bare AuNW in vacuum and the effects of additional initial defects such as dislocations. In addition, we compare these results to the melting behaviour of a NW that is coated by surfactants exhibiting an attractive interaction with the gold surface atoms [1].

For that purpose three different initial configurations have been prepared: (a) a bare NW consisting of 200 layers containing 18 Au atoms in each layer arranged in a perfect fcc lattice. This corresponds to a cross section of $1.2 \times 1.2 \text{ nm}^2$ and a length of about 400 nm. This size is comparable to the typical size of NWs in experiments. (b) A NW as in (a) but with an additional initial dislocation. (c) A NW that is coated with surfactant molecules.

These NW models have then been subject to free evolution in a temperature range of 100 - 1500 K to determine the melting point and investigate the melting behaviour and influence of

the modifications on the latter. The equations of motion have been integrated with the velocity Verlet algorithm with a variable time step in the order of 0.1-10 fs. The total simulation time has been about 500 ps at each temperature. All calculations have been carried out with the DL_POLY 4 software [2].

As a model surfactant n-aminopentane ($\text{NH}_2\text{-CH}_2\text{-CH}_2\text{-CH}_2\text{-CH}_2\text{-CH}_3$; AP) has been chosen, where the amine group exhibits an attractive interaction with gold atoms but behaves like a methyl group otherwise.

The interactions between gold atoms have been modelled by the Sutton-Chen many-body potential [3, 4]. The total conformational energy of the AP molecules is given as the sum of bonding, bending and dihedral potentials as well as the intermolecular potentials which are of the 12-6 Lennard-Jones (LJ) type. In particular, the energy parameter of the LJ-potential describing the strength of the attractive interaction between amine groups and gold atoms has been varied between 1 and 7 kcal/mol to investigate the influence of coating on the melting point. All other force field parameters have been taken from the CHARMM [5] and united (UFF) force fields [6].

2. Results

Before investigating the melting process of a bare NW in vacuum we checked the appropriateness and proper implementation of the Sutton-Chen potential by investigating the melting of bulk gold. For ease of comparison with earlier publications [7] we simulated a bulk system consisting of 4000 gold atoms. The latter were arranged in a perfect fcc structure in a cell subjected to cubic periodic boundary conditions. The phase transition from solid to liquid state takes place at around 1380 K in good agreement with experiment (1338 K). The validity of the Sutton-Chen potential for the melting behaviour of bulk gold implies also some confidence that it can also capture qualitative trends in finite systems. This was further checked against available simulation data by simulating small gold nanoparticles of 256 gold atoms. The melting temperature was found at about 550-575 K, virtually the same as reported in earlier studies [8, 9] with the – in principle more sophisticated – TB-SMA potential [10] for modelling the Au-Au interaction.

After these checks we determined the melting temperature of the perfect bare NW (see (a) in section 1) to be about 750 K. This result together with the above result for the Au nanoparticle is in good agreement with the well-known melting point depression [11] for small metal nanosystems.

The effect of adding surfactant molecules (AP) is best observed by plotting the normalized root mean square displacement (RMSD in Å per ps) as well as the diffusion coefficient (approximately corresponding to the derivative of the RMSD) of the gold atoms versus the temperature, see figure 1. For an Au-NH₂ potential parameter $\epsilon < 4.5$ kcal/mol an

abrupt change in the NRMSD, accompanied by the corresponding peak of the diffusion coefficient, can be observed in the temperature region around 750 K. However, for values larger than 4.5 kcal/mol the jump in the NRMSD and the peak in the diffusion coefficient, respectively, is shifted to substantially higher temperatures, indicating a corresponding increase of the melting temperature.

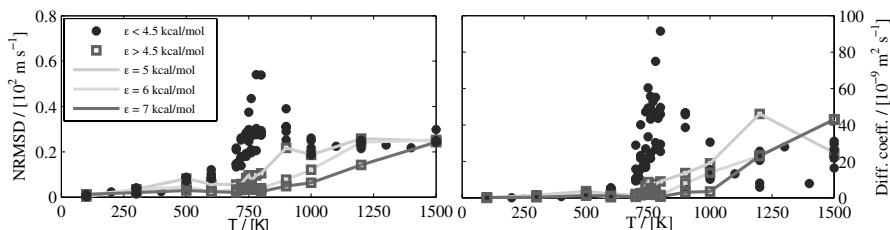


Figure 11: NRMSD (left) and diffusion coefficient (right) of Au atoms in dependence of temperature and various values of ϵ .

The threshold value of about 4.5 kcal/mol equals approximately $6 \times kT/2$, where T is the melting temperature of the bare AuNW in vacuum and k is Boltzmann's constant. This corresponds nicely to the surfactant model which effectively gives rise to a behaviour of AP resembling a near-linear string with six degrees of freedom (three translational, two rotational and one vibrational). Equipartition of the energy leads then straightforwardly to the smallest necessary depth of the well of the LJ potential. The melting of the NW is suppressed until the AP molecules are no longer permanently absorbed and only a dynamical exchange of them on the surface remains. At temperatures $T < \epsilon/3k$, where $\epsilon > 4.5$ kcal/mol, the isotropic pressure, due to the attractive interaction between AP molecules and surface atoms, suppresses the thermal motion of the gold atoms and thus, the melting of the NW.

Conclusion

The melting behaviour of thin gold NWs has been investigated. Besides a qualitative reproduction of the well-known melting point depression [11], our simulations suggest that such NWs can be thermally stabilized by coating them with surfactants, given that the attractive interaction between Au atoms and surfactants exceeds a certain threshold which can be explained from simple thermodynamic considerations.

Acknowledgements

This work was supported by the Austrian Ministry of Science BMWF as part of the university infrastructure program of the scientific computing platform at LFU Innsbruck. Support from the DK+ on computational interdisciplinary modelling is gratefully acknowledged. C.W. and J.L. thank the National Science and Technology Development Agency (NSTDA Chair Professor and National Nanotechnology Center), the National Research University Project of Thailand (NRU) and the Thailand Research Fund for support. Support from the Austrian Research Council (FWF: I200-N19 and RFBR: 09-03-91001-a) is acknowledged. We thank Prof. Kersti Hermansson for fruitful discussions and suggestions concerning our work.

References

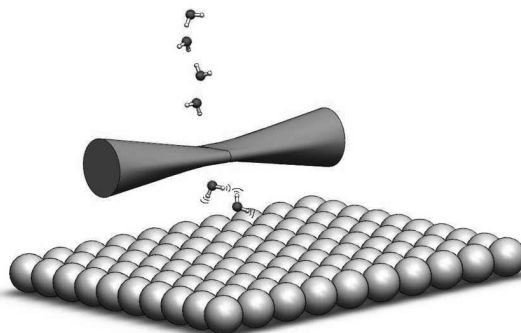
- [1] S.E. Huber, C. Warakulvit, J. Limtrakul, T. Tsukuda, M. Probst, *Nanoscale* (2011), DOI: 10.1039/c1nr11282a.
- [2] I.T. Todorov, W. Smith, K. Trachenko, M.T. Dove, *J. Mater. Chem.*, 16 (2006) 1911-1918.
- [3] A.P. Sutton, J. Chen, *Phil. Mag. Lett.*, 61 (1990) 139-146.
- [4] H. Rafii-Tabar, A.P. Sutton, *Phil. Mag. Lett.*, 63 (1991) 217-224.
- [5] P.v.R. Schleyer, e. al., *The Encyclopedia of Computational Chemistry*, in, John Wiley & Sons, Chichester, 1998, pp. 271-277.
- [6] A.K. Rappe, C.J. Casewit, K.S. Colwell, W.A. Goddard, W.M. Skiff, *J. Am. Chem. Soc.*, 114 (1992) 10024-10035.
- [7] Y. Zhang, Y.-H. Wen, J.-C. Zheng, Z.-Z. Zhu, *Phys. Lett. A*, 373 (2009) 3454-3458.
- [8] Q. Pu, Y. Leng, X. Zhao, P.T. Cummings, *Nanotechnology*, 18 (2007) 424007/424001-424005.
- [9] Q. Pu, Y. Leng, L. Tsetseris, H.S. Park, S.T. Pantelides, P.T. Cummings, *J. Chem. Phys.*, 126 (2007) 144707/144701-144707/144706.
- [10] F. Cleri, V. Rosato, *Phys. Rev. B*, 48 (1993) 22-33.
- [11] O. Guelsersen, F. Ercolessi, E. Tosatti, *Phys. Rev. B*, 51 (1994) 7377-7380.

Quantum-state Resolved Studies of the Physisorption of Water on Ice

P. Morten Hundt¹, Régis Bisson², Hirokazu Ueta¹, and Rainer D. Beck¹

¹ *Laboratoire de Chimie Physique Moléculaire, Ecole Polytechnique Fédérale de Lausanne, Switzerland. Corresponding author : Rainer.Beck@epfl.ch*

² *CNRS, PIIM, Université de Provence, Marseille, France.*



Water ice is a major component of the circumstellar environments of evolved stars. Hence, the condensation probability of water molecules on ice is an important parameter in the modeling of water ice growth on dust grains around evolved stars. Previous molecular beam experiments have measured H_2O and D_2O sticking coefficients on ice as a function of incidence energy and angle but the role of selective vibrational and rotational excitation of the incident water molecules in physisorption has never been investigated until now.

In our study, we combine a molecular beam/surface science apparatus with a powerful continuous wave (cw) infrared laser to investigate the influence of selective vibrational excitation on the physisorption of D_2O on amorphous D_2O -ice. Water molecules are excited to specific ro-vibrational states with one quantum of O-D stretch by cw laser excitation in a molecular beam before they collide with defined speed and incident angle with the solid surface in ultrahigh vacuum. Physisorption probabilities are measured by a mass spectrometer using a modulated beam reflection technique based on the King and Wells method.

Laser preparation of different vibrational modes of water enables us to probe for mode specificity in its physisorption. The results of our studies will help to clarify the role of vibrational energy transfer in the sticking of water on ice and will contribute to a detailed predictive understanding of these important processes.

Formation of molecular hydrogen in the interstellar medium

Benjamin J. Irving¹, Anthony J. H. M. Meijer[†]

¹ *University of Sheffield, Sheffield, UK, S3 7HF, chp08bjj@sheffield.ac.uk*

[†] *a.meijer@sheffield.ac.uk*

Molecular hydrogen, H₂, is one of the fundamental constituents of the universe, acting as the molecular feedstock for much of the chemistry occurring within the interstellar medium (ISM). Although gas phase models of the chemistry of interstellar clouds have been successful in explaining the abundances of some gas phase molecules, it has long been established that they cannot account for the large abundance of molecular hydrogen. The general consensus of the astronomical community is that carbonaceous interstellar dust grains assume a catalytic role in the formation of H₂ molecules within interstellar clouds.

First-principles calculations using the *VASP* (Vienna *ab initio* simulation package) software package have been performed in order to scrutinise the hydrogen-dust grain interaction. Furthermore, the collinearly-dominated Eley-Rideal H₂ formation pathway has been studied by quantum dynamical means using the Multi Configuration Time Dependent Hartree (MCTDH) algorithm in conjunction with a novel PES accounting for energy transfer from the nascent H₂ bond to the dust grain surface.

Experimental determination of conditions in the trap: reaction temperature and reactant density

P. Jusko¹, I. Zymak¹, D. Mulin¹, Š. Roučka¹, R. Plašil¹, D. Gerlich^{1,2}, J. Glosík¹

¹ Department of Surface and Plasma Science, Faculty of Mathematics and Physics, Charles University in Prague, V Holešovičkách 2, Praha 8, 180 00, Czech Republic, pavol.jusko@mff.cuni.cz

² Department of Physics, Technische Universität Chemnitz, 09107 Chemnitz, Germany

A variable temperature 22-pole rf trap with buffer gas ion cooling is used for various astrophysically relevant studies. Currently we are studying binary and ternary association reaction of H^+ and H_2 at temperature 11–22 K. The actual reaction temperature is very sensitive to parameters of the trap and to experimental conditions. We used ternary association reaction of $\text{He}^+ + \text{He} + \text{He} \rightarrow \text{He}_2^+ + \text{He}$ to characterize temperature and density in particular.

Determining reactant density and temperature

The actual temperature at which the reaction takes place is determined by the temperature of the ions and the temperature of the buffer gas. The resulting reaction temperature T can be expressed as:

$$T = (m_I T_B + m_B T_I) / (m_I + m_B), \quad (1)$$

where m_I , m_B , T_I , T_B are the masses and temperatures of ions and buffer gas respectively [1,2].

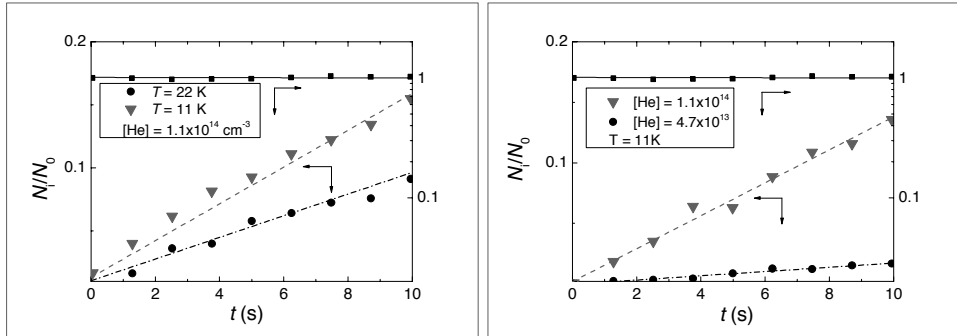


Figure 1: Time evolution of relative numbers of reactant He^+ (squares, right ordinate) and product ions He_2^+ (triangles, full circles left ordinate) in the trap. Left: two different temperatures at $[\text{He}] = 1.1 \times 10^{14} \text{ cm}^{-3}$. Right: two different He number densities at $T = 11 \text{ K}$. Primary ions He^+ and association product He_2^+ relative numbers are plotted. Numbers of ions in the trap are normalized to initial number N_0 of primary ions (see Fig. 34. [1]), which is $N_0 \sim 200$ at both conditions. Solid line at the top of each figure represents fit in form of $\exp(-t/\tau)$ with $\tau > 60 \text{ s}$. Solid line (and squares) also represent numbers of primary He^+ for He_2^+ product plotted using full circles.

The temperature of the 22-pole trap walls is measured by a silicon diode mounted on the 22-pole trap housing. The density in the trap at given temperature is calculated from the pressure measured by a spinning rotor gauge (operates at room temperature) [2].

To determine the actual temperature of the ions and of the neutrals we decided to investigate the temperature in the trap using a ternary association of He^+ and He. This reaction can be used as a thermometer as shown in [2,3,4], helium assisted association has been studied in various experimental setups e.g. liquid nitrogen cooled flowing afterglow [5], liquid helium cooled drift tube [6] and helium closed cycle cryostat cooled rf traps [2]. Temperature dependences of the form $k_3 \sim T^\kappa$ have been determined ($\kappa = -0.38$ [5] and -0.60 [6]). In ion traps it is possible to measure apparent rate constant k^* , by monitoring He_2^+ ion formation (see Fig. 1.), described at $[\text{He}_2^+] \ll [\text{He}^+]$ as $[\text{He}_2^+] \sim [\text{He}^+] k^* [\text{He}] t$. The ternary rate coefficient k_3 is connected with k^* [2]:

$$k^* = k_3[\text{He}] + k_r, \quad (2)$$

where k_r is the radiative and k_3 the ternary rate coefficient.

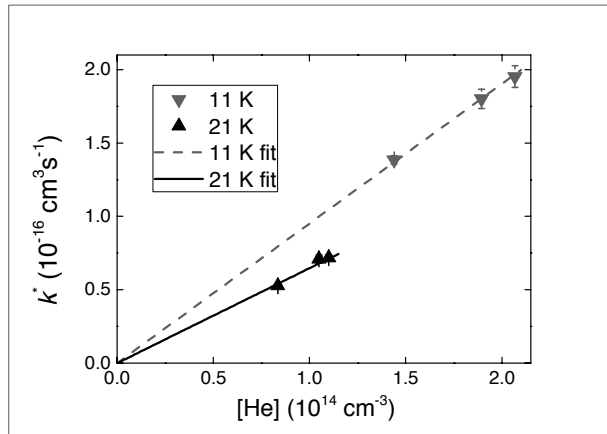


Figure 2: Apparent binary rate coefficient dependence on number density of He buffer gas measured at two different temperatures. Lines indicate linear fit through data and axes origin.

Fig. 2. shows the helium pressure dependence of the apparent rate constant k^* . Data in Fig. 1. illustrates results of particular experiment. Total number of primary ions (He^+) and association products (He_2^+) are measured as a function of time for different conditions. Fig. 2. also shows that we are measuring in helium density range where ternary association is a dominant process and eventual binary radiative association is negligible (we neglect k_r in Eq. 2). Measured ternary association rate coefficient k_3 are plotted in Fig. 3. together with

previously measured values [3,4,5,6,7,8]. Temperature on the abscissa is the temperature of the trap.

Conclusion

Increase of the ternary rate coefficient with decreasing temperature is apparent. Present values are higher than previously measured values (23% at lowest temperature compared to value given in ref. [4]), however at higher temperatures data sets agree within their experimental error. Our recent measurements confirm our expectations that we are able to attain reaction temperatures down to 10 K in the 22-pole trap at least for mass 4 ion in helium. Measurement with lower masses (H^+) are done with different operating conditions of the trap, because of effective potential dependence on the mass (for details see ref. [1]), to achieve the lowest temperature higher rf frequencies may be needed (22 instead of 18 MHz).

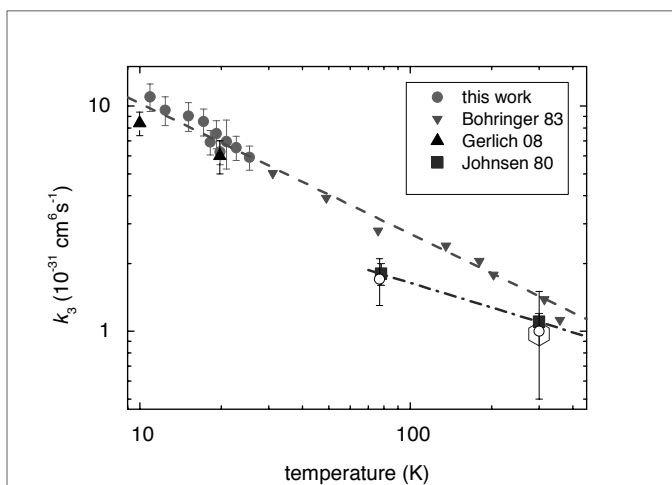


Figure 3: Ternary association rate coefficient (k_3) as a function of temperature. Full circles – present 22-pole trap measurements (data measured at 11 and 21 K are plotted in Fig. 2.). Triangles (down) – drift tube measurements [6]. Squares – flowing afterglow measurements [5]. Triangles (up) – older rf trap measurements [4]. Circles – older drift tube measurements [7]. Pentagon – older stationary afterglow measurements [8]. Dashed line – fit from [6]. Dash-dot line – fit from [5]. It looks like measured $k_3 \sim T^\kappa$ increases (with constant exponent $\kappa = -0.56 \pm 0.1$) down to 10 K.

Acknowledgments

Financial support of the DFG (FOR 388) is gratefully acknowledged. This work is a part of the research plan MSM 0021620834 and grant OC10046 financed by the Ministry of Education of the Czech Republic and was partly supported by GACR (202/07/0495, 205/09/1183, 202/09/0642), by GAUK 25709, GAUK 406011, GAUK 388811 and by COST Action CM0805 (The Chemical Cosmos).

References

- [1] D. Gerlich, *Advances in Chemical Physics* **82**, 1-176 (1992)
- [2] D. Gerlich, S. Horning, *Chemical Reviews* **92**, 1509-1539 (1992)
- [3] D. Gerlich, *The study of cold collisions using ion guides and traps*, chapt 3 in: Low temperatures and cold molecules (ed. I.W.M. Smith), Singapore, 121-174 (2008)
- [4] W. Paul, *Reaktionsdynamik schwach gebundener ionischer Cluster - Doctoral thesis*, TU Chemnitz, 48-49 (1996)
- [5] R. Johnsen, A. Chen, M.A. Biondi, *J. Chem. Phys.* **73**, 1717-1720 (1980)
- [6] H. Böhringer, F. Arnold, *Int. J. Mass Spectrom. Ion Phys.* **49**, 61-83 (1983)
- [7] E. C. Beaty, P. L. Patterson, *Phys. Rev.* **137**, A346 (1965)
- [8] R. Hackam, J. J. Lennon, *Proc. Phys. Soc. London* **84**, 133 (1964)

Influence of higher-order dispersion coefficients on near-threshold bound and continuum states

Alexander Kaiser¹, Tim-Oliver Müller² and Harald Friedrich²

¹Universität Innsbruck, Inst. für Ionenphys., A-6020, Technikerstraße 25/3, alexander.kaiser@uibk.ac.at

²Technische Universität München, James-Franck-Straße 1, D-85748 Garching

The interaction potential of dimers consisting of atoms, ions or molecules is usually not known for all distances in general. However, the asymptotic forces are often very well known at large distances r . Typical examples are the van der Waals potentials between two neutral species, behaving as $-C_6/r^6$ for large r , or the atom-ion interaction behaving as $-C_4/r^4$ asymptotically, where C_6 , C_4 are system-specific dispersion coefficients. Higher-order expansions of the asymptotic form of the potential are available in the literature, e.g. [1, 2], for many cases. For deep potentials with attractive tails vanishing more rapidly than $1/r^2$ at large distances, highly excited bound states and low-energy scattering states are largely determined by the properties of the potential tail, which can be accounted for by a small number of *tail functions*. The effects of interaction in the close region (small r) are incorporated via two parameters, the threshold quantum number ν_D and an additional small correction proportional to energy E , with a coefficient γ_{sr} , further referred to as second short-range parameter. The threshold quantum number first introduced by LeRoy, Bernstein [3] and Stwalley [4] is in general non-integer and reflects the proximity of the least-bound state to the dissociation threshold. The threshold quantum number and the second short-range parameter can be obtained, e.g., by fitting to spectroscopically measured levels of highly excited states. These two parameters can then be used to extrapolate to other bound states in the near-threshold regime or to calculate low-energy scattering properties.

A brief summary of the theory for vanishing and non-vanishing angular momentum J , including conditions of validity is given. An application, where a single inverse power-law tail $V_{\text{tail}} \propto -1/r^\alpha$ is not sufficient to achieve a proper separation of the tail effects is the strontium dimer. In this case, the theory can be applied by including higher-order dispersion coefficients.

Theory

The theory is based on the recognition that WKB waves of the form

$$\psi_{\text{WKB}} \propto \frac{A(E)}{\sqrt{p(r,E)}} \cos\left(\frac{1}{\hbar} \int_r p(r',E) dr' - \frac{\phi(E)}{2}\right) \quad (1)$$

with the local classical momentum $p = \sqrt{2\mu(E - V(r))}$, an energy-dependent reflection phase $\phi(E)$ and an amplitude $A(E)$, are good approximate solutions of the radial Schrödinger equation in certain regions of space and energy for a given potential and its tail. The quality of the WKB approximation is a local property and can be investigated using the quantity function $Q(r, E)$ [5] for the full potential or for its tail. For a potential tail more singular than $-1/r^2$ for small r the WKB representation of the solution of the radial Schrödinger equation with V_{tail} becomes increasingly accurate with decreasing distance and is in fact exact in the limit $r \rightarrow 0$. The quality of the WKB approximation as a function of r and E can be seen in Figure 1a) for a typical interatomic potential and in Figure 1b) for its tail. In the dark regions (i.e. $|Q(r, E)| \approx 1$) the WKB representation is a highly accurate solution of the radial Schrödinger equation, in the bright regions (i.e. $|Q(r, E)| \gg 1$) the WKB waves fail.

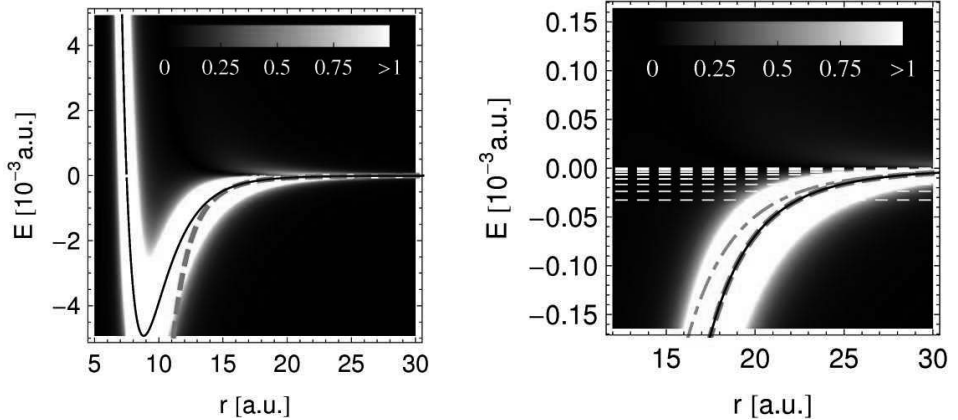


Figure 1: a) Density plot of $|Q(r, E)|$ as a function of both r and E for the full analytical potential energy curve [6] for the strontium dimer $^{88}\text{Sr}_2$, $J = 0$ in $X^1\Sigma_g^+$ configuration. The full potential (solid) and its tail (dashed) are shown. b) A zoom to energies near the dissociation threshold. The ten least bound states (white dashed) and the homogeneous tail $-C_6/r^6$ (dot-dashed) are shown additionally.

□

For our purpose the existence of a connected WKB region at close distances is required. Within a connected WKB region, WKB amplitudes A and phases ϕ do not change with r . This inner connected WKB region has to overlap with the region, where the full potential is very accurately approximated by its tail. Under these conditions, the exact solution of the

Schrödinger equation with the potential tail can be matched to appropriate WKB waves for the inner part of the wave function as shown in Ref. [7]. For the bound states this procedure leads to the quantization rule

$$F_{\text{tail}}(E_\nu) + f_{\text{sr}}(E_\nu) = \nu_D - \nu \quad (2)$$

where the quantization function F_{tail} only depends on the potential tail and is calculated solving the Schrödinger equation with V_{tail} and comparing the solution at small r to the WKB form Eq. (1). The small correction function $f_{\text{sr}}(E) \propto \gamma_{\text{sr}} E$ accounts for residual effects of the short-range interaction, which are not included in the threshold quantum number ν_D .

For the low-energy scattering states above threshold, the relevant quantity is the scattering phase shift $\delta_J(E)$, which directly translates into elastic scattering cross sections via the partial wave expansion. The matching procedure from Refs. [8, 9] yields

$$\tan(\delta_J) = \frac{A_s \sin(\pi(\nu_D - f_{\text{sr}}) - \xi_t + \phi_s)}{A_c \cos(\pi(\nu_D - f_{\text{sr}}) - \xi_t + \phi_c)} \quad (3)$$

for the phase shifts, where A_s, A_c, ϕ_s, ϕ_c are WKB amplitudes and phases which are, together with the function ξ_t , simply-structured tail-dependent functions and can be calculated numerically for a given tail in a straightforward way. With Eqs. (2) and (3) the near-threshold properties of the bound and continuum states are determined by the tail dependent functions and two additional parameters ν_D and γ_{sr} . These two parameters can be obtained, for example, by using the energies of two spectroscopically measured highly excited states.

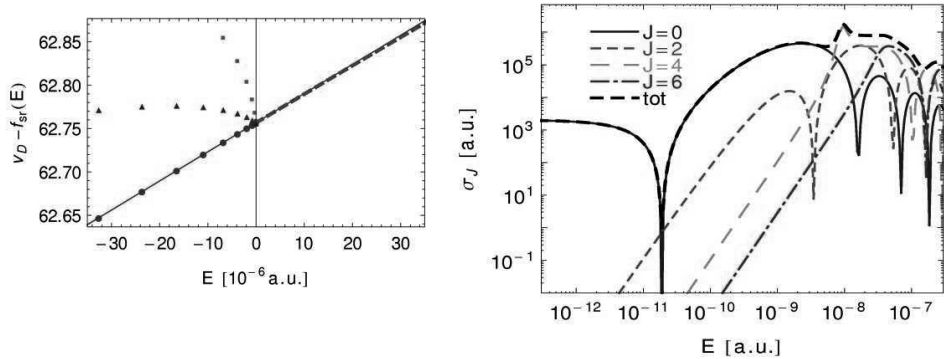
Application to strontium dimer

In order to demonstrate the applicability of the theory for a real example we chose the strontium dimer $^{88}\text{Sr}_2$. This example is very convenient because it has recently been studied extensively by Stein et al. [6] via Fourier Transform Spectroscopy. From these measurements a potential energy curve for the electronic ground state has been extracted by fitting to the experimental data. This full potential energy curve, shown in Fig. 1, is taken as a reference to test the accuracy of the theory. Including three dispersion coefficients in the potential tail

$$V_{\text{tail}} = -\frac{C_6}{r^6} - \frac{C_8}{r^8} - \frac{C_{10}}{r^{10}} \quad (4)$$

the tail functions $A_s, A_c, \phi_s, \phi_c, \xi_t$ are obtained for each energy E and angular momentum J by numerically solving the Schrödinger equation with for various initial conditions above and below threshold as described in Ref. [9]. The quality of the quantization function is analyzed

by plotting $F_{\text{tail}}(E_v) + v$ on the left of Fig. 2a) for the least 10 bound states of the full potential from Stein et al. [6]. Using only one (squares) or two (triangles) dispersion coefficients of Eq. (4) does not lead to satisfactory results. By using all three dispersion coefficients (filled circles) recommended in Ref. [6], the 10 bound states are described by the two parameters v_D , γ_{sr} very well. Using these parameters, as obtained by fitting a line through the filled



circles below threshold, and the tail functions for above threshold the scattering phase shifts are readily calculated and the resulting partial scattering cross sections are shown in Fig. 2b) for different angular momenta J .

Figure 2: a) Test of the quantization function Eq. (2) and the formula for the phase shift Eq. (3) for the s -wave of the strontium dimer ($E < 0$). For positive energies: smooth transition of the short-range function $f_{\text{sr}}(E)$ through threshold using Eq. (3). b) elastic scattering cross section using Eq. (3) and the parameters from below threshold.

References

- [1] J. Mitroy, M. W. J. Bromley, Phys. Rev. A **68**, 052714 (2003)
- [2] S. G. Porsev and A. Derevianko, Phys. Rev. A **65**, 020701 (2002)
- [3] R. J. LeRoy and R.B. Bernstein, J. Chem. Phys. **52**, 3869 (1970)
- [4] W. Stwalley, Chem. Phys. Lett. **6**, 241 (1970)
- [5] H. Friedrich, J. Trost, Phys. Rep. **397**, 359 (2004)
- [6] A. Stein, H. Knöckel, E. Tiemann, Eur. Phys. J. D **57**, 171 (2010)
- [7] P. Raab, H. Friedrich, Phys. Rev. A **78**, 022707 (2008)
- [8] T.-O. Müller, A. Kaiser, H. Friedrich, Phys. Rev. A **84**, 032701 (2011)
- [9] A. Kaiser, T.-O. Müller, H. Friedrich J. Chem. Phys. **135**, (accepted 2011)

Hydrogen-fullerene interactions at low temperatures

Alexander Kaiser, Stefan E. Huber, Oksana Ismailova and Michael Probst

Universität Innsbruck, Institut für Ionenphysik und Angewandte Physik, Technikerstraße 25/3, A-6020, alexander.kaiser@uibk.ac.at

Interactions between fullerenes or graphene and hydrogen have recently been the subject of a number of studies. On the technological side, their possible use as a medium for hydrogen storage [1, 2] causes this interest while, for example, the possible abundance of fullerene-hydrogen clusters in the interstellar medium has been discussed in astrophysics. There, in outer space, hydrogen-covered fullerenes might contribute to diffuse interstellar bands [3] of hitherto unknown origin. The detection of C_{60} and C_{70} in the IR spectra of planetary nebula indicated that fullerenes can be produced in space [4].

In this work, we give an overview of our calculations on the physisorption and chemisorption of hydrogen to fullerenes and relate it to recent experiments on hydrogen-fullerene clusters in liquid helium droplets.

The dissociation of hydrogen molecules is suppressed at low temperatures by a high energy barrier, e.g. in the vicinity of neutral C_{60} the reaction has to overcome $3.7eV$ according to [1]. A possible binding mechanism at low temperatures is physisorption of H_2 above the carbon surface as described and observed, e.g. in [1, 3]. In the mass spectrometry experiments of [3] fullerenes were prepared in superfluid helium nanodroplets doped also with hydrogen. Their results show interesting features, one of them being the appearance of magic numbers, i.e. the probability of finding a fullerene with a certain number of physisorbed H_2 in the spectrum drops manifestly from 32 to 33 hydrogen molecules on C_{60} and from 37 to 38 molecules attached to C_{70} . This number correlates with the number of faces, where in case of C_{60} there are 12 pentagons and 20 hexagons, totaling in 32 faces. This supports the theory that one hydrogen molecule is physisorbed above each face in a first shell. Another interesting observation in [3] is a tendency to form $C_{60}H_x$ with x odd more likely than x even. This could be governed by the formation of H_3^+ during the ionization process, which gives its proton to C_{60} , having a larger proton affinity.

Method

We use the PBE0 model [5], which is a hybrid model of Hartree Fock and density functional theory. PBE0 is based on a GGA functional developed by Perdew, Burke and Ernzerhof [6],

which in turn makes use of the Perdew-Wang correlation functional [7]. In this PBE functional all parameters, except that of the local spin density, are fundamental constants. PBE0 is in general not sufficient to describe long-range van der Waals interactions. However, in this case we have a charged system with stronger binding than in an uncharged system. For such systems PBE0 is supposed to give at least good trends of binding energies because it accurately describes static polarisabilities [8]. The 6-31G(*d*,*p*) basis set of contracted gaussians with additional polarization functions is used. All the calculations are done with the Gaussian09 implementation.

Results

In contrast to H_2 , H_3^+ dissociates without barrier in the vicinity of C_{60} into H_2 which is repelled and a proton that binds covalently to the nearest C-atom. Hydrogen covalently bound to C_{60} leads to a somewhat distorted fullerene, where the C-atom below the atomic hydrogen is elevated 0.2\AA in the $C_{60}H^+$ system in the attempt to reach sp^3 configuration, compare Figure 1. The C - H bond length is 1.106\AA .

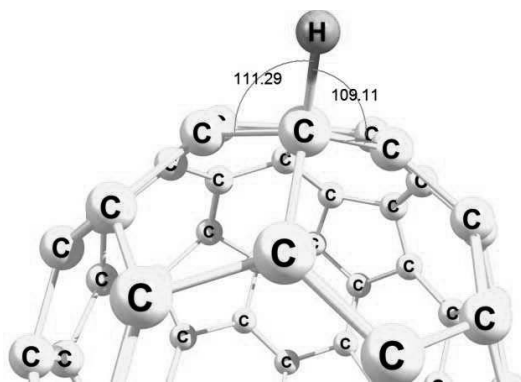


Figure 1: Fullerene with hydrogen: $C_{60}H^+$

The positive charge of $C_{60}H^+$ is equally distributed over the whole system. This can be seen in Figure 2 in a density plot of the electrostatic potential for three different cuts through the molecule. One cuts through the center of the molecule and through the hydrogen. The others are parallel to this first plane, where the second one cuts through the second layer of C-atoms and the third one is situated halfway between the second and third layer of C-atoms.

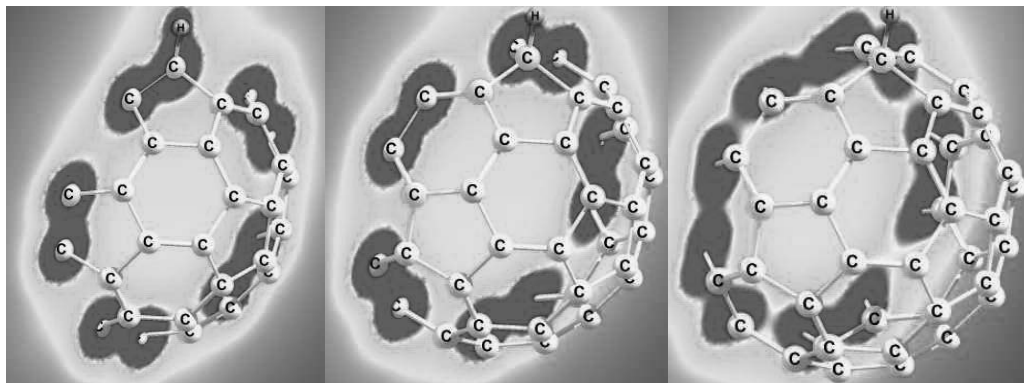


Figure 2: Electrostatic potential of $C_{60}H^+$ for different cuts through the molecule.

An optimization of H_3^+ in the vicinity of C_{60} leads to an equilibrium geometry with a physisorbed H_2 in a distance of about 3.4\AA to the surface of the fullerene. Both the distance and the binding energy of the physisorbed H_2 vary with its angular position due to the corrugation of the surface. The binding energy of the physisorbed H_2 also depends on the position of H_2 in respect to the chemical bound hydrogen atom. For the equilibrium geometry of the left hand side of Figure 3 a binding energy of 25.5meV is reached, for the right hand side of Figure 3 it is 29.7meV . The situation changes dramatically for H_2 opposite to the covalent bound atomic hydrogen with a binding energy of only 17.4meV .

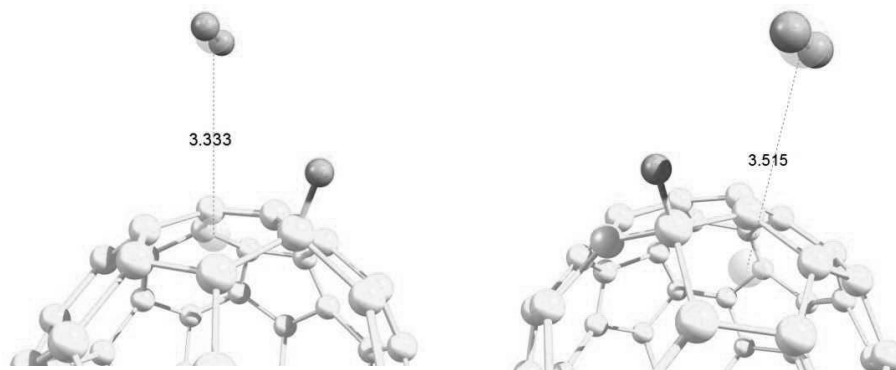


Figure 3: Two possible equilibrium geometries of $(C_{60}H)^+ H_2$

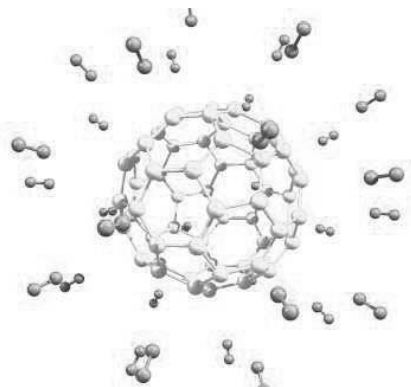


Figure 4: Neutral C_{60} coated with 32 H_2 . Each face is occupied by one H_2 .

A neutral fullerene coated with 32 hydrogen molecules is shown in Figure 4. In this configuration a binding energy of only 12meV per H_2 is obtained. The distance of H_2 to the center of the faces 3.56\AA for the hexagons and 3.6\AA for pentagons is slightly larger than in the $C_{60}H_3^+$ case. Such small binding energies can only be observed in cold surroundings. At room temperature the bond would probably dissociate immediately and these van der Waals bound clusters would have a very short life time.

We could confirm the possibility of creation of a stable $C_{60}H^+$ out of neutral buckminsterfullerenes in the presence of H_3^+ . A second collision with H_3^+ is unlikely due to the coulomb repulsion between $C_{60}H^+$ and H_3^+ . The $C_{60}H^+$ complex can be coated at low temperatures with molecular hydrogen.

References

- [1] T. T. Vehviläinen, M. G. Ganchenkova, L.E. Oikkonen and R.M. Nieminen, Phys. Rev. B **84**, 085447 (2011)
- [2] A. Sigal, M. I. Rojas, and E. P. M. Leiva, Phys. Rev. Lett. **107**, 158701 (2011)
- [3] C. Leidlmair, P. Bartl, H. Schöbel, S. Denifl, M. Probst, P. Scheier, and O. Echt, Astrophys. J. Lett. **738**, L4 (2011)
- [4] J. Cami, J. Bernard-Salas, E. Peeters, S. E. Malek, Science **329**, 1180 (2010)
- [5] C. Adamo, V. Barone, J. Chem. Phys. **110**, 6158 (1999)
- [6] J. P. Perdew, K. Burke, M. Ernzerhof, Phys. Rev. Lett. **77**, 3865 (1996)
- [7] J. P. Perdew, Y. Wang, Phys. Rev. B **33**, 8800 (1988)
- [8] C. V. Caillie, R. D. Amos, Chem. Phys. Lett. **328**, 446 (2000)

Cs–He_N Rydberg series

Florian Lackner, Günter Krois, Moritz Theisen, Markus Koch and Wolfgang E. Ernst

Institute of Experimental Physics, Graz University of Technology, Petersgasse 16, A-8010 Graz, Austria, markus.koch@tugraz.at

Single caesium (Cs) atoms located on helium nanodroplets (He_N) of several thousand helium atoms are excited into Rydberg states up to the ionization limit [1]. A two-step laser excitation through the well-defined intermediate state $6^2P_{1/2}$ is used to reach nS , nP , and nD states. Cs–He_N Rydberg excitations are resolved up to about $n = 20$. The energies are compared with those of free Cs atom Rydberg states and quantum defects as well as the on-droplet ionization threshold are derived.

Helium nanodroplet isolation spectroscopy has been developed as a powerful tool to study basic properties of single, isolated atoms, molecules, and clusters in an ultracold (0.38 K) environment [2]. Alkali-metal (Ak) atoms, which reside on the surface of the He_N, are an ideal test system and the lowest electronic transitions $n^2P_{1/2} \leftarrow n^2S_{1/2}$ and $n^2P_{3/2} \leftarrow n^2S_{1/2}$, historically known as D1 and D2 lines, respectively, are well characterized. However, relatively few experiments have investigated higher excited states of Ak–He_N complexes. For Rydberg states, where the spatial distribution of the Ak valence electron becomes comparable in size to the diameter of the droplet, the question of the structure of the Ak*–He_N system naturally arises (the * denotes an excited atom). It is known that upon photoionization Rb and Cs ions immerse into the droplet [3,4]. The formation of a system consisting of an Ak ion-core immersed into a He_N and the electron in an orbital outside represents a system of fundamental interest but is an experimental challenge (see also ref. [5]).

Experimental

He_N with an average number of about 10^4 helium atoms and a diameter of ~ 10 nm are generated by a supersonic expansion under typical nozzle conditions (5 μm diameter, 14 K temperature, 60 bar stagnation pressure) and doped by means of a resistively heated pickup cell (80°C to 100°C) loaded with Cs metal [1]. To record Rydberg series, two different spectroscopic methods are used: for lower states the excitation is monitored by laser induced fluorescence (LIF), and for higher states resonant three-photon-ionization time-of-flight (R3PI-TOF) spectroscopy is applied. Both schemes exploit the fact that Cs atoms remain on the He_N when excited into the $6^2P_{1/2}$ state [3]. This non-desorbing state is excited by laser L1 (fixed at 11197 cm^{-1}) and is used as an intermediate state for further excitations with laser L2, which is scanned across the Rydberg states. In case of the LIF scheme fluorescence light is collected from the $6^2P_{3/2} \rightarrow 6^2S_{1/2}$ (D2 line) transition. For the R3PI-TOF scheme two pulsed lasers are used. Ionization from a Rydberg state (the third step) is realized by a photon of

either laser. Ions are detected with the TOF mass spectrometer in the time window corresponding to the Cs-He_m ($m = 1-8$) masses, as a function of the laser L2 wavelength.

Results and discussion

Figure 1 shows the Cs-He_N absorption spectrum as recorded with LIF (red) and with R3PI-TOF (blue) spectroscopy.

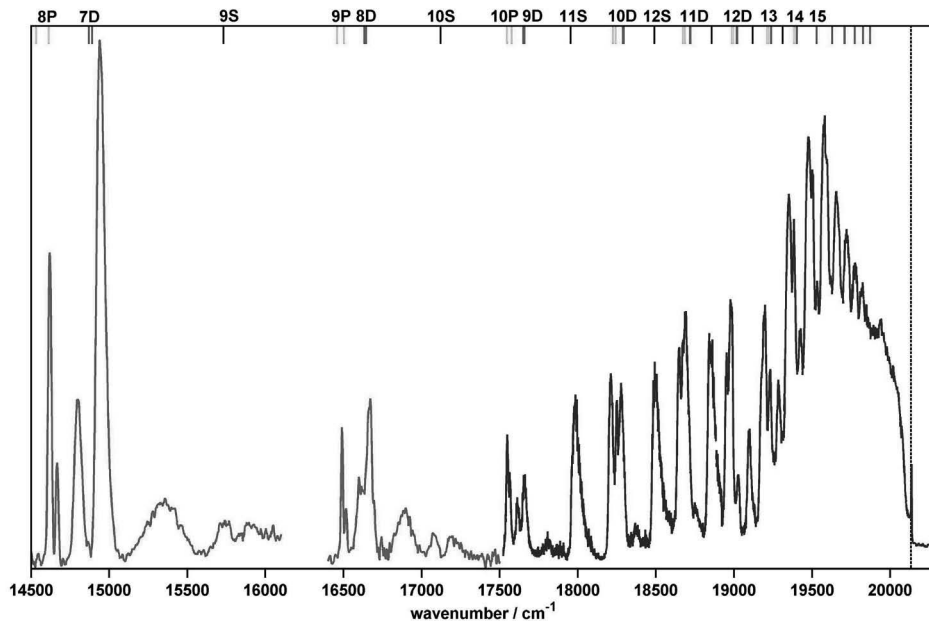


Figure 1: Absorption spectrum of Cs-He_N as function of the wavelength of L2 observed with LIF spectroscopy (red) and R3PI-TOF spectroscopy (blue). While L1 is kept at the fixed wavelength of 11197 cm^{-1} , L2 is scanned and excites Cs-He_N from the non-desorbing $6^2P_{1/2}$ intermediate state to Rydberg states. Corresponding transitions of bare Cs atoms are indicated at the top. The ionization threshold of free Cs atoms is indicated as dashed line.

The P states are split into three substates according to the pseudo-diatomic molecule model⁵: ${}^2\Pi_{1/2}$, ${}^2\Pi_{3/2}$ and ${}^2\Sigma_{1/2}$ (from lower to higher energy). The first two can be separated up to $n = 11$ where the spin-orbit interaction seems to become comparable to the perturbation by the droplet. Above $n = 12$ the $P({}^2\Sigma_{1/2})$ states merge with the D(Δ) states. For the D states spin-orbit interaction is neglected and three diatomic states are observed: Δ , Π , Σ . Spectral peaks can be resolved up to $n \sim 20$.

The spectrum in figure 1 agrees well with the pseudo-diatomic model. Note that in addition to nS and nD levels also excitations into nP levels are observed. According to the molecular electric-dipole selection rules ($\Delta\Lambda = 0, \pm 1$ and $\Delta\Omega = 0, \pm 1$) it is possible to excite from the $6^2P_{1/2}({}^2\Pi_{1/2})$ state (the intermediate state) into ${}^2\Sigma_{1/2}$, ${}^2\Pi_{1/2}$, ${}^2\Pi_{3/2}$, and ${}^2\Delta_{3/2}$ states, which is confirmed by the spectrum.

Towards the ionization limit. The spectrum presented in figure 1 allows to follow the principal quantum number dependence of the shift $\Delta\tilde{\nu}$ of individual on-droplet spectral peaks with respect to the corresponding free-atom lines. The on-droplet peaks turn out to be blue-shifted for $n \delta 10$ and red-shifted for $n \tau 10$. The energy of both the free-atom states and the on-droplet states is assumed to be given by the Rydberg formula $E_n = E_I - R_\infty / (n - d)^2$, where E_I is the ionization energy, R_∞ is the Rydberg constant, and d is the quantum defect. Thus, $\Delta\tilde{\nu}$ can be simulated as the difference of on-droplet Rydberg energies and free-atom Rydberg energies:

$$\Delta\tilde{\nu} = E_{I,dr} - \frac{R_\infty}{(n - d_{dr}(n))^2} - \left(E_{I,at} - \frac{R_\infty}{(n - d_{at}(n))^2} \right) \quad (1)$$

While $E_{I,at}$ (31406.5 cm^{-1}) and $d_{at}(n)$ for bare Cs atoms are known (see ref. [1] and refs. therein), $E_{I,dr}$ and $d_{dr}(n) = d_{at}(n) + \Delta d_{dr}$ are taken as free parameters in a non-linear least squares fit (see table 1).

The model in equation 1 fits the spectral peaks in figure 1 very well, which demonstrates the Rydberg character of the system and results in small uncertainties for the parameters. The results for the ionization energy $E_{I,dr}$ of different states of the Cs-He_N system are in excellent agreement and the average value is $E_{I,dr} = 31\,355(1) \text{ cm}^{-1}$, corresponding to a decrease of the ionization energy compared to the bare atom of $\Delta E_I = -52(1) \text{ cm}^{-1}$. A lowering of E_I is perfectly reasonable because of polarization effects and the resulting attractive interaction

⁵ In the pseudo-diatomic molecule model the He_N is treated as one atom of a diatomic molecule with the molecular axis connecting the center of the droplet with the Ak nucleus. For states with strong SO interaction Hund's case (a) seems appropriate. The standard notation is: ${}^{2S+1}\Lambda_\Omega$, where Λ is the projection of the orbital angular momentum L on the molecular axis and Ω is the projection of the total electronic angular momentum J on the molecular axis.

between the Cs^+ core and the He_N . In contrast, the differences in the droplet induced changes of the quantum defect Δd_{dr} are not surprising because of the strong mixing of configurations in highly excited states which can be assumed to be different for individual states. The decrease of Δd_{dr} , which is the case for all states, indicates that the configuration mixing at high states, after all, decreases the electron probability inside the positive core.

Table 1: Parameters for the on-droplet part parameters of equation (1), as obtained from a non-linear least squares fit to spectral peaks in figure 1.

state	$E_{1,\text{dr}} / \text{cm}^{-1}$	Δd_{dr}	d_{dr}	d_{at}
S(Σ)	31 356(2)	-0.128(5)	3.92(1)	4.049
P($\Sigma_{1/2}$)	31 355(3)	-0.114(4)	3.44(1)	3.559
P($\Pi_{1/2}$)	31 353(2)	-0.063(3)	3.53(1)	3.592
P($\Pi_{3/2}$)	31 357(3)	-0.047(3)	3.51(1)	3.559
D(Π)	31 354(7)	-0.26(1)	2.21(1)	2.476
D(Δ)	31 354(3)	-0.071(5)	2.40(1)	2.476

Our current work concentrates on the Rb– He_N system, which exhibits advantages in the energy level distribution and thus facilitates an unambiguous assignment of the D state manifold.

References

- [1] F. Lackner, G. Krois, M. Theisen, M. Koch and W. E. Ernst, Phys. Chem. Chem. Phys. **13**, 18781–18788 (2011)
- [2] C. Callegari and W. E. Ernst, *Helium Droplets as Nanocryostats for Molecular Spectroscopy—from the Vacuum Ultraviolet to the Microwave Regime*, in *Handbook of High-Resolution Spectroscopy*, eds. M. Quack and F. Merkt, John Wiley & Sons, Chichester, 2011.
- [3] M. Theisen, F. Lackner and W. E. Ernst, J. Chem. Phys. **135**, 074306-074306 (2011)
- [4] M. Theisen, F. Lackner and W. E. Ernst, Phys. Chem. Chem. Phys. **12**, 14861–14863 (2010)
- [5] E. Loginov and M. Drabbels, Phys. Rev. Lett. **106**, 083401 (2011)

Cr clusters in helium nanodroplets

Matthias Hasewend, Andreas Kautsch, Martin Raschek, Markus Koch and Wolfgang E. Ernst

Institute of Experimental Physics, Graz University of Technology, Petersgasse 16, A-8010 Graz, Austria, markus.koch@tugraz.at

A high temperature pickup source based on electron bombardment was constructed and built for the synthesis and investigation of transition metal clusters inside superfluid helium nanodroplets (He_N) [1]. With this source the aggregation of chromium (Cr) clusters inside He_N is demonstrated with mass spectrometry. The Cr- He_N complex is investigated spectroscopically by means of laser induced fluorescence (LIF) and resonant two-photon-ionization (R2PI) with mass sensitive ion detection. First preliminary spectroscopic results will be presented at the symposium.

In molecules as well as in nanoclusters the distribution of charges and of orbital and spin angular momenta may lead to observable electric and magnetic dipole moments, respectively. Magnetic nanoclusters feature significant practical promise as building blocks for novel magnetic materials. While isolated atoms of almost all elements show a non-vanishing magnetic moment (described by Hund's rule), in the solid state only very few elements preserve a magnetization, which is a consequence of electron delocalization, favouring equal population of states with antiparallel spin orientation. Thus the understanding of property change in the transition from a dense electron gas in isolated atoms to a dilute electron gas in solids is one of the main goals in cluster theory.

The unique environment of He_N provides fundamentally new opportunities to synthesize and investigate tailored clusters of atoms and molecules [2]. The applicability of He_N as host for magnetic studies of isolated particles has recently been demonstrated with the realization of electron spin resonance in single alkali-metal atoms, where very slow spin relaxation, slow dephasing and very little influence of the droplet were found [3].

Clusters of transition metals with nearly half filled shells, such as chromium (Cr) and manganese, are of particular interest due to the large number of unpaired electrons per atom and the related possibility of huge local spin polarization. Stern-Gerlach deflection experiments of Cr_n ($n = 20-133$) find superparamagnetic response and magnetic moments per atom often exceeding the moment per atom present anywhere in a bulk antiferromagnetic lattice [4].

Figure 1 demonstrates the first synthesis of Cr clusters in He_N . Shown is the most prominent region of the mass spectrum of Cr_9 (black bars) together with a simulated mass distribution (grey bars). Each of the observed masses is a result of different isotopic combinations (natural abundances: ^{50}Cr (4.3 %), ^{52}Cr (83.8 %), ^{53}Cr (9.5 %), ^{54}Cr (2.4 %)). The simulated mass distribution and the composition of each peak is described by a multinomial distribution. For example, the peak at 468 u consists of $^{52}\text{Cr}_9$ (78 %), $^{50}\text{Cr} + ^{52}\text{Cr}_6 + ^{53}\text{Cr}_2$ (13 %), $^{50}\text{Cr} + ^{52}\text{Cr}_7 + ^{54}\text{Cr}$ (8%), and other combinations (<1%). The spectrum was recorded with large He_N ($\bar{N} = 24000$) and pickup conditions optimized for multiple Cr pickup.

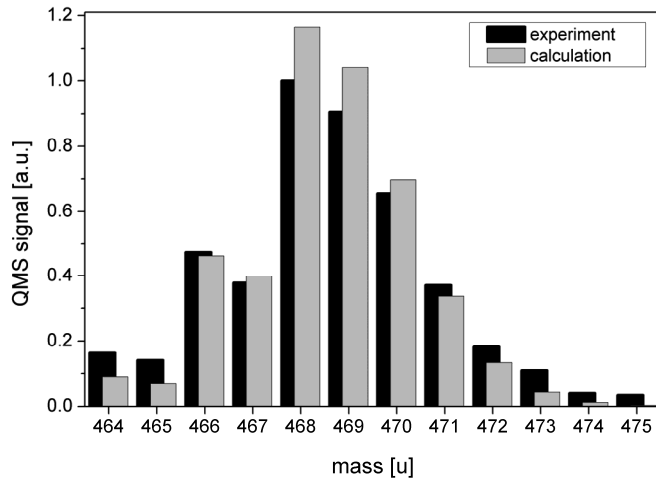


Figure 1: Mass spectrum of the most prominent region of the isotopic mixture of Cr_9 , obtained with large He_N ($\bar{N} = 24000$).

References

- [1] M. Ratschek, M. Koch, and W. E. Ernst, in preparation (2011)
- [2] C. Callegari and W. E. Ernst, *Helium Droplets as Nanocryostats for Molecular Spectroscopy—from the Vacuum Ultraviolet to the Microwave Regime*, in *Handbook of High-Resolution Spectroscopy*, eds. M. Quack and F. Merkt, John Wiley & Sons, Chichester, 2011.
- [3] M. Koch, G. Auböck, C. Callegari and W. E. Ernst, *Phys. Rev. Lett* **103**, 035302 (2009)
- [4] F.W. Payne, Wei Jiang, and L.A. Bloomfield, *Phys. Rev. Lett* **97**, 193401 (2006)

Developing new accurate *ab initio* PES for Metal Nitrosyls

B. Murali Krishna and Roberto Marquardt

Laboratoire de Chimie Quantique

Institut de Chimie UMR 7177 CNRS/ Université de Strasbourg

4 rue Blaise Pascal - CS90032 - 67081 Strasbourg cedex – France

murali.krishna@etu.unistra.fr

Abstract

The lowest singlet and triplet electronic levels of A' and A'' symmetry of the neutral copper nitrosyl (CuNO) system are calculated by *ab initio* methods. Calculations at the multi-reference configuration interaction (MRCI) level of theory using atomic bases of the valence triple-zeta type (VTZ) are proven to be necessary for accurate results, with single and double excitations from an active space involving 22 valence electrons, 13 molecular orbitals and 12 roots. The present calculations yield a singlet A ground state for CuNO with a binding energy of (2188 cm⁻¹)

Introduction

CuNO and its ion has been observed in matrix isolation[1,2], and infrared spectra in argon[3]. To get an insight into homogeneous catalysis, accurate prediction of the nature of the interaction is necessary in the gas phase[4,5].

For CuNO, the theoretical studies have not yet been able to unambiguously assign the ground state. Coupled cluster calculations with single and double excitations (CCSD) give a triplet ground state of CuNO, whereas perturbative inclusion of triple excitations (CCSD(T)) gives a singlet ground state of ¹A' symmetry[6] with an end-on bent structure and an estimated binding energy of 18.8 kcal/mol. In calculations using the density functional theory (DFT), pure density functionals assign a singlet ground state[3], while hybrid functionals favor a triplet state as the lowest electronic energy state[7, 8].

It is important to note that the aforementioned methods are essentially mono-configurational. Therefore, in the present study, a systematic investigation of calculation settings related to an accurate prediction of the electronic wave function for the ground and excited states is carried out at the multi-configurational self-consistent-field (MCSCF) and internally contracted multi-reference configuration interaction (MRCI) levels of theory, albeit restricted to single and double excitations.

Methods

The calculations on the ground and excited electronic states were performed using the MCSCF method followed by MRCI method of Werner and Knowles[9,10] as implemented in the MOLPRO[11] suite of programs. The CI orbitals were obtained by state averaged

MCSCF calculations using C_S , with equal weights for all the participating states. In the calculations, we use augmented correlation-consistent polarized n-tuple zeta basis sets aug-cc-pVTZ, (AVTZ) of Dunning and co-workers[12]. A reduced basis set obtained from the AVTZ basis by omission of the g function of Cu and f functions in N and O, called RVTZ here, also yields the relative energies with the expected accuracy (m E_h).

Results

The neutral linear system of N, O and Cu atoms

The ground state of the copper atom is 2S ($[Ar]s^1d^{10}$) and the first excited state is 2D ($[Ar]s^2d^9$). NO has a Π ground state with a calculated bond length of 115 pm at AVTZ basis and MRCI level of theory. The three dimensional configuration space may be spanned by the coordinates r_{NO} , r_{Cu} and θ_{Cu} shown in Figure 1, where r_{Cu} is the distance of the copper atom from the point at the center of the NO distance.

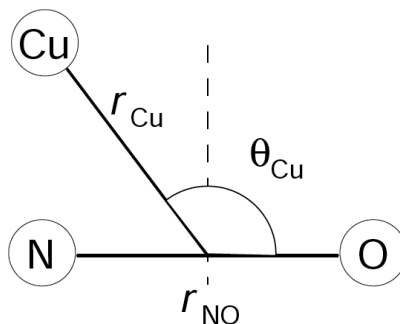


Figure 1: General coordinates for the {Cu, N, O} system; r_{NO} is the distance of the copper atom from the point bisecting r_{NO} ; $0 \leq r_{NO} \leq \infty$, $0 \leq r_{Cu} \leq \infty$, $\theta_{Cu} \leq 180$.

MCSCF calculations

In this study, we carefully chose the number of states computed in each symmetry to overcome convergence failures at the MCSCF level. An unbalanced number of roots leads to broken symmetries. Also, severe root-flipping problems occur when we fail to include all states of an electronic multiplet in the MCSCF calculations.

Clearly, Cu s and d orbitals are very close lying and one might anticipate that all these orbitals need to be included in the active space. A calculation in C_S corresponding to $6 \times ^1A'$ and $6 \times ^1A''$ and roots is very physical and comes out naturally from the symmetry species of asymptotic states of CuNO. An active space which consists of 13 orbitals, $9 \times ^1A'$ and $4 \times ^1A''$, with 22 electrons, denoted CAS (22,13), gives clean convergence.

However, MCSCF calculations with 12 roots and CAS (22,13), converge to 2S as the excited state and a degenerate 2D as the ground state with an energy difference of more than $90 mE_h$ at the asymptote. Experimentally, for Cu, the 2D lies above the 2S by about 11200 cm^{-1} . This inversion of the states at MCSCF calculation is also observed for the Cu atom alone if we include the 3d orbitals in the active space[13].

MRCI calculations

The natural orbitals obtained from the MCSCF calculation is then used to perform single and double excitations included in the MRCI from 13 orbitals as active orbitals, thereby correlating 22 electrons, i.e. a CAS (22,13). The MRCI calculations flip the states into the correct order at the asymptote. A non degenerate 1A component is the ground state. It should be noted that all the configurations giving rise to the lowest 6 states pertaining to each symmetry species are necessary to correctly calculate the ground state of the system, making the calculation truly multi-referential and highly multi-configurational.

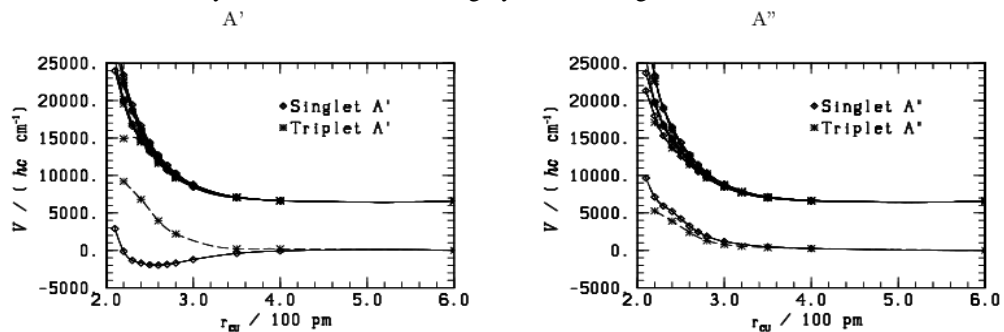


Figure 2: MRCI potential energy functions for the lowest singlet and triplet states of A' and A'' symmetry at the fixed values $\theta_{Cu}=130$ and $r_{NO}=115 \text{ pm}$.

Figure 2 shows the bound state. It also shows 5 excited states, which become degenerate at the asymptote (2D level of Cu) in the 1A , while the $6 \times ^3A'$ and $6 \times ^1A''$ and $6 \times ^3A''$, and states are essentially repulsive. The bound state structure is at about the bottom of the potential well of the lowest 1A state in Figure 2 with a binding energy of $10 mE_h$ (2188 cm^{-1}), for the CAS (22,3) with the RVTZ basis. While the present MRCI calculations confirm the order of singlet and triplet states from previous results [6], where a stable $^3A''$ is predicted to lie $11 mE_h$ higher than the 1A state, they yield larger relative triplet-singlet energies around the minima (about $23 mE_h$ here). Furthermore, they do not indicate that bound triplet states exist, contrary to what is suggested in [6].

Conclusions

In this study, we successfully optimised all the parameters to calculate the ground state of the neutral [N,O,Cu] system. It has been shown that MCSCF calculation involving 12 roots is necessary to get a clean convergence but gives asymptotically inverted states. To describe the ground state properly we use the computationally expensive MRCI calculations over 6 states per symmetry species simultaneously. Also we show by MRCI calculations, that the active space should contain the all 3d electrons of Cu to accurately describe the system. Here we use the CAS (22,13) which is close to the full valence space of the system. The bound state is an 1A state with a binding energy of 2188 cm^{-1} . These MRCI calculations using our method of calculating six states provides the lowest as well as excited states to a good accuracy for the PES which can then used to do quantum dynamical calculations on the complex.

Acknowledgment

We thank the Centre National de la Recherche Scientifique (CNRS) and the Région Alsace for funding and K.A. Peterson, V. Robert, C. Daniel and H. Schwarz for fruitful discussions.

References

- [1] Sülzle, D. and Schwarz, H. and Mookb, K. H. and Terlouw, J. K., *Int. J. Mass Spec. and Ion. Proc.*, **108**, 269 (1991).
- [2] D. W. Ball and J. A. Chiarelli, *J. Mol. Spectrosc.*, **372**, 113-125 (1996).
- [3] M. Zhou and L. Andrews, *J. Phys. Chem. A*, **104**, 2618-2625 (2000).
- [4] Bohme, D. K. and Schwarz, H., *Angew. Chem. Int. Ed.*, **44**, 2336-2354 (2005).
- [5] W. B. Tolman, *Angew. Chem. Int. Ed.*, **49**, 1018-1024 (2010).
- [6] J. Hrusak, W. Koch, and H. Schwarz, *J. Chem. Phys.*, **101**, 3898-3905 (1994).
- [7] J. L. C. Thomas, J. C. W. Bauschlicher, and M. B. Hall, *J. Phys. Chem. A*, **101**, 8530-8539 (1997).
- [8] E. L. Uzunova, *J. Phys. Chem. A*, **113**, 11266-11272 (2009).
- [9] H.-J. Werner and P. J. Knowles, *J. Chem. Phys.*, **82**, 5053 (1985).
- [10] H.-J. Werner and P. J. Knowles, *J. Chem. Phys.*, **89**, 5803 (1988).
- [11] R. D. Amos, A. Bernhardsson, A. Berning, P. Celani, D. L. Cooper, M. J. O. Deegan, A. J. Dobbyn, F. Eckert, C. Hampel, G. Hetzer, P. J. Knowles, T. Korona, R. Lindh, A. W. Lloyd, S. J. McNicholas, F. R. Manby, W. Meyer, M. E. Mura, A. Nicklass, P. Palmieri, R. Pitzer, G. Rauhut, M. Schütz, U. Schumann, H. Stoll, A. J. Stone, R. Tarroni, T. Thorsteinsson, and H.-J. Werner. Molpro, a package of ab initio programs designed by H.-J. Werner and P. J. Knowles, version 2009.1, (2009).
- [12] R. A. Kendall, T. H. Dunning Jr., and R. J. Harrison, *J. Chem. Phys.*, **96**, 6797-6806 (1992).
- [13] N. B. Balabanova and K. A. Peterson, *J. Chem. Phys.*, **125**, 074110 (2006).

Chemistry and photochemistry on mixed water/nitric acid ice nanoparticles studied in molecular beams

Jozef Lengyel^{1,2}, Viktoriya Poterya¹, Andriy Pysanenko¹ and Michal Fárník¹

¹ J. Heyrovský Institute of Physical Chemistry, Academy of Sciences of the Czech Republic, Dolejškova 3, 182 23 Prague 8, Czech Republic. jozef.lengyel@jh-inst.cas.cz, michal.farnik@jh-inst.cas.cz

² Department of Physical Chemistry, Institute of Chemical Technology, Technická 5, 166 28 Prague 6, Czech Republic

Heterogeneous chemistry and photochemistry on surfaces of polar stratospheric cloud (PSC) particles play a key role in stratospheric chemistry in the annual ozone depletion [1]. The PSCs can be composed either of mixed water/nitric acid ice particles (Type I PSCs), e.g., nitric acid trihydrate (NAT) crystals or ternary mixtures of nitric acid/ice particles with microdroplets of sulfuric acid, and pure ice nanoparticles (Type II PSCs) [1].

To mimic the stratospheric processes in our laboratory in order to gain their detailed molecular level understanding, we have recently studied a UV photochemistry of hydrogen halides (HCl, HBr, HI) on pure ice nanoparticles $(\text{H}_2\text{O})_n$, $n \approx 10^2$ - 10^3 , in molecular beam experiment. [2-7]. The next step in our studies is to investigate the $(\text{HNO}_3)_m \cdot (\text{H}_2\text{O})_n$ clusters, and subsequently the photochemistry of hydrogen halide molecules deposited on these mixed nanoparticles.

Recently, Gomez *et al.* have presented theoretical calculations at the B3LYP/aug-cc-pVQZ level [8,9] and interpreted a thermodynamical stability of small mixed $\text{H}_2\text{O}/\text{HNO}_3/\text{HCl}$ clusters by calculation of the estimated Gibbs free energy values. They found 15 stable species and predicted that these clusters can form aggregates with atmospheric implications. These ternary systems have not yet been experimentally studied.

So far only formation of binary $(\text{HNO}_3)_m \cdot (\text{H}_2\text{O})_n$ complexes was studied experimentally. Kay *et al.* made one of the first relevant experimental study about formation and solvation of mixed $(\text{HNO}_3)_m \cdot (\text{H}_2\text{O})_n$ clusters [10]. They investigated nitric acid dissociation in water clusters by jet expansion coupled to mass spectrometry. The question of HNO_3 acidic dissociation in small water clusters was addressed in their studies with the result that at least $n=5$ water molecules are necessary to complete the ion-pair formation. The same group also studied the reaction of HNO_3 with protonated water clusters in a fast-flow reactor operated over wide temperature range [11]. Consistently with the previous study it was shown that at low temperatures the incorporation of HNO_3 occurs only for clusters exceeding a specific size leading to $\text{D}^+ \cdot (\text{D}_2\text{O})_n \cdot \text{DNO}_3$ ($n \geq 5$). Further nitric acid molecule can be incorporated only into water clusters having a considerably higher degree of solvation.

The photodissociation of HNO_3 has been studied as a bare molecule [12] and in clusters [13].

Ion-pair formation in mixed $(\text{HNO}_3)_m \cdot (\text{H}_2\text{O})_n$ clusters

In our experiment the $(\text{HNO}_3)_m \cdot (\text{H}_2\text{O})_n$ clusters are prepared by supersonic expansion through a conical nozzle into the vacuum. The mixed water/nitric acid clusters are prepared from a solution of concentrated nitric acid in water and it is heated inside a reservoir in temperature range of 298-373 K. The resulting vapor is mixed with helium or argon as carrier gases, with stagnation pressures ranging from 1 to 3 bar. The clusters are ionized by electrons and the fragment mass spectra are recorded by quadrupole mass spectrometer. In the photodissociation experiment the clusters are interrogated by UV lasers (193 nm and 243 nm) and charged fragments are detected by TOF techniques. Further details of the apparatus can be found elsewhere, e.g., in Ref. [14].

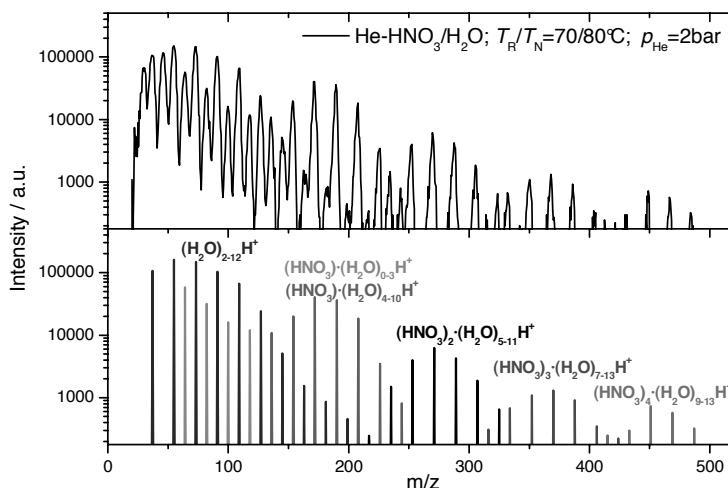


Figure 1: Mass spectrum of clusters produced in expansion of $\text{HNO}_3/\text{H}_2\text{O}$ in He-carrier gas at 2 bar stagnation pressure: the measured spectrum (top) and its analysis (bottom)

Typical mass spectrum of these clusters with helium as a carrier gas is shown in figure 1. Several groups of mass peaks can be identified in the spectrum: Protonated water clusters $(\text{H}_2\text{O})_k\text{H}^+$ (blue) decrease in intensity exponentially with the size k . The group of cluster $\text{HNO}_3 \cdot (\text{H}_2\text{O})_n\text{H}^+$ fragments decreases first to $n=4$ (orange) followed by an increase with a maximum intensity for $n=6$ (red). This dependence was interpreted as due to the onset of the acidic dissociation in the neutral clusters. Further groups of fragments with more than one HNO_3 molecule occur at higher masses. It indicates that the next molecule can be incorporated in the cluster when there are enough water molecules to acidically dissolve the previous molecule(s) and solvate the ion pairs. These observations are in general agreement with the previous experiments of Castleman's group with $\text{DNO}_3/\text{D}_2\text{O}$ [10,11].

Photochemistry of mixed $(\text{HNO}_3)_m \cdot (\text{H}_2\text{O})_n$ clusters

Next, we investigate the photolysis of HNO_3 molecules in the clusters. In our previous studies with water clusters doped with hydrogen halides [2-6] we have observed that the acidic dissociation led to a generation of a charge-transfer-to-solvent state (CTTS) after the photoexcitation and subsequently to an H_3O radical generation and substantial enhancement of H-fragment signal from the H_3O dissociation. Similar mechanism has been sought for in the $\text{HNO}_3/\text{H}_2\text{O}$ system. However, very little H-fragment signal has been observed in the current experiment. In addition the kinetic energy distribution of the measured H-fragments exceeds to significantly higher energies than our previously measured spectra from H_3O .

Thus we conclude that in the $\text{HNO}_3/\text{H}_2\text{O}$ system despite the acidic dissociation in the ground state either the CTTS state is not reached by the photoexcitation at 193 nm (6.4 eV) or the photodissociation mechanism is different from the $\text{HX}/\text{H}_2\text{O}$ system.

The hydrogen is not one of the major fragments in the HNO_3 photodissociation. We also observed nonresonantly multiphoton ionized NO fragment in our photodissociation experiment and measure their kinetic energy distributions. It corresponds to a statistical distribution, and based on this we propose that the photodynamics of an excited HNO_3 molecule in the clusters leads to quenching into the ground state and subsequent statistical decay, Fig. 2.

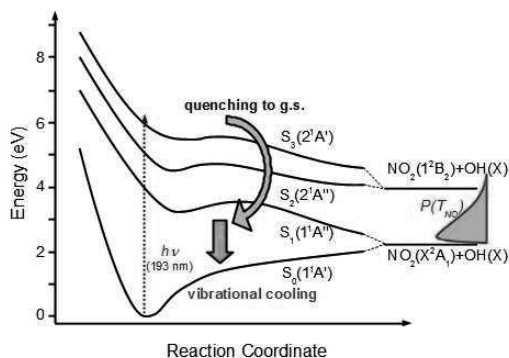


Figure 2: Schematic picture of the quenching mechanism and statistical decay of HNO_3 in clusters after the photoexcitation.

Acknowledgement: This work has been supported by the Grant Agency of the Czech Republic Project Nos. 203/09/0422 and P208/11/0161

References

- [1] S. Solomon, *Rev. Geophys.* **37**, 275 (1999).
- [2] V. Poterya, M. Fárník, P. Slavíček, U. Buck, V. V. Kresin, *J. Chem. Phys.* **127**, 071101 (2007).
- [3] V. Poterya, J. Fedor, A. Pysanenko, O. Tkáč, J. Lengyel, M. Ončák, P. Slavíček, M. Fárník, *Phys. Chem. Chem. Phys.* **13**, 2250 (2011).
- [4] M. Fárník, U. Buck, *Phys. Scr.* **76**, 73 (2007).
- [5] M. Ončák, P. Slavíček, V. Poterya, M. Fárník, U. Buck, *J. Phys. Chem. A* **112**, 5344 (2008).
- [6] M. Ončák, P. Slavíček, M. Fárník, U. Buck, *J. Phys. Chem. A* **115**, 6155 (2011).
- [7] V. Poterya, M. Fárník, M. Ončák, P. Slavíček, *Phys. Chem. Chem. Phys.* **10**, 4835 (2008).
- [8] P. C. Gómez, O. Gálvez, R. G. Mosteo, C. Puzzarini, R. Escribano, *Phys. Chem. Chem. Phys.* **12**, 4617 (2010).
- [9] P. C. Gómez, O. Gálvez, R. Escribano, *Phys. Chem. Chem. Phys.* **11**, 9710 (2009).
- [10] B. D. Kay, V. Hermann, A. W. Castleman Jr., *Chem. Phys. Lett.* **80**, 469 (1981).
- [11] X. Zhang, E. L. Mereand, A. W. Castleman Jr., *J. Phys. Chem.* **98**, 3554 (1994).
- [12] J. R. Huber, *ChemPhysChem* **5**, 1663 (2004).
- [13] Q. Li, J. R. Huber, *Chem. Phys. Lett.* **345**, 415 (2001).
- [14] M. Fárník, *Molecular Dynamics in Free Clusters and Nanoparticles Studied in Molecular Beams*, ICT Prague Press, Institute of Chemical Technology, Prague, (2011).

The solvated electron alias H_3O radical: Photochemistry on ice nanoparticles:

Jozef Lengyel^{1,2}, Viktoriya Poterya¹, Andriy Pysanenko¹, Milan Ončák², Petr Slaviček^{1,2} and Michal Fárník¹

¹*J. Heyrovský Institute of Physical Chemistry, Academy of Sciences of the Czech Republic, Dolejškova 3, 182 23 Prague 8, Czech Republic, michal.farnik@jh-inst.cas.cz*

²*Department of Physical Chemistry, Institute of Chemical Technology, Technická 5, 166 28 Prague 6, Czech Republic*

In this contribution we present our recent molecular beam investigations of large water clusters $(\text{H}_2\text{O})_n$, $n \approx 10^2$ - 10^3 (ice nanoparticles) and water clusters with embedded hydrogen halide molecules $\text{HX} \cdot (\text{H}_2\text{O})_n$ ($X = \text{Cl}, \text{Br}, \text{I}$). It has been suggested in recent theoretical calculations [1,2] that the neutral H_3O radical molecule represents the cluster model for solvated electron, from the point of view of its electronic wavefunction. We provide an experimental evidence for the H_3O generation in ice nanoparticles upon UV-light excitation. Our experiments are supported and interpreted by state-of-the-art theoretical calculations.

In our laboratory large water clusters composed of several hundreds of water molecules -ice nanoparticles- are investigated in molecular beams in vacuum. In a typical experiment we dope the ice nanoparticles with foreign molecules and interrogate them with UV lasers investigating the photochemistry of these species. Such processes can mimic the chemistry in the upper atmosphere or outer space.

Hydronium radical

The very first experimental confirmation of the generation of the H_3O species has been provided by our laboratory [3]. In this study we confirmed that the acidic dissociation of HBr molecules takes place on ice nanoparticles and the contact ion pair is generated in the ground state. The zwitterionic system $\text{H}_3\text{O}^+ \cdot \text{Br}^- \cdot (\text{H}_2\text{O})_n$ is excited by the UV radiation into a charge-transfer-to-solvent (CTTS) state, from which transition into a biradical state occurs (Fig. 1). During the CTTS step, the electron is transferred from the halide anion to the protonated solvent, the proton and the electron mutually neutralize and hydronium radical H_3O is formed. This rather general mechanism has been confirmed in a series of experimental and theoretical studies for various hydrogen halides [4-7]. Besides, we have provided an experimental evidence for the H_3O generation in excited pure water clusters [8].

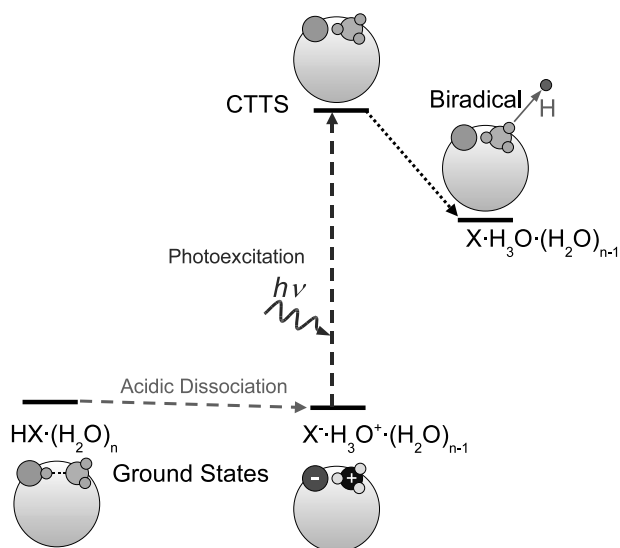


Figure 1: Schematic mechanism of H₃O radical generation and subsequent dissociation in hydrogen halide doped water clusters.

Solvated electron

Recently it has been suggested that a direct dissociative electron attachment (DEA) to freon molecules (CFC) on PSC particles can lead to the generation of Cl· radicals [9]. In this process the so called solvated (hydrated, aqueous) electrons e_{aq}^- are proposed to play the essential role.

As mentioned above, it has been suggested [1,2] that the neutral H₃O radical molecule represents the cluster model for the solvated electron. Thus the first step in the chemistry involving aqueous electrons e_{aq}^- can be now mimicked in our experiments. Further studies will involve doping the ice nanoparticles with the solvated electrons with other molecules present in the space and investigating their chemistry and photochemistry with the participation of e_{aq}^- , e.g., reactions such as dissociative electron transfer (DET) illustrated in Fig. 2 can be studied.

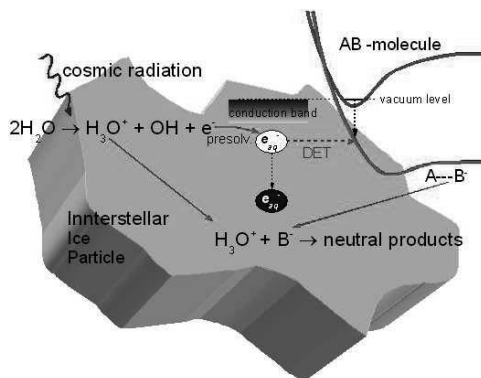


Figure 2: Schematic illustration of a possible solvated electron initiated dissociative electron transfer (DET) on ice nanoparticles.

Acknowledgement: This work has been supported by the Grant Agency of the Czech Republic Project Nos. 203/09/0422 and P208/11/0161

References

- [1] A. L. Sobolewski, W. Domcke, *J. Phys. Chem. A* **107**, 1557 (2003).
- [2] W. Domcke, A. L. Sobolewski, *Phys. Chem. Chem. Phys.* **9**, 3818 (2007).
- [3] V. Poterya, M. Fárník, P. Slavíček, U. Buck, V. Kresin, *J. Chem. Phys.* **126**, 071101 (2007).
- [4] M. Fárník, U. Buck, *Phys. Scr.* **76**, 73 (2007).
- [5] M. Ončák, P. Slavíček, V. Poterya, M. Fárník, U. Buck, *J. Phys. Chem. A* **112**, 5344 (2008).
- [6] V. Poterya, J. Fedor, A. Pysanenko, O. Tkáč, J. Lengyel, M. Ončák, P. Slavíček, M. Fárník, *Phys. Chem. Chem. Phys.* **13**, 2250 (2011).
- [7] M. Ončák, P. Slavíček, M. Fárník, U. Buck, *J. Phys. Chem. A* **115**, 6155 (2011).
- [8] V. Poterya, M. Fárník, M. Ončák, P. Slavíček, *Phys. Chem. Chem. Phys.* **10**, 4835 (2008).
- [9] Q.-B. Lu, L. Sanche, *Phys. Rev. Lett.* **87**, 078501 (2001).

Quantum Simulations of Helium Clusters with Open Shell and Ionic Dopants

J. Jiang, M. Lewerenz, and M. Mladenović

*Laboratoire MSME, UMR 8208 CNRS, Université Paris Est (Marne la Vallée),
5, Blvd. Descartes, 77454 Marne la Vallée Cedex 2, France*

Introduction

Many experiments on pure and doped helium clusters result in the production of a broad distribution of charged fragment ions after electron impact or laser ionisation. These ion yield distributions occasionally exhibit distinct stability patterns. We use the diffusion quantum Monte Carlo technique to study these stability patterns and structural features of helium clusters with open shell atomic and molecular dopants, which can also arise from photodissociation processes. Spectroscopic experiments have shown that the controlled assembly of unusual intermolecular arrangements and of reactive complexes is possible inside liquid helium droplets [1]. Reactive processes leading to light emission [2] have been observed and more recently photodissociation experiments have been carried out which indicate interesting pathways for energy dissipation and caging [3]. The latter experiments addressed in particular the photodissociation of CH_3I which is extremely well studied in the gas phase. Simulations of these processes require a powerful many body quantum method for the treatment of nuclear motion and reliable many-body potentials which we construct from high level ab initio CCSD(T) calculations for several electronic states mixed by spin-orbit coupling and including non-additive interactions arising from induction. For small clusters numerically exact calculations of rovibrational properties are used to establish the quality of our potential surfaces.

Photofragments

We present steps towards the modelling of the photodissociation $\text{CH}_3\text{I} \rightarrow \text{CH}_3 + \text{I}$ inside helium droplets which are part of the ANR project DYNHELIUM. Potential energy curves have been calculated for several electronic states of $\text{I}^q\text{-He}$, $q=-1,0,+1,+2$ with the CCSD(T) method and effective core potentials and are used for the construction of many body models for mixed clusters of the type $\text{I}^q\text{@He}_n$ which have been observed as photofragments ($q=0$) and in electron impact ionisation experiments ($q=-1,+1,+2$). The potential models include non additive induction effects and spin-orbit mixing.

Stability patterns computed with the diffusion quantum Monte Carlo technique indicate the existence of soft shells for $q=-1,0$ and a pronounced shell closure at $n=16$ for $q=+2$ in excellent agreement with recent experiments. Angular distribution functions indicate that in

spite of sharp density maxima these shells are not solid. The accuracy of our many body potential model is illustrated by calculations for the experimentally well known Ar^+He_n clusters.

Three-dimensional potential energy surfaces for the weak van der Waals interaction between a helium atom and a CH_3 radical in several geometries ranging from planar to pyramidal have been computed by RCCSD(T) calculations with large diffuse basis sets and fitted to a compact analytical form which reproduces all ab initio interaction energies with in 0.05 cm^{-1} . The assembly of these building blocks for a global potential energy function will eventually allow dynamical studies of fragmentation and product size and energy distributions.

Open shell molecular ions

We present first results for CO^+ ions in helium clusters. He-CO^+ is an interesting astrophysical collision system but its interest for helium cluster studies is the similarity of the CO^+ rotational constant with the one of neutral CO. Our present understanding of rotation inside helium clusters relies on studies of molecules where changing the molecule implies changing dynamical parameters and the interaction potential. The CO/CO^+ case allows to study the specific effect of changing only the interaction energy. $\text{CO}^+@\text{He}_n$ should be relatively easy to make by cluster ionisation or aggregation in ion drift tubes and its strong dipole and vibrational transition moment make it an easy target for high resolution spectroscopy. We have computed accurate ab initio surfaces for the two lowest electronic states of He-CO^+ to predict rovibrational spectroscopic and collisional properties. A many-body model using these surfaces is used to study larger CO^+He_n clusters.

References

- [1] J.M. Merritt, J. Küpper, and R.E. Miller, *Phys. Chem. Chem. Phys.* **7**, 67-78 (2005);
J.M. Merritt, S. Rudić and R.E. Miller, *J. Chem. Phys.* **124**, 084301 (2006);
M.Y. Choi, G.E. Douberly, T.M. Falconer, W.K. Lewis, C.M. Lindsay, J.M. Merritt,
P.L. Stiles and R.E. Miller, *Int. Rev. Phys. Chem.* **25**, 15-75 (2006)
- [2] E. Lugovoj, J.P. Toennies and A.F. Vilesov, *J. Chem. Phys.* **112**, 8217-8220 (2000),
see also Contribution by Gaveau et al.
- [3] A. Braun and M. Drabbels, *Phys. Rev. Lett.* **93**, 253401 (2004);
J. Chem. Phys. **127**, 114303 (2007); *J. Chem. Phys.* **127**, 114304 (2007);
J. Chem. Phys. **127**, 114305 (2007)

Advanced modelling of He droplets

Andreas Mauracher^{1,2}, Kersti Hermansson² and Daniel Spångberg²

¹ *Institute of Ion Physics and Applied Physics, Leopold-Franzens-University Innsbruck, Technikerstr. 25/3, A-6020 Innsbruck, Austria, andreas.mauracher@uibk.ac.at*

² *Department of Materials Chemistry, The Ångström Laboratory, Lägerhyddsvägen 1, SE-751 21 Uppsala, Sweden*

The theoretical work presented at the SASP 2012 was inspired by different experimental studies carried out by the group of Paul Scheier [1,2]. Although a lot of information can be obtained from the experimental data, some important features cannot be derived, e.g. the arrangement of the Helium atoms around the ions. We will show the characteristic steps to carry out MD simulations capable of describing the weak bonds, which are involved in Helium-Helium interactions.

In the first step of the project the interaction of Helium atoms with small atomic and molecular systems is studied using quantum mechanical electronic structure (ab initio) methods. These calculations are performed using different levels of theory and large basis sets – additionally corrected for the basis set superposition error – of different accuracy to determine the level required for a reliable description of small gas phase clusters containing these ions, as well as one to several Helium atoms. The interaction of Helium atoms with ions is very weak and therefore it is essential to use a method that can reliably compute these weak bonds. In the second step the derived level of theory and basis set are used to calculate potential energy surfaces for different systems. The third step is the derivation of an advanced state-of-the-art many-body force-field for the Helium-solvated systems. In the fourth step the functions fitted in step 3 are used in MD simulations of the solvation of the molecules in small liquid Helium droplets.

First, classical MD simulations are performed to acquire a general understanding of how the Helium atoms want to coordinate. Secondly, since the Helium atoms are very light, and the temperatures used in the experiment are very low, quantum mechanical motion (delocalization) of the nuclei is an important effect to incorporate. For this reason, the method of PIMD is used to study the preferred solvation of the molecular ions by Helium. A representative system and the obtained results from the simulations will be presented at the meeting. We compare quantities derived from MD and PIMD, such as radial distribution function but also number of helium atoms in first and second solvation shells, to experimental data to judge the quality of the methods employed in this work.

Acknowledgement

This project is funded by the Austrian Research Fund (FWF, Vienna) via an Erwin-Schrödinger-abroad fellowship (J 2973-N20), and supported by the Swedish Research Council.

References

- [1] S Denifl *et al*, *J. Am. Chem. Soc.* 15/**130** 5065 (2008)
- [2] A Mauracher *et al*, *SA Phys. Chem. Chem. Phys.* 37/**11** 8240 (2009)

Three-level system depletion spectroscopy by absorption with cavity ringdown

Fabio J. Mazzotti, Ranjini Raghunandan, Aaseef M. Esmail , Lizandra Barrios

University of Basel, KlingelbergStrasse 80, CH-4055 Basel

Theoretical quantitative considerations as well as experimental data are presented for a technique based on absorption depletion spectroscopy coupled with cavity ringdown spectroscopy. The evolution of the radiative losses inside the cavity is determined by solving the coupled rate equations by numerical integration. Optical effects taken into account are the photons involved in absorption, cavity losses (mirror reflectivity) as well as stimulated emission. The principle is based on monitoring a transition by cavity ringdown spectroscopy while a second transition (bearing a state in common) is being resonantly excited by the decaying radiation trapped inside a collinear ringdown optical cavity. A numerical example is given with atomic lines of Neon by plotting atomic level densities and radiation intensity decaying curves. The effect of translational velocity of the jet modifying the rate equations was further added in the model. An experiment on resonant atomic transitions in a supersonic expansion discharge is carried out in one of the three-level schemes in order to demonstrate the feasibility of the technique.

Inversion tunneling in normal and substituted anilines from infrared spectroscopy and quasiadiabatic channel reaction path Hamiltonian calculations.

Eduard Miloglyadov, Robert Prentner, Georg Seyfang, Martin Quack

Physical Chemistry, ETH Zurich, CH-8093 Zurich, Switzerland, miloglyadov@ir.phys.chem.ethz.ch

We report the spectra and assignment of the NH-stretching modes up to the second overtone in the room temperature FTIR spectra of ortho-C₆H₄FNHD and C₆F₅NHD as well as the direct measurement of ground state tunneling splittings in the both molecules. The decrease of the tunneling splitting in ortho-C₆H₄FNHD and C₆F₅NHD with higher NH-stretching excitation demonstrates the inhibiting nature of the NH-stretching mode in these substituted anilines. Results of theoretical investigations on the basis of DFT calculations with B3LYP/6-31G** and the quasi-adiabatic channel Reaction Path Hamiltonian (RPH) model showed a good agreement with the experimental results.

Introduction

The inversion of the NH₂ group in aniline over the plane of the phenyl ring is a prototypical example of tunneling dynamics. An early determination led to a barrier for the tunneling process of about 450 cm⁻¹ [1]. The tunneling process through the barrier splits the ground state and also many vibrationally excited states into two tunneling components. The dependence of the inversion tunneling process upon the excitation of other vibrational modes was approximately treated using the quasi adiabatic channel Reaction Path Hamiltonian (RPH)[2] and is strongly mode specific. Room temperature FTIR spectroscopy and supersonic jet ISOS spectroscopy [5] have been used in our group to investigate the dependence of the tunneling process on the NH-stretching excitation of the normal and deuterium substituted anilines, showing the NH-stretching to be an inhibiting mode [2,3,4,5,6]. In our current work we extended the investigations to the fluorinated NHD-anilines. We report the results of the measurement and assignment of the NH stretching states and corresponding tunneling splittings from the ground state up to the second overtone (N=3). Our investigation shows that the inhibiting behavior of the NH-stretching mode persists in fluorinated anilines.

Reaction path Hamiltonian approach for the inversion tunnelling in aniline

Tunneling splittings were calculated using the quasi-adiabatic channel Reaction Path Hamiltonian [2]. Therefore it was necessary to calculate the electronic potential along the inversion angle, which was done by freezing the inversion angle and optimizing the structure along all other coordinates (clamped coordinate approach). The energy, structure and frequencies were calculated at each point of the inversion angle with Gaussian09 using the B3LYP density functional with a 6-31G** basis set. In the RPH approximation the full dimensional problem is approximated by effective one-dimensional potential functions, which result from coupling of the inversion mode adiabatically to the remaining 3N-7 vibrational modes. The resulting one dimensional Schrödinger equation can then be solved on a equidistant grid to yield vibrational frequencies and tunneling splittings.

Inhibition of stereomutation tunneling by NH-stretching excitation in normal, pentafluoro- and orthofluoro- anilines-NHD

Experimental setup

Spectra in the range of 2000-11000 cm^{-1} have been recorded on BOMEM DA-002 Fourier transform spectrometer. The system has a maximum mirror displacement of 1.25 m and correspondingly an instrument function with a best unapodized resolution of 0.0024 cm^{-1} . All spectra were measured using a tungsten lamp or globar as a light source and a multipass White-type cell with 20 passes corresponding to the absorption path length of about 35 m. To cover the range of 2000-12000 cm^{-1} different combinations of beam splitters and detectors were used. For the range of the fundamental and first overtone in the range of 2000-8000 cm^{-1} , a CaF_2 beam splitter together with an InSb detector was used. To record the range of 8000-11000 cm^{-1} for the second overtone measurements a fused silica beam splitter was used in conjunction with an InSb cold window detector and a germanium detector. For the measurements of the transition between lower tunneling components in the far infrared a 25 μ and 50 μ Mylar films as the beamsplitters, a mercury lamp as a light source and a bolometer have been used. To extract the spectra of the partially deuterated species the spectra of penta- and orthofluoroaniline with different degree of deuteration have been measured. The instrumental resolution was varied between 0.1 and 0.5 cm^{-1} .

Results and discussion

Assignments of the measured NH-stretching fundamental, first and second overtone bands of NH stretching vibration, as well as corresponding tunneling splittings in the ortho- C_6H_4FNHD and C_6F_5NHD anilines and the results of the theoretical calculations for both molecules are summarized in the Table 1. The calculated adiabatic channel barrier height for the inversion is about 443.5 cm^{-1} in C_6H_4FNHD and 382.3 cm^{-1} in C_6F_5NHD .

Assignment	C_6H_4FNHD						C_6F_5NHD			
	Experiment		DFT+RPH				Experiment		DFT+RPH	
	$\tilde{\nu}$ cm^{-1}	$\Delta\tilde{\nu}$ cm^{-1}	$\tilde{\nu}_a$ cm^{-1}	$\Delta\tilde{\nu}$ cm^{-1}	$\tilde{\nu}_b$ cm^{-1}	$\Delta\tilde{\nu}$ cm^{-1}	$\tilde{\nu}$ cm^{-1}	$\Delta\tilde{\nu}$ cm^{-1}	$\tilde{\nu}$ cm^{-1}	$\Delta\tilde{\nu}$ cm^{-1}
Ground state	0	33.3	0	35.1	0	22.5	0	42.3(2)	0	41.3
ν_{NH} (u,u)	3459.7	20.9		21.0		11.9	3468.5	31(2)		24.7
ν_{NH} (l,l)	3472.1		3667.1		3646.1		3480		3669.3	
$2\nu_{NH}$ (u,u)	6768	12.3		11.9		5.8	6786.4	20.1		13.8
$2\nu_{NH}$ (l,l)	6789		7320.6		7277.6		6808.6		7324.0	
$3\nu_{NH}$ (u,u)	9937	-		6.5		2.8	9950.3	10.6		7.3
$3\nu_{NH}$ (l,l)			10961.9		10897.6		9982.0		10964.8	

Table 1. Assignment of NH-stretching fundamental and overtone bands of ortho- C_6H_4FNHD and C_6F_5NHD aniline. The transition wavenumber $\tilde{\nu}$ connects the upper, upper (u, u) and lower, lower (l, l) inversion sublevels. $\tilde{\nu}_a$ and $\tilde{\nu}_b$ are the transition wavenumbers of two isotopomers of the ortho- C_6H_4FNHD with different positions of the D (or H) atom with respect to fluorine ($\tilde{\nu}_a$ for H adjacent). $\Delta\tilde{\nu}$ is the inversion splitting of the vibrational state

A comparison of the experimental and theoretical data for the tunneling splitting shows good agreement for the ortho-fluoroaniline-NHD, but larger difference between the theoretical and experimental values of tunneling splitting for the NH-stretching modes of the pentafluoroaniline-NHD. One of the reasons for the this larger difference may be the overestimation of the experimental values of the tunneling splitting for the vibrational states due to the strong congestion of the room temperature spectra by the hot bands. These data require additional justification by measurements in a molecular beam which are currently planned and in progress. Another point for the discussion is related to two isotopomers of the ortho- C_6H_4FNHD with different positions of the D (or H) atom with respect to fluorine. Both isotopomers have the same potential energy surface in the limit of the Born-Oppenheimer

approximation, but relying on the RPH calculation they have different tunneling splittings due to difference in the zero point energy corrections. The direct observation of the first tunneling transition revealed only a transition at 33.3 cm^{-1} , another possible transition was out of the spectral range of the measurements. While the quasiharmonic theoretical calculations are still preliminary, the present results confirm the general character of the inhibiting behavior of the NH-stretching mode in anilines that has been first demonstrated in normal aniline [4,5,6].

Acknowledgements. Our work is financially supported by ETH Zürich and the Schweizerischer Nationalfonds. We thank Michael Hippler and Andreas Schneider for help and discussions and Reto Ulrich and Guido Grassi for the synthesis of the $\text{C}_6\text{F}_5\text{ND}_2$ and $\text{C}_6\text{H}_4\text{FND}_2$.

References

- [1] M. Quack, M. Stockburger, *J. Mol. Spectrosc.*, **43**, 87 (1972)
- [2] B. Fehrensen, D. Luckhaus, M. Quack, *Z. Phys. Chem.*, **209**, 1 (1999);
B. Fehrensen, D. Luckhaus, M. Quack, *Chem. Phys.*, **338**, 90 (2007)
- [3] B. Fehrensen, M. Hippler, M. Quack, *Chem. Phys. Lett.*, **298**, 320 (1998)
- [4] E. Miloglyadov, A. Kulik, M. Quack and G. Seyfang (2010) *Contributions of the 17th Symposium on Atomic, Cluster and Surface Physics 2010* (SASP 2010), ISBN 978-3-902719-52-2, Milewski, I., Kendl, A., Scheier, P. (eds), Innsbruck University Press (IUP), Innsbruck, 216
- [5] M. Hippler, E. Miloglyadov, M. Quack, G. Seyfang, in *Handbook of High Resolution Spectroscopy*, Vol. 2, p. 1069-1118, M. Quack and F. Merkt (eds), Wiley, Chichester, 2011
- [6] B. Fehrensen, "Infrarotspektroskopie und Quantendynamik der Stereomutation von Anilin und H_2O_2 und ihren Isotopomeren", Ph.D. thesis, ETH Zurich (1999)

Low Energy Ion Surface Irradiation Experiment

Elena-Andra Muntean, Tom Field and Bob McCullough

Queen's University Belfast, School of Mathematics and Physics, Centre for Plasma Physics

Email: emuntean01@qub.ac.uk, N. Ireland, UK

The space between the stars is not empty but filled with a very diffuse gas with extremely low densities and temperatures, which is a unique laboratory with conditions not normally encountered on Earth. A new ion irradiation experiment is being developed at QUB to investigate irradiation of astrophysical ice analogues formed on a cooled substrate surface at temperatures down to 10 K. Preliminary experiments have been performed to investigate ion irradiation of a titanium surface.

Beams of H_2^+ , D_2^+ , C^+ and O^+ from a 10 Ghz permanent magnet ECR ion source were directed onto a Ti surface at 22.5 deg and 45 deg with respect to the normal of the target surface. A quadrupole mass spectrometer capable of detecting neutral, positive and negative species desorbed or sputtered from the surface was positioned with its entrance 30mm the impact point of the ion beam on the target. Negative ions from the surface were directed into the quadrupole by applying a negative bias of 27V to the target. The mass spectra show that the principle ion formed in all cases was H^- and in the case of D_2^+ any D^- signal was below the noise level. This suggests that the negative ion observed were from atoms and molecules already on the titanium surface and were formed by sputtering.

The H^- observed in this experiment were produced by sputtering and not formed directly from atoms in the primary ion beam. The H^- yield observed is well modeled by a simple theoretical sputtering equation. The sputtered H^- yield showed a linear dependence with incident H_2^+ ion beam intensity as is expected for this process. It may be that any H^- formed directly from H_2^+ had too much kinetic energy to be detected in the quadrupole mass spectrometer.

Spin and orbital moments of isolated clusters – synchrotron radiation elucidates nanomagnetism

Sergey Peredkov ^a, Matthias Neeb ^b, Wolfgang Eberhardt ^b, Jennifer Meyer ^c,
Matthias Tombers ^c, Heinrich Kampschulte ^c, and Gereon Niedner-Schatteburg ^c

^a Technische Universität Berlin, Institut für Optik und Atomare Physik, Hardenbergstr. 36, 10623 Berlin, Germany; ^b Helmholtz-Zentrum Berlin für Materialien & Energie, BESSY II, Albert-Einstein-Str. 15, 12489 Berlin, Germany; ^c Fachbereich Chemie und Forschungszentrum OPTIMAS, Technische Universität Kaiserslautern, 67663 Kaiserslautern, Germany

The determination of spin and orbital magnetic moments from the free atom to the bulk phase is an intriguing challenge for nano science, in particular since most magnetic recording materials are based on nanostructures. We present temperature-dependent X-ray magnetic circular dichroism (XMCD) spectra of isolated transition metal clusters as obtained by virtue of the novel GAMBIT setup [1] at the synchrotron radiation source BESSY II.

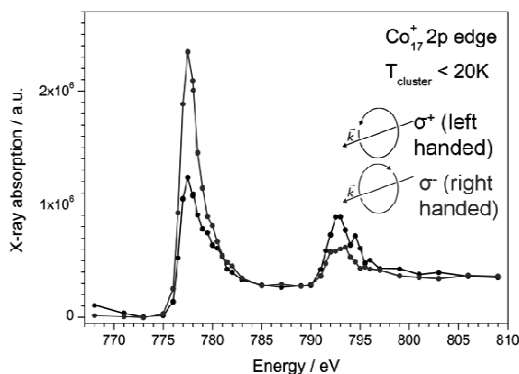


Figure 1: XMCD spectrum of size selected and isolated Cobalt cluster cations ($n=17$)

In particular, we apply so called sum rule analysis and thereby deduce the intrinsic spin and orbital magnetic moments of the non-interacting magnetic nanoparticles, such as e.g. free clusters of Iron, of Cobalt [2], and of Nickel. An exceptionally strong, element specific, enhancement of the orbital moment is verified for free magnetic clusters which is up to 4 times larger than the bulk value. Our temperature-dependent measurements reveal that the spin orientation along the external magnetic field is nearly saturated at ~ 20 K and 7 T while the orbital orientation is clearly not.

Total magnetic moments as deduced from our XMCD data might also help to reconcile divergent results as obtained from Stern-Gerlach experiments published earlier.

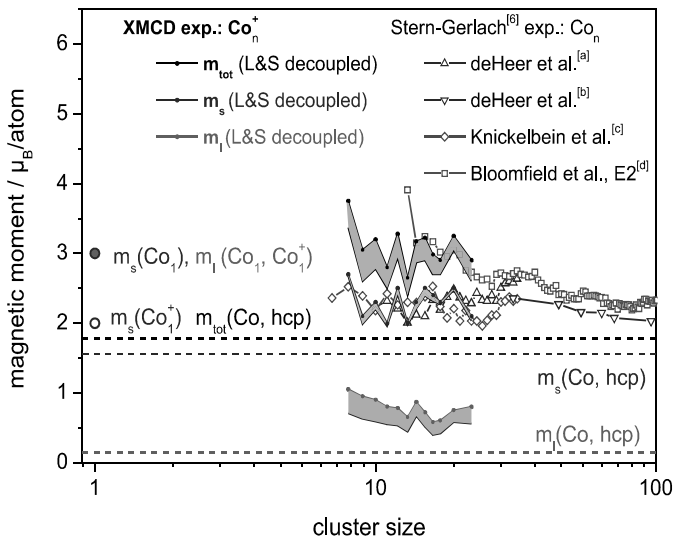


Figure 2: Spin- and orbital contributions to the magnetic moments of isolated cobalt clusters. [6] [a] de Heer et al., *Science* **265**, 1682 (1994); [b] de Heer et al., *Phys. Rev. Lett.* **95**, 237209 (2005); [c] Knickelbein, *J. Chem. Phys.* **125**, 44308 (2006); [d] Bloomfield et al., *Phys. Rev. B* **75**, 94431 (2007); Co(hcp) Chen *et al.*, *Phys. Rev. Lett.* **75**, 152 (1995)

References

- [1] S. Peredkov et al., *J. Electr. Spectr. Related Phenom.* **184**, 113-118 (2011)
 [2] S. Peredkov et al., *Phys. Rev. Lett.* **107**(23), 233401 (2011)

Low-temperature Surface Reactions of Non-energetic OH Radicals of Astrophysical Interest.

Yasuhiro Oba¹, Naoki Watanabe¹, Tetsuya Hama¹, Akira Kouchi¹, and Valerio Pirronello²

¹ Institute of Low Temperature Science, Hokkaido University, N19W8, Kita-ku, Sapporo, Hokkaido 060-0819 JAPAN, oba@lowtem.hokudai.ac.jp

² Dipartimento di Fisica e Astronomia, Università di Catania, 95125 Catania, Sicily, ITALY

It has been considered that hydroxyl radicals (OH) play a significant role in chemical reactions on grain surfaces in molecular clouds. In particular, OH-related surface reactions at low temperatures lead to the formation of simple molecules such as H₂O and CO₂, which are present in interstellar icy grain mantles as the main constituents. Previous studies experimentally demonstrated that these molecules were actually produced through surface reactions under astrophysically relevant conditions. For example, solid CO₂ was formed through reactions of CO with OH, which was produced by photolysis of H₂O [1]. Such photo-induced reactions would have a considerable contribution to chemical reactions in interstellar environments. Note that solid CO₂ is also present in dense molecular clouds where the UV field is very weak. In such a situation, photo-induced CO₂ formation is unlikely to occur; non-energetic pathways are necessary. However, due to technical difficulties, surface reactions related to non-energetic OH, including CO + OH, were not experimentally investigated so far.

We have recently succeeded in producing non-energetic, cold OH as reactants for various surface reactions at as low as 10 K. The OH was produced by dissociation of H₂O in microwave-induced plasma and was cooled down to 100 K before reactions. Here, we report experimental results on the formation of various species through surface reactions of cold OH at very low temperatures. Reactions investigated in the present study are schematically summarized in Figure 1.

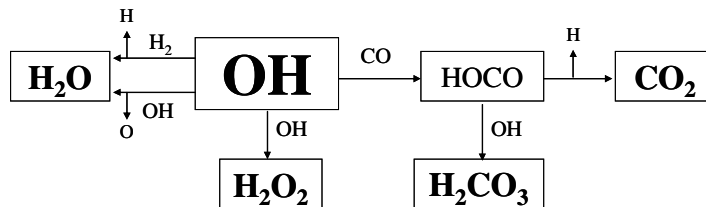


Figure 1 A schematic illustration of surface reaction pathways investigated in this study.

References

- [1] N. Watanabe, A. Kouchi, *Astrophys. J.* **567**, 651 (2002)

Comparative Study on Hydrogenated and Deuterated Amorphous Carbon Films Deposited by RF PECVD

Vilma Bursikova^{1,2}, Adrian Stoica², Vratislav Perina³, Romana Miksova³, Pavel Slavicek¹, Valentin Mocanu¹

¹ Masaryk University, Faculty of Science, , Regional R&D center for low-cost plasma and nanotechnology surface modifications, Kotlarska 2, 61137 Brno, Czech Republic,

² Masaryk University, Ceitec, Kotlarska 2, 61137 Brno, Czech Republic, vilma@physics.muni.cz

³ Institute of Nuclear Physics, Academy of Sciences of the Czech Republic, Rez near Prague, Czech Republic

The aim of this work is to characterize and compare the properties of hydrogenated carbon thin films (HDLC) and deuterated carbon thin films (DDL) deposited by r.f. plasma enhanced chemical vapor deposition (PECVD) from two different precursor mixtures methane/hydrogen (CH_4/H_2) and methane/deuterium (CH_4/D_2) on single crystalline silicon substrates. Complete atomic compositions, including hydrogen and deuterium content, were determined by combination of RBS and ERD analyses. We focused our attention on the following coating properties: hardness, elastic modulus, fracture toughness, film-substrate adhesion and internal stress. The results were completed by advanced plasma diagnostics performed by means of optical emission spectroscopy (OES).

1. Introduction

Amorphous hydrogenated diamond-like carbon (a-C:H, HDLC) films have attracted increased attention due to their extraordinary properties like high hardness, low friction coefficient, high electrical resistivity, chemical inertness and excellent wear resistance. Due to their biocompatibility, chemical inertness and being impermeable to liquids, HDLC coatings could protect biological implants against corrosion and serve as diffusion barriers [1-2]. Various materials derived from a-C:H structure have been developed incorporating nitrogen, silicon, oxygen, fluorine or various metal atoms into its structure in order to modify and improve the a-C:H film properties [2-5]. Deuterated amorphous carbon films (a-C:D, DDL) were also investigated for some specific applications, like storing ultra cold neutron devices [6] or as neutron mirrors [7]. There are several techniques suitable for preparation of HDLC and DDL films; our work will focus on low pressure radio frequency plasma enhanced chemical vapor deposition (PECVD). The main objective of the present work was to study the effects of replacing hydrogen by deuterium in the deposition mixture commonly used for HDLC film preparation (CH_4/H_2).

2. Experimental part

Hydrogenated amorphous carbon (a-C:H, HDLC) and deuterated amorphous carbon (a-C:D, DDLC) films were deposited on glass and single crystalline silicon substrates by r.f. plasma enhanced chemical vapor deposition (PECVD). The films were deposited from a mixture of CH₄ with H₂ and CH₄ with D₂, with the following values of the flow rates (Q): Q_{CH₄} = 1.4 – 2.8 sccm, Q_{H₂} = 0.4 sccm and Q_{D₂} = 0.4 sccm. The reactor was a vertically mounted Pyrex cylinder closed by two stainless steel flanges. The bottom graphite electrode was coupled to an r.f. generator (13.56 MHz) via a blocking capacitor. The upper graphite electrode was grounded. The r.f. power was kept at 50 W. The related negative self bias voltage (U_b) varied from - 260 to - 360 V as a function of the gas feed composition. The total pressure was 20 Pa. The films were deposited on mirror polished silicon and glass substrates placed on the bottom electrode. Optical emission spectroscopy monitored the deposition process.

The complete atomic composition (carbon, hydrogen, deuterium and oxygen content) of the deposited films was determined by ion beam methods combining Rutherford backscattering (RBS) and elastic recoil detection analysis (ERDA). The RBS and ERDA measurements were evaluated by computer codes GISA 3 [12] and SIMNRA [13], using enhanced non-Rutherford cross-section values from a SigmaBase (also part of SIMNRA Code).

The depth sensing indentation (DSI) method was used for determination of mechanical properties of the films using Fischerscope H100 tester equipped with Berkovich indenter. The applied load was registered as a function of indentation depth during loading/unloading cycles in order to determine the effective elastic modulus $Y = E/(1-\nu^2)$ (E is the Young's modulus and ν is the Poisson's ratio of the films) the film hardness H. At least ten different maximum loads were chosen in the interval from 2 to 300 mN. Each test was repeated at least 16 times in order to minimize the experimental errors. The calculated mechanical parameters were averaged and the 95% confidence level was determined for each studied parameter. The macroscopic internal stress in the films was determined from the sample-curvature measurements using the Stoney method [14].

3. Results and discussion

Two sets of diamond-like samples were prepared, the HDLC set without and the DDLC set with deuterium incorporation. In contrast to experiments described in [6-11] the deuterium incorporation was not achieved by using deuterized methane CD₄ but with mixing D₂ with CH₄. Fig. 1 shows parts of the emission spectrum recorded from the discharge in CH₄/D₂ gas mixture, during one of the experimental depositions of the carbon layers. The major optical emission lines from atomic H and D can be observed. Fig. 2 shows the dependence of the film hardness and elastic modulus on the bias voltage. An increase in substrate bias led to the

increase of hardness and elastic modulus, which reach values up to 22 GPa and 165 GPa, respectively. All studied films exhibited compressive stress. Increase in negative bias voltage decreased the values of the compressive stress in the deposited film. DDLC films presented slightly higher values (in the range from -1.2 to -2.1 GPa) of the compressive stress than the HDLC prepared at the same deposition conditions. The interfacial fracture toughness K_{int} characterizing the film/substrate adhesion was relatively high it ranged for both films from 0.3 to 0.5 MPam^{0.5}.

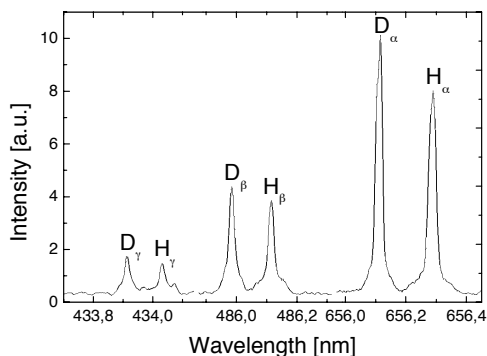


Figure 1: Parts of the optical emission spectrum recorded from the discharge in $\text{CH}_4 + \text{D}_2$ gas mixture, during the deposition of the DDLC1 film.

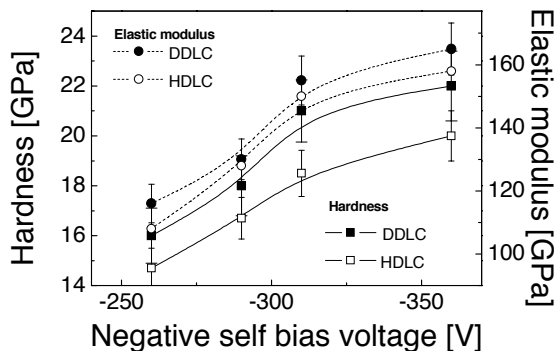


Figure 2: Comparison of the dependence of the hardness and elastic modulus of the DDLC and HDLC films on the bias voltage.

In Table 1 the atomic compositions of DDLC and HDLC films are compared. The increase in bias voltage caused decrease in atomic percentage of hydrogen as well as deuterium in case of

DDLDC films. The methane fragmentation is more effective at higher bias voltage, consequently the atomic percentage of carbon increased, even if only half of the methane flow was used comparing with films prepared at the low bias voltage.

Sample	Q_{CH_4} [sccm]	$-U_b$ [V]	C[at%]	H[at%]	D[at%]	O[at%]
DDLDC1	1.40±0.02	360±5	65.00	30.00	2.00	3.00
HDLC1	1.40±0.02	360±5	65.70	32.50	-	1.80
DDLDC4	2.80±0.02	257±7	59.06	32.32	4.62	4.00
HDLC4	2.80±0.02	257±7	56.75	37.30	-	5.95

Table 1: Atomic composition of DDLDC and HDLC films together with the methane flow rate Q_{CH_4} and negative bias voltage U_b .

4. Conclusion

The atomic composition and mechanical properties of thin films deposited from CH_4/H_2 and CH_4/D_2 mixtures using RF PECVD were compared. With increasing bias voltage the hardness, elastic modulus and compressive stress of films increased and both H as well as D content in films decreased. The deuterium addition into the deposition mixture can enhance the hardness and the elastic modulus of DLC films.

Acknowledgement

This work has been supported by the contract GACR202/07/1669, by the Ministry of Education, Youth and Sports of the Czech Republic, contract MSM 0021622411 and OP R&DI CZ.1.05/2.1.00/03.0086.

References

- [1] J. Robertson, *Material Science and Engineering R*, **37**, 129 (2002)
- [2] A. Grill, *Thin Solid Films* **355–356**, 189(1999).
- [3] M. Grishke et.al. *Diamond Rel. Mater.* **7**, 454, (1998)
- [4] C. De Martino et.al. *Diamond Rel. Mater.* **6**, 559 (1997)
- [5] V. Buršíková, et.al. *Optoelectron. Adv. Mater. - Rapid Commun.* **1**, 491 (2007)
- [6] M.G.D. van der Grinten et al., *Nucl. Instr. and Meth. in Phys. Res. A* **423**, 421 (1999)
- [7] Y. Kawabata, M. Hino, T. Horie, S. Tasaki, K. Yoshida, I. Kanno, M. Nakayama, *Nuclear Instruments and Methods in Physics Research Section A*, **9**, 1-3, 84 (2004)
- [8] M.E.H. Maia da Costa, F.L. Freire Jr., *Surface & Coatings Technology* **204**, 1993 (2010)
- [9] N. Mathis, C. Meunier, G. Guibert, S. Mikhailov, G. Berthout, *Surface & Coatings Technology* **202**, 2349 (2008)

- [10] F. Chai, N. Mathis, N. Blanchemain, C. Meunier, H.F. Hildebrand, *Acta Biomater.* **4(5)** 1369 (2008)
- [11] N. Mathis, C. Meunier, F. Munnik, S. Mikhailov, *Thin Solid Films* **516**, 1508 (2008)
- [12] J. SaariLahti, E. Rauhala, *Nucl. Instrum. Methods Phys. Res., Sect. B* **64**, 734 (1992)
- [13] M. Mayer, *SIMNRA User's guide*, Technical report IPP 9/113, Max-Planck-Institut für Plasmaphysik, Garching, Germany (1997)
- [14] G. Stoney, *Proc. R. Soc. London, Ser. A* **82**, 172 (1908)

Excited state relaxation of diarylethenes: a gas phase study on isolated and deposited molecules on Ar_n clusters

G. Piani*^{1,2}, **A. Lietard**^{1,2,3}, **R. Pollet**⁴, **L. Poisson**^{1,2}, **B. Soep**^{1,2}, **J.-M. Mestdagh**^{1,2}

¹ CNRS, IRAMIS, SPAM, Laboratoire Francis Perrin, URA 2453, F-91191 Gif-sur-Yvette, France;

² CEA, IRAMIS, SPAM, Laboratoire Francis Perrin, URA 2453, F-91191 Gif-sur-Yvette, France

³ Univ Paris Sud 11 - ED470 Chimie de Paris Sud, F-91405 Orsay CEDEX (France)

⁴ CEA, IRAMIS, SIS2M, UMR 3299, F-91191 Gif-sur-Yvette, France

* giovanni.piani@cea.fr

A gas phase study of isolated molecules is an easy way to have an experimental access to their intrinsic properties and to perform direct comparison with calculations. Our concern is to unravel the dynamics of photoexcited diarylethenes at the femtosecond timescale as they relax their internal energy along a reaction pathway.

We have used ultrafast ionization spectroscopy techniques to investigate the excited state dynamics of different diarylperfluorocyclopentenes. Following the temporal evolution of the photoelectron spectrum generated with a REMPI (1+n') scheme, we are able to point out the presence of a reaction (the diarylethene ring closure) mediated by the electronic excited state.

The experimental evidences can be explained in the theoretical framework presented by other authors in the literature, basing on a relaxation from the open form excited state to the closed form ground state *via* a Conical Intersection. Differences in the dynamics have been found, that can be attributed to the different substitution on the diarylethene frame.

We are reporting also experimental results on the influence that a controlled environment can have on the excited state relaxation of these molecules. Experiments carried out after deposition of the sample on Ar_n clusters have pointed out a slower relaxation dynamics, due to solvation.

Analysis of the products of reactions induced in methane-nitrogen plasma generated in the glow discharge

Lucie Polachova^{1,3}, Gabriel Horvath^{2,3}, Jon Watson⁴, Nigel J. Mason³, Frantisek Krcma¹, Miroslav Zahoran² and Stefan Matejcik²

¹*Faculty of Chemistry, Brno University of Technology, Purkynova 118, 612 00, Brno, Czech Republic*

²*Department of Experimental Physics, Comenius University, Mlynska dolina F-2, 842 48 Bratislava, Slovakia*

³*Department of Physics and Astronomy, Open University, Walton Hall, Milton Keynes MK7 6AA, United Kingdom*

⁴*Planetary and Space Sciences Research Institute, Open University, Milton Keynes MK7 6AA, United Kingdom*

e-mail: xcpolachova@fch.vutbr.cz

The exploration of Our understanding of planetary atmospheres is being advanced by the exciting results arising from the Cassini-Huygens mission to Titan, Saturn's most famous moon. The complex chemistry revealed in Titan's, leading to the synthesis of more complex molecules is providing new insights into our understanding of how life on Earth developed. In our experiments Titan's atmosphere is simulated in a glow-discharge formed from a mixture of CH₄-N₂ gas. Samples of the discharge gas were analyzed by GC-MS and FTIR. The major products identified in the GC-MS spectra were: ethane, ethene, acetylene, hydrogen cyanide and acetonitrile. These molecules may be precursors for other more complicated molecular structures including amino acids, the 'seeds of life'.

Introduction

Titan is the largest moon in Saturn's lunar system and has been a subject of interest to astronomers and planetary scientists for a long time because its atmospheric conditions are thought to have resembled to those conditions found on the Earth several billion years ago [1]. The most important minor compounds detected by Cassini-Huygens space mission are nitriles (HCN, HC₃N, HC₅N, C₂N₂) believed to be formed as a result of dissociation of nitrogen and methane either by solar induced photolysis or by electron impact [2] and hydrocarbons (C₂H₂, C₂H₄, C₂H₆, C₃H₈, C₃H₄ [2]). In order to understand the physical and chemical processes leading to such observed phenomena additional laboratory simulations are required.

Discharges have been shown to be good mimics of planetary atmospheres providing insights into both the physical and chemical processes present in these atmospheres. DBD, glow, microwave, RF and corona discharges [3-10] have been all used in order to study electron-molecule and ion-molecule reactions in planetary atmospheres and in recent years several of these discharges have been used to mimic Titan's atmosphere and shown that various complex compounds can be formed, for example the higher hydrocarbons, nitriles or even amino acids. This paper presents the results of organic synthesis in a Titan like atmosphere operated in a glow discharge.

Experiment

The apparatus used in our experiments is shown schematically in Figure 1. The measurements were carried out in a flowing regime at atmospheric pressure and room temperature. The discharge electrode system had a pair of stainless steel holders positioned in parallel to the iron electrodes. A stable, abnormal glow plasma occurred between the electrodes at their shortest distance of 2 mm, thus forming plasma channel with diameter of 1 mm. The reactor chamber had a volume of 0.3 L. The discharge was powered by a DC HV source. The discharge was ignited when voltage of 5500 V was applied to the electrodes, then voltage drop reached a value at about 400 V. The present experiments were performed for different $N_2:CH_4$ ratios in range from 1 % to 5 % of CH_4 in N_2 plus 1 % of CO_2 and 1 % of H_2 . Gaseous samples of products formed in the discharge were taken out for GC-MS analysis through a gas outlet into a cold trap. The cold trap was subsequently heated and the resultant gas sample for GC-MS analysis was taken using a lock syringe.

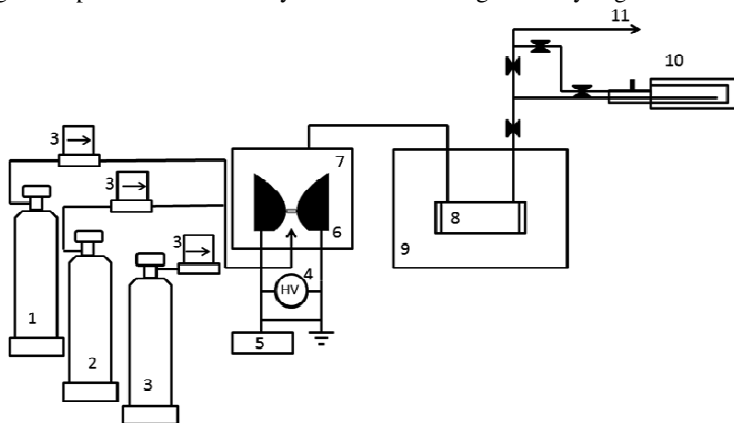


Figure 1. Experimental setup: 1- storage bottle of nitrogen, 2-storage bottle of methane, 3-storage bottle of hydrogen or carbon dioxide, MKS mass flow controllers, 4- DC power supply, 5- oscilloscope, 6- electrode system, 7- reactor body 8- lock needle for GC-MS, 9- IR gas cell, 10- FTIR spectrometer, 11- exhaust.

Results and discussion

A FTIR spectrometric study of the products formed in the glow discharge fed by a varying mixture of methane in nitrogen (1 % of CH_4) was performed in a flowing regime. A typical infrared spectrum is shown in Figure 2. Hydrogen cyanide was found to be the most abundant product at wavelength 1435 cm^{-1} . The other major products were NH_3 (966 cm^{-1}) and C_2H_2 (729 cm^{-1}). Carbon monoxide and water were detected as reaction products in methane-nitrogen gas mixture with 1% of carbon dioxide. The product concentrations are strongly dependent on compositions of the methane-nitrogen gas mixtures. Increasing the initial CH_4 content from 1 to 5 % causes an increase in the products yield (see Figure 3a. and 3b.). The dependence of product concentrations on the flow rate and a gas mixture CH_4-N_2 plus 1 % of

H_2 contents gives the same observed behaviour with respect to the major products and increases the concentration of lower hydrocarbons (C_2H_2 , C_2H_4 and C_2H_6).

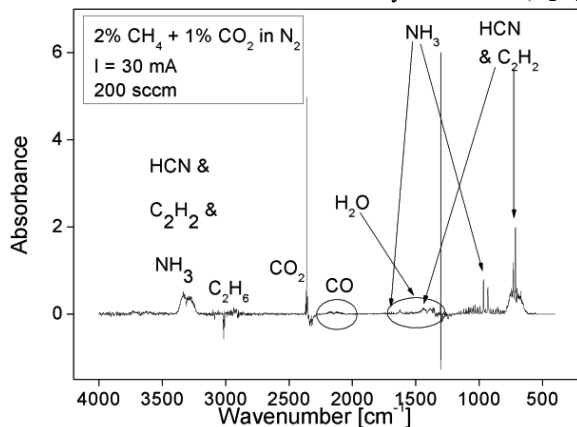
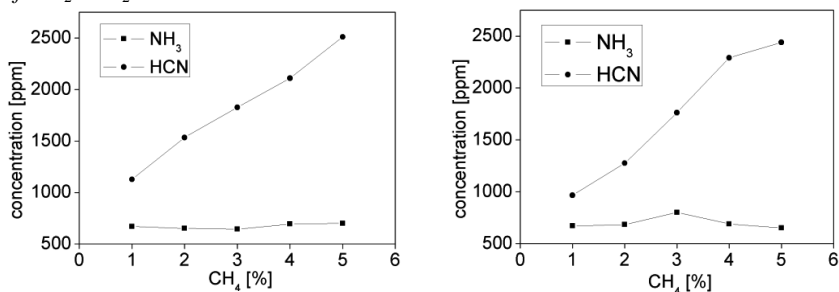
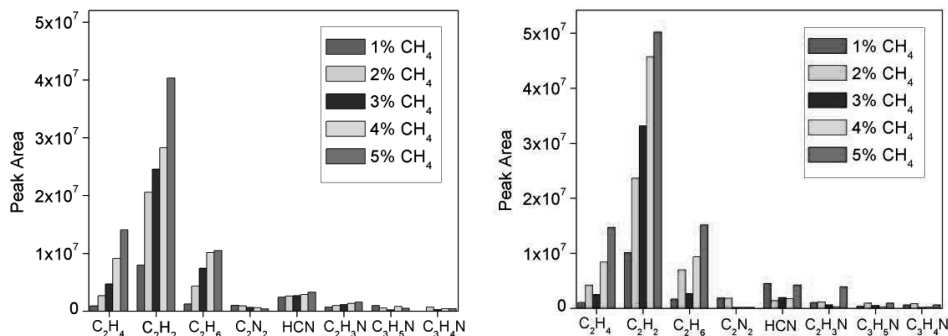


Figure 2. Sample spectrum of analysed products formed in a gas mixture 2 % of CH_4 + 1 % of CO_2 in N_2 .



Figures 3a. and 3b. The dependence of products concentrations on initial CH_4 concentrations **a**: 200 sccm flow rate and discharge current 30 mA in N_2 plasma, and **b**: CH_4 - N_2 gas mixture with 1 % of hydrogen.

Some of the results obtained from a GC-MS analysis of the plasma effluent are shown in Figure 4a. and 4b. The quantitative unit is represented by a peak area. As it is shown in Figure 4a., the concentration depends on the initial methane content. Increasing the initial CH_4 content from 1 to 5 % causes an increase in the product yield (see Figure 4a.). Figure 4a. and 4b. shows the concentrations of the major products (ethene, acetylene, ethane, cyanogen, hydrogen cyanide, acetonitrile, propenenitrile, propanenitrile). The dependence of product concentrations on the flow rate and a gas mixture of CH_4 - N_2 plus 1 % of H_2 showed the same behaviour with respect to the major products and increases the concentration of lower hydrocarbons (C_2H_2 , C_2H_4 and C_2H_6). However, there was a more significant effect on some hydrocarbon-like products than others: the yield of all N-containing products increased rapidly but was less dramatic in the hydrocarbons and hydrogen cyanide yields.



Figures 4a. and 4b. The dependence of product concentrations as a function of initial CH₄ concentrations for **a**: 200 sccm flow rate and discharge current 30 mA, **b**: 200 sccm flow rate and discharge current 30 mA, CH₄-N₂ gas mixture with 1 % of hydrogen.

Conclusion

In this contribution we present the results of a FTIR and GC-MS study of stable gaseous products formed in a glow discharge of methane and nitrogen. The major products detected by FTIR were: HCN, NH₃ and C₂H₂. Carbon monoxide and water were detected as reaction products in methane-nitrogen gas mixture with 1% of carbon dioxide. Ex situ GC-MS analysis of the gaseous revealed additional products, for example the hydrocarbons: ethene, acetylene, ethane, propene, propane, propyne, 1,2-propadiene, 1-butene-3-yne, 1,3-butadiene and 1,3-butadiyne. The following nitriles were also identified: hydrogencyanide, acetonitrile, cyanogen, 2-propenenitrile, 2-propanenitrile, 2-methylpropenenitrile and 2-methylpropanenitrile. Benzene and toluene were detected as the aromatic compounds. Such experiments will aid our understanding of processes in Titan's atmosphere.

References

- [1] Aplin K. L., Surveys in Geophysics, vol. 27, pp 63-108, 2006.
- [2] Vinatier S. et al., Icarus 188, pp 120-138, 2007.
- [3] Bernard J M, Quirico E, Brissaud O, Montagnac G, Reynard B, McMillan P, Coll P, Nguyen M J, Raulin F and Schmitt B, Icarus 185 301, 2006.
- [4] Pintassilgo C. D., Loureiro J., Cernogora G. And Touzeau M., Plasma Sources Sci. Technol. 8 463, 1999.
- [5] Szopa C., Cernogora G., Boufendi L., Correia J. and Coll P., Planetary and Space Science 54 394, 2006.
- [6] Imanaka H., Khare B. N., Eلسا J. E., Bakes E. L. O., McKay C. P., Cruikshank D. P., Sugita S., Matsui T. and Zare R. N., Icarus 168 344, 2004.
- [7] Sekine Y., Imanaka H., Matsui T., Khare B. N., Bakes E. L. O., McKay C. P., and Sugita S, Icarus 194 186, 2008.
- [8] Coll P., Coscia D., Gazeau M. C., de Vanssay E., Guillemin J. C. and Raulin F., Adv. Space Res. 16 93, 1995.
- [9] Ponnampertuma C. and Woeller F., Nature 203 272, 1964.
- [10] Gonzalez R. N. and Ramirez S. I., Adv. Space Res. 19 1121, 1997.

The structure of liquid ethylene glycol: MD simulations

Oksana Ismailova and Michael Probst

Institute of Ion Physics and Applied Physics, University of Innsbruck, Technikerstraße 25, 6020 Innsbruck, Austria; michael.probst@uibk.ac.at

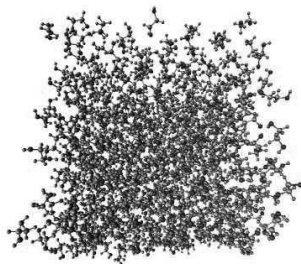
Ethylene glycol (EG) has important applications and is an interesting molecule, due to its flexible and symmetric H-O-C-C-O-H chain structure. The physical properties of ethylene glycol depend on chain angles and aggregation. The purpose of this work is to investigate dynamical and structural properties of pure ethylene glycol in wide temperature ranges.

Various properties of ethylene glycol (EG) were studied using molecular dynamics simulations. An all-atom OPLS force field was used to describe the intermolecular and intramolecular interactions of liquid EG:

$$\Sigma_{\text{bond}} = \Sigma_{\text{bond}} K_r (r - r_{\text{eq}})^2$$

$$\Sigma_{\text{angle}} = \Sigma_{\text{angle}} K_{\theta} (\theta - \theta_{\text{eq}})^2$$

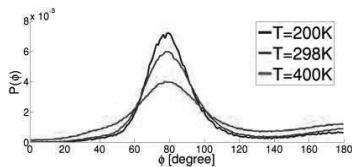
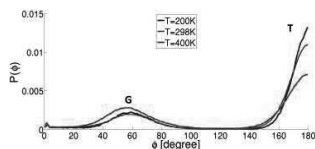
$$\Sigma_{\text{torsion}} = \Sigma_i \frac{V_1}{2} [1 + \cos \phi_i] + \frac{V_2}{2} [1 - \cos 2 \phi_i] + \frac{V_3}{2} [1 + \cos 3 \phi_i]$$



The average molecular dipole moment and the diffusion constants from this model are in good agreement with experimental values.

MD simulations were performed using the DL_POLY package.

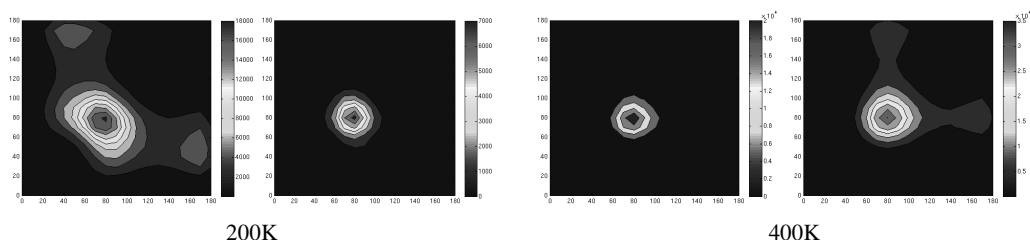
Trajectories of a few nanoseconds each were analyzed with respect to structural probability distributions and to dynamical properties. Results from the former can be understood in terms of intramolecular angles:



Dihedral angle distribution of O-C-C-O (left) and H-O-C-C (right) at temperatures of 200-400K.

An analysis of the trajectories shows that the probability distribution of the intramolecular angles are not independent of each other.

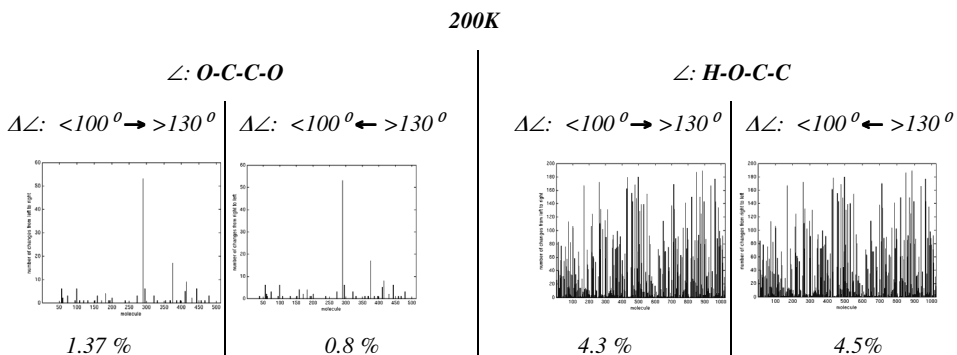
Below the mutual dependence of the rotation of the H-O bonds at the ends of the molecule are shown for different angles in the middle: For small values of $\angle O-C-C-O$, the probability of finding one $\angle H-O-C-C$ angle in a trans conformation is larger.



200K 400K

Correlation between the two H-O-C-C angles (one on x, the other on the y-axis) for EG molecules with small ($\angle O-C-C-O < 100^\circ$; left) and large ($\angle O-C-C-O > 130^\circ$) C-C torsion angles in the middle. 200K and 400K.

As an example of time-dependent processes, also the dynamics of angle flipping were investigated in detail. The graphs below show the trajectories of angle flipping. If a molecule starts to change its angles, it normally does so many times. The percentages of molecules involved is also given:



Characterization and manipulation of explosive compounds and homologues

S. Ralser¹, M. Hager¹, D. Gschliesser¹, J. Rodríguez Fernández², C. Urban², J. M. Gallego³, R. Otero² and P. Scheier¹

¹*Institut für Ionenphysik und Angewandte Physik, Universität Innsbruck, Technikerstraße 25b, 6020 Innsbruck, Austria*

²*LASUAM, Departamento de Física de la Materia Condensada, Universidad Autónoma de Madrid, Cantoblanco 28049 Madrid, Spain*

³*Instituto de Ciencia de Materiales, CSIC. Cantoblanco. 28049 - Madrid. Spain*

Dissociative electron attachment (DEA) to explosive compounds like pentaerythritol tetranitrate (PETN) [1], Royal Demolition Explosive (RDX) [2] and trinitrotoluene (TNT) [3] leads to formation of low-mass anions and stable neutral fragments like CO, CO₂, NO₂, H₂, N₂ and H₂O, with concomitant release of substantial kinetic energy. This underlines the explosive character of these substances. For gas phase experiments this is well known, but the interaction of explosives with tunneling electrons from a scanning tunneling microscope has not been investigated so far.

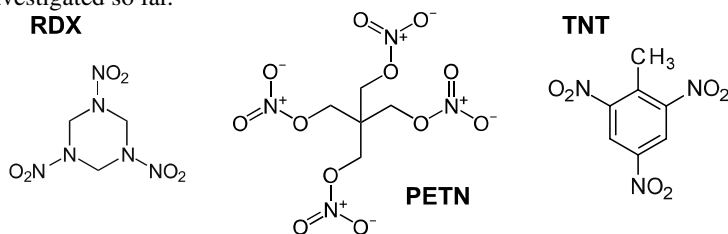


Figure 1: Chemical structure of RDX, PETN and TNT

Besides the locally well-defined deposition of an electron the effect of the surface may modify strongly the subsequent reactions upon electron attachment. To bridge the gap between gas phase and surface experiments electron attachment to helium nanodroplets doped with explosives are performed. The surrounding He matrix efficiently acts as a heat sink, similar to the metal surfaces utilized in STM studies and thereby stabilizes fragments by evaporative cooling. In this latter case, the explosives are deposited on a clean copper surface and arrangement such as self-assembling and manipulation them with a tip of a scanning tunneling microscope are studied. Particular emphasis is given to DEA, induced by tunneling electrons [4], as a trigger for phase transitions and micro-explosions.

Gas phase experiments

Gas phase and helium nano-droplet measurements are performed utilizing a double focusing sector field mass spectrometer. Figure 2 shows a mass scan of fragment anions produced

upon low-energy electron attachment to gas phase RDX (orange line) and RDX doped helium nano-droplets (blue line). High-mass fragments are strongly enhanced from the He droplets due to evaporative cooling of the helium matrix.

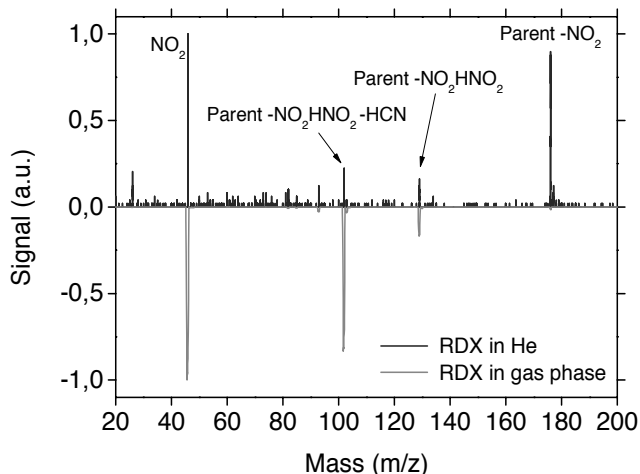


Figure 2: Mass spectra of product anions upon low-energy electron attachment to RDX in the gas phase and embedded in He nanodroplets.

Besides a stabilization of high-mass fragment anions the He-matrix leads to a pronounced modification of the electron energy dependence of the cross section of formation of the anions. DEA to gas phase RDX reveals high anion yields close to 0eV only, whereas from doped He nanodroplets also at much higher electron energies anion formation is observed. Scavenging of fast electrons via electronic excitation of He leads to a repetition of the peak sequence at 20eV and 40eV.

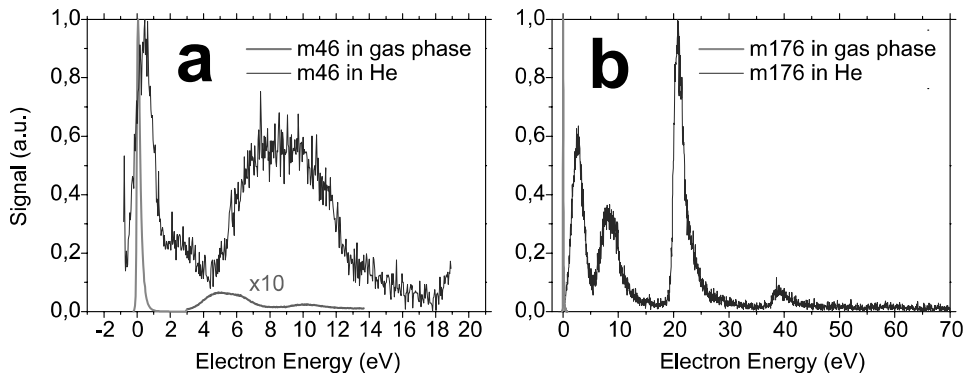


Figure 3: Anion efficiency curves of NO_2^- and $[\text{RDX-NO}_2]^-$ upon electron attachment to RDX in gasphase (orange line) and inside He nanodroplets (blue line)

STM Experiments

Surface cleaning of Cu single crystals is achieved by a standard sputtering and annealing procedure [5]. Deposition is performed by evaporation. The so prepared surface is measured and manipulated using a variable temperature STM.



Figure 4: Pentaerythritol

STM measurements of pentaerythritol (PETP, Figure 4), a homologue of PETN, are performed. Figure 5 shows PETP molecules on the surface in amounts of less than a monolayer, measured at room temperature. During time, a change in morphology from rectangular to striped phase is observed.

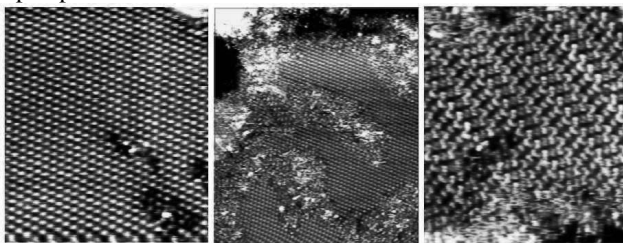


Figure 5: Self-assembly of PETP on Copper (110) at room temperature: from rectangular to striped phase (Image sizes: $164 \times 192 \text{ \AA}$, $328 \times 383 \text{ \AA}$ and $328 \times 383 \text{ \AA}$)

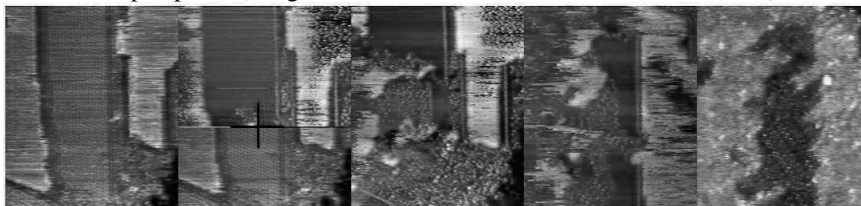


Figure 6: Chemical reaction of PETP molecules induced by a voltage ramp – a time dependent study

Stabilization of the rectangular structure appears at temperatures below 230K. At this temperature, a morphological change of the molecules on the surface is induced applying a voltage pulse, as shown in figure 6. In the first two images, one can see a rectangular structured island of PETP at the position where the voltage pulse (-3V) was applied. From

this point, the morphological change of the molecules propagates isotropically and after several scans, the whole island shows a new order. The acquisition time of each image is 20 seconds. Similar measurements are currently performed with PETN, RDX and TNT.

References

- [1] P. Sulzer et al, J. Chem. Phys. (2009) 131
- [2] A. Edtbauer et al, J. Chem. Phys. (2010) 132
- [3] A. Mauracher et al, Phys. Chem. Chem. Phys. (2009) 37/11
- [4] P. A. Sloan, R. E. Palmer, Nature, 434 (2005).
- [5] R.G. Musket et al., Applications of Surface Science 10 (1982), 143-207

Collisional Radiative Recombination of H_3^+ Ion in Low Temperature Plasma

Štěpán Roučka, Petr Dohnal, Michal Hejduk, Jozef Varju, Peter Rubovič, Sergii Opanasiuk, Radek Plašil and Juraj Glosík

Charles University, Faculty of Mathematics and Physics, Department of Surface and Plasma Science, V Holesovickach 2, Praha 8, 180 00, Czech Republic, stepan@roucka.eu

Introduction

The term *collisional radiative recombination* (CRR) describes a process of electron-ion recombination by cascading of electrons from the free continuum states to the ground state via intermediate Rydberg states. The transitions between these states are either radiative or collisional with participation of an additional electron, hence the name collisional radiative recombination. The process of CRR for atomic ions has been studied both theoretically [1, 2, 3] and experimentally [4, 5] for a long time. A convenient approximate formula for the recombination coefficient α_{cr} as a function of temperature T in kelvins and electron concentration n_e in cm^{-3} was found by Stevefelt et al. [3]

$$\alpha_{cr} = 1.55 \times 10^{-10} T^{-0.63} + 6.0 \times 10^{-9} T^{-2.18} n_e^{0.37} + 3.8 \times 10^{-9} T^{-4.5} n_e \text{ cm}^3 \cdot \text{s}^{-1}, \quad (1)$$

which is valid for atomic ions at low temperatures and He_2^+ molecular ion. The CRR of He_2^+ has also been studied experimentally at temperatures above 300 K [6, 7]. However, to our knowledge, there is no proper theory or measurement of CRR of molecular ions with exception of He_2^+ . Under the high electron concentrations ($n_e > 10^9 \text{ cm}^{-3}$) present in our experiments, the radiative and mixed terms of expression (1) can be neglected to obtain a simpler expression

$$\alpha_{cr} = A_{CRR} T^{-4.5} n_e \text{ cm}^3 \cdot \text{s}^{-1}; \quad A_{CRR} = 3.8 \times 10^{-9}. \quad (2)$$

Here we introduce a parameter A_{CRR} , which will be used as a fitting parameter in the analysis of our measurements. In the process of CRR, the energy from the recombination is partially transferred to the electron gas. The amount of energy ΔE per recombined ion is of the order of several $k_B T$ and corresponds to the energy of a particular Rydberg state n of the recombining atom (molecule) [3]. We use $n=10$ and $\Delta E = 0.13 \text{ eV}$ as a reasonable estimate. It was verified, that variation of ΔE by factor 2 does not influence our conclusions. This contribution summarizes the recent experimental results regarding CRR of H_3^+ [8, 9] obtained in our laboratory.

Experimental

All our presented experiments employ a plasmatic afterglow technique. The evolution of the electron density n_e on the axis of a discharge tube during the afterglow can be described by the equation

$$\frac{dn_e}{dt} = -K_{CRR}(T_e(n_e)) n_e^3 - \alpha_{\text{eff}} n_e^2 - \frac{n_e}{\tau_D}, \quad K_{CRR} = \alpha_{CRR}/n_e, \quad (3)$$

Where α_{eff} is the effective binary recombination coefficient consisting of contribution from binary recombination and helium assisted ternary recombination; τ_D stands for the characteristic diffusion time of the principal diffusion mode. The dependence of the K_{CRR} and electron temperature T_e on electron concentration is caused by the heating of electron gas due to CRR.

The measurements with H_3^+ were performed using a Stationary Afterglow – Cavity Ring Down Spectrometer (SA-CRDS). This device is operated with a pulsed discharge in a He/Ar/H₂ mixture and the decay of ion concentrations is observed during the afterglow. The CRDS technique used in our laboratory is described in detail elsewhere, see e.g. [8, 9]. Here we only explain, that it is a highly sensitive absorption spectroscopy technique, which allows us to measure the absolute concentrations of ions in particular quantum states in the decaying plasma. The rotational thermal equilibrium was verified by observing ion populations in multiple rotational levels. The kinetic temperature of ions was measured from the Doppler broadening of the absorption lines. Both the kinetic and rotational temperatures were found to be in close agreement with the buffer gas temperature [8, 9]. The electron temperature was calculated using a mathematical model, which includes the heating by CRR, elastic collisions with He, rotational (de-)excitation of H_3^+ , and coulombic collisions with ions [8]. The total electron concentration was calculated from the concentration of ions in the ground state with the assumption of thermal equilibrium.

Results and discussion

The measured electron density evolutions (see Fig. 1) were analyzed by fitting the numerical solution of equation (3) using a nonlinear least squares method. Fig. 1 shows, that the most general fit (line (a), where A_{CRR} and α_{eff} were fitted as free parameters) is a very good representation of the measured data. This fit produces α_{eff} in agreement with previous FALP results [10], but essentially zero value of $A_{CRR} = (0 \pm 2) 10^{-10}$, which is in contradiction with the theory [3]. To visualize the significance of this result, another fit was calculated using the fixed theoretical value $A_{CRR} = 3.8 \times 10^{-9}$ (line (b)) and α_{eff} as a fitting parameter. Furthermore, since α_{eff} is known from our different FALP experiment [10], we have drawn a line according to the known value of α_{eff} and theoretical value of A_{CRR} (line (c)). The discrepancy between the lines according to the theory of CRR and the measured data is obvious. We conclude from this graph, that the observed electron density decay is due to dissociative recombination with diffusion and not due to CRR. Equivalent analysis was performed on 10 datasets with weighted average result $A_{CRR} = (0.0 \pm 1.7) 10^{-11}$, which is at least two orders of magnitude lower than the theoretical value. However, we have to keep in mind, that the referred theory is developed only for atomic ions and He_2^+ (see [3] and discussion in [11]). We can expect a contribution of the CRR process to the overall recombination of H_3^+ , because the mechanism is very general, but the actual interplay between CRR and other recombination processes is not known to us. Because the measured data are well explained by effective binary recombination, we neglect the ternary term of equation (3) in our further analysis.

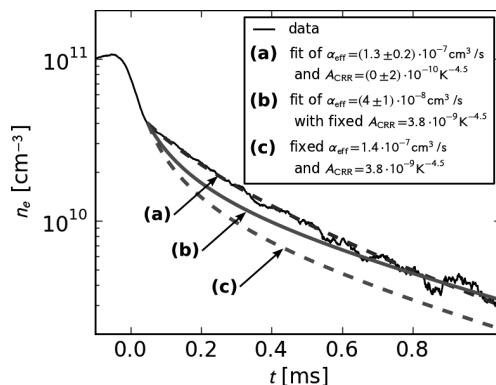


Figure 1: Electron density evolution measured in the stationary afterglow of H_3^+ plasma at 77 K and results of fits with various constraints. For details see text.

To support our hypothesis, that the observed decay is dominated by binary and helium-assisted dissociative recombination, we plot the temperature dependence of the binary recombination coefficient obtained by SA-CRDS together with the data from FALP in Fig. 3. The theoretical contributions of CRR to the recombination at two different electron concentrations $n_e=3 \times 10^{10} \text{ cm}^{-3}$ and $n_e=5 \times 10^9 \text{ cm}^{-3}$ are indicated in the graph. The FALP data were obtained at lower concentrations $\leq 2 \times 10^9 \text{ cm}^{-3}$, where the contribution of CRR should in theory be negligible. If the SA-CRDS data were influenced by CRR, we should observe a sharp increase of the coefficient at the lowest temperature in contrast to the FALP data. However, the FALP and SA-CRDS data are in a good mutual agreement. Moreover, the measured data also agree well with the theoretical curve for binary recombination [12].

Conclusion

The fitting analysis of our data indicates no measurable contribution of CRR to the observed recombination. The upper limit on CRR determined from the fits is by two orders of magnitude smaller than the theoretical value [3]. This observation is supported by the consistency of measured SA-CRDS data with the FALP experiment and with theoretical value for dissociative recombination. A possible explanation for low CRR is slightly higher temperature of electrons. Such explanation may apply to experiment by Amano [13], who was also unable to observe the theoretical CRR in his H_3^+ experiment. However, the detailed model of electron energy balance used in our fitting procedure was not able to account for such a discrepancy. A reasonable explanation is, that the theory of CRR for H_3^+ needs some corrections to account for the interplay between CRR and binary dissociative recombination.

Acknowledgment

This work is a part of the research plan MSM 0021620834 and grant OC10046 financed by the Ministry of Education of the Czech Republic and was partly supported by GACR (202/07/0495, 202/08/H057, 205/09/1183, 202/09/0642), by GAUK 92410, GAUK 353811, GAUK 54010, GAUK 25709 and by COST Action CM0805 (The Chemical Cosmos).

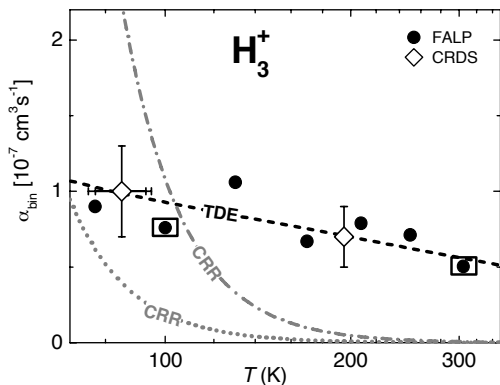


Figure 2: The temperature dependence of the binary recombination coefficient in H_3^+ . Data obtained from SA-CRDS [8, 9] and FALP [10] experiments are shown. The points enclosed in black rectangles were obtained by combining data from SA-CRDS and FALP. The theoretical curve for dissociative recombination in thermodynamical equilibrium (TDE) [12] is shown together with theoretical dependence of effective binary CRR at concentrations $n_e=3\times 10^{10} \text{ cm}^{-3}$ (dash-dotted line) and $n_e=5\times 10^9 \text{ cm}^{-3}$ (dotted line).

References

- [1] D'Angelo, N., *Phys. Rev.*, **121**, 505-507 (1961)
- [2] Bates, D. R. & Kingston, A. E., *Proc. Phys. Soc.*, **83**, 43-47 (1964)
- [3] Stevefelt, J.; Boulmer, J. & Delpech, J.-F., *Phys. Rev. A*, **12**, 1246-1251 (1975)
- [4] Collins, C. B. *et al.*, *Phys. Rev. A*, **6**, 1545-1558 (1972)
- [5] Skrzypkowski, M. *et al.*, *Chem. Phys.*, **296**, 23 - 27 (2004)
- [6] Robertson, W. W., *J. Chem. Phys.*, **42**, 2064-2070 (1965)
- [7] Deloche, R.; Monchicourt, P. *et al.*, *Phys. Rev. A*, **13**, 1140-1176 (1976)
- [8] Dohnal, P.; Hejduk, M.; Varju, J.; Rubovic, P.; Roucka, S.; Kotrik, T.; Plasil, R.; Johnsen, R.; Glosik, J., *Proc. Roy. Soc.*, (2012), (in preparation).
- [9] Varju, J. *et al.*, *Phys. Rev. Lett.*, **106**, 203201 (2011)
- [10] Glosik, J.; *et al.*, *Phys. Rev. A*, **79**, 052707 (2009)
- [11] Bates, D. R.; Guest, M. F. & Kendall, R. A., *Planet. Space Sci.*, **41**, 9-15 (1993)
- [12] dos Santos, S. F.; Kokoouline, V. & Greene, C. H., *J. Chem. Phys.*, **127**, 124309 (2007)
- [13] Amano, T., *Astrophys. J. Lett.*, **329**, L121-L124 (1998)

IR-Laser Induced Population Transfer from Highly Populated Rotational Levels of NH₃ in a Molecular Beam

Peter Dietiker¹, Martin Quack¹, Andreas Schneider¹, Georg Sevfang¹ and Fatih Ünlü¹

¹ Physical Chemistry, ETH Zürich, 8093 Zürich, Switzerland. quack@ir.phys.chem.ethz.ch

Although the theoretical calculation of the parity violating energy difference in molecules is now well established its experimental verification is still missing. In principle this energy difference can be measured in sophisticated high-resolution spectroscopic experiments or alternatively in a well defined time resolved experiment as it has been proposed 25 years ago [1]. In the paper we present an experimental scheme and the first experimental results towards the detection of the parity violating energy difference in molecules by the proposed time resolved technique.

Introduction

Electromagnetic quantum chemistry predicts the ground state energies of enantiomers of chiral molecules to be exactly equal by symmetry. According to our current understanding, however, the electroweak interaction breaks this symmetry and introduces a slight energy difference ΔE_{PV} of the ground states of enantiomers, corresponding to a reaction enthalpy $\Delta_{\text{PV}}H_0^\circ$ for the stereomutation [1-3]

$$R = S, \quad \Delta_{\text{PV}}H_0^\circ = N_A \Delta E_{\text{PV}} \quad (1)$$

The experimental verification of parity violation in molecules is still one of the great challenges in physics and chemistry [3-5]. There are several proposals based on high-resolution experiments to measure the frequency shift between enantiomers of chiral molecules like CHFClBr or CDBrFI [6-10]. Experiments pursuing this scheme have yet to achieve the required resolution to detect this extremely small frequency shift [2,5]. These experiments cannot detect the parity violating energy difference ΔE_{PV} , but only a difference of such differences [1,3]. Another promising experiment is to observe the effect of parity violation in the time domain [1,5]. In this time resolved method an excited state with well defined parity has to be populated in a two- or multiple-step preparation process and the inter conversion of the two parity states is observed by time resolved methods. For the limiting case where the parity violating energy difference $\Delta_{\text{PV}}E$ between two enantiomers is much larger than the tunnelling splitting ΔE_{\pm} the period of inter conversion of the two parity states is determined by the parity violating energy difference $\Delta_{\text{PV}}E$.

In preparation for the above-mentioned experiment we have chosen the achiral molecule NH₃ as a test molecule. The molecule has large rotational constants and only the lowest rotational levels ($J = 0,1$) are populated in a molecular beam. A two step population transfer process to

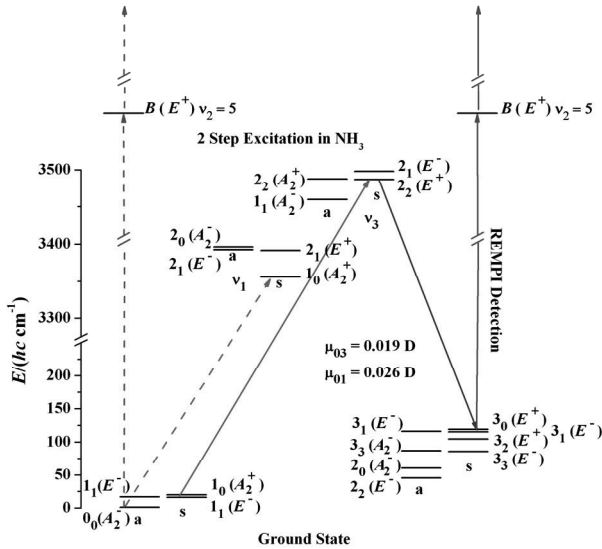
rotationally higher excited levels can be studied through an IR-absorption/stimulated IR-emission process with a rotational level of the NH-stretching vibrations (ν_1 or ν_3) as the intermediate state. The laser frequencies necessary for these absorption and stimulated emission steps are in a spectral range where very reliable and powerful cw lasers (OPO) are available. In addition, the UV-spectrum of NH_3 is well understood and molecules prepared in the higher rotational levels can be probed efficiently by a 2+1 or 3+1 REMPI scheme through the electronically excited \tilde{A} -state (E^-) or the B -state (E^+) states [11]. The two step preparation scheme, including the REMPI detection step is shown schematically in figure 1.

Experimental Setup

To obtain the necessary state selection and to shield the prepared molecules from any interaction with their surrounding like collisions or interaction with any electric or magnetic fields the experiments have to be performed in a molecular beam. About 5 cm downstream of the skimmer the molecular beam is crossed by two IR laser beams to prepare the molecules in a molecular level of defined parity in a two-photon absorption/stimulated emission process. After the preparation step the molecules are transferred, ideally without any further interaction with the surrounding, to the centre of a time of flight mass spectrometer where they are detected with high sensitivity in the opposite parity state by resonant enhanced multiphoton ionization (REMPI). For the first experiments a distance of 20 cm was chosen between the preparation and detection zone. As the beam diameter of the REMPI laser is very small ($D \approx 100 \mu\text{m}$) only the fraction of the molecules prepared with a very small velocity component perpendicular to molecular beam are detected in the REMPI step.

Two continuous wave OPOs (Linco OS4000 and OS4600) are used for the preparation step. The OS4000 has a doubly resonant cavity (pump + signal) and the idler radiation is tuneable from $2500 - 4150 \text{ cm}^{-1}$ with a maximum power of 60 mW. The OS4600 is only resonant for the signal wave and the idler wave is tuneable from $2100 - 4350 \text{ cm}^{-1}$ with a power of up to 1 Watt. Both OPOs are stabilized to a frequency comb (Menlo Systems FC 1500-250). For the singly resonant OS4600 the pump and the signal beam are locked to different modes of the frequency comb and a long-term frequency stability is obtained which is given by the stability of the microwave GPS reference standard. For the doubly resonant OS4000 only the pump beam is locked to the frequency comb and the frequency stability of the idler beam is determined by the width of the resonance of the signal beam. With a proper temperature stabilization and a good isolation from external laboratory perturbations a frequency stability well below 1 MHz should be possible, as it could be derived from the stability of the beat signal between the idler beams of the OS4000 and the OS4600.

The UV-radiation for the multiphoton ionization in the detection step is delivered from a frequency doubled dye laser (Radiant Dyes, Narrow Scan D) pumped by the second harmonic



of an Nd-YAG laser (Continuum 9010). To avoid AC-Stark broadening of the REMPI signal the UV pulse energy had to be reduced to 1 mJ.

Figure 1: Reduced rovibrational level scheme of NH_3 . The proposed two step preparation sequence, including the REMPI detection, is given by the full line whereas the one photon depletion step is shown with a dashed line. The rotational levels (J_K) are characterized according to the symmetry group S_3^* [3]

Measured Depletion Spectrum

In a first step we have investigated the population transfer from the vibrational ground state to the symmetric NH-stretching vibration v_1 . The OS4600 is tuned to the R_0 -transition and the depletion of the population from the ($J = 0, K = 0$) is measured by a (2+1) REMPI process using the $v_2 = 5$ level of the electronically excited B -state (E^+) as an intermediate [12]. In figure 2 the depletion of the population in the ($J = 0, K = 0$)

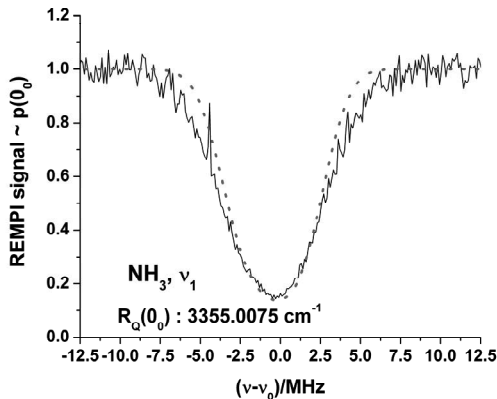


Figure 2: REMPI-Signal (full line) of the population depletion of the ($J=0, K=0$)- level of the vibrational ground state. The dashed line shows a result of a simulation of the excitation process. The Liouville von Neuman equation is integrated for a laser intensity of 0.6 W, a laser beam diameter of 0.55 mm and a linear chirp $d\omega/dt = 10.1 \text{ MHz}/\mu\text{s}$.

state due to the interaction with the radiation from the strong infrared laser field is shown. To guarantee an efficient population transfer a linear chirp was imposed to the laser frequency by the adiabatic passage method. The dashed line shows the result of a simulation of the excitation process. The Liouville von Neuman equation is integrated for a laser intensity of 0.6 W, a laser beam diameter of 0.55 mm and a linear chirp $d\omega/dt = 10.1 \text{ MHz}/\mu\text{s}$. For the simulation the nuclear hyperfine structure due to the ^{14}N -nuclear spin ($I_N = 1$) is taken into account using the same quadrupole coupling constant eQq for the ground and vibrational excited state. The width (5 – 6 MHz) of the measured and simulated spectrum is nearly identical showing only minor contributions from a velocity component perpendicular to the beam direction. The precision of the measured line position is determined by the angle between the laser and molecular beam. A deviation of 1° from the exact perpendicular direction would result in a frequency shift of 3 MHz which is much larger than the uncertainty of our laser frequency.

Conclusion

We have set up an experiment, which allows the efficient population transfer from an initially populated molecular level to a second level by a two-photon IR-absorption/stimulated IR-emission process. The two lasers involved in the preparation step have been locked to a reference frequency with very high stability and accuracy. The efficient population transfer for the first step of the preparation process has been verified in a molecular beam through the vibrational excitation of NH_3 .

Acknowledgment: Our work is supported financially by the ETH Zürich and the Schweizerischer Nationalfonds. We thank A.Laso and E. Peyer for technical support.

References

- [1] M. Quack, *Chem. Phys. Lett.* **132**, 147 (1986).
- [2] M. Quack and J. Stohner, *Phys. Rev. Lett.* **84**, 3807 (2000).
- [3] M. Quack, 'Fundamental Symmetries and Symmetry Violations from High-resolution Spectroscopy', in *Handbook of High-resolution Spectroscopy*, Vol.1, M. Quack and F. Merkt (eds.), Wiley 2011
- [4] A. Bakasov, T.-K. Ha, M. Quack, *J. Chem. Phys.* **109**, 7263 (1998).
- [5] M. Quack, J. Stohner, M. Willeke, *Annu. Rev. Phys. Chem.* **59**, 741 (2008).
- [6] O. N. Kompanets, A. R. Kukudzhanov, V. S. Letokhov, L. L. Gervits, *Opt. Commun.* **19**, 414 (1976).
- [7] E. Arimondo, P. Glorieux, and T. Oka, *Opt. Commun.* **23**, 369 (1977).

-
- [8] A. Bauder, A. Beil, D. Luckhaus, F. Müller, M. Quack, *J. Chem. Phys.* **106**, 7558 (1997).
- [9] C. Daussy, T. Marrel, A. Amy-Klein, C. T. Nguyen, C. Bordé, and C. Chardonnet, *Phys. Rev. Lett.* **83**, 1554 (1999).
- [10] J. Crassous, F. Monier, J. P. Dutasta, M. Ziskind, C. Daussy, C. Grain, C. Chardonnet, *Chem. Phys. Chem.* **4**, 541 (2003).
- [11] M. N. R. Ashfold, C. Bennett, R. J. Stickland, *Com. At. Mol. Phys.* **19**, 181 (1987).
- [12] M. Hippler, E. Miloglyadov, M. Quack, G. Seyfang, 'Mass and Isotope Selective Infrared Spectroscopy' in *Handbook of High-resolution Spectroscopy*, Vol.2, M. Quack and F. Merkt (eds.), Wiley 2011

Photofragmentation of amino acids containing a disulfide (S-S) bond

S. Soorkia,¹ B. Lucas,¹ J. A. Fayeton,¹ M. Barat¹ and C. Juvet^{1,2}

¹ *Institut des Sciences Moléculaires d'Orsay, CNRS UMR 3214, Université Paris-Sud, France, satchin.soorkia@u-psud.fr*

² *Centre Laser Université Paris-Sud, CNRS FR 2764, France*

We have shown that electronegative centers play a central role in photofragmentation mechanisms as in singly protonated molecules containing a carboxylic acid group.¹⁻³ In principle, disulfide bonds are also electronegative centers where the active electron could attach, leading to specific bond breaking. While the fragmentation efficiency in Collision Induced Dissociation (CID) conditions for S-S bonds is fairly low,⁴ we show that bond cleavage reactions at the disulfide bridge dominate following UV excitation. In this study, Tryptophan-Cystine (WCC) is chosen as a model of aromatic amino acid with a disulfide bridge. Photofragmentation of the corresponding protonated species (WCC⁺), produced in an Electrospray Ionization source, by 263 nm photons are studied with a unique experimental technique based on the detection in coincidence of the ionic and neutral fragments. Time and position resolved measurements allow distinguishing between direct and sequential dissociation of the parent ion following UV excitation. However, the measured fragmentation times (on the order of a few μ s) of the different product ions suggest that a more complex mechanism is at play.

References

- [1] V. Lepere, B. Lucas, M. Barat, J. A. Fayeton, V. J. Picard, C. Juvet, P. Carcabal, I. Nielsen, C. Dedonder-Lardeux, G. Gregoire, and A. Fujii, *J. Chem. Phys.* **127**, 134313 (2007)
- [2] B. Lucas, M. Barat, J. A. Fayeton, M. Perot, C. Juvet, G. Gregoire, and S. B. Nielsen, *J. Chem. Phys.* **128**, 164302 (2008)
- [3] M. Perot, B. Lucas, M. Barat, J. A. Fayeton, and C. Juvet, *J. Phys. Chem. A* **114**, 3147 (2010)
- [4] H. Lioe and R. A. J. O'Hair, *Anal. Bioanal. Chem.* **389**, 1429 (2007)

Control of chemical synthesis by electrons: The making and breaking of bonds

Th. Hamann, E. Böhler, T. Borrmann, J. H. Bredehöft, P. Swiderek

*Universität Bremen, Fachbereich 2 (Chemie/Biologie), Institute of Applied and Physical Chemistry,
Leobener Straße / NW 2, Postfach 330440, 28334 Bremen, Germany*

The transformation of structurally simple molecules into more complex ones is the central challenge of chemical research. This concerns not only the area of material synthesis but also the question of the origin of life. In an ideal process, a well-defined initiating step would drive a system towards a specific product that is made from the initial molecular building blocks. Low-energy free electrons provide an approach to control chemical reactions. Depending on their incident energy (E_0), fragmentation of molecules can proceed via attachment of the electron thus forming a temporary negative ion that decays to a negative and a neutral fragment (Dissociative electron attachment, DEA) according to $AB + e^- \rightarrow AB^{*-} \rightarrow A^- + B$. At higher E_0 dissociation can result from electron impact ionisation (EII) which is, in the simplest case, represented by $AB + e^- \rightarrow A^+ + B + 2 e^-$. Furthermore, excitation to neutral states can also induce dissociation of the molecule. In the condensed phase, reactive fragments thus produced undergo further reactions. If specific fragments can be produced in the initiating dissociative electron-molecule interaction, it may thus be possible to also drive the subsequent reactions with adjacent molecules towards specific products. In this contribution we discuss and compare the potential of DEA and EII concerning the control of electron-induced reactions in the condensed phase and at surfaces.

Control by Dissociative Electron Attachment

Depending on the energy of the incoming electron (E_0), dissociative electron attachment (DEA) (essentially, molecular dissociation into a neutral and anionic fragment following initial electron capture into short-lived molecular anion or “*resonance*”) leads to the rupture of specific bonds [1,2]. A particularly fine example was provided by a suite of gas phase experiments on the nucleobase thymine which demonstrated that each single hydrogen atom can be selectively dissociated from the molecule by proper choice of the energy of the incoming electron (E_0) [3]. A recent study on formamide (HCONH_2) also provided evidence for a similar selectivity [4].

It has been shown that DEA can trigger reactions that lead to the modification or functionalisation of surfaces. One example is the electron-induced fluorination of an amorphous hydrogen-terminated Si surface [5]. In this reaction, dissociative electron attachment (DEA) to CF_4 deposited as a thin layer on the Si surface leads to fragmentation of CF_4 as monitored by electron-stimulated desorption (ESD) of F^- . The reactive fragments thus produced react with the surface so that F is attached to Si. Also, it was recently demonstrated that acetonitrile (CH_3CN) can be attached to a diamond surface [6]. This reaction yielding CH_2CN^- and an H radical is initiated by DEA to CH_3CN deposited onto the surface. The H radical can activate the initially hydrogen-terminated diamond surface. It was assumed that the radical fragment remaining after detachment of the electron from CH_2CN^- then recombines with the radical site at the activated surface to become covalently attached.

Despite these obvious successes of applying DEA to the control of surface reactions, the situation may be less satisfactory in the condensed phase. As an example, CD_3 radicals produced by DEA to CD_3CN in condensed mixtures of CD_3CN and C_2H_6 statistically attack both types of neighboring molecules. This has been shown by thermal desorption spectrometry [7] which gives at E_0 below the ionisation threshold evidence of the production of both CD_3H and CD_4 (see Figure 1).

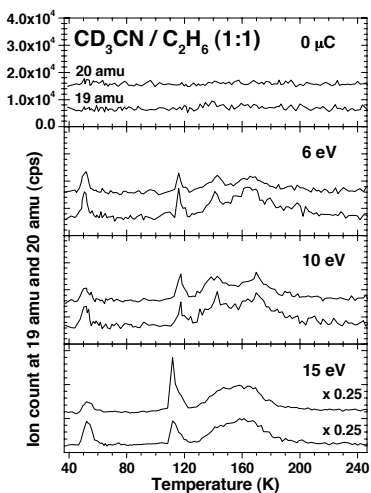


Figure 1: TDS measurements at 19 amu and 20 amu for 15-layer films of $\text{CD}_3\text{CN}/\text{C}_2\text{H}_6$ mixtures (1:1) before and after electron exposure of $5000 \mu\text{C}$ at the stated incident energies. The magnification is the same for all curves.

Control by Electron Impact Ionisation

Recent studies on electron-induced processes in condensed molecular films have shown that near-threshold electron impact ionisation (EII) can also initiate molecular synthesis. Strong Coulomb forces arising after ionisation lead to attractive interaction and subsequent reaction between adjacent molecules. As an example, irradiation of a condensed mixture of C_2H_4 and NH_3 at electron energies (E_0) just above the ionisation threshold induces such a reaction leading to formation of ethylamine ($C_2H_5NH_2$) [8]. Ionisation of one of the reaction partners removes the electrostatic repulsion between the lone pair of NH_3 and the electron-rich double bond of C_2H_4 and thus sufficiently lowers the activation barrier of the reaction between the two molecules so that the adduct formation can take place (Figure 2). The reaction thus proceeds on a cationic potential energy surface and the neutral product is formed by recapture of a thermalised electron present within the molecular layer while electron exposure continues. This mechanism is particularly appealing because it does not imply fragmentation of the reaction partners so that a more complex product is readily accessible.

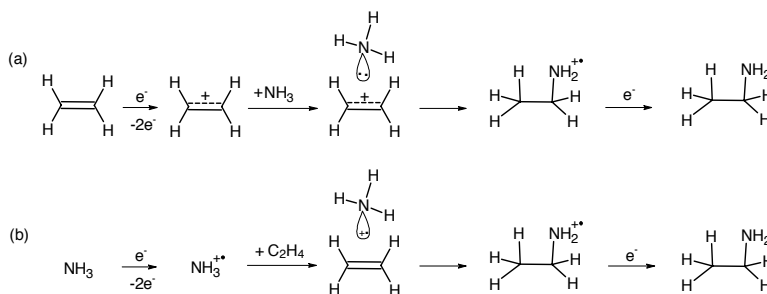


Figure 2: Electron impact ionisation-driven hydroamination of

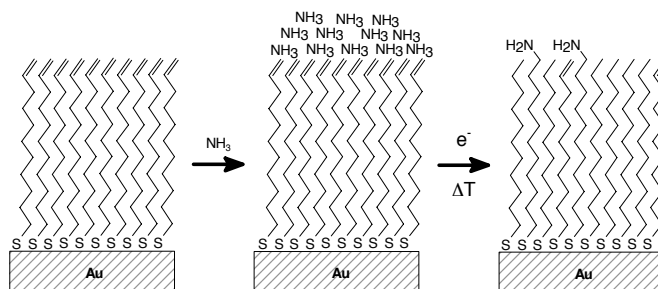


Figure 3: Schematic representation of an electron-driven process for amination of a SAM carrying a terminal CC double bond [9]. The process relies on the reaction mechanism

The reaction shown in Figure 2 has also been applied to the functionalization of self-assembled monolayers (SAMs) terminated by CC double bonds [9]. XPS results show that this approach in fact can produce a SAM surface carrying roughly 25% nitrogen-containing groups (see Figure 3). Reduction of the double bond by hydrogen released upon electron-induced dissociation of NH_3 is observed as a concurrent process. As an important finding, however, the reducing action of a sufficiently thick NH_3 layer upon electron exposure also protects the SAM from damage caused by electron irradiation.

Conclusions

Low-energy electrons provide a means of controlling chemical reactions and can lead to the controlled synthesis of specific products. At E_0 below the ionisation threshold DEA provides access to selective bond cleavage by proper tuning of incident electron energy. For example, fragments produced by DEA can initiate surface functionalisation. However, in the condensed phase radical species produced by DEA often undergo unselective reactions. At E_0 above but near the ionization threshold EII can be used to control reactions. We have shown here that Coulomb forces resulting from ionisation can drive chemical synthesis starting from simple building blocks. For example, ionisation can initiate the surface functionalisation (hydroamination) of unsaturated SAMs. However, it is important to consider that ionisation yields intact molecular cations only near the threshold.

References

- [1] I.Bald, J.Langer, P.Tegeger, O.Ingolfsson, *Int. J. Mass Spectrom.* **277**, 4 (2008).
- [2] E.Illenberger, J.Momigny, Gaseous Molecular Ions, Steinkopff Darmstadt (1992).
- [3] P.Swiderek, *Angew. Chem. Int. Ed.* **45**, 4056 (2006) and references therein.
- [4] T.Hamann, A.Edtbauer, F.Ferreira da Silva, S.Denifl, P.Scheier, P.Swiderek, *Phys.Chem. Chem.Phys.* **13**, 12305 (2011).
- [5] W.Di, P.Rowntree, L.Sanche, *Phys.Rev. B* **52**, 16618 (1995).
- [6] A.Lafosse, M.Bertin, D.Caceres, C.Jäggle, P.Swiderek, D.Pliszka, R.Azria, *Eur. Phys. J. D* **35**, 363 (2005).
- [7] I.Ipolyi, W.Michaelis, P.Swiderek, *Phys.Chem.Chem.Phys.* **8**, 180 (2007).
- [8] T.Hamann, E.Böhler, P.Swiderek, *Angew.Chem.Int.Ed.* **48**, 4643 (2009).
- [9] T.Hamann, L.Kankate, E.Böhler, J.H.Bredehöft, F.Zhang, A.Göhlzäuser, P.Swiderek, *Langmuir*, in print.

Modification of polydimethylsiloxane coatings by H₂ RF plasma, Xe₂^{*} excimer VUV radiation, and low-energy electron beams

P. Swiderek¹, E. Jolondz¹, J.H. Bredehöft¹, T. Borrmann¹, C. Dölle², M. Ott², C. Schmäser², A. Hartwig², V. Danilov³, H.-E. Wagner³, J. Meichsner³

¹ Universität Bremen, Fachbereich 2 (Chemie/Biologie), Institute of Applied and Physical Chemistry, Leobener Straße / NW 2, Postfach 330440, 28334 Bremen, Germany

² Fraunhofer Institute for Manufacturing Technology and Applied Materials Research, Wiener Straße 12, D-28359 Bremen, Germany

³ University of Greifswald, Institute of Physics, Felix-Hausdorff Straße 6, D-17489, Greifswald, Germany

Polydimethylsiloxanes (PDMS) have a wide range of applications including uses as release agents, rubber molds, water repellents or adhesives but also in biomedical devices, personal care products and dielectric encapsulation as well as microfluidic devices or corrosion protective coatings. PDMS has an outstanding viscosity, optical transparency, and chemical inertness, and it is non-toxic and non-volatile [1-4]. In coating technology, PDMS is suitable for application techniques such as spin-coating, dip-coating or aerosol-coating to generate thin films which can also be loaded with nanoparticles (e.g. Ag, TiO₂) to provide antibacterial properties or photocatalytic activity [5-7]. Most importantly, the liquid and hydrophobic PDMS layers can be converted into hydrophilic SiO_x solid thin films. However, a thermal treatment aiming at this conversion requires temperatures above 800°C [8] and is therefore impractical for large scale applications and thermally sensitive materials. On the other hand, a conversion at room temperature can be achieved by tools like VUV irradiation [9] or plasma processing [10].

As an alternative method for the modification of surfaces or thin films, electron beam processing has been used previously to crosslink different siloxanes [11-13]. However, none of the early studies on electron-induced crosslinking of siloxanes has provided detailed information on the reaction mechanisms. Therefore the aim of the present contribution is twofold. First, this study provides a direct comparison of the modifications in liquid PDMS layers achieved by H₂ RF plasma, Xe₂^{*} excimer VUV, and low-energy electron beam treatment and thus investigates the option of controlling the properties of the coatings by choosing the physical tool applied in the processing. Second, the fundamental chemical reactions initiated by the different types of projectiles are reviewed to provide an explanation for the observed differences between the modifications achieved by the three processes.

Modification of liquid PDMS coatings

The modifications of liquid PDMS layers by three different processes, namely, H₂ RF plasma treatment, Xe₂* excimer VUV irradiation, and exposure to a low-energy electron beam have been investigated and compared using reflection absorption infrared spectroscopy (RAIRS). The results show that the outcome differs between the three processes. Plasma treatment leads to an abrupt transition of the uppermost layers to a SiO_x-like material. In contrast, much deeper regions of the coating are reached by VUV radiation from both the plasma or light sources like a Xe₂* excimer lamp as applied here. This leads to a gradual and controllable transition from PDMS to a SiO_x-like material in the presence of O₂ [9]. In contrast, RAIRS does not provide evidence of an increasing oxidation of PDMS in the case of electron exposure even in the presence of O₂ although a sufficiently high electron energy can equally remove the methyl groups of PDMS. Each of the three processes thus provides a means to produce coatings with distinct properties.

Mechanisms of the conversion of liquid PDMS

VUV radiation from both the plasma or light sources like a Xe₂* excimer lamp as applied here reaches relatively far into the coating. The photolytic processes induce homolytic cleavage of CH and SiC bonds and consequent radical reactions and thus lead to a successive decline of organic side groups in PDMS. This reaction equally facilitates the formation of an oxidized product because the produced radicals can readily react with O₂ to form peroxy radicals which then decay to more strongly oxidized Si species [9,14]. However, a gradual and controllable transition from PDMS to a SiO₂-like material in the presence of O₂ offers the perspective to tune the material properties over a wide range [9].

In contrast, electron exposure of siloxanes and thus also PDMS induces reactions predominantly by electron impact ionisation, the dominant initiating reaction being dissociation into CH₃ and a cation with charge residing on a Si atom [15]. This latter intermediate has a much smaller affinity to bind O₂ than a Si radical. In consequence, oxidation of the material is not favoured to the same extent as under VUV or plasma treatment.

Finally, the modification by plasma is more complex because it is driven by the combined effects of ions, electrons, energetic neutrals, and VUV radiation. In particular, it is very likely that particles impinging onto the material during plasma processing induce the rapid and

direct transformation to SiO_x of the near-surface regions of a PDMS layer [10]. Such particles can enter a polymer layer only to a depth of a few nm and the induced reactions depend critically on the nature of the projectile [16]. For example, it was shown that proton bombardment at energies as low as 10 eV leads to crosslinking of polymeric materials initiated by C-H bond cleavage [16]. Here, the severe damage caused by such processes leads to a rapid transition of the uppermost PDMS layers.

In conclusion, the reaction mechanisms initiated in PDMS by absorption of VUV photons, by impact of electrons, and by ions and neutral particles as additional agents in plasma processing are fundamentally different. This can be traced back to specific initiating elementary reaction steps and can explain the distinctly different modification of PDMS coatings by the three processes.

References

- [1] A.C.M.Kuo, in *Polymer Data Handbook*, edited by J. E. Mark (Oxford University Press, New York, 1999), pp. 411.
- [2] S.K.Sia, G.M.Whitesides, *Electrophoresis*, **24**, 3563 (2003).
- [3] J.C.McDonald, G.M.Whitesides, *Acc.Chem.Res.* **35**, 491 (2002).
- [4] S.W.Duo, M.S.Li, M.Zhu, Y.Zhou, *Mater.Chem.Phys.* **112**, 1093 (2008).
- [5] M.Wagener, B.Günther, *Progr. Colloid Polymer Sci.*, **111**, 78 (1998).
- [6] C.Dölle, C.Schmüser, M.Ott, *Jahrbuch Oberflächentechnik* **66**, 96 (2010).
- [7] M.Ott, C.Dölle, V.Danilov, A.Hartwig, J.Meichsner, D.Salz, C.Schmüser, O.Schorsch, M.Se bald, H.-E.Wagner, K.D.Vissing, *Plasma Proc. Polym.*, submitted.
- [8] D.Seyferth, *Adv.Chem.Ser.* **224**, 565 (1990).
- [9] C. Dölle, M.Papmeyer, M.Ott, K.Vissing, *Langmuir* **25**, 7129 (2009).
- [10] V.Danilov, H.-E.Wagner, J.Meichsner, *Plasma Proc. Polym.* **8**, 1059 (2011).
- [11] R.W.Christy, *J. Appl. Phys.* **31**, 1680 (1960).
- [12] Y.Yatsui, T.Nakata, K.Umehara, *J.Electrochem.Soc.* **116**, 94 (1969).
- [13] E.D.Roberts, *J.Electrochem.Soc.* **120**, 1716 (1973).
- [14] V.-M.Graubner, R.Jordan, O.Nuyken, B.Schnyder, T.Lippert, R.Kötz, A.Wokaun, *Macromolecules* **37**, 5936 (2004).
- [15] I.Ipolyi, E.Burean, T.Hamann, M.Cingel, S.Matejcik, P.Swiderek, *Int.J.Mass Spectrom.* **282**, 133 (2009).
- [16] Z.Zheng, X.Xu, X.Fan, W.M.Lau, R.W.M.Kwok, *J.Am.Chem.Soc.* **126**, 12336 (2004).

Quantum dynamics study on muonium chemical reactions

Toshiyuki Takayanagi¹, Tomokazu Tanaka¹ and Takanori Kobayashi²

¹ Department of Chemistry, Saitama University, Saitama City, Japan, tako@mail.saitama-u.ac.jp

² Division of Materials Science and Chemical Engineering, Yokohama National University

Muonium (Mu) is an ultralight isotope of hydrogen, consisting of a positive muon (μ^+) and an electron, since the mass of μ^+ is about 1/9 of the proton mass. The lifetime of Mu (or μ^+) is short ($\sim 2.2 \mu\text{s}$), but this timescale is long enough for investigating chemical reactions containing Mu. Since Mu is a well-behaved hydrogen isotope in a molecule, studying chemical reactions of Mu provides important information about quantum mechanical effects including tunneling, resonance, and quantized vibrations.

In this presentation, we will talk about our recent theoretical studies for the $\text{Mu} + \text{F}_2 \rightarrow \text{MuF} + \text{F}$ (and $\text{F} + \text{MuF} \rightarrow \text{FMu} + \text{F}$) [1,2] and $\text{Mu} + \text{R}_1\text{R}_2\text{C}=\text{S}$ reactions (where R_i denotes a certain functional group) [3]. In the former reaction system, we found that quantum tunneling plays an essential role in low-temperature rate constants as well as in anomalous threshold behaviors at low collision energies. On the other hand, in the latter reaction, we found that the atomic addition site is different between Mu and H due to a large quantized vibrational energy. This means that the H and Mu addition reactions may yield different reaction products. It should be emphasized that this behavior has never been observed in H/D reactions.

As for the MuFF (HFF) reaction system, we have firstly developed an accurate global potential energy surface using the *ab initio* multi-reference configuration interaction method with a large basis set and then perform quantum dynamics calculations on the developed surface using both time-dependent and time-independent quantum scattering methods. Fig. 1 compares the calculated thermal rate constants of Mu (H and D) + $\text{F}_2 \rightarrow \text{MuF} + \text{F}$ reaction with available experimental data. It should be emphasized that a strongly curved behavior of $\text{Mu} + \text{F}_2$ due to quantum tunneling is reproduced at a very good level. Notice that quantum tunneling is significantly enhanced by the existence of the attractive van der Waals well located in the entrance region of the potential energy surface. We have also performed quantum dynamics

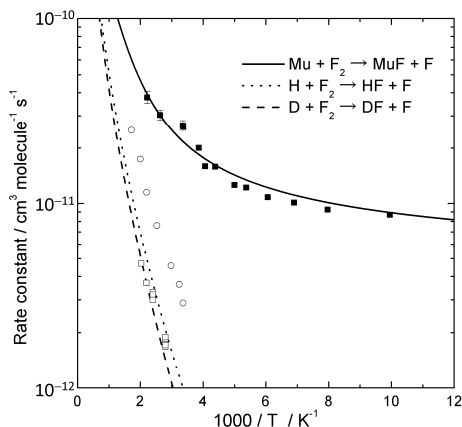


Fig. 1: Comparison of theoretical and experimental rate constants for the $\text{X} + \text{F}_2$ ($\text{X} = \text{Mu}, \text{H}, \text{D}$) reactions.

attractive van der Waals well located in the entrance region of the potential energy surface. We have also performed quantum dynamics

calculations for the $F + \text{MuF}' \rightarrow \text{FMu} + \text{F}'$ exchange reaction using the same potential energy surface. Fig. 2 displays the reaction probabilities for the $F + \text{MuF}'(v = 0, j = 3, 4 \text{ and } 5) \rightarrow \text{FMu} + \text{F}'$ reaction, where v and j are diatomic vibrational and rotational quantum numbers, respectively. Interestingly, one can see very large peaks with a step-like structure around reaction threshold energies. Our detailed analyses show that these come from the combined effect of both quantum tunneling and quantum resonance associated with the $\text{F} \cdots \text{MuF}'$ hydrogen-bond-like complex.

Next, we will present the results of high-level electronic structure calculations for $\text{Mu}(\text{H})$ addition to the C and S atoms of $\text{C}=\text{S}$ containing molecules ($R_1R_2\text{C}=\text{S}$). Stationary points including addition (exchange) transition states and addition products have been obtained with the CASPT2, CCSD(T) and B3LYP levels of theory. We found that the barrier height for the C-addition is generally large, while the S-addition takes place with a very low barrier of without a barrier. This indicates that the S-addition reactions are always kinetically favored. However, it is found that the situation of the thermodynamics stability of the C- and S-adducts is somewhat complicated.

For relatively small functional groups for R_1 - and R_2 -, the C-adducts are more stable than the S-adducts since the C–H bond is generally stronger than the S–H bond. However, for some larger $\text{C}=\text{S}$ containing molecules, S-adducts are more stable than the C-adducts in Mu addition, while the S-adduct are less stable than the C-adducts in H addition. A typical example for the $\text{Mu}/\text{H} + \text{CH}_3(\text{NH}_2)\text{C}=\text{S}$ (thioacetamide) reaction is shown in Fig. 3, obtained at the CCSD(T)/avtz level of theory. It is interesting to notice that the Mu-addition thermodynamically favors the S-site addition, while the H-

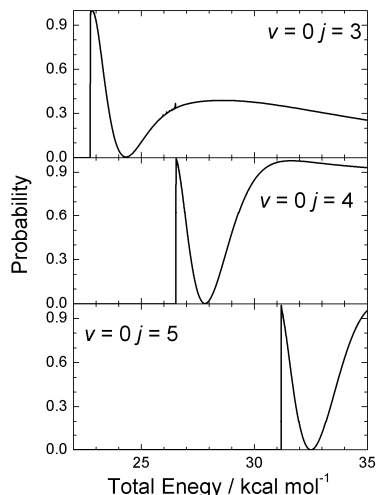


Fig. 2 : Reaction probabilities for the $F + \text{MuF}'(v = 0, j = 3-5) \rightarrow \text{FMu} + \text{F}'$ reaction as a function of the total energy.

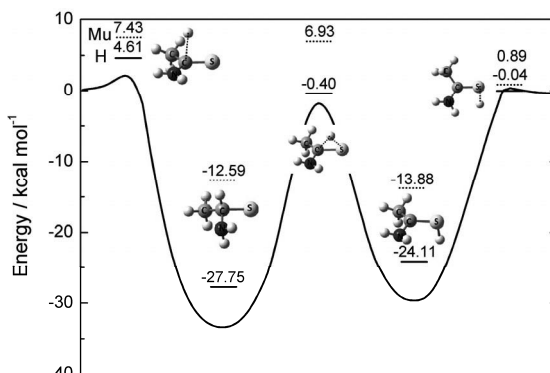


Fig. 3 : Schematic energy diagram of the potential energy surface for the $\text{H}(\text{Mu}) + \text{CH}_3\text{NH}_2\text{C}=\text{S}$ reaction.

notice that the Mu-addition thermodynamically favors the S-site addition, while the H-

addition favors the C-site addition. This result mainly comes from very large quantized vibrational energies of Mu-containing molecules. Our computational results indicate that there is the possibility that Mu and H reactions do give different reaction products through different reaction mechanisms. This might be a new kind of isotope effects between Mu and H/D.

References

- [1] T. Tanaka, T. Takayanagi, *Chem. Phys. Lett.*, **496**, 248–253 (2010).
- [2] T. Tanaka, T. Takayanagi, *Chem. Phys.* in press.
- [3] T. Kobayashi, K. Seki, T. Tanaka, T. Takayanagi, *Comp. Theo. Chem.*, **963**, 256–262 (2011).

Decay of the dialanine anion formed upon free electron attachment

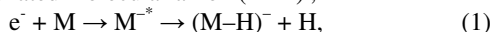
Katrin Tanzer, David Gschliesser, Violaine Vizcaino, Michael Probst, Paul Scheier and Stephan Denifl

Institut für Ionenphysik und Angewandte Physik and Center for Molecular Biosciences Innsbruck, Universität Innsbruck, Technikerstraße 25, 6020 Innsbruck, Austria

The dehydrogenated parent anion $(M-H)^-$ is one of the most dominant anions formed in dissociative electron attachment to various small biomolecules like nucleobases and amino acids. In the present study the $(M-H)^-$ channel for the dipeptide dialanine is investigated with two different instruments: an electron monochromator and a two-sector-field mass spectrometer. At electron energies below 2 eV the measured high resolution ion efficiency curve shows two peaks around 1 eV. Based on quantum chemical calculation determining the threshold energy of $(M-H)^-$ we ascribe the resonances to H loss from different sites in the dialanine molecule.

Introduction

The electron attachment process to biomolecules gained considerable interest since it was discovered that low energy electrons can induce single and double strand breaks in DNA ^[1]. In such a reaction a free electron with a specific kinetic energy attaches resonantly to a molecule leading to a temporary negative ion state (TNI). Once formed, one of the most likely relaxation processes of the TNI is the dissociation of the molecule (DEA). The dissociation process following electron capture needs to be thoroughly understood for modeling and predicting damage by ionization radiation since low energy electrons are generated in abundance by the interaction or ionizing radiation with biological tissue ^[1]. Electron scattering processes with amino acids are also relevant for modeling radiation damage. Amino acids represent the building blocks of peptides and proteins, and the DNA is packed and arranged around proteins. For small biomolecules like amino acids attachment of a low energy electron with a typical kinetic energy of few eV leads often dominantly to the closed-shell dehydrogenated molecular anion $(M-H)^-$,



where M^{-*} is the TNI formed by the resonant electron capture. Above the threshold of electronic excitation the decay pattern changes in favor to smaller fragment anions which for some species are also accompanied by multiple bond ruptures in the molecules. While the fragmentation of dialanine for electron attachment has already been studied ^[2], we focus now in this study on the hydrogen loss upon electron attachment. Utilizing a hemispherical electron monochromator providing an electron resolution of about 120 meV we have determined in the present study the $(M-H)^-$ ion yield as a function of the electron energy for

the dipeptide dialanine. Since for dialanine more sites are available for hydrogen loss than for single amino acids, we have carried out quantum chemical calculations to investigate the site of H-loss. Moreover, utilizing a two-sector-field mass spectrometer we investigated metastable induced decays of $(M-H)^-$ at different resonance energies.

Experimental Setup

The high resolution electron attachment experiment was performed with a crossed beam-setup in combination with a quadrupole mass spectrometer (HEM) ^[3]. A commercially available dialanine sample from Sigma-Aldrich (stated purity $\geq 99\%$) was placed in an oven and heated to temperatures of about 413 K. The oven was attached to a copper capillary with 1 mm opening which ended close to the collision chamber of the electron monochromator. Anions formed were extracted by a weak electric field into a quadrupole mass spectrometer. The mass selected anions were finally detected by a channel electron multiplier which was operated in single pulse counting mode. The electron energy spread was about 120 meV in the measurement (at electron current of about 20 nA). The energy spread was determined with the well-known s-wave attachment reaction leading to Cl^- from CCl_4 . This resonance at about zero eV was also used for the calibration of the energy scale.

Metastable decays of the dehydrogenated dialanine anion $(M-H)^-$ were studied with a two-sector-field instrument (2-SF-MS) ^[4] of reversed Nier-Johnson magnetic sector-electric sector configuration. The ion source of the mass spectrometer was a standard Nier-type ion source where an effusive beam of dialanine molecules, evaporated in an oven (heating temperature typically 398 K), was crossed with an electron beam of about 1 eV resolution. Anions formed were accelerated by 8kV and subsequently mass and energy analyzed. After passing the electric sector anions were detected with a channel electron multiplier operated in single pulse counting mode.

Results and Discussion

Figure 1 shows the anion efficiency curve of the dehydrogenated parent anion $(M-H)^-$ for dialanine between 0 – 7 eV measured with both experimental apparatus, the 2-SF-MS and the HEM.

$(M-H)^-$ around 1 eV

The ion yield from the 2-sector-field instrument only shows one resonance at 1 eV while with the high resolution electron monochromator we can resolve two peaks at 0.85 eV and 1.2 eV respectively. In amino acids, a distinct asymmetric peak shape with a vertical onset was observed; the ion yield was assigned to the hydrogen loss from the carboxyl group. In the

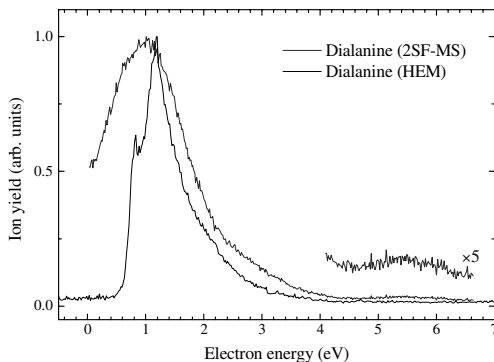


Figure 1: Anion efficiency curve of the dehydrogenated parent anion ($M-H$) for dialanine measured with the high resolution electron monochromator (HEM; electron energy spread about 120 meV) and with the 2-sector-field mass spectrometer (2SF-MS; electron spread about 1 eV).

case of dialanine however the calculated thermodynamic thresholds for other ($M-H$)⁻ isomers show that a hydrogen loss from the amide group is now also energetically possible. The thresholds were calculated using the G4(MP2)^[5] method and are 0.91 eV for the H loss from the carboxyl group and 0.8 eV from the amide group. The thresholds are obtained as difference between the ground-state energies of products and reactants and have an estimated accuracy of ± 0.1 eV. The two peaks in the low energy resonance are therefore very likely to form from H loss from two different sites. More precisely the peak at 0.85 eV is assigned to the H loss from the amide group due to the lower threshold and the peak at 1.2 eV forms by H loss from the carboxyl group.

($M-H$)⁻ - and metastable decays at 5.5 eV

While the ion yield from the 2-sector-field instrument shows a resonance at around 1 eV and 5.5 eV, only the lower energy resonance is visible with the HEM. Because of the much shorter timescales (high extraction acceleration) in the 2-SF-MS we can observe a resonance of the ($M-H$)⁻ anion at 5.5 eV while in the HEM the anion already decays into smaller fragments before it is detected. The metastable decay of ($M-H$)⁻ turned out to be strongly dependent on the initial electron energy. The mass analyzed ion kinetic energy scans (MIKE) scans do not show any metastable decays below 2.5 eV. At 1 eV the anions do not carry enough excess energy to drive further dissociation. The ($M-H$)⁻ formed at the 5.5 eV resonance however decays into three fragments (see Figure 2):

- (i) m/z 88 which was ascribed previously to $(NHCH(CH_3)COOH)^-$, i.e. from the cleavage of the peptide bond OC-NH between the two alanine moieties,

- (ii) m/z 115 identified as $(M-H-CO_2)^-$, and
- (iii) m/z 141 identified as $(M-H-H_2O)^-$

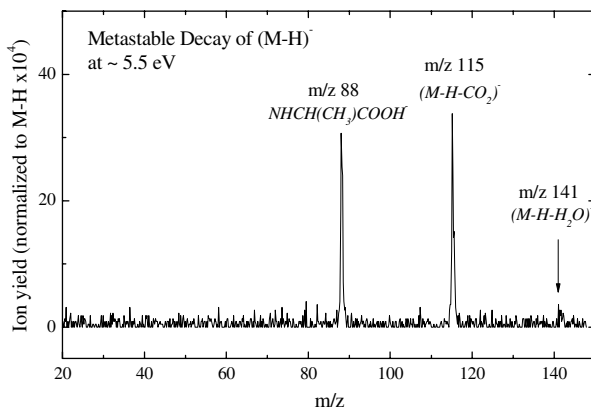


Figure 2: MIKE scan of the metastable decay of $(M-H)^-$ formed at the electron energy of 5.5 eV.

Acknowledgements

This work was supported in part by the Austrian Science Fund, Wien (FWF, projects P22665, P19073), and the Austrian Ministry of Science (infrastructure grant to the LFU scientific computing platform). M.P. acknowledges support from the RFBR-FWF projects 09-03-91001-a and I200-N19 and V.V. acknowledges a Lise Meitner grant from the FWF (M1203).

References

- [1] B. Boudaiffa, P. Cloutier, D. Hunting, M.A. Huels, L. Sanche, *Science* **287**, 1658-1660 (2000)
- [2] E. Alizadeh, D. Gschliesser, P. Bartl, M. Hager, A. Edtbauer, V. Vizcaino, A. Mauracher, M. Probst, T.D. Märk, S. Ptasinska, N. J. Mason, S. Denifl, P. Scheier, *J. Chem. Phys.* **134**, 054305-1-9 (2011)
- [3] S. Ptasinska, S. Denifl, P. Candori, S. Matjcik, P. Scheier, T. D. Märk, *Chem. Phys. Lett.* **403**, 107-112 (2005)
- [4] D. Huber, M. Beikircher, S. Denifl, F. Zappa, S. Matjcik, A. Bacher, V. Grill, T. D. Märk, P. Scheier, *J. Chem. Phys.* **125**, 084304-1-7 (2006)
- [5] L. A. Curtiss, P. C. Redfern, K. Raghavachari, *J. Chem. Phys.* **127**, 124105-1-8 (2007)
- [6] Y. V. Vasil'ev, B. J. Figard, V. G. Voinov, D. F. Barofsky, M. L. Deinzer, *J. Am. Chem. Soc.* **128**, 5506-5515 (2000)

Multilayer and multiparameter grain surface modeling in prestellar cores and hot corinos

Vianney Taquet, Cecilia Ceccarelli, Claudine Kahane

¹ *Institut de Planétologie et d'Astrophysique de Grenoble, vianney.taquet@obs.ujf-grenoble.fr*

The understanding of the formation of Complex Organic Molecules (COMs), observed in large quantities in massive hot cores since two decades (Blake et al. 1987), has gained a renewed interest in the last few years after the detection of abundant COMs also in solar type protostars, specifically in hot corinos (Cazaux et al. 2003), and in the clouds of the Galactic Center (Requena-Torres et al. 2007). Many of these COMs are assumed to be mainly formed on interstellar grains, which act as catalysts for chemical reactions (Tielens & Hagens 1982).

The state of art astrochemical models tend to underestimate the abundance of most of COMs. Indeed, they assumed that radicals (such as CH_3O , CH_2OH and HCO) are produced by the photodissociation of species frozen onto the grain mantles by CR induced FUV emission, a difficult effect to quantify and, therefore, relatively uncertainty. Here, we have developed a new model which shows that radicals can be naturally trapped in grain mantles during the cold and dense pre-collapse phase, namely in prestellar cores.

The new model is based on three key points: 1) the adoption of a multilayer approach, where we distinguish the chemical processes that happen in the mantle inert bulk and on the reactive surface, as also suggested by the results of the Monte Carlo models by Cuppen and collaborators (Cuppen et al. 2009); 2) the influence of the porous structure of grains, which allows light particles to stay on the surface for a longer time than in non-porous grains, as also suggested by Perets & Biham (2006); 3) the study of the distribution of the chemical compositions coming from the variation and uncertainty of key physical, chemical and surface parameters.

First, we will present the influence of the multilayer approach and grain porosity on the formation of grain mantles. We will then show how the variation of parameters induces uncertainties in the mantle chemical compositions. Finally, we will show firsts results on the deuterium chemistry in prestellar cores, and on the formation of complex organic molecules at the surface of grain mantles caused by the warming-up occurring in the hot corinos.

References

- [1] G. Blake, E. C Sutton, C. R Masson, T. G Phillips 1987, *ApJ*, 315, 621
- [2] S. Cazaux, A. G. G. M Tielens, C. Ceccarelli et al. 2003, *A&A*, 593, L51
- [3] M. A Requena-Torres, N Marcelino, I Jiménez-Serra et al. 2007, *A&A*, 655, L37
- [4] A. G. G. M. Tielens, W. Hagen 1982, *A&A*, 114, 245
- [5] H. Cuppen, E. F. van Dishoeck, E. Herbst, A. G. G. M Tielens 2009, *A&A*, 508, 275
- [6] H. Perets, O. Biham 2006, *MNRAS*, 365, 801

Vibrationally bond-selective chemisorption of methane on Pt(111) studied by reflection absorption infrared spectroscopy

Li Chen¹, Hirokazu Ueta¹, Régis Bisson^{1,2} and Rainer D. Beck¹

¹ Laboratoire de Chimie Physique Moléculaire, Ecole Polytechnique Fédérale de Lausanne, Switzerland.

² Aix-Marseille Univ, PIIM, 13397, Marseille, France.

We describe a new molecular beam/surface science apparatus (Fig.1) for quantum state resolved studies of gas/surface reactions using state specific laser reagent preparation by tunable continuous infrared laser radiation in combination with reflection absorption infrared spectroscopy (RAIRS) for the online detection of surface bound the reaction products. Unlike previously used detection methods such as Auger electron spectroscopy, secondary ion mass spectrometry and temperature programmed desorption, RAIRS provides direct structural information on the surface bound product species and is a non-invasive detection method that can be applied online during a molecular beam deposition experiment to obtain a complete product uptake curve in a single deposition run. (Fig. 2)

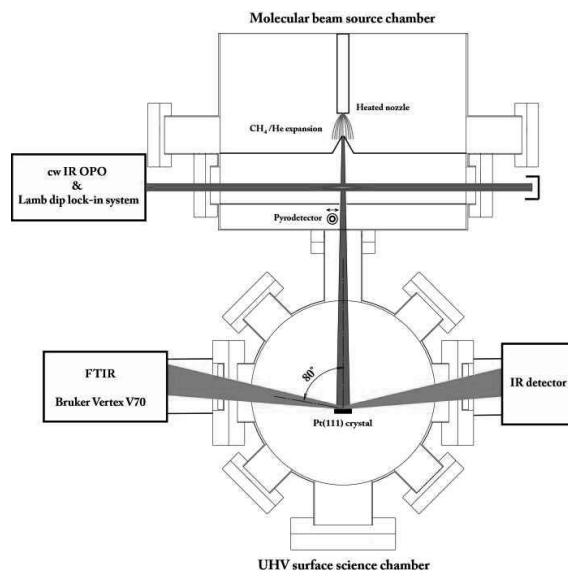


Figure 12: Schematic of molecular beam/surface science apparatus using state specific reagent preparation by infrared laser pumping of a molecular beam incident on a single crystal surface in ultra-high vacuum. Surface bound reaction products are detected by RAIRS

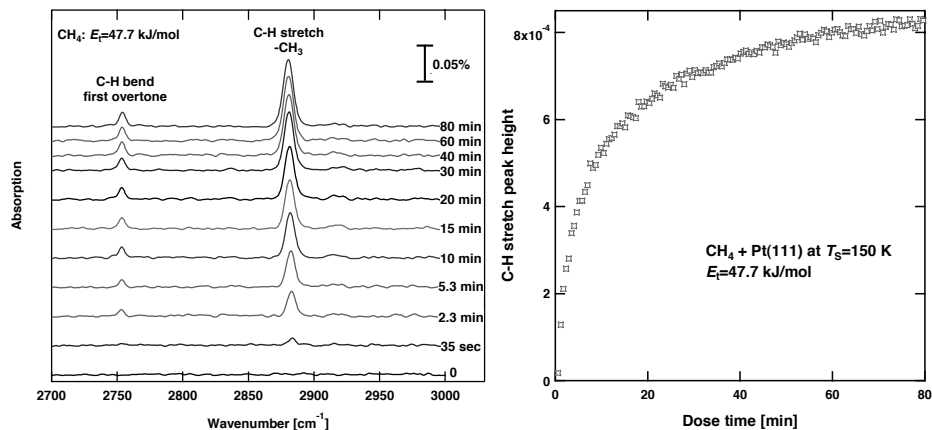


Figure 13: Series of RAIRS spectra of CH₃(ads) and resulting uptake curve produced by the dissociative chemisorption of CH₄, incident with 47.7 kJ/mol translational energy on a Pt(111) surface at a surface temperature of 150 K.

The experimental uptake curves of the chemisorption products can be analyzed to yield the initial sticking coefficient S_0 of the incident methane on the clean Pt(111) from the initial slope of the uptake curve, the coverage dependence $S(\theta)$ of the sticking coefficient and the saturation coverage of the adsorbates.

In initial experiments with this new setup, we have applied the RAIRS detection technique to probe for bond selectivity in the chemisorption of several methane isotopologues on Pt(111). Thermal activation of the dissociation by incident translational and vibrational energy is observed to lead to a near statistical distribution of C-H and C-D cleavage products. In contrast, state specific infrared laser reagent excitation of an infrared active C-H stretch vibration leads to highly selective C-H bond cleavage for any of the partially deuterated isotopologues CH₃D, CH₂D₂, and CHD₃ which will be described in detail in a separate contribution to SASP 2012.

State-selected ion-molecule reactions relevant to the chemistry of Titan's ionosphere

B. Cunha de Miranda^{1,2,3}, S. Chefdeville¹, V. Vuitton⁴, J. Zabka⁵, M. Polasek⁵, C. Romanzin¹, and C. Alcaraz^{1,2}

¹ Lab. de Chimie Physique, Bât 350, UMR 8000 CNRS-Université Paris-Sud 11, 91405 Orsay, France, (christian.alcaraz@u-psud.fr, claire.romanzin@u-psud.fr)

² Synchrotron SOLEIL, L'Orme des Merisiers, Saint Aubin BP 48, 91192 Gif sur Yvette Cedex, France,

³ Universidade Federal Fluminense, Instituto de Física, Av. Gal. Milton Tavares de Souza, Boa Viagem, 24210-346 - Niteroi, RJ – Brasil (barbara.miranda@synchrotron-soleil.fr)

⁴ Institut de Planétologie et d'Astrophysique de Grenoble, UMR 5274, Bât. D de Physique, BP 53, 38041 Grenoble cedex 9, France (veronique.vuitton@obs.ujf-grenoble.fr)

⁵ J. Heyrovsky Institute of Physical Chemistry of the ASCR, v. v. i. Dolejškova 2155/3, 182 23 Prague 8, Czech Republic (jan.zabka@jh-inst.cas.cz, miroslav.polasek@jh-inst.cas.cz)

Abstract

To quantify the production of neutral oxygen O atoms from atomic O⁺ ions, the reactions of state-selected O⁺(⁴S, ²D, ²P) atomic ions (¹⁶O⁺ and ¹⁸O⁺) with methane (CH₄ and CD₄) have been studied. Absolute cross sections for the ionic product formations have been measured as a function of electronic excitation of O⁺ and collision energy. With electronic excitation of the O⁺ parent ion from the ground state ⁴S to the long lived excited states ²D and ²P, a reduction of the total cross section and a complete inversion of the branching ratio between the main products (CH₄⁺ and CH₃⁺) are observed.

1. Introduction

The objectives of this work are derived from the very recent debate on the role of oxygen species in the chemistry of Titan atmosphere [1]. It appears that these species could be initiated by O⁺ cations that are injected on Titan from another Saturn satellite, Enceladus, as confirmed by the observation of precipitating O⁺ flux by the Cassini Plasma Spectrometer [2]. The charge transfer (CT) of O⁺ ions producing neutral O atoms would be the starting point of the chemistry of oxygen in Titan neutral atmosphere. Thus, it appears very important to characterize as well as possible the reactions of O⁺ with the two most abundant neutrals of Titan's atmosphere, N₂ and CH₄. In previous works, the reaction of ground state O⁺(⁴S) with methane was studied in details by Levandier *et al.* as a function of collision energy [3] and the reactions of O⁺(⁴S, ²D, ²P) with N₂ were characterized by Li *et al* [4].

2. The $O^+(^4S, ^2D, ^2P) + CH_4$ reaction

2.1 Experiment

The reaction of O^+ atomic ions with methane has been studied on the guided ion beam apparatus, CERISES [5]. To avoid mass overlaps and to discriminate against secondary reactions, the three isotopically labeled reactions, $^{16}O^+ + CH_4$, $^{16}O^+ + CD_4$ and $^{18}O^+ + CH_4$, have been considered. Absolute reaction cross sections have been measured at selected collision energies for the reaction of O^+ in its ground state $O^+(^4S)$ and first two excited metastable states $O^+(^2D)$ and $O^+(^2P)$ which have very long lifetimes ($\tau(^2D) = 1.6\text{-}9.1$ h and $\tau(^2P) = 4.9\text{-}6.3$ s).

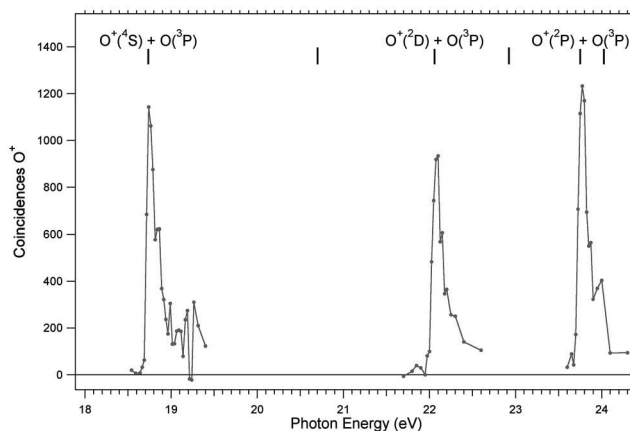


Figure 1: Production of state-selected $O^+(^4S, ^2D, ^2P)$ cations in coincidence with threshold photoelectrons (TPEPICO) by dissociative photoionisation of O_2 with VUV synchrotron radiation.

As shown on Fig. 1, pure state selection of O^+ cations produced by dissociative photoionisation of O_2 has been achieved by using a double threshold technique [5], in which O^+ ions with no recoil kinetic energy were extracted from the source in coincidence with threshold photoelectrons. The experiment was done with VUV radiation in the 18-25 eV range delivered by the DESIRS beamline at the french synchrotron SOLEIL and takes advantage of the 8-bunch operating mode of SOLEIL, in which the interval between two bunches of photons is 148 ns.

2.2 Results

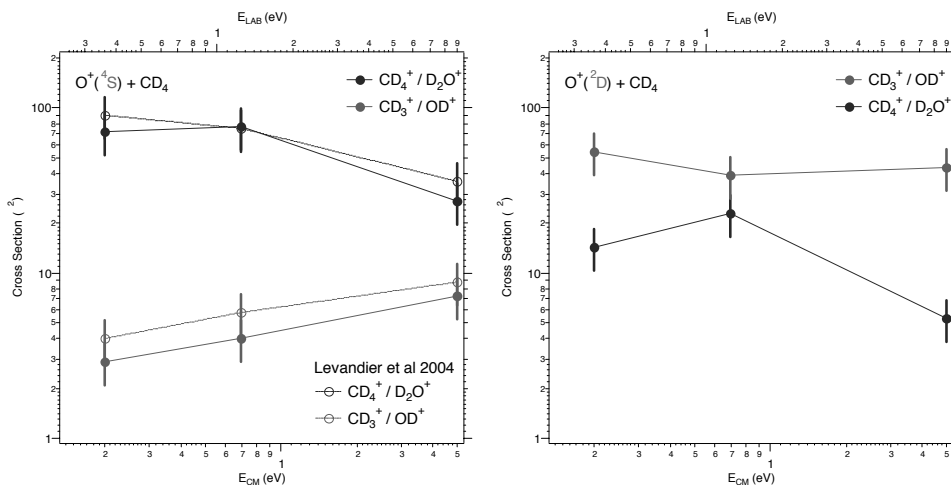


Figure 2: Cross sections for the production of CD₄⁺ and CD₃⁺ in the reaction of ¹⁶O⁺(⁴S and ²D) with CD₄ as a function of collision energy

Absolute cross sections for the reactions of O⁺(⁴S, ²D, ²P) with methane have been measured at three collision energies. Some of these measurements for the two main products, CD₄⁺ and CD₃⁺, are shown on Fig. 2 for the reactions O⁺(⁴S, ²D) + CD₄. Isotope labeling has allowed us to show that D₂O⁺ and OD⁺, which have the same nominal *m/z* as CD₄⁺ and CD₃⁺ (20 and 18 resp.) are minor products even when O⁺ is excited. As visible on Fig. 2, we observe a moderate reduction of the total cross section with excitation of O⁺ to the ²D state, but a complete inversion of the branching ratio between the two products, in favor of the CD₃⁺ product. This is also true for the O⁺ excitation to the ²P state. We are currently analysing the product velocities to find if the CH₃⁺ products are associated with the formation of OH or O + H, which would be very different for the oxygen chemistry. These new laboratory data can be now integrated in Titan's ionosphere models, as was done for the reaction N⁺(³P, ¹D) + CH₄ [6].

Acknowledgements

Synchrotron SOLEIL, RTRA « Triangle de la Physique » (Project « Radicaux » 2009-007T), Pôle Planétologie du PRES Universud (contract 2008-53), Programme National de Planétologie (PNP), COST (Action CM0805 « The Chemical Cosmos »), France-Brazil Program CAPES-COFECUB (n°525/06) and Université Paris-Sud (PhD grant B. Cunha de Miranda), Czech Science Foundation (P208/11/0446) and France-Czech Republic Program CNRS-AVCR (n°20201).

References

- [1] S.M. Hörst, V. Vuitton, and R.V. Yelle, *J. Geophys. Res.* **113**, E10006 (2008).
- [2] R.E. Hartle, E.C. Sittler, F.M. Neubauer, et al, *Planet. Space Sci.* **54** (12), 1211 (2006).
- [3] D.J. Levandier, Y.H. Chiu, R.A. Dressler, L.P. Sun, and G.C. Schatz, *J. Phys. Chem. A* **108** (45), 9794 (2004).
- [4] X. Li, Y.L. Huang, G.D. Flesch, C.Y. Ng, *J. Chem. Phys.* **106**(4), 1373-81 (1997)
- [5] C. Alcaraz, C. Nicolas, R. Thissen, J. Zabka, and O. Dutuit, *J. Phys. Chem. A* **108** (45), 9998 (2004).
- [6] N. Carrasco, C. Alcaraz, O. Dutuit, S. Plessis, R. Thissen, V. Vuitton, R. Yelle, P. Pernot, *Planet. Space Sci.* **56**(12), 1644-57 (2008).

Orienting polar molecules without multipole lenses: Optical state selection with adiabatic orientation

Tim Schäfer¹, Nils Bartels¹, Nils Hocke¹, Xueming Yang³, Alec M. Wodtke^{1,2,4}

¹Institute for Physical Chemistry, Georg-August University of Göttingen, Göttingen, Germany

²Max Planck Institute for Biophysical Chemistry, Göttingen, Germany

³Dalian Institute for Chemical Physics, Dalian, PRC

⁴Department of Chemistry and Biochemistry, University of California Santa Barbara

The spatial configuration of atoms serves as well as any as a definition for molecular identity, structure and to a large degree function. In direct analogy to the central role played by atomic spatial configuration in molecular function, how a molecule's atoms are spatially configured with respect to its surroundings similarly defines its functional interactions with its environment. This helps explain the long standing motivation to develop means of controlling molecular orientation.

For polar molecules, applying an external electric field exerts a force that is capable of orienting the molecule with respect to the direction of the field. By varying the direction of the electric field with respect to a fixed direction in the laboratory frame of reference, one may alter the direction the molecule points in space. One of the most successful approaches to orienting polar molecules has been to selectively focus specific rotational states with quadrupole¹ and hexapole² lenses. Quadrupole fields produce sinusoidal re-focusing trajectories for certain states of linear molecules and have been used, for example, to investigate the angular dependence of dipole-induced dipole interactions between TIF and a series of rare gases³. Hexapoles, which produce sinusoidal refocusing trajectories for symmetric top molecules, have been more extensively employed, in particular, for orienting symmetric top molecules for surface scattering experiments⁴.

Consider the case of hexapole focusing of a polar symmetric top molecule. In the language of quantum mechanics, the orientation is described in terms of the populations of its rotational states, $|J, K, M\rangle$. Here, J is the total angular momentum quantum number, K is the projection quantum number along the symmetry axis of the molecule and M is the projection quantum number along the axis of the electric field.

For molecules with a 1st order Stark effect, the focal length, l , of the hexapole lens is given by Eq. (1)².

$$l^2 = \frac{\pi^2 r_0^3}{3} \frac{MK}{J(J+1)\mu_{el}V_{hex}} \frac{\frac{1}{2}mv^2}{J(J+1)} \sim \frac{MK}{J(J+1)} \frac{\text{Kinetic Energy}}{\text{Stark Energy}} \quad (1)$$

A similar expression has been given for quadrupole lenses¹. Specific rotational states are focused through an aperture, placed in the focal plane of the lens. Other states are less efficiently imaged or indeed defocused. The hexapole lens thus acts as a rotation state selector. The selected rotational state is then transferred to an orientation field. This field need not be constant. By slowly varying the direction of the orientation field along the path of the

molecule, the orientation of the molecule will adiabatic follow the changing direction of the electric field.

Optical pumping is an attractive alternative to multipole lens state-selection. Here, specific rotational states prepared by laser excitation are directly injected into the orientation field. Under the adiabatic condition, the laser prepared states are transformed into quantum mechanically optimal orientation states for use by the experimentalist. This approach offers certain advantages over other methods. First, the focal length of multipole lens scales quadratically with the kinetic energy of the molecule. See Eq. (1). This means that perfect focusing is only possible for molecules of a single kinetic energy. Hence, the multipole state resolving power is rapidly reduced by any velocity spread in the sample and may even require use of a velocity selector¹⁻². Furthermore, especially for molecules with small dipole moments, only modest kinetic energies can even be refocused^{4a, 4c, 5}. Chemical studies of oriented molecules at high kinetic energy are especially interesting, since reorienting forces in chemical reactions – sometimes called steering effects – can be overcome.

In this work, we demonstrate optical state selection with adiabatic orientation. Using stimulated emission pumping of NO, we prepare single parity states (*e* or *f*) in the rotational level of the $X^2\Pi_{1/2}(v=16, J=1/2)$ state in a field free region. The molecules then fly into an electric field and we follow the adiabatic re-coupling producing oriented NO by laser induced fluorescence spectroscopy as a function of the strength of the external electric field. In contrast to use of multipole lenses, the methods demonstrated here are essentially insensitive to the kinetic energy of the molecular sample. Not only may one work with samples with broad kinetic energy distributions, high kinetic energies are as easily oriented as low ones. There is not a focusing condition. The electrode needed for orientation is small compared to a multipole lens. Thus, the distance from the source to the experiment can be reduced, with concomitant higher flux. Another feature of this method is the ability to orient both low field and high field seeking states. This allows rapid optical switching between orientation states using a static orientation field.

The experiments are carried out in a molecular beam apparatus similar to that described in previous papers⁶. A pulsed supersonic molecular beam of rotationally cold NO molecules ($T_{\text{ROT}} \sim 6\text{K}$) is produced by expanding either a 50% NO/Kr ($\text{KE} = 0.035\text{ eV}$) or a 1% NO in H_2 ($\text{KE} = 1.0\text{ eV}$) mixture into the vacuum through a piezoelectric valve (1mm ϕ nozzle, 10 Hz, 3 Atm. stagnation pressure). After passing a 2 mm electro-formed skimmer (Ni Model 2, Beam dynamics, Inc.) 3 cm downstream, the beam enters a differentially pumped region, where Stimulated Emission Pumping⁷ (SEP) is carried out. Populations of NO $X^2\Pi_{1/2}(v''=16)$

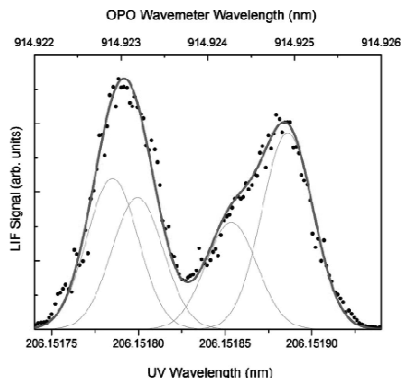


Figure 1: Resolved $R_{11}(1/2)$ A-douplets of the $B^2\Pi_{1/2}(v'=3) \leftarrow X^2\Pi_{1/2}(v''=0)$ transition.

in single parity levels of the $J=1/2$ state are produced by exciting the $B^2\Pi_{1/2}(v'=3) \leftarrow X^2\Pi_{1/2}(v''=0) R_{11}(1/2)$ (PUMP) transition followed by de-exciting the $B^2\Pi_{1/2}(v'=3) \rightarrow X^2\Pi_{1/2}(v''=16) P_{11}(3/2)$ (DUMP) transition. The PUMP step requires light at 206.15nm, produced by a narrow bandwidth homebuilt OPO-SFG laser system (250 MHz resolution, 1 mJ/pulse)⁸. The PUMP step is carried out in a field free region where parity selection rules are strongly obeyed. The high resolution OPO-SFG light source is capable of resolving the $R_{11}(1/2)$ Λ -doublet transitions. See Figure 1. This produces states of defined parity (e or f). Stimulated emission transfers population to the $X^2\Pi_{1/2}(v''=16, J=1/2)$ preserving the parity selected in the PUMP step. This is carried out using the 458.1nm fundamental of a Nd:YAG pumped (PRO-270, Spectra Physics) dye laser (PRSC-DA-24, Sirah) with a pulse energy of 8 mJ and a bandwidth of 3000 MHz. The SEP preparation is monitored by Laser induced fluorescence and fluorescence depletion spectroscopy using a quartz lens and a photomultiplier tube (Hamamatsu, R7154)⁹.

The state prepared NO molecules in single parity levels of $X^2\Pi_{1/2}(v''=16, J=1/2)$ fly downstream in the molecular beam into another differentially pumped vacuum chamber and pass along the symmetry axis of a cylindrical (7 cm long) stainless steel electrode positioned 1 cm in front of a grounded Au(111) sample, which is used to apply electric fields up to 18 kV/cm parallel to the propagation axis of the molecular beam. The Au(111) surface is located 15 cm downstream from the SEP state preparation zone. The 450nm output of a Nd:YAG pumped (Powerlite 7010, Continuum) dye laser (CSTR-DA-24, Sirah) is used to detect the NO($v=16$) molecules in the orientation field by resonantly exciting the molecules to the $A^2\Sigma(v=2)$ state and monitoring the LIF on a PMT in a setup similar to that described above. For detection of the PMT signals we utilize a digital oscilloscope (LT344, LeCroy) interfaced to a computer.

The strength of the orientation field averaged over the ($\sim 1 \text{ mm}^3$) probe volume located between the cylindrical electrode and the gold surface is determined by measuring the Stark splitting of the $B^2\Pi_{1/2}(v'=3) \leftarrow X^2\Pi_{1/2}(v''=0) R_{11}(1/2)$ PUMP transition as a function of the electric field. Since all molecular constants needed to calculate these splitting are known¹⁰, the observed splitting can be used to derive the strength of the electric field.

Results and Discussion

The rotational states of NO are described by symmetric top wave functions

$$\langle J, K, M | \hat{H} | J, K, M \rangle = \sum_{\chi} \mathcal{D}_{\chi, K, M}^{J, K, M} \langle J, K, M | \hat{H} | J, K, M \rangle$$

Where $\mathcal{D}_{\chi, K, M}^{J, K, M}(\chi, \theta, \phi)$ are the Wigner rotation matrices, θ is the polar angle with respect to the electric field, ϕ is the azimuthal angle and χ is the internal azimuthal angle describing the radical electron orbiting the NO bond axis. The Eigenstates of parity relevant to these SEP experiment are given as follows.

$$|J\rangle, |\Omega\rangle, M, \pm = \frac{1}{\sqrt{2}} (|J, \Omega, M\rangle \pm |J, -\Omega, M\rangle)$$

Without an electric field, these states are split by a few 100 MHz (Λ -splitting). The parity state mixing induced by the electric field leads to orientation states.

$$\frac{1}{\sqrt{\alpha(E)^2 + \beta(E)^2}} \{ \alpha(E) |J, |\Omega\rangle, M, +\rangle \pm \beta(E) |J, |\Omega\rangle, M, -\rangle \}$$

The mixing coefficients, $\alpha(E)$ and $\beta(E)$, can be determined from experimental transition strengths in the $A^2\Sigma^- \leftarrow X^2\Pi$ system¹¹. Fig. 2 shows the result of such a determination for $J = \frac{3}{2}$. Circles are derived from transition strengths and the solid lines are results of a theory with no adjustable parameters also given in Ref. 11. When $2\alpha(E)\beta(E) = 1$, the molecules achieve maximal orientation, with an orientational probability distribution, $f_{l, \pm}(\theta) \sim (\cos\theta \pm 1) \sin\theta$, a limit that is for practical purposes reached in this work. We also note the red stars, which are measurements for NO molecular beams with 1.0 eV translational energy.

Finally, we point out that the quantum mechanics described here is valid for all symmetric top molecules. In particular, infrared excitation to single K-doublets with defined parity followed by adiabatic orientation represents a new way to carry out orientation experiments on a wide variety of molecules. Indeed, we see no reason why these ideas should not be applicable to near symmetric top molecules.

References

- [1] HG Bennewitz *et al.*, *Z. Physik* **141**, 6 (1955).
- [2] KH Kramer *et al.*, *J. Chem. Phys.* **42**, 767 (1965).
- [3] HG Bennewitz *et al.*, *Z. Physik* **177**, 84 (1964).
- [4] (a) EW Kuipers *et al.*, *Chem. Phys.* **138**, 451 (1989); (b) MG Tenner *et al.*, *Chem. Phys. Lett.* **168**, 45 (1990); (c) MG Tenner *et al.*, *Surf. Sci.* **236**, 151 (1990).
- [5] M Okada *et al.*, *European Physical Journal B* **75**, 71 (2010).
- [6] (a) D Matsiev *et al.*, *J. Chem. Phys.* **118**, 9477 (2003); (b) J Chen *et al.*, *Chem. Phys.* **301**, 161 (2004).
- [7] (a) X Yang *et al.*, *J. Phys. Chem.* **97**, 3944 (1993); (b) M Silva *et al.*, *Annu. Rev. Phys. Chem.* **52**, 811 (2001).
- [8] L Velarde *et al.*, *Rev. Sci. Instrum.* **81**, (2010).
- [9] JD White *et al.*, *J. Chem. Phys.* **124**, (2006).
- [10] M Drabbels *et al.*, *Chem. Phys. Lett.* **256**, 8 (1996).
- [11] MJL de Lange *et al.*, *Chem. Phys. Lett.* **294**, 332 (1998).

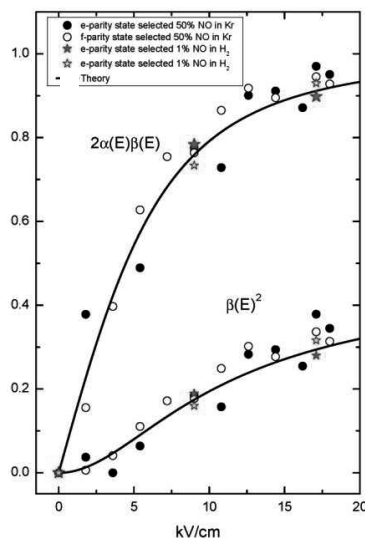


Figure 2: Experimentally derived mixing coefficients as in Ref. 11. Black/White symbols indicate experiments carried out with NO beams with 0.05 eV and stars 1.0 eV kinetic energy.

Quantum simulations for double proton transfer processes

T. Yoshikawa, T. Takayanagi

Department of Chemistry, Saitama University, Japan

I. Introduction

Multiple proton transfer is one of the most fundamental chemical reactions and has been observed in a wide range of molecular systems. A basic question to be solved is whether the transfer occurs via a concerted or stepwise mechanism. This question has been frequently addressed by using static electronic structure calculations of the potential energy surface. However, this simplified picture cannot be generally applied without considering nuclear quantum effect, including tunneling and zero-point vibrational quantization.

In this work, path-integral molecular dynamics simulations (PIMD), that can give important information on the nuclear quantum effects, have been performed for porphycene [1] and hydrated glycine clusters [2] in order to understand the double proton transfer mechanism from a quantum mechanical viewpoint. In the former molecule, we found that the nuclear quantum effects are playing an important role in determining the proton transfer mechanism. In the latter system, we found that the double proton transfer occurs between glycine and water molecules for specific cluster sizes.

II. Calculation

To understand the role of quantum effects, we have performed PIMD simulations. In the porphycene molecule, the molecular dynamics simulations were carried out with 24 – 40 beads depending on the system temperature as well as isotopic substitution (HH, HD or DD) of the inner two protons. The time increment was set to $\Delta t = 0.12 - 0.24$ fs. On the other hand, in hydrated glycine cluster case, the PIMD simulations were performed with 64 – 96 beads depending on the system temperature. The time increment was same as the porphycene case.

III. Results and Discussion

Porphycene is porphyrin isomer and it can convert into the other *trans*-form, which

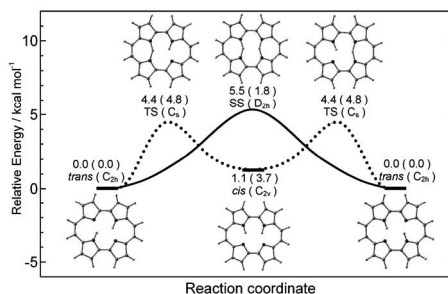
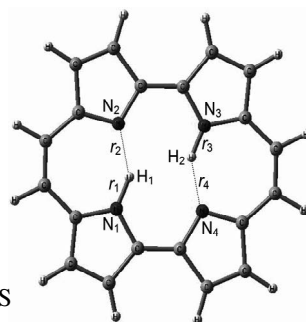


Fig 1. Schematic potential energy diagram of porphycene tautomerism.

is most stable structure, through two mechanisms (Fig. 1). One is the concerted pathway in which two protons simultaneously move to the other sites. The other is stepwise pathway in which single proton transfer occurs in a stepwise manner. In this case, the reaction includes intermediate *cis*-form. Fig. 2 displays the 2D contour plots of the inner proton/deuteron distributions obtained by the PIMD simulations at 300 K and 500 K. In porphycene-HH at 300 K, we obtained significant distributions along the line

●*trans*, ■*cis*, ×TS, +SS



connecting the two minima through SS, which is second order saddle point. This result indicates that the double proton transfer between the *trans* configurations at 300 K mainly occurs through the concerted mechanism. At 500 K, it is seen that the contribution of the stepwise mechanism increases. Therefore, thermal effects are correlated with the proton transfer mechanisms. In the case of isotopically substituted porphycene molecules, DD and HD, we found that the proton transfer mechanism is completely changed. Thus we found that the double proton transfer mechanism in porphycene depends on both temperature and isotopic substitution effects.

Glycine is the simplest naturally occurring amino acid and is one of the most fundamental molecules in biological systems. Since glycine has two functional groups of different polarity, an amino group ($-\text{NH}_2$) and a carboxylic group ($-\text{COOH}$), it can exist either as nonionized neutral form or as zwitterionic tautomer form with ammonium ion ($-\text{NH}_3^+$) and carboxylate ion ($-\text{COO}^-$) units. More specifically, it is well-known that glycine predominantly exists in its neutral form in the

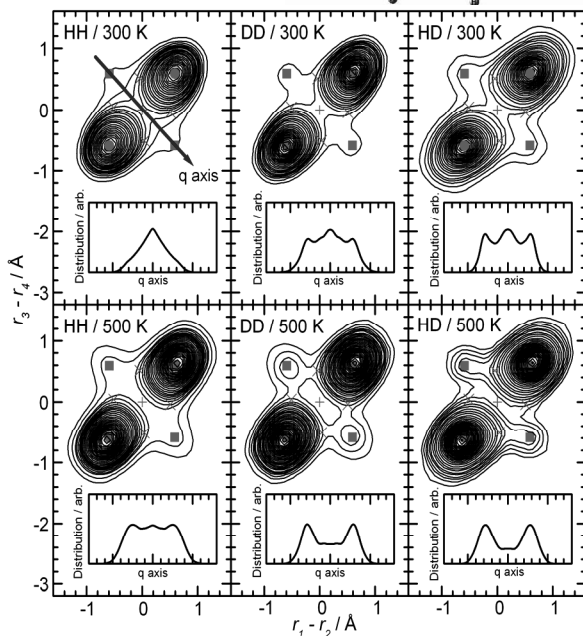


Fig. 2 Two-dimensional contour plots of the inner proton/deuteron distributions and its isotopic variants as a function of r_1-r_2 and r_3-r_4 coordinates obtained by the PIMD simulations at $T = 300$ K (top) and 500 K

gas phase and that in contrast glycine adopts zwitterionic form in bulk aqueous solution and in crystalline state. This fact indicates that polar solvent environments significantly affect a thermodynamic equilibrium between neutral and zwitterionic forms [3]. Therefore,

we are interested in inter-molecular

proton transfer processes for hydrated glycine clusters. Fig. 3 shows the contour plots of the proton density distributions obtained from the PIMD results for the

glycine·(H₂O)_n (n = 5 and 6) clusters. It is seen that the obtained distributions are somewhat broad but two reaction pathways are clearly seen. Two arrows in each plot

in Fig. 3 are associated with synchronous (S path) and asynchronous (AS path) proton transfer pathways. Interestingly, it is found that both mechanisms play a role in the proton transfer processes for the glycine·(H₂O)_n (n = 5 and 6) clusters.

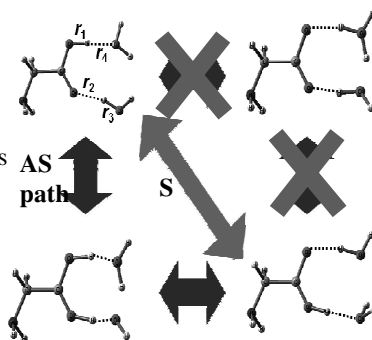
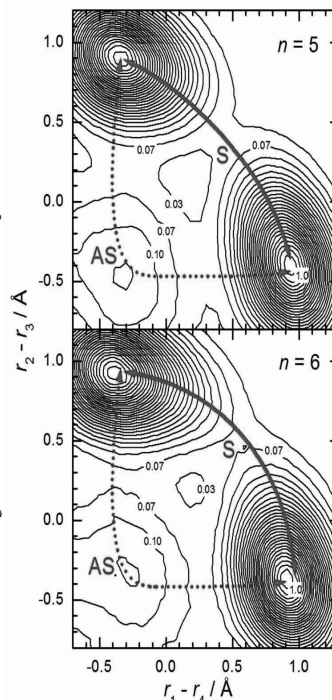


Fig. 3 Two-dimensional contour plots of the proton distributions as a function of r_1-r_4 and r_2-r_3 coordinates obtained by the PIMD simulations at T = 200 K.



IV. References

- [1] T. Yoshikawa, S. Sugawara, T. Takayanagi, M. Shiga, and M. Tachikawa, *Chem. Phys. Lett.* **496** (2010) 14-19.
- [2] T. Yoshikawa, H. Motegi, A. Kakizaki, T. Takayanagi, M. Shiga, and M. Tachikawa, *Chem. Phys.*, **365** (2009) 60-68.
- [3] S. M. Bachrach, *J. Phys. Chem. A*, **112** (2008) 3722.

Author Index

Akhgarnusch, A.	141	Cederquist, H.	23
Albert, S.	86	Chang, Ch.	119
Alcaraz, C.	123, 287	Chen, L.	140, 285
Amiaud, L.	133	Chefdeville, S.	287
An der Lan, L.	92, 156	Chigai, T.	53
Arndt, M.	134	Choi, J.-H.	150
Ascenzi, D.	101	Cooper, R.	62
Asvany, O.	90	Cornaton, Y.	151
Auerbach, D.J.	62	Cunha de Miranda, B.	287
Azria, R.	133		
		Danilov, V.	273
Bajo, J.J.	96	Daxner, M.	92, 156
Balaj, O.P.	141	Dell'Angelo, D.	160
Balucani, N.	127	Denifl, S.	92, 156, 279
Barat, M.	268	Dietiker, P.	263
Barrios, L.	233	Dölle, C.	273
Bartels, Ch.	62	Dörre, N.	134
Bartels, N.	291	Dohnal, P.	162, 259
Bartl, P.	92, 156	Dong, W.	59
Bauerecker, S.	44	Dulieu, F.	29
Bazin, A.	127	Dutuit, O.	127, 180
Beck, R.D.	140, 198, 285		
Benoit, D. M.	49	Eberhardt, W.	239
Beyer, M.K.	141	Echt, O.	92
Bisson, R.	140, 198, 285	Ellis, A.M.	92, 156
Böhler, E.	142, 147, 269	Ernst, W.E.	212, 216
Borrmann, T.	269, 273	Eschner	118
Bredenhöft, J.H.	40, 142, 269, 273	Esmail, A.M.	233
Briant, M.	174		
Brünken, S.	90	Fárník, M.	73, 166, 222, 226
Bursikova, V.	242	Faure, A.	37
Busnengo, H.F.	59	Fayeton, J.A.	268
Buttersack, T.	44	Fedor, J.	73
		Fendt, A.	118
Campargue, A.	45	Field, T.	238
Ceccarelli, C.	283		

Fischmann, K.	141	Horvath, G.	248
Forget, F.	22	Huber, S.E.	190, 194, 208
Friedrich, H.	204	Humblot, V.	133
		Hundt, P.M.	198
Gallego, J.M.	255		
Gaveau, M.-A.	174	Irving, B.J.	51, 199
Geyer, Ph.	134	Ismailova, O.	208, 252
Geppert, W.	24		
Gerlich, D.	67, 200	Jäger, K.Ph.	141
Giri, K.	51	Jiang, J.	229
Glosík, J.	162, 200, 259	Joblin, Ch.	33
Golibrzuch, K.	62	Jochem, R.	156
González, L.	96	Jolondz, E.	273
González-Vázquez, J.	96	Jouvet, C.	268
Govers, Th.R.	176	Jungwirth, P.	85
Grätzel, M.	66	Jusko, P.	200
Gröller, H.	180		
Gschliesser, D.	92, 147, 255, 279	Kahane, C.	283
		Kaiser, A.	204, 208
Guillon, G.	160	Kampschulte, H.	239
		Kandratkensa, A.	62
Hager, M.	92, 255	Kassi, S.	45
Hall, F.H.J.	111	Kautsch, A.	216
Hama, T.	53, 184, 241	Keim, A.	186
Hamann, Th.	269	Kepler Albert, K.	86
Hao, Q.	141	Kimura, Y.	53
Harnisch, M.	186	Kobayashi, T.	276
Hartwig, A.	273	Koch, M.	212, 216
Hasewend, M.	216	Kočišek, J.	73
Haslinger, Ph.	134	Kojima, T.M.	131
Hejduk, M.	162, 259	Kouchi, A.	53, 184, 241
Hell, T.	190	Krěma, F.	248
Herman, Z.	186	Krishna, B.M.	218
Hermansson, K.	231	Krois, G.	212
Hertz, R.	118	Kulikov, Yu.N.	180
Hidaka, H.	53, 131		
Hocke, N.	291	Lackner, F.	212
Höckendorf, R.F.	141	Lafosse, A.	133
Hornberger, K.	134	Lammer, H.	180
Hornekær, L.	61	Leidlmaier, Ch.	92, 156

Lengyel, J.	73, 222, 226	Oba, Y.	53, 241
Lerch, Ph.	86	Oltean, M.	77
Lewerenz, M.	229	Ončák, M.	73, 226
Li, Z.	62	Opanasiuk, S.	162, 259
Lichtenegger, H.I.M.	180	Ostermann, A.	190
Lietard, A.	247	Osterwalder, A.	104
Limtrakul, J.	194	Otero, R.	255
Lindinger, A.	105	Ott, M.	273
Litman, J.H.	72		
Lucas, B.	268	Park, M.-J.	150
		Patzner, A.B.C.	119
Mack, O.	92	Peredkov, S.	239
Märk, T.D.	156, 186	Perina, V.	242
Maier, J.P.	71	Pfleger, M.	180
Marquardt, R.	151, 170, 218	Piani, G.	247
Marquetand, Ph.	96	Pirronello, V.	241
Maršálek, O.	85	Plašil, R.	162, 200, 259
Mason, N.J.	248	Poisson, L.	247
Matejcik, S.	248	Polachova, L.	248
Mauracher, A.	231	Polasek, M.	123, 287
Mazzotti, F.J.	233	Pollet, R.	247
McCullough, B.	238	Poterya, V.	73, 166, 222, 226
Meichsner, J.	273	Postler, J.	92, 147
Meijer, A.J.H.M.	51, 199	Pradier, C.-M.	133
Mestdagh, J.-M.	174, 247	Prentner, R.	234
Meyer, J.	239	Price, S.D.	114
Miksova, R.	242	Probst, M.	190, 194, 208, 252, 279
Milet, A.	77	Puschnigg, B.	92
Miloglyadov, E.	234	Pysanenko, A.	73, 222, 226
Mladenović, M.	229		
Mocanu, V.	242	Quack, M.	86, 234, 263
Monturet, S.	56		
Müller, T.-O.	204	Raghunandan, R.	233
Mulin, D.	200	Rahinov, I.	62
Muñoz-Caro, G.	76	Ralsler, S.	255
Muntean, E.-A.	238	Raschek, M.	216
		Richter, M.	96
Nakai, Y.	131	Rodewald, J.	134
Neeb, M.	239	Rodríguez-Fernández, J.	255
Niedner-Schatteburg, G.	239		
Nimmrichter, J.	134		

Romanzin, C.	123, 287	Takayanagi, T.	276, 295
Rothard, H.	25	Tanaka, T.	276
Roučka, Š.	200, 259	Tanzer, K.	279
Rubovič, P.	162, 259	Taquet, V.	283
		Theisen, M.	212
Saalfrank, P.	56	Tombers, M.	239
Sanglan, P.	66	Tong, X.	111
Sanov, A.	108	Tosi, P.	101
Santamaria, J.	96	Tremblay, J.Ch.	56
Schäfer, T.	291	Tully, J.C.	62
Scheier, P.	92, 147, 156, 186, 255, 279	Ünlü, F.	263
Schlemmer, S.	90	Ueta, H.	140, 198, 285
Schmitt, B.	81	Uhlig, F.	85
Schmüser, C.	273	Uras-Aytemiz, N.	77
Schneider, A.	263	Urban, C.	255
Schöbel, H.	92, 156		
Seyfang, G.	234, 263	Van der Linde Ch.	141
Shematovich, V.I.	180	Varju, J.	162, 259
Shen, X.J.	59	Viel, A.	160
Shenvi, N.	62	Vizcaino, V.	92, 279
Signorell, R.	72	Vuitton, V.	127, 287
Siu, C.-K.	141		
Slavíček, P.	73, 166, 226	Wagner, H.E.	273
Slavicek, P.	242	Warakulwit, Ch.	194
Smith, M.A.	108	Ward, M.D.	114
Soep, B.	247	Watanabe, N.	53, 131, 184, 241
Sola, I.	96		
Soorkia, S.	268	Watson, J.	248
Spångberg, D.	231	Watson, R.E.	114
Spighi, G.	174	Wester, R.	100
Stohner, J.	38	Willitsch, S.	111
Stoica, A.	242	Wodtke, A.M.	62, 291
Streibel, T.	118		
Sülzle, D.	119	Xiao, Y.	59
Svrčková, P.	73		
Swiderek, P.	142, 147, 269, 273	Yan, X.H.	59
		Yang, X.	291
Šištík, L.	166	Yelle, R.V.	127

Yoder, B.	72
Yoshikawa, T.	295
Yuan, B.	108
Zabka, J.	123, 287
Zahoran, M.	248
Zimmermann, R.	118
Zöttl, S.	92, 186
Zymak, I.	200